1 2 9 0

UNIVERSIDADE D
COIMBRA

Raquel Sofia Freitas Boia

ACTIVATION OF A_3 ADENOSINE RECEPTOR USING INTRAOCULAR BIODEGRADABLE IMPLANTS AS A STRATEGY FOR THE TREATMENT OF GLAUCOMA

Tese de Doutoramento do Programa Interuniversitário de Doutoramento em Envelhecimento e Doenças Crónicas orientada pela Professora Doutora Ana Raquel Santiago e pela Professora Doutora Gabriela Silva e apresentada à Faculdade de Medicina da Universidade de Coimbra.

Dezembro de 2020

Faculdade de Medicina da Universidade de Coimbra

ACTIVATION OF A_3 ADENOSINE RECEPTOR USING INTRAOCULAR BIODEGRADABLE IMPLANTS AS A STRATEGY FOR THE TREATMENT OF GLAUCOMA

Raquel Sofia Freitas Boia

Tese de Doutoramento do Programa Interuniversitário de Doutoramento em Envelhecimento e Doenças Crónicas orientada pela Professora Doutora Ana Raquel Santiago e pela Professora Doutora Gabriela Silva e apresentada à Faculdade de Medicina da Universidade de Coimbra.

Dezembro 2020

1 2 9 0

UNIVERSIDADE D COIMBRA

Support

This work was supported by Foundation for Science and Technology (FCT), Portugal (PhD Fellowship PD/BD/114115/2015; R&D project PTDC/NEU-OSD/3123/2014; Strategic Projects Pest UID/NEU/04539/2013, UID/NEU/04539/2019, UIDB/04539/2020 and UIDP/04539/2020); COMPETE-FEDER (POCI-01-0145-FEDER-016849 and POCI-01-0145-FEDER-007440); BRAINHEALTH 2020 (CENTRO-01-0145-FEDER-000008).

Agradecimentos

E chegando a esta reta final é fascinante fazer um resumo de todas as etapas fundamentais no decorrer de todo o trabalho e, é um enorme sentimento de gratidão perceber que realmente isto só é possível tendo pessoas boas ao nosso lado. Engana-se quem pensa que investigação se faz sozinha, e eu tenho tido imensa sorte nas pessoas que se têm cruzado no meu percurso.

Sem dúvida que a pessoa a quem devo todo o sucesso deste trabalho é à minha orientadora, Doutora Raquel Santiago. Em todo o percurso desde a preparação para entrevista do programa doutoral, idealização do projeto, concretização do projeto e escrita da tese, a Raquel foi fundamental. Durante este percurso houve alguns contratempos! Perceber se iríamos conseguir ter os implantes atempadamente para fazer os ensaios. Um modelo animal que não funcionou e que a meio do percurso poderia ter comprometido o progresso do projeto. Perceber se realmente os implantes estariam a libertar o fármaco. Foi uma luta! Mas conseguimos! E em todos os momentos em que eu poderia não estar a ver qual o melhor caminho e qual o próximo passo a seguir, a Raquel conseguiu sempre ajudar-me a ver a luz ao fundo túnel. E isto é o melhor que se pode ter de um orientador! Agradeço do fundo do coração todas as palavras amigas e todas as oportunidades que me foram dadas ao longo destes anos, que muito contribuíram para o meu percurso e crescimento enquanto investigadora. Obrigada!

Agradeço ao Doutor Francisco Ambrósio, líder do grupo Retinal Dysfunction and Neuroinflammation Lab, pela oportunidade que me deu em integrar o grupo desde 2011 e desde então me proporcionar todas as condições necessárias para desenvolver o meu trabalho. Para além disto em muito agradeço ao Doutor Francisco a oportunidade em integrar diferentes projetos que sem dúvida têm contribuído muito para o meu percurso enquanto investigadora.

Agradeço à Doutora Gabriela Silva, co-orientadora desta tese, pelo acompanhamento e pelas suas palavras amigas ao longo do meu percurso.

Agradeço ao Doutor Henrique Girão, coordenador do Programa de Doutoramento, pela amizade e disponibilidade demonstrada ao longo destes anos. Agradeço também o facto de liderar um grupo onde a boa disposição que se consegue encontrar do outro lado do corredor faz toda a diferença num dia de trabalho. Obrigado a todos pela paciência nos meus longos dias de immunopanning! Obrigada Mónica por todo o tempo e dedicação dedicado ao processimento das minhas amostras para microscocopia eletrónica.

Quero também agradecer ao Professor Herminio Sousa, à Doutora Mara Braga e ao Paulo Dias, fundamentais no processo de desenvolvimento dos implantes. Este projeto aliou duas áreas totalmente diferentes com um objetivo final em comum, e só tenho a destacar o quão bem esta colaboração funcionou muito fruto do empenho de todos.

I would like to thank to the people from the group of Professor Manuel-Vidal Sanz, from the University of Murcia for receiving me so nicely. A special acknowledgment to Professor Manuel Vidal-Sanz for receiving me in his lab, and for giving me all the conditions to perform part of the experiments presented in this thesis. It was a very hardworking month, which without the help of several people it would not be possible to perform all of the work that was done. A special thank to Cari for all the help during these years and to receive me so warmly in Murcia.

O meu agradecimento especial vai para o grupo Retinal Dysfunction and Neuroinflammation Lab! Muitos têm sido os que vêm e vão, muitos têm sido os que vêm e ficam e, destes muitos marcaram de alguma forma o meu percurso. A boa disposição e o companheirismo deste grupo são das características mais importantes que levo para a vida! Sem dúvida que tenho de destacar algumas pessoas como fundamentais neste processo.

Rita Gaspar, minha parceira desde o início deste percurso! Agradeço-te o grande companheirismo e amizade desde o início e que foi fundamental no nosso primeiro ano de doutoramento. Tive o prazer de partilhar contigo os restantes anos de doutoramento bem de perto e, fazer desta uma viagem menos solitária.

Catarina Neves, sempre com uma palavra amiga e muita acertada! Obrigado por me ouvires, obrigado por toda a paciência. E não te preocupes Neves, estarei sempre cá para tudo o que tu precisares. Eu tenho a certeza de que irás fazer um caminho na ciência brilhante!

Maria, grande companheira desde o início deste projeto e, sempre mais certa que eu de que isto iria resultar! Obrigada Mary por tudo! Obrigada pelos ensinamentos! Obrigada pela oportunidade de ter ido contigo a Múrcia ajudar no trabalho, nem sabes o quanto isso me ajudou na minha estadia.

Inês minha parceira de gabinete e que tanto aturou as minhas epifanias! Obrigada por todos os discursos motivacionais. Obrigado por toda a tua boa disposição e descontração que tanto me faz rir! Obrigada por todas as palavras amigas que ajudaram a seguir em frente e tomar as decisões certas!

Fi que tem sido uma pessoa fundamental e das mais importante desde a minha chegada ao grupo. Fi um grande obrigada pela tua amizade sincera e genuína! Esta é uma amizade para a vida.

Celocas obrigada por teres feito parte deste processo sempre com uma palavra amiga e sempre com bons conselhos a seguir.

Quero também agradecer ao Marco e à Sofia, amigos do PhDOC, pela boa disposição ao longo de todas as rotações, aulas e retiros.

Agradeço à Kath e à Vera todo o companheirismo desde o início do curso. Apesar de longe, vocês têm acompanhado o processo bem de perto sempre com uma palavra amiga. Vera um grande obrigado por todos os dias me ouvires e aconselhares, acho que não houve um único dia que não tenha recorrido a ti para seguir em frente!

Agradeço à Dani que é a minha amiga de uma vida e para a vida! Já nos conhecemos há mais de 20 anos, não falamos todos os dias e nem estamos juntas sempre, mas quando estamos é como se o tempo não tivesse passado. Ela está em todos os momentos da minha vida, assim como eu dos dela, e os anos de preparação desta tese não foram exceção. Obrigada minha Dani.

Sem dúvida que as 3 pessoas mais importantes para que tudo isto fosse possível são os meus pais e a minha irmã! Podia não existir mais ninguém mas é aqui, ao meu núcleo familiar, onde todos os dias encontrei e irei sempre encontrar a razão e força para seguir em frente. Com eles aprendo todos os dias que com muito trabalho e dedicação tudo é possível. Agradeço muito à minha irmã a grande ajuda ao longo destes anos e, acima de tudo agradeço muito a ajuda fundamental em tornar esta tese tal como tinha imaginado! E sem dúvida uma última palavra para os meus pais que têm feito o possível e impossível para que hoje pudesse concluir esta etapa. A vocês devo tudo, devo tudo aquilo que sou hoje!

Table of contents

Activation of adenosine A_3 receptor protects retinal ganglion cells from degeneration induced by ocular hypertension

Porous poly(ε-caprolactone) implants: A novel strategy for efficient intraocular drug delivery

Activation of A_3 adenosine receptor using intraocular biodegradable implants protects retinal ganglion cells from ischemic injury

Publications

The presented thesis contributed to the following reviews:

1. Santiago AR, Madeira MH, **Boia R**, Aires ID, Rodrigues-Neves AC, Santos PF, Ambrósio AF. Keep an Eye on Adenosine: Its Role in Retinal Inflammation. Pharmacol Ther. 2020 Jun;210:107513. doi:10.1016/j.pharmthera.2020.107513

2. **Boia R**, Ruzafa N, Aires ID, Pereiro X, Ambrósio AF, Vecino E, Santiago AR. Neuroprotective Strategies for Retinal Ganglion Cell Degeneration: Current Status and Challenges Ahead. Int J Mol Sci. 2020 Mar 25;21(7):2262.
doi: 10.3390/ijms21072262

The results presented in this thesis were published in peer-reviewed international scientific journals:

1. **Boia R***, Dias PAN*, Martins JM, Galindo-Romero C, Aires ID, Vidal-Sanz M, Agudo-Barriuso M, de Sousa HC, Ambrósio AF, Braga MEM, Santiago AR. Porous poly (Ɛ-caprolactone) implants: A novel strategy for efficient intraocular drug delivery. J Control Release. 2019 Dec 28;316:331-348.
doi:10.1016/j.jconrel.2019.09.023
* Authors contributed equally to this work

2. **Boia R**, Salinas-Navarro M, Gallego-Ortega A, Galindo-Romero C, Aires ID, Agudo-Barriuso M, Ambrósio AF, Vidal-Sanz M, Santiago AR. Activation of adenosine A_3 receptor protects retinal ganglion cells from degeneration induced by ocular hypertension. Cell Death Dis. 2020 May 27;11(5):401.
doi: 10.1038/s41419-020-2593-y

Abbreviations

A_1R	Adenosine A_1 receptor
$A_{2A}R$	Adenosine A_{2A} receptor
$A_{2B}R$	Adenosine A_{2B} receptor
A_3R	Adenosine A_3 receptor
ADA	Adenosine deaminase
ADK	Adenosine kinase
ADP	Adenosine diphosphate
AMD	Age-related macular degeneration
AMP	Adenosine monophosphate
ATP	Adenosine 5'-triphosphate
a.u.	Arbitrary units
BDNF	Brain-derived neurotrophic factor
BRB	Blood-retinal barrier
BSA	Bovine serum albumin
Ca^{2+}	Calcium
cAMP	Cyclic adenosine monophosphate
CD39	Apyrase
CD73	Ecto-5'-nucleotidase
ChAT	Choline acetyltransferase
CNS	Central nervous system
CNTF	Ciliary neurotrophic factor
Cop-1	Copolymer-1
CO_2	Carbon dioxide
CTB	Cholera toxin B subunit
DAPI	4',6'-diamidino-2-phenylindole
DARC	Detection of Apoptosing Retinal Cells
DIV	Day *in vitro*
DMSO	Dimethyl sulfoxide
DOC	Deoxycholate
DTT	Dithiothreitol
DXMT	Dexamethasone
ECL	Enhanced chemiluminescence
ECF	Enhanced chemifluorescence
ED	Embryonic day
EGTA	Ethylene glycol tetraacetic acid
EHP	Elevated hydrostatic pressure
ELISA	Enzyme-linked immunosorbant assay
EPO	Erythropoietin
ERG	Electroretinography
EVA	Ethylene vinyl acetate
FBS	Fetal bovine serum

FCNN	Fully convolutional neural network
FDA	Food and Drug Administration
FG	Fluorogold
G	Glycofurol
GABA	γ-aminobutyric acid
GCL	Ganglion cell layer
GFAP	Glial fibrillary acidic protein
GLP	Good Laboratory Practices
HBSS	Hanks' balanced salt solution
HEPES	4-(2-hydroxyethyl)piperazine-1-ethanesulfonic acid
HM	Hot melting
HPLC	High performance liquid chromatography
Iba1	Ionized calcium-binding adaptor molecule 1
iBRB	Inner blood-retinal barrier
IL-1β	Interleukin-1β
ILM	Inner limiting membrane
INL	Inner nuclear layer
IOP	Intraocular pressure
IPL	Inner plexiform layer
I-R	Ischemia-reperfusion
IS/OS	Inner segments/outer segments
ISO	International Organization for Standardization
Ki	Inhibitory constant
KLF	Krüppel-like family
K^+	Potassium
LGN	Lateral geniculate nucleus
MAG	Myelin-associated glycoprotein
MEM	Eagle's minimum essential medium
mRNA	Messenger RNA
mTOR	Mammalian target of rapamycin
NeuN	Neuronal nuclear protein
NFL	Nerve fiber layer
NGF	Nerve growth factor
NgR	Nogo receptor
NMDA	N-methyl-D-aspartate
NOS	Nitric oxide synthase
nSTR	Negative scotopic threshold response
NT-501 ECT	NT-501 encapsulated cell therapy
NTs	Nucleoside transporters
oBRB	Outer blood-retinal barrier
OCT	Optical coherence tomography

OHT	Ocular hypertension
OLM	Outer limiting membrane
ONH	Optic nerve head
ONL	Outer nuclear layer
OPL	Outer plexiform layer
PBS	Phosphate-buffered saline
PCL	Poly(Ɛ-caprolactone)
PFA	Paraformaldehyde
PGA	Poly(glycolic acid)
PI3K	Phosphoinositide 3-kinases
PKC-α	Protein kinase C-α
PLA	Poly(lactic acid)
PLGA	Poly(D,L-lactic-co-glycolic)acid
PND	Postnatal day
pSTR	Positive scotopic threshold response
PTEN	Phosphatase and tensin homologue
PVA	Polyvinyl alcohol
PVDF	Poly(vinylidene difluoride)
RGCs	Retinal ganglion cells
rhNGF	Recombinant human NGF
RIPA	Radioimmunoprecipitation assay
RMSE	Root-mean-square error
ROI	Region of interest
RPE	Retinal pigmented epithelium
SAH	S-adenosylhomocysteine
SC	Superior colliculus
$scCO_2$	Supercritical carbon dioxide
SCi	Superior colliculi
SDS-PAGE	Sodium dodecyl sulphate-poly(acrylamide) gel electrophoresis
SEM	Standard error of the mean
Sema3A	Semaphorin-3A
SFM	Supercritical carbon dioxide-assisted foaming/mixing method
STR	Scotopic threshold response
TBS-T	Tris-buffered saline with Tween-20
TEM	Transmission electron microscopy
TNF	Tumor necrosis factor
TUNEL	Terminal deoxynucleotidyl transferase-mediated dUTP nick-end labeling
VEGF	Vascular endothelial growth factor
Zn^{2+}	Zinc
Δ1	Delta 1
Δ2	Delta 2
$[Ca^{2+}]_i$	Intracellular Ca^{2+} concentration

Abstract

Glaucoma is a leading cause of irreversible blindness that is characterized by optic nerve damage and retinal ganglion cell (RGC) death. Elevated intraocular pressure (IOP) is an important risk factor in glaucoma and the only that is modifiable. Indeed, current treatments are directed towards IOP lowering, however many patients continue to lose vision despite successful IOP control. Therefore, new and more effective treatments are necessary, and targeting neuroprotection of RGCs is considered to be an additional therapy. RGCs express adenosine A_3 receptor (A_3R) and its activation confers protection to RGCs following an excitotoxic stimulus, as occurs in glaucoma. These findings strongly support that A_3R activation can protect RGCs from glaucomatous damage. Therefore, we aimed to study the protective properties of A_3R agonist against glaucomatous insult (Chapter 2). Ocular hypertension (OHT) was induced by laser photocoagulation of the limbal veins and A_3R agonist (2-Cl-IB-MECA, 5 μl, 1.2 μM) was delivered intravitreally immediately after the induction of OHT. The outcome was assessed 7 days post injection. The treatment with A_3R agonist increased RGC survival and attenuated the impairment in retrograde axonal transport induced by OHT, which is consistent with the preservation of the optic nerve structure. These beneficial effects of A_3R activation may be contributing to the maintenance of the RGC function in OHT animals. Therefore, A_3R can be suggested as a good therapeutic target to protect RGCs from glaucomatous damage.

Drug delivery into the posterior part of the eye is mainly achieved by intravitreal injection. However, frequent intravitreal injections can lead to retinal detachment, cataract, and endophthalmitis. Therefore, the design of sustained drug delivery systems for the posterior segment of the eye can encompass a therapeutic breakthrough. The development of these systems has been a challenge for many years, but it is nowadays used in clinical practice for some retinal diseases. Biodegradable implants present an additional advantage since they are degraded into nontoxic products and, then safely eliminated, contrary to nonbiodegradable implants. Aiming to overcome the need of multiple intravitreal injections, herein a new biodegradable intraocular implant (porous poly(ε-caprolactone) (PCL)-based intraocular implants) was developed for controlled drug release in collaboration with the Chemical Engineering Department of the Faculty of Sciences and Technology of the University of Coimbra (Chapter 3, supplementary information). Thus, the potential of PCL-based implants to be used as intraocular drug delivery device was assessed (Chapter 3). The presence of the PCL implant or the degradation products did not cause neuronal cell death, particularly did not affect the number of RGCs, in retinal primary neural cell cultures and retinal organotypic cultures, reinforcing the possibility of testing these implants in animal models. The PCL-based implants were surgically introduced in the vitreous of Wistar rats, and the outcome was evaluated at 4 and 8 weeks after the surgery. The presence of the PCL implant or the procedure did not change retinal function (evaluated by electroretinography, ERG) nor retinal structure (evaluated by optical coherence tomography, OCT). Moreover, PCL implant did not induce alterations in retinal neurons and had no toxic effect in RGCs *in vivo*, since the number of RGCs was not altered. The impact to retinal glial cells was assessed, and both the procedure and the presence of PCL implant may induce Müller cell gliosis, without affecting microglial cells and astrocytes. The assessment of retinal structure

and Müller cell reactivity 1 year after surgery demonstrated that the structure was not altered and that Müller cell gliosis observed in early time points was a transient effect. Taking into consideration the lack of retinal toxicity of PCL implants, this new device can now be loaded with drugs to tackle retinal diseases. Indeed, since the activation of A_3R confers protection to the retina, in particular to RGCs, implants loaded with 2-Cl-IB-MECA can be hypothesized as a new strategy to protect the retina from degeneration (Chapter 4).

2-Cl-IB-MECA-loaded PCL implants were developed in collaboration with the Chemical Engineering Department of the Faculty of Sciences and Technology of the University of Coimbra (Chapter 4, supplementary information). The PCL implant loaded with 2-Cl-IB-MECA presented an extended drug release of around 30 days. Then, the drug released from the implant maintained functional activity, as determined *in vitro* by single-cell Ca^{2+} imaging of RGCs. 2-Cl-IB-MECA-loaded PCL implants were immersed in a saline solution for 24 h that was able to reduce the glutamate-evoked increase in intracellular Ca^{2+} concentration in immunopurified RGC cultures. Drug-free and 2-Cl-IB-MECA-loaded PCL implants were introduced in the vitreous after inducing transient retinal ischemia, and the outcome was assessed 1 month after lesion induction. The presence of 2-Cl-IB-MECA-loaded PCL implants in the vitreous preserved the structure of the optic nerve and preserved the anterograde axonal transport. Moreover, the survival of RGCs was increased and the function of RGCs was maintained upon transient retinal ischemia, indicating that RGCs are protected from ischemia-reperfusion damage.

These results suggest that A_3R represents a potential drug target for the development of novel therapeutic strategies for glaucoma. Moreover, the incorporation of 2-Cl-IB-MECA in a biodegradable intraocular implant may be a promising therapeutic strategy for glaucoma.

Keywords: Adenosine A_3 receptor, glaucoma, intraocular biodegradable implants, neurodegeneration, neuroprotection.

Resumo

O glaucoma é umas das principais causas de cegueira, sendo caracterizado por danos no nervo ótico e morte das células ganglionares da retina (CGR). A pressão intraocular elevada (PIO) é um fator de risco e é o único que é modificável. Os tratamentos atualmente usados na clínica são direcionados para o controlo da PIO, contudo muitos pacientes continuam a perder visão, apesar do controlo da PIO. Assim, torna-se necessário desenvolver novas abordagens terapêuticas e a proteção das CGR é considerada uma abordagem com potencial. As CGR expressam o recetor A_3 de adenosina (A_3R) e a sua ativação confere proteção às CGR após estímulos excitotóxicos. Assim, o objetivo principal foi estudar os efeitos protetores do agonista do A_3R contra o dano glaucomatoso (Capítulo 2). Utilizou-se um modelo animal de glaucoma induzindo hipertensão ocular por fotocoagulação das veias do limbo e o agonista do A_3R (2-Cl-IB-MECA, 5 μl, 1.2 μM) foi administrado por injeção intravítrea imediatamente após a indução de hipertensão ocular. Os resultados foram analisados 7 dias após a injeção intravítrea. O tratamento com o agonista do A_3R aumentou a sobrevivência das CGR e atenuou o défice no transporte axonal retrógrado induzido pela hipertensão ocular. Estes resultados são consistentes com a preservação da estrutura do nervo ótico. Os efeitos benéficos observados pela ativação do A_3R poderão estar a contribuir para a manutenção da função das CGR nos animais com hipertensão ocular. Desta forma, podemos considerar o A_3R um bom alvo terapêutico para conferir proteção às CGR contra o dano glaucomatoso.

A entrega de fármacos para a parte posterior do olho é maioritariamente conseguida através de injeções intravítreas. Contudo, repetidas injeções podem levar ao descolamento da retina ou ao desenvolvimento de catarata. Assim, apesar do desenvolvimento de sistemas de libertação de fármacos para a parte posterior do olho ser um desafio, é já uma prática clínica para algumas doenças da retina. Os implantes biodegradáveis apresentam a vantagem de serem degradados em produtos não tóxicos e facilmente eliminados, ao contrário dos implantes não biodegradáveis. Com o objetivo de ultrapassar a necessidade de múltiplas injeções intravítreas foi desenvolvido um novo implante intraocular (à base de poli(Ɛ-caprolactona)) para libertação controlada de fármacos. Este implante foi desenvolvido em colaboração com o Departamento de Engenharia Química da Faculdade de Ciências e Tecnologia da Universidade de Coimbra (Capítulo 3, informação suplementar). Assim, o potencial deste implante de PCL ser usado como sistema de libertação intraocular de fármaco foi avaliado (Capítulo 3). A presença do implante de PCL, assim como os produtos de degradação, não causaram morte neuronal, e, em particular, não afetaram o número de CGR, em culturas primárias neuronais de retina e em culturas organotípicas de retina, reforçando a possibilidade de avaliar a segurança do uso destes implantes em modelos animais. Os implantes de PCL foram cirurgicamente introduzidos no vítreo de ratos Wistar e os resultados foram analisados 4 e 8 semanas após a cirurgia. A presença do implante de PCL, assim como o procedimento, não alteraram nem a função da retina (avaliado por electroretinografia, ERG) nem a estrutura da retina (avaliado por tomografia de coerência ótica, OCT). Além disso, os implantes de PCL não induziram alterações nos neurónios da retina e não alteraram o número de CGR. O impacto para as células da glia da retina foi também avaliado e, tanto o procedimento como a presença do implante induziram reatividade das células de Müller, sem

afetar as células da microglia e os astrócitos. A avaliação da estrutura da retina e da reatividade das células da retina, após 1 ano após a cirurgia, mostrou que a estrutura se mantém inalterada e que a gliose das células de Müller observada nos tempos de experiência iniciais foi uma reação transitória. Sabendo que os implantes de PCL não induzem toxicidade para a retina, os implantes intraoculares de PCL podem ser carregados com um fármaco de forma a conferir proteção às CGR. Uma vez que a ativação do A_3R confere proteção para a retina, e, em particular para as CGR, os implantes de PCL carregados com 2-Cl-IB-MECA podem ser formulados como uma nova estratégia terapêutica para a proteção da retina (Capítulo 4).

Os implantes carregados com 2-Cl-IB-MECA foram desenvolvidos em colaboração com o Departamento de Engenharia Química da Faculdade de Ciências e Tecnologia da Universidade de Coimbra (Capítulo 4, informação suplementar). O implante de PCL carregado com 2-Cl-IB-MECA apresentou uma libertação prolongada de fármaco durante 30 dias. Além disso, o fármaco libertado a partir do implante manteve a sua atividade funcional para o recetor, tal como foi determinado por imagiologia de cálcio. Os implantes carregados com 2-Cl-IB-MECA foram submersos em solução salina durante 24 h o que reduziu o aumento da concentração de cálcio intracelular induzido por glutamato, em culturas purificadas de CGR. Implantes carregados com 2-Cl-IB-MECA, assim como implantes sem fármaco, foram introduzidos no vítreo após a indução de isquémia da retina e, os resultados foram avaliados 1 mês depois. Os implantes carregados com 2-Cl-IB-MECA preservaram a estrutura do nervo ótico e aumentaram o transporte axonal anterógrado. Além disso, aumentou a sobrevivência das CGR, assim com preservou a sua função após isquémia transitória, o que indica que as CGR estão protegidas do dano causado pela isquémia-reperfusão.

Estes resultados sugerem que o A_3R representa um alvo para o desenvolvimento de uma nova estratégia terapêutica para o glaucoma. Além disso, a incorporação de 2-Cl-IB-MECA nos implantes intraoculares biodegradáveis pode ser uma estratégia terapêutica promissora.

Palavras-chave: Glaucoma, implantes biodegradáveis intraoculares, neurodegenerescência, neuroproteção, recetor A_3 de adenosina.

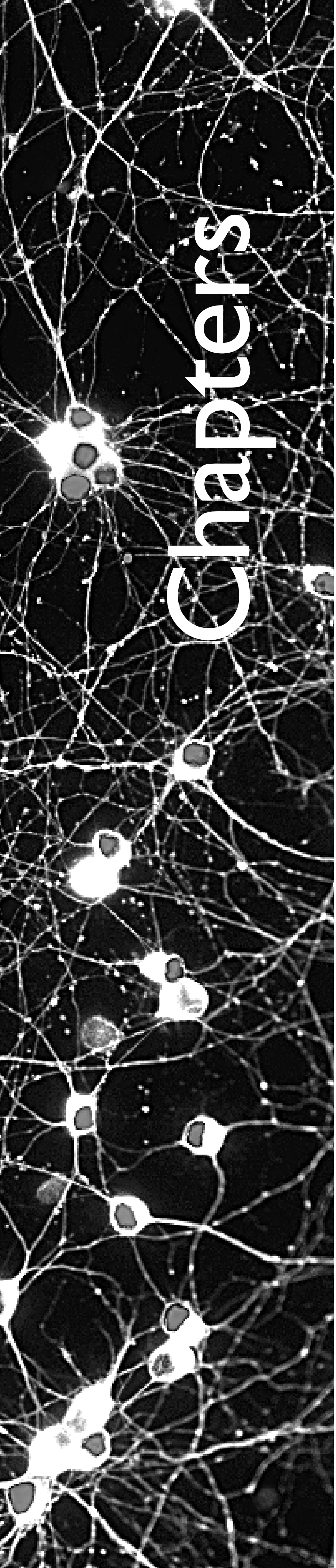

Chapters

General introduction

1

1. The visual system

1.1. The eye

The eye is the primary organ of vision and is divided into three layers: the outermost layer, composed by sclera and cornea; the middle layer (or uveal tract), composed by choroid, ciliary body, and iris; and the inner layer, composed by retinal pigment epithelium (RPE) and the retina which is the neurosensory stratum of the eye (Galloway et al., 2006, Malhotra et al., 2011). The eye is divided in three different compartments: anterior chamber, posterior chamber and vitreous chamber filled by aqueous humor (anterior and posterior chambers) and vitreous humor (vitreous chamber) (Galloway et al., 2006) (Figure 1). Light rays pass through the cornea and enters into the eye and are focused on the neurosensory retina (Kaplan 2007).

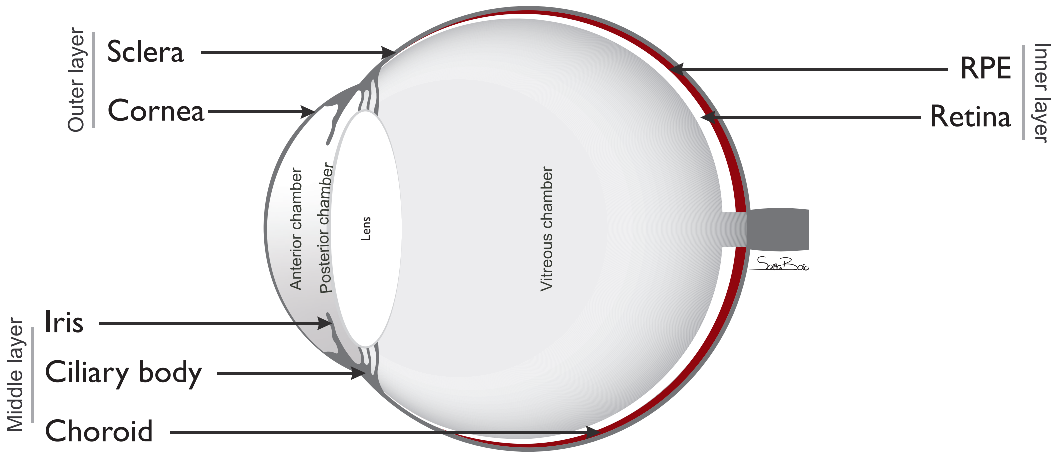

Figure 1 | Schematic cross-section of the eye demonstrating its major anatomical features.

1.2. The retina

The retina is part of the central nervous system (CNS) and is constituted by neurons (photoreceptors, bipolar cells, horizontal cells, amacrine cells and retinal ganglion cells (RGCs)), glial cells (astrocytes, Müller and microglial cells), epithelial cells (RPE) and vascular cells (endothelial cells and pericytes) (Kolb et al., 1995). The retinal tissue is limited by the RPE that regulates the transport of nutrients and waste products to and from the retina (Boulton et al., 2001) and by the inner limiting membrane (ILM) that is a basement membrane that defines the border between the retina and the vitreous cavity (Halfter et al., 2008).

1.2.1. Retinal neuronal cells

The neuronal component of the retina is composed by six types of neurons: photoreceptors (rods and cones), bipolar cells, horizontal cells, amacrine cells and RGCs. Photoreceptors, whose nuclei are located in the outer nuclear layer (ONL), respond to light and make synapses with second-order neurons. The cell bodies of retinal interneurons (horizontal, bipolar and amacrine cells) are located predominately in the inner nuclear layer (INL) and modify and relay the visual information from the photoreceptors to the RGCs that are located in the innermost layer of the retina, the ganglion cell layer (GCL) (Figure 2). RGCs are the output cells of the retina that convey the visual signals to the brain visual targets. The axons of RGCs run initially in the nerve fiber layer (NFL) and converge into the optic disc, cross the lamina cribrosa at the optic nerve head (ONH), and form the optic nerve (Figure 2) (Kolb et al., 1995). The neurons interconnect through synapses in the outer plexiform layer (OPL), where photoreceptors make synapses with bipolar and horizontal cells, and in the inner plexiform layer (IPL) where bipolar and amacrine cells make connections with RGCs (Kolb et al., 1995).

Photoreceptors

Photoreceptors are light-sensitive cells and transduce light into an electrical signal. There are two types of photoreceptors: rods and cones. Both photoreceptors consist of 1) an outer segment (OS) containing the visual pigment molecules; 2) an inner segment (IS) that contains mitochondria as an energy-producing region; 3) a cell body with the nucleus; and 4) a synaptic terminal where neurotransmission with bipolar or horizontal cells occurs.

Rod photoreceptors are responsible for scotopic vision, at low light levels, since rods are the only that present sensitivity to capture the few photons that are available at those conditions. Cone photoreceptors are responsible for photopic vision, under higher light levels, since cones respond selectively to photons in different regions of the visible spectrum (Wassle 2004, Hurley 2009).

Bipolar cells

Bipolar cells receive neurotransmission signals from photoreceptors and transmit them to RGCs, linking the outer retina to the inner retina (Herrmann et al., 2011). It was described, among species, one type of rod driven bipolar cells and several types of bipolar cells that receive inputs from cones, for instance in mouse retina it was proposed 11 types of cone bipolar cells (Wassle et al., 2009). Bipolar cells are functionally divided into two main groups: ON and OFF bipolar cells, according to their response to light. ON bipolar cells are depolarized by light whereas OFF bipolar cells are hyperpolarized by light (Euler et al., 2014).

Retinal ganglion cells (RGCs)

RGCs are the output neurons of the retina into the brain, collecting signals from bipolar and amacrine cells and transmits them through their axons to the brain. Several different types of RGCs were identified, and in an adult mouse retina there are approximately 30 functional subtypes of RGCs (Sanes et al., 2015, Baden et al., 2016). The RGC morphological maturation during development occurs, in a mouse, in the first week after birth even before the bipolar cells to make synapses with RGCs (Diao et al., 2004). RGCs have been identified by physiological, morphological and molecular criteria, however, some classifications are not yet definitive (Wong et al., 2012, Sanes et al., 2015).

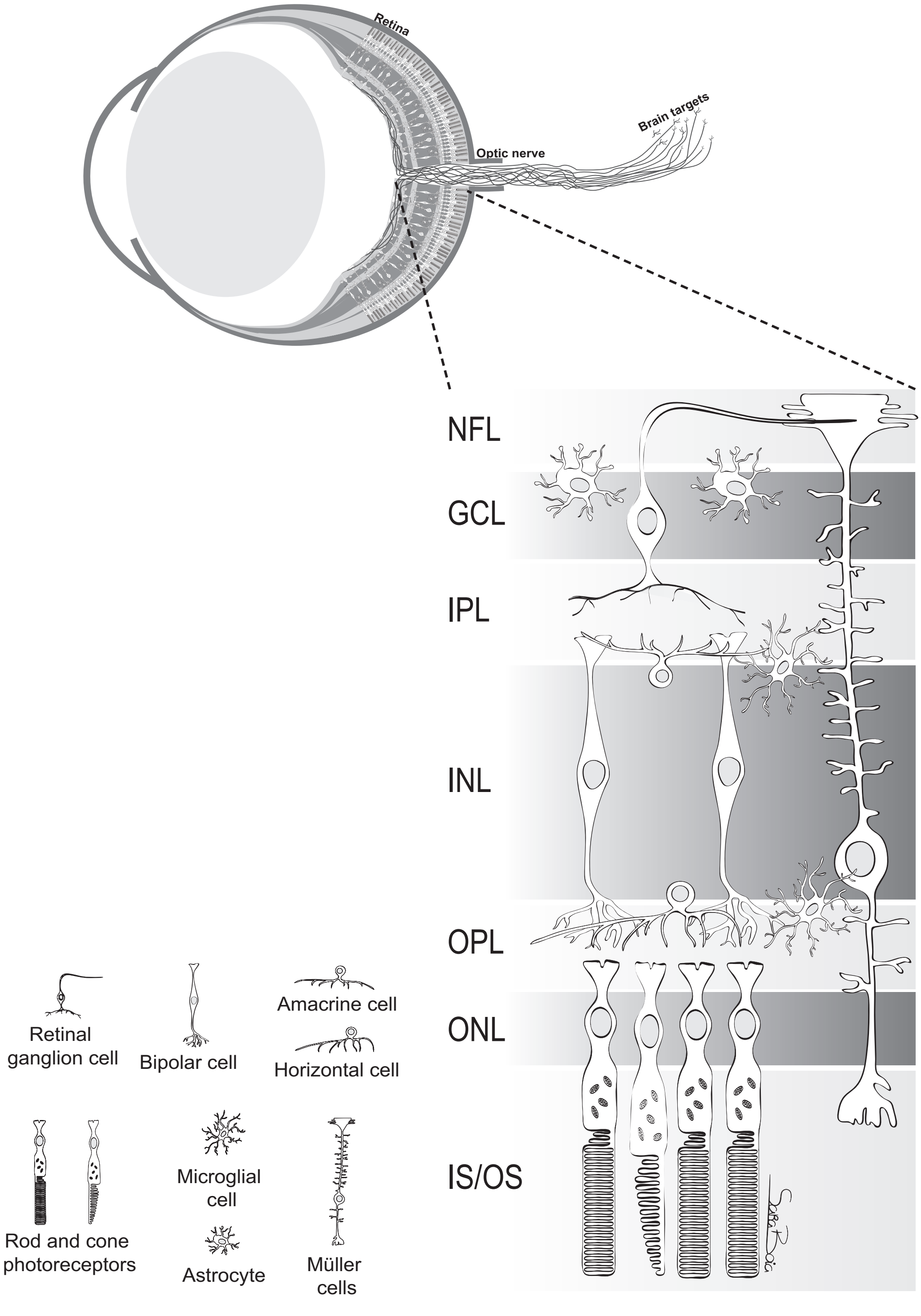

Figure 2 | Schematic representation of the neural sensory retina, depicting the organization of the cells into nuclear and plexiform layers. The nuclei of photoreceptors, rods and cones, are located in the outer nuclear layer (ONL) and nuclei of interneurons, amacrine, bipolar and horizontal cells, are located predominately in the inner nuclear layer (INL). The cell bodies of RGCs are in the ganglion cell layer (GCL) and their axons run in the nerve fiber layer (NFL). There are two types of macroglia: Müller cells that span vertically the entire retina and astrocytes that are present in the GCL. Microglial cells are localized predominately in the inner retina and in the outer plexiform layer (OPL). IPL, inner plexiform layer; IS/OS, inner and outer segments of photoreceptors (Boia et al., 2020).

Horizontal cells

Horizontal cells are retinal interneurons and the second neurons that contact directly with photoreceptors and bipolar cells in OPL. Horizontal cells provide lateral inhibitory feedback to rods and cones contributing to the maintenance of visual sensitivity to luminance contrast (Wassle 2004).

Amacrine cells

Amacrine cells are interneurons that interact with bipolar cells and RGCs at the level of IPL (Kolb et al., 1995). The majority of amacrine cells have their soma in the INL, but there is also some displaced amacrine cells at GCL (Curcio et al., 1990). Displaced amacrine cells represented 3% of the total cells in central retina and nearly 80% in the far periphery (Curcio et al., 1990).

1.2.2. Retinal glial cells

In the retina there are three main types of glial cells: Müller cells, astrocytes, and microglia (Figure 2). Microglial cells are the first line of defence in the retina, however, Müller cells and astrocytes also collaborate in this activity (Vecino et al., 2016).

Müller cells

Müller cells are the predominant glial cells in the retina that span vertically the entire width of the retina from inner border at outer limiting membrane (OLM) to the distal end of the ONL (Vecino et al., 2016). Müller cells present several functions in order to support the normal function of the retina (Reichenbach et al., 2013), as uptake and recycling of neurotransmitters, retinoic acid compounds, and ions (such as potassium K^+), control the metabolism and nutrients supply to the retina, and regulation of blood flow and maintenance of the blood-retinal barrier (BRB) (Reichenbach et al., 2013).

Gliotic Müller cells have been described upon retinal injury, namely in human glaucoma (Wang et al., 2002). Upregulation of glial fibrillary acidic protein (GFAP) is a non-specific response of Müller cells to retinal injury, constituting a good maker of Müller cell gliosis (Bringmann et al., 2006). A crosstalk between Müller cells and other retinal glial cells, as microglia, appears to be required for the induction of gliosis (Wang et al., 2011, Wang et al., 2014).

Astrocytes

Astrocytes are star-shaped glial cells and in the retina are mostly located in NFL and GCL (Vecino et al., 2016). Astrocytes are part of BRB, since their processes envelop blood vessels being very important in the maintenance of the integrity of BRB. Moreover, astrocytes also provide neurotrophic support, a very important function since they are in close contact with RGC soma and axons (Vecino et al., 2016). In response to an injury, astrocytes proliferate, change their morphology and increase the expression of GFAP, a process designated as astrogliosis (de Hoz et al., 2016).

Microglia

Microglial cells are the resident immune cell type in the CNS and are engaged in the surveillance of the microenvironment. Retinal microglial cells present several preponderant roles in neurogenesis (Huang et al., 2012), synaptic pruning (Schafer et al., 2012), maintenance of synaptic structure and function (Wang et al., 2016b) and modulation of inflammatory reactions (Wang et al., 2014, Madeira et al., 2016a). In the retina, microglia mainly reside in the OPL and IPL, but some microglial cells are also found surrounding the soma of RGCs and their axons (Yu et al., 2020). This close contact of microglial cells with plexiform layers allow the maintenance of synaptic structure and function that underlie the retina's electrophysiological response to light (Wang et al., 2016b). In the adult retina in physiological conditions, microglia present a ramified morphology with highly dynamic processes that provide a coverage of the retinal milieu (Silverman et al., 2018). However, upon injury, microglia present a more amoeboid morphology and increase their motility in order to move towards the injured site (Lee et al., 2008). Microglia-mediated neuroinflammation is a common feature of several retinal degenerative diseases, as glaucoma, further contributing to RGC loss (Madeira et al., 2015a). In fact, early microglial activation has been reported in animal models of glaucoma (Bosco et al., 2011, Bosco et al., 2015), and targeting microglia-mediated neuroinflammation has been demonstrated to prevent the retinal neurodegenerative process (Madeira et al., 2015a, Madeira et al., 2016a, Boia et al., 2017).

1.2.3. The vascular retina

Central retinal artery and the short posterior ciliary arteries give the blood supply to the retina and to the choroid, respectively (Das et al., 2014). Thus, occlusion of the central retinal artery leads to complete loss of blood supply to the retina that culminates in retinal cell death and vision loss (Farris et al., 2020). The blood supply to the inner retina is composed of three different vascular plexuses embedded in the neural tissue: a layer of vessels that lies within the NFL with branches extending into the GCL, and two layers lying along each side of the INL (Figure 3) (Santiago et al., 2018). The photoreceptors and RPE are nourished by the vessels within the choroid (Figure 3) (Kaplan 2007) .

In order to maintain an appropriate, tightly regulated microenvironment of the retina, BRB plays a crucial role in preserving retinal function and, therefore, vision (Cunha-Vaz 2004). BRB is divided in two major components: the inner blood-retinal barrier (iBRB) and the outer blood-retinal barrier (oBRB) (Cunha-Vaz 2004). The iBRB is constituted by the endothelial cells of the capillaries in the inner retina, and consist of a monolayer of endothelial cells joined by tight junctions, a basement membrane that surrounds the endothelial cells, and pericytes outside that are modified smooth muscle cells of capillaries and may have contractile functions to regulate vascular flow by dilating and contracting (Das et al., 2014). The oBRB is composed by the endothelium of the choriocapillaris, Bruch's membrane and RPE (Das et al., 2014). Several mechanisms for BRB dysfunction and vascular leakage have been proposed for some diseases, such as diabetic retinopathy, age-related macular degeneration (AMD), retinal vein occlusion and uveitis (Das et al., 2014).

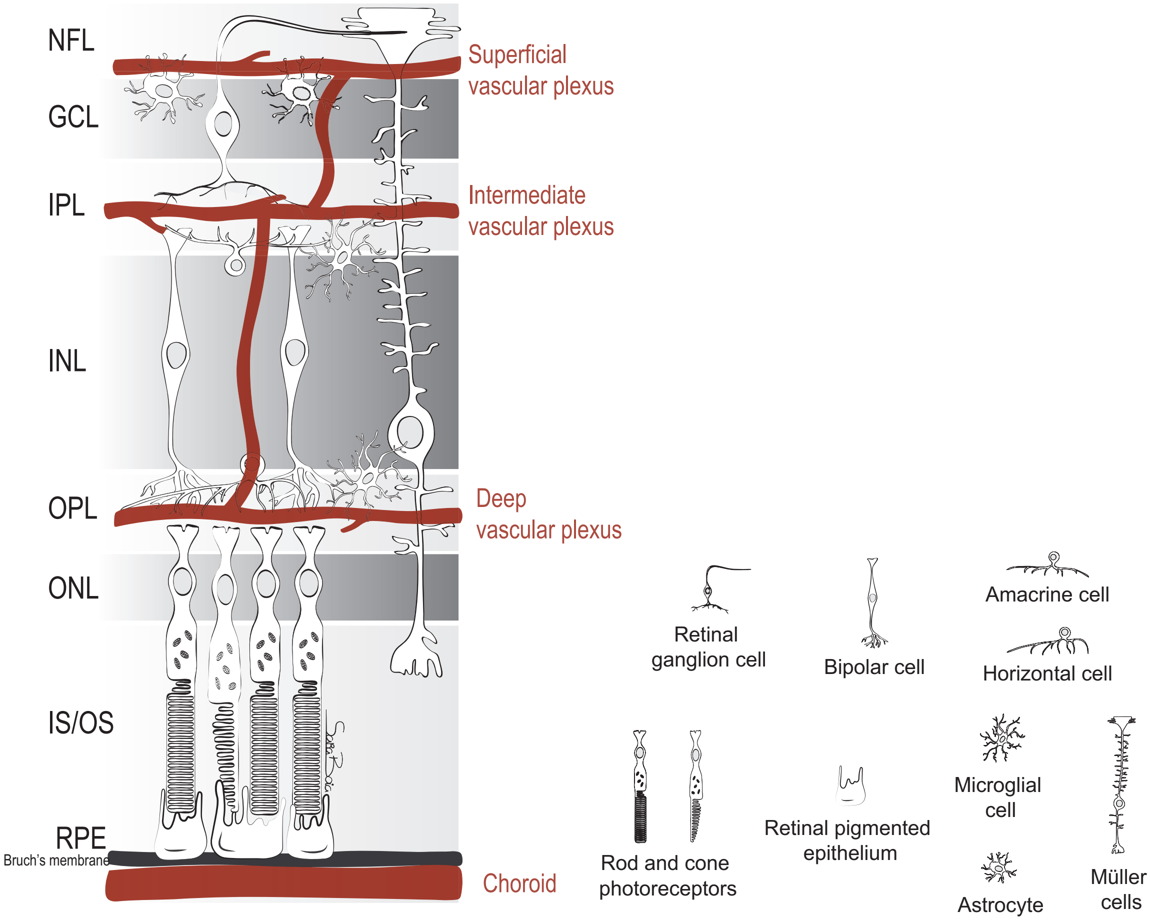

Figure 3 | Schematic representation of retinal structure showing the retinal blood vessels lining the inner surface of the retina and the choroid. There are three layers of retinal vascular plexuses that are embedded among retinal neurons: the superficial layer lies within the inner nerve fiber layer (NFL) and the intermediate and deep capillary plexuses align along each sides of the inner nuclear layer (INL). The choroid that is between retinal pigment epithelium (RPE) and sclera supplies blood to the outer portion of the retina. GCL, ganglion cell layer; IPL, inner plexiform layer; OPL, outer plexiform layer; ONL, outer nuclear layer; IS/OS, inner and outer segments of photoreceptors.

1.3. Phototransduction and retinal circuitry

When light reaches the retina, it passes through the inner retina and the photons are absorbed by the visual pigments of the photoreceptors, and then the neural flow proceeds back in the opposite direction of the incident light. The process that comprises the absorption of light by photoreceptors and the conversion of the energy into a neural response in called by phototransduction and occurs in the OS of photoreceptors (Hurley 2009). Rod photoreceptors contain rhodopsin as photopigment, while cone photoreceptors contain several photopigments (opsins) (Nathans 1999). Unlike rods, in vertebrates, there are several subtypes of cone photoreceptors that are divided by their opsin expression. Generally, the most common cone subtypes include long wavelength (red or L-), middle wavelength (green or M-) and short wavelength (blue or S-) sensitive cones (Nathans 1999). In dim light conditions, the detection by rods predominates, since they are extremely sensitive in poorly light conditions (scotopic vision). The activity of cones predominates in photopic conditions, when the retina is responsive to a broader range of light wavelengths, under bright illumination (Remington 2012).

Under dark conditions, the photoreceptors are not being stimulated by light and are depolarized, continuously releasing glutamate. The process of phototransduction begins with the absorption of light photons by photoreceptors that causes the breaking of a double bond in 11-cis-retinal forming the isomer all-trans-retinal which leads to conformational changes in rhodopsin. This leads to a cascade of events that culminate in an alteration of the electrical activity of the cell, causing membrane hyperpolarization of the photoreceptor (Hurley 2009). Thus, at the photoreceptor synaptic terminals in OPL, the light-evoked signals are transferred onto postsynaptic neurons by the release of glutamate, which is high in darkness and is reduced by light. Photoreceptors synapse with bipolar cells or with horizontal cells. Based on two different types of bipolar cells, the two major functional visual pathways, ON and OFF, are generated. Under light conditions, horizontal and OFF cone bipolar cells are hyperpolarized, and transfer their signals in the IPL through excitatory synapses onto OFF RGCs. At the same light conditions, ON cone bipolar cells are depolarized, and form synapses with ON RGCs. Therefore, OFF RGCs are excited by stimuli that are darker than the background, and ON RGCs by stimuli that are brighter than the background (Wassle 2004).

The major and direct signal flow (vertical signal pathway) is from photoreceptors to RGCs via bipolar cells (Yang 2004). The modulation of this vertical signal pathway is provided by horizontal and amacrine cells in the OPL and IPL, respectively (horizontal pathway) (Yang 2004). The main neurotransmitters that mediate these two pathways are glutamate, γ-aminobutyric acid (GABA) and glycine. Glutamate is the main excitatory neurotransmitter in the retina and it is responsible for the vertical flow of visual signal. GABA and glycine are both inhibitory neurotransmitters that modulate the synaptic transmission in the horizontal pathway (Yang 2004). Thus, RGCs are the last cell type to be depolarized and transmit the visual signal into the brain targets (Remington 2012) that will be described below.

2. Optic neuropathies

Optic neuropathies comprise a group of ocular diseases, like glaucoma (the most common), anterior ischemic optic neuropathy and retinal ischemia, in which RGCs are the main affected cells (Carelli et al., 2017). Blindness secondary to optic neuropathies is irreversible since RGCs lack the capacity for self-renewal and have a limited ability for self-repair (Goldberg et al., 2002a). The exact mechanism that leads to RGC degeneration and death is still unknown, but axonal injury has been proposed as an early event that culminates in apoptosis of RGCs (Dratviman-Storobinsky et al., 2008). It is estimated that glaucoma worldwide will affect 111.8 million people in 2040 (Tham et al., 2014). However, there is no effective therapeutic strategy now in the clinics for this disease.

2.1. Glaucoma

Glaucoma is a progressive optic neuropathy and, although the primary site of glaucoma injury is not well understood, this disease is characterized by death of RGCs and loss of their axons as well as optic nerve atrophy (Shahsuvaryan 2013). The measurement of retinal NFL thickness and macular GCL plus IPL thickness was shown to be useful in the early detection of glaucomatous optic neuropathy (Nouri-Mahdavi et al., 2013). Although both glaucomatous optic neuropathy and non-glaucomatous optic neuropathy cause thinning of NFL and macular GCL plus IPL (Mwanza et al., 2012, Jeoung et al., 2013, Larrea et al., 2014), the damage pattern and extent of NFL and macular GCL plus IPL from the two forms of diseases are distinct (Xiao et al., 2020). Glaucoma is a multifactorial disease, however, intraocular pressure (IOP) elevation and aging are the most common risk factors for disease development (Weinreb et al., 2014). Elevated IOP are currently the only modifiable risk factor that is strongly associated with rates of progressive NFL loss (Jammal et al., 2020), that way the only therapy in glaucoma management aims to lower IOP in order to slow the rate of visual field deterioration (EGS 2017). In fact, it was demonstrated that ocular hypotensive medication leads to a reduction in the visual field deterioration (AGIS 2000, De Moraes et al., 2012) and in the rates of progressive NFL loss (Jammal et al., 2020). Nevertheless, even in patients with IOP in normal ranges, approximately one-third of cases present optic nerve degeneration (Wiggs 2013).

IOP is determined by the balance between the rate of aqueous humour production and outflow from the eye. Aqueous humour is produced by the ciliary body in the posterior chamber and flows into the anterior chamber. There are two pathways responsible for the drainage of aqueous humour from the eye that are the conventional pathway through trabecular meshwork or by unconventional pathway through the ciliary muscle (Goel et al., 2010) (Figure 4). The iridocorneal angle (the junction of the iris and the cornea) is the most important site of fluid drainage from the human eye, and abnormalities of this iridocorneal angle may interfere with ocular fluid drainage that can lead to glaucoma (Smith et al., 2001).

There are two different groups of glaucoma: primary and secondary glaucoma. Primary glaucoma, like open-angle glaucoma, normal-tension glaucoma, angle-closure glaucoma and congenital glaucoma, are defined as isolated and idiopathic disease of the anterior chamber of the eye and optic nerve. Secondary glaucoma, like neovascular glaucoma, pigmentary glaucoma,

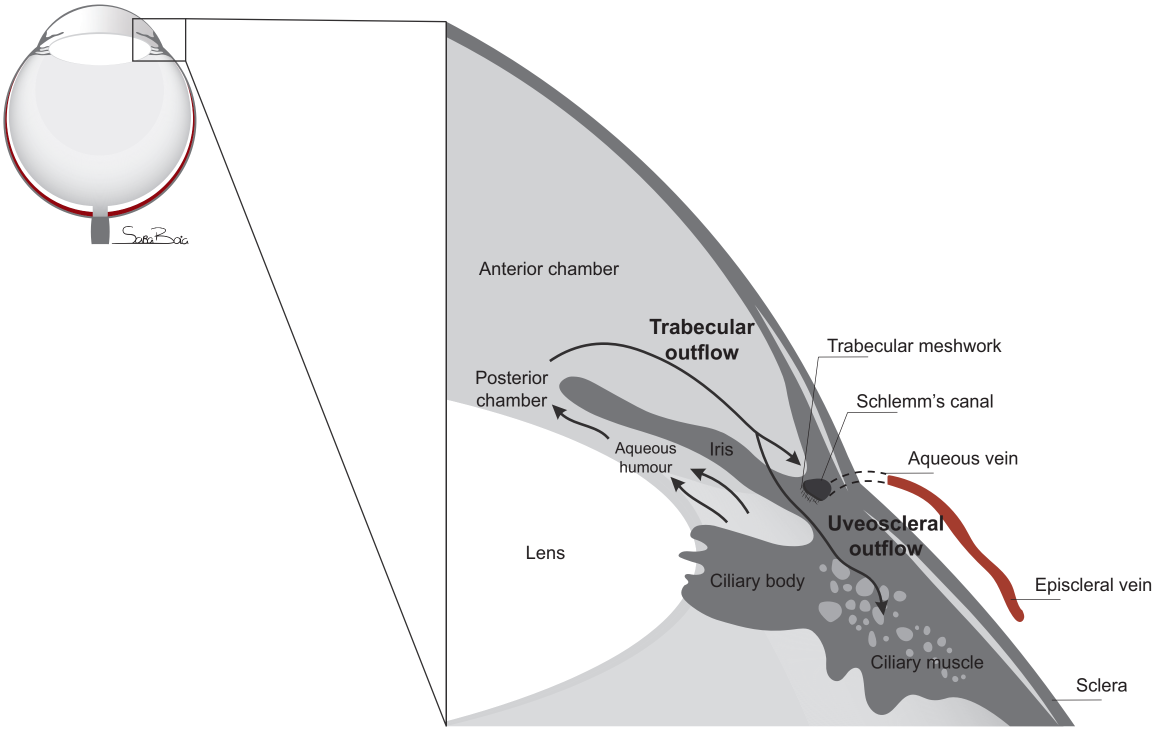

Figure 4 | Schematic representation of iridocorneal angle anatomy and aqueous humour circulation and drainage. Aqueous humour is produced by the epithelium of the ciliary body, entering the anterior chamber through the pupil, and then flowing toward the iridocorneal angle where it leaves the eye. The conventional outflow pathway of aqueous humour is through trabecular meshwork, while the uveoscleral pathway is through the ciliary muscle.

exfoliation glaucoma and uveitic glaucoma, are associated with known predisposing events as development abnormalities, systemic diseases, drug therapy or trauma (Wiggs 2013). The two main types of glaucoma are primary open-angle glaucoma and angle-closure glaucoma, that are broadly distinguished by the anatomic configuration of iridocorneal angle (Figure 5). Open-angle glaucoma presents a wide-open iridocorneal angle, that allows unimpeded fluid outflow through trabecular meshwork, however, there is an increased resistance to drainage humour aqueous that contribute to elevated IOP. Angle-closure glaucoma present a narrow iridocorneal angle with obstructed aqueous humour outflow. However, glaucoma can still occur at normal IOP. In fact, patients with normal-tension glaucoma develop optic nerve damage and visual field loss without ever having elevated IOP (Killer et al., 2018).

The primary site of glaucoma injury is not well defined, and whether RGC loss occurs prior visual field loss is controversial (Hood 2019). However, it is recognised that visual field and NFL defects occur after a significant loss of RGCs (Harwerth et al., 2007, Medeiros et al., 2013).

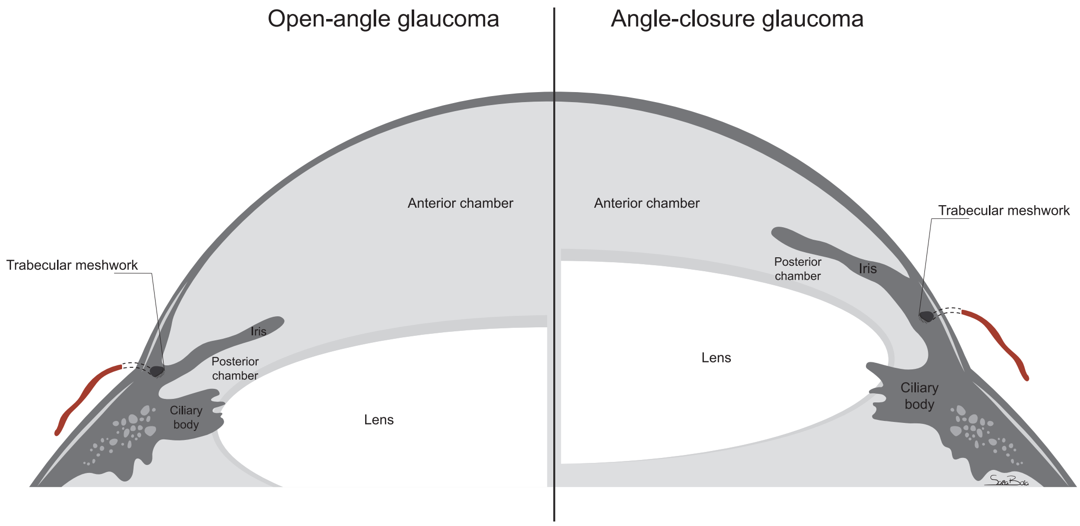

Figure 5 | The anatomical differences in iridocorneal angle between open-angle glaucoma and angle-closure glaucoma.

2.1.1. Clinical diagnosis of glaucoma

Generally, glaucoma is an assymptomatic disease until it is severe, presenting at this stage substantial amounts of neural damage, and because of this, glaucoma diagnosis is frequently delayed (Schuster et al., 2020). In fact, one third of subjects with previously undetected glaucoma present an advanced or later-stage disease in at least one eye (Heijl et al., 2013).

Since elevated IOP is the major risk factor for development and progression of glaucoma, the measurement of the IOP (tonometry) on initial diagnosis is mandatory (Quigley 2018a). IOP lowering delays the progression of disease and preserves adequate visual function in most, but not in all glaucoma patients (Kass et al., 2002). Reduction of IOP removes stress causing glaucomatous optic nerve damage, but it does not stimulate cell survival or cell resilience to withstand pathological insults or prevent cells' death. However, the relationship between elevated IOP and vision loss is not straightforward. Normal-tension glaucoma presents the same ONH features that are characteristic of glaucoma (Shields 2008), suggesting that the pathological mechanisms in the different types of glaucoma might be similar and independent of ocular hypertension (OHT).

An accurate diagnosis of glaucoma subtype requires meticulous assessment of the anterior chamber angle. Ophthalmological examination of the anterior chamber can be achieved by slit-lamp gonioscopy that is considered the gold-standard technique for anterior chamber angle evaluation. However, this technique presents some shortcomings, like poor reproducibility and the long learning curve on how to perform the technique (Riva et al., 2020). Several new imaging techniques for angle evaluation have been developed in the recent years, like ultrasound biomicroscopy or anterior segment optical coherence tomography (OCT), however, gonioscopy is still the clinical reference standard for the assessment of the iridocorneal angle (Riva et al., 2020). The evaluation of the anterior chamber angle is used only to determine if the angle is physically open or closed in order to recognize signs of conditions that can produce elevated IOP (Schuster et al., 2020).

Despite the differences in the etiology of the different forms of glaucoma, all share a common characteristic that is the degeneration of RGCs and their axons, accompanied by remodelling of the lamina cribrosa of the ONH (Alqawlaq et al., 2019). There is now a significant body of evidence suggesting that multiple non-IOP factors contribute to RGC degeneration and loss, an issue that remains to be clarified (Almasieh et al., 2012, Munemasa et al., 2013). Changes in the optic disc and visual field are similar between angle-closure glaucoma and open-angle glaucoma (Boland et al., 2008). That way examination with OCT of the progressive excavation of the optic disc, tissue loss at the neuroretinal rim and the thinning of the NFL are the mainstay for glaucoma diagnosis (Schuster et al., 2020). The visual fields should also be examined to evaluate the degree of functional impairment resulting from the loss of optic nerve fibers, and to provide a guide to treatment (Schuster et al., 2020). A thinning of NFL in glaucomatous eyes was first described in 1995 (Schuman et al., 1995), and it was demonstrated a high degree of correlation with functional status of the optic nerve, as measured by visual field examination (Schuman et al., 1995, Leung et al., 2005).

Early diagnosis and treatment can prevent vision loss from the disease which raises the issue that there is an unmet need for earlier markers of disease (Beykin et al., 2020). Detection of Apoptosing Retinal Cells (DARC) technology is a novel method to visualise apoptotic retinal cells in the retina in humans that is predictive of disease progression (Cordeiro et al., 2017), and it is now in a phase 2 clinical trial (ISRCTN10751859) as an earlier biomarker of glaucoma.

2.1.2. Current treatments for glaucoma

Lowering of elevated IOP is currently the only proven treatment strategy to delay the progression of glaucoma (Heijl et al., 2002, Leske et al., 2003). Glaucoma medications reduce IOP by increasing aqueous outflow and/or reducing aqueous production. There are several effective classes of topical therapies for glaucoma, including prostaglandin analogues, β-blockers, α-adrenergic agonists and carbonic anhydrase inhibitors, and parasympathomimetic drugs (Figure 6) (Cvenkel et al., 2020). Combining different medications with different mechanism of action leads to superior IOP-lowering efficacy compared to each of the components used alone (Harasymowycz et al., 2016). A new class of IOP-lowering medications for glaucoma has been developed, such as Rho-kinase inhibitors and nitric oxide-donating prostaglandin analogues that were both approved by Food and Drug Administration (FDA) in 2017 (Cvenkel et al., 2020). However, all of these IOP-lowering agents are administered in the form of eye drops that are accompanied by poor patient compliance due to the need of multiple daily administrations, difficulties in accurately administering the drug to the eye, and side-effects (Claxton et al., 2001, Sleath et al., 2006). Indeed, the persistence in continuing the treatment is generally below 50% at 1 year, making the poor patient adherence to treatment one of the major reasons for treatment failure in patients with glaucoma (Harasymowycz et al., 2016).

Glaucoma treatment is also accomplished by laser treatment to the eye or ocular surgery, as second-line treatment, when the eye drops are not so effective. In laser trabeculoplasty, laser energy is delivered to the trabecular meshwork aiming IOP lowering by increasing aqueous outflow (Gazzard et al., 2019). Recently, laser trabeculoplasty was proposed as a first-line treatment since by removing or lessening the need for complex treatment regimens it reduces the risk of non-adherence (Gazzard et al., 2019). Moreover, ocular surgery has been used as glaucoma therapeutic strategy and trabeculectomy is the most commonly performed incisional surgical procedure to lower IOP (Weinreb et al., 2014).

Nowadays glaucoma is largely recognized as a neurodegenerative disease (Gupta et al., 2007a, Jutley et al., 2017), however, despite meaningful improvements in the knowledge of the pathophysiology of the disease, there is no non-IOP lowering medications approved and patients continue to go blind from glaucoma (Susanna et al., 2015). Therefore, there is a urgent need for non-IOP therapeutic strategies, and the neuroprotection of RGCs may arise as a new therapeutic strategy for the treatment of glaucoma (Almasieh et al., 2017).

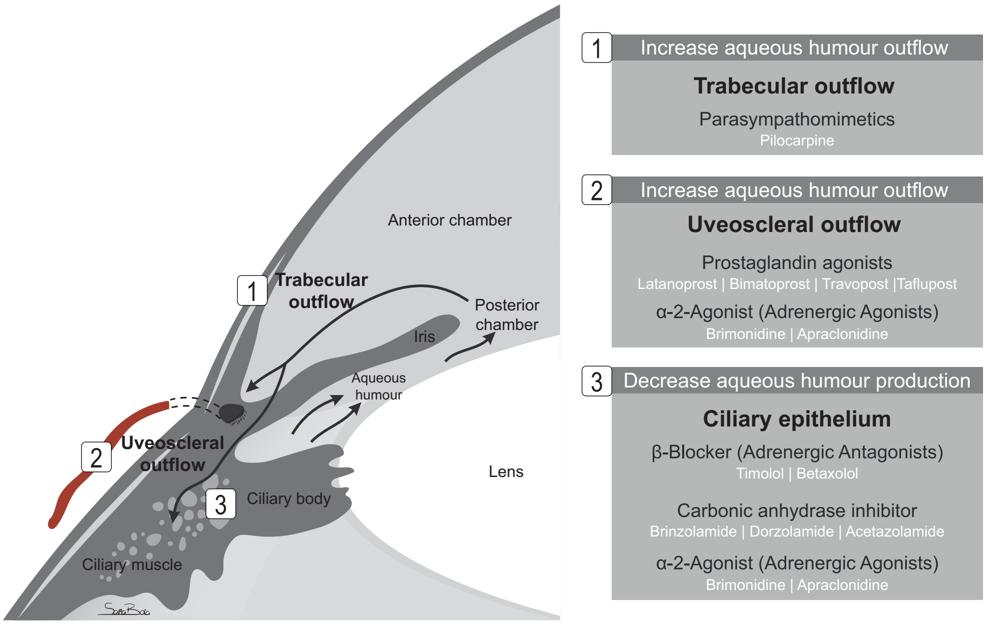

Figure 6 | IOP-lowering drugs for the management of glaucoma depicting their site of action.

2.2. Modelling glaucoma to study retinal cell degeneration: *in vitro* and animal models

The beneficial effect of decreasing IOP levels in attenuating the loss of the visual field, led to a great interest in understanding how the mechanical forces of IOP affect the function of different ocular cells (Wax et al., 2000). Different *in vitro* and animal models have been developed to mimic some features of the disease and have greatly contributed to unravel important aspects in the neurodegeneration and RGC death in glaucoma (Johnson et al., 2010). Models of glaucoma are fundamental to improve the knowledge of the pathogenesis of the disease and to develop new potential therapeutic strategies to change the course of the disease.

2.2.1. *In vitro* models

Culture of dissociated cells allows to study a cell response of individual cell population in a controlled environment without the interference of other cell types, against noxious conditions. Most of retinal cell types have been cultured including neurons and glial cells (Santiago et al., 2006, Aires et al., 2019a). The cultures of RGCs prepared by sequential immunopanning allow to study protective agents directed to neuroprotection of RGCs (Barres et al., 1988, Martins et al., 2015). The main disadvantage of this preparation may be the fact that the components used to maintain the culture environment may cause a cellular response that differs from the *in situ* response and cells may lose cellular features normally expressed *in vivo* (Weinreb et al., 2005). Retinal organotypic cultures are a more complex model that maintains the anatomical structure. The opportunity to investigate whole tissue cultures poses clear advantages compared with a monolayer of cells, allowing the study of cell-to-cell interactions *in vitro* (Pattamatta et al., 2016). Elevated hydrostatic pressure (EHP) has been used to mimic OHT *in vitro* (Aires et al., 2017). Because of its simplicity, the application of hydrostatic pressure to cultured cells appears very attractive for examining the effects of elevated IOP to retinal cells. EHP proved to be a useful model to test the effectiveness of neuroprotective drugs (Madeira et al., 2015b, Madeira et al., 2016a, Aires et al., 2019a).

In fact, *in vitro* models allow to answer important questions in a more rapid and less expensive way, however, *in vitro* models do not mimic the intricacy of glaucomatous disease nor replace animal models.

2.2.2. Animal models

Several animal models have been developed to model the human condition. Rodent models of glaucoma are essential in understanding disease mechanisms and assessing efficacy of therapeutic interventions. Since elevated IOP is the main risk factor, relevant animal models for glaucoma have been developed around the challenge of producing experimental IOP elevation. However, other non-related IOP animal models have been developed (Johnson et al., 2010).

The quantitative evaluation of RGC loss is a commonly used end point to assess experimental glaucomatous degeneration. However, the degree of RGC loss may affect the usefulness of the animal model to assess a therapeutic intervention efficacy. It means that a glaucoma animal model that induces loss of only a small proportion of RGCs or induced an injury by which the most RGC die present several disadvantages. In the first case it is because the number of animals in a group must be very large to determine if there has been an effect, and in the second case it is because if most RGC die, again it may be difficult to produce a protective effect without a truly huge protective power. That way, a useful glaucoma model should generate RGC loss of 25-50% (Quigley 2018b).

Glaucoma animal models that rely on IOP increase

Animal models of glaucoma with elevated IOP rely on the mechanism of aqueous humour circulation, mainly by reducing the outflow of aqueous humour.

Episcleral vein cauterization

Episcleral vein cauterization was the first reported rat model of experimental glaucoma that is induced by cauterization of two or three episcleral veins (Garcia-Valenzuela et al., 1995). This elevates IOP by reducing venous outflow, thereby increasing aqueous fluid pressure, and leads to RGC loss (Garcia-Valenzuela et al., 1995).

Hypertonic saline OHT model

The Morrison's model of rat OHT was described in 1997, and it is induced by the injection of hypertonic saline solution (NaCl, 1.8 M) into the limbal vascular plexus (into an episcleral vein) (Morrison et al., 1997). A successful injection of hypertonic saline will cause a sclerotic damage of the trabecular meshwork with variable angle closure, resulting in gradual reduction of aqueous outflow and IOP elevation (Morrison et al., 2015). The extent of IOP elevation can be variable, depending on the degree of angle scarring (Morrison et al., 2015), however, a significant positive correlation between RGC apoptosis and OHT in rats was demonstrated (Cordeiro et al., 2017).

Laser photocoagulation

In the limbal laser-photocauterization to induce OHT, the laser is applied to the trabecular meshwork, the perilimbar and episcleral veins and, it was already described in mice (Salinas-Navarro et al., 2009a) and in rats (Salinas-Navarro et al., 2010). The laser photocoagulating of the limbal vasculature, that is involved in drainage of aqueous humour, induces a chronic angle closure that results in increased resistance of aqueous humour outflow (Vidal-Sanz et al., 2012). Laser photocoagulation of the aqueous outflow pathway produces a moderate IOP increase that raises in the first 24 h induction and it is constantly maintained elevated during the first week, decreasing slowly thereafter (Salinas-Navarro et al., 2010). Such OHT results in significant damage to the RGC population, as shown by RGC loss and decrease in the axonal transport (Levkovitch-Verbin et al., 2002, Salinas-Navarro et al., 2009a, Salinas-Navarro et al., 2010).

Microbead occlusion model

The microbead occlusion model was described more recently in 2010 (Sappington et al., 2010). IOP was elevated by the injection of polystyrene microbeads into the anterior chamber to occlude aqueous outflow through trabecular meshwork, which leads to a 30% elevation in IOP (Sappington et al., 2010). The use of paramagnetic microbeads, instead of polystyrene microbeads, allows the occlusion of the iridocorneal angle producing a sustained elevation of IOP with fewer injections (Samsel et al., 2011). Microbeads model allows to manipulate IOP magnitude and duration in a relatively simple way, simply by altering the number of microbeads injected (Morgan et al., 2015). The increase in IOP produced using the microbeads (30% elevation in IOP) resembles more the changes in untreated human eyes (38% elevation in IOP above 15 mm Hg) (Sappington et al., 2010). This IOP elevation elicits thinning of the axon population in the optic nerve (Sappington et al., 2010). Moreover, chronic IOP elevation resulted in disruption of axonal transport and damage of optic nerve axons (Crish et al., 2010, Abbott et al., 2014).

Spontaneous glaucoma (DBA/2J mouse strain)

DBA/2J mouse strain is a well characterized glaucoma animal model. It is a genetically based model that presents pigment dispersion, iris transillumination, iris atrophy, and anterior synechia which leads to a blockade of the aqueous outflow (Anderson et al., 2002) and consequent OHT by the age of 9 months (Libby et al., 2005a). This is accompanied by death of RGCs, optic nerve atrophy and cupping, and visual deficits (Libby et al., 2005a). The disease is not synchronous in all eyes and not all eyes develop glaucoma, maybe because some mice do not experience IOP elevation and/or some eyes may not have sufficient exposure to damaging IOPs (Libby et al., 2005a). Additionally, this DBA/2J mouse also develops a slowly typical glaucoma damage, which makes that the experiments with this animal model are inevitably year-long.

Glaucoma animal models that do not rely on IOP increase

Pressure-independent animal models have been used to model normal-tension glaucoma, and they have provided insights into the neurodegenerative mechanisms of RGC loss, like optic nerve crush, optic nerve transection, and retinal ischemia-reperfusion (I-R) injury (Johnson et al., 2010).

<u>Optic nerve crush or transection</u>

Optic nerve crush or transection (complete or partial) has been utilized to trigger a specific loss of RGCs. Upon exposure, the optic nerve may be crushed using forceps to deliver a consistent amount of force or the optic nerve may be transected with care be taken to preserve the integrity of the retinal arterial blood supply (Johnson et al., 2010). RGC degeneration begins quickly being RGC loss significant at day 3 and progressing over time (Sánchez-Migallón et al., 2018). These models are of particular importance when investigating how axonal injury plays a role in glaucomatous pathology, and in elucidating mechanisms that may support optic nerve regeneration.

<u>Retinal ischemia-reperfusion injury</u>

The induction of retinal I-R occurs by the cannulation of the anterior chamber of the eye with a needle connected to a reservoir infusing sterile saline solution. By setting the IOP to about 110 mmHg, the blood flow through the retinal and uveal vasculature is suppressed. This method may represent a model of acute angle closure glaucoma (Osborne et al., 2004). When ischemic exposure period is over, the reperfusion is established and IOP values are normalized. Since this model involves the induction of acute elevation of IOP, the neurodegenerative effect is thought to be primarily mediated through the ischemic insult, though it is possible that other IOP-induced damage to RGCs, similar to that seen in chronic glaucoma models, may also play a role (Johnson et al., 2010). Besides the damage of RGCs, damage also occurs throughout the various layers of the retina (Madeira et al., 2016a, Boia et al., 2017, Palmhof et al., 2019), which makes this model to be considered for global retinal degeneration.

<u>2.2.3. Monitoring glaucoma progression: translation to animal models</u>

Rodent animal models of glaucoma provide several advantages for addressing neurobiological questions concerning the issues of retinal degeneration, regeneration and neuroprotection in glaucoma. Accurate monitoring of glaucoma patients is vital to preserve their visual function, and the main advantage is that several diagnostic methods used in humans are easy to perform and minimally invasive, being possible to utilize them in animal models (Ban et al., 2018).

Currently, the main evaluation tool used in clinical practice is tonometry for the measurement of IOP. The development of tonometric devices that accurately measure IOP in animals helped in glaucoma research (Hu et al., 2018). Measuring IOP with a tonometer is possible to perform in awake rats after a short period of training (Boia et al., 2017).

The structural changes in the ONH and NFL loss, features of glaucoma, are accompanied by visual field damage. Measuring the rate of NFL loss by OCT might be a useful tool to identify patients who are at a higher risk of developing visual field loss (Miki et al., 2014). Additionally, advances in optic nerve imaging techniques have enabled clinicians to detect structural changes in patients (Lisboa et al., 2012, Na et al., 2013). OCT is a non-invasive procedure used to visualize the anterior and posterior segments of the eye at high resolution, and substantial progress has been made in order to use this technique in animals (Kawaguchi et al., 2006, Nagata et al., 2009).

Visual field testing remains one of the most important tools for characterizing and monitoring vision loss in glaucoma (Wu et al., 2018). It was demonstrated that when visual field changes are detectable there is a substantial number of RGCs that is lost (Medeiros et al., 2013). That way the progression of visual field defects may be used as a functional measurement of RGC loss. Visual field test is not possible to perform in animals since it requires a response to a light spot that is repeatedly present in different areas of the visual field (Ban et al., 2018). However, retinal function and, in particular, the function of RGCs can be assessed both in humans and in animals by electroretinography (ERG). ERG is an important diagnostic tool that allows to identify the electrical activity of each cell type of the retina in response to a light stimulus (Wilsey et al., 2016). However, the full-field flash ERG has not been useful for glaucoma diagnosis since it is dominated by the responses of photoreceptors and bipolar cells (a- and b-wave, respectively, in both scotopic and photopic conditions) (Wilsey et al., 2016). In animal models of disease, ERG is widely used to detect changes in retinal function (Martins et al., 2011). Generally, when retinal function deteriorates, the light-induced electrical activity in the retina reduces (Rosolen et al., 2008). Despite the full-field flash ERG does not reflect the responses of RGCs, the scotopic threshold response (STR) that is recorded under deep dark adaptation and upon exposure to a very dim light flashes, can be used to determine the electrical activity of RGCs (Mead et al., 2016).

The tests and techniques performed to diagnose and monitor glaucoma progression can be used, with the necessary adaptations, in animal models. This allows the evaluation of therapeutic strategies with parallel outcomes in animal models.

3. Retinal ganglion cells (RGCs)

RGCs serve as "feature detectors" that each encode specific components of the visual world and convey them to the brain. Based on morphology, functional properties, presynaptic partners and central projection patterns, approximately 30 different RGC subtypes have been characterised in the mouse retina (Rheaume et al., 2018). Differentiation of nascent RGCs into identifiable RGC subtypes occurs postnatally and is regulated by differential transcription factor expression (as reviewed in Murcia-Belmonte et al., 2019). Based on single cell ribonucleic acid (RNA)-seq transcriptome profiling, most subtypes of RGCs appear to be present proportionally in both eyes, although a few RGC subtypes predominate in one eye compared to the other (Rheaume et al., 2018). Increasing evidence suggests that there is a type-specific vulnerability of RGCs to different injuries (Boia et al., 2020).

3.1. Connecting the retina to the brain: RGCs projections

RGCs are the output cells of the retina, extending their axons through the optic nerve to a specific set of targets in the brain (Erskine et al., 2014). Optic nerve forms a link between the neurosensory retina and the brain and it is an important segment of the visual pathway. During development, there are several molecular factors that instigate RGC axonal grow away from the retina to synapse in target areas of the brain (reviewed in Kutsarova et al., 2016). After birth, there is a peak in cell death that in rodents occurs between postnatal days 2 and 5 (PND 2-5), ensuring that only RGCs that reached their targets survive (reviewed in Guerin et al., 2006).

The RGC axons from both eyes decussate within the optic chiasm, where the axons segregate to form two optic tracts on either the same or the opposite side of the brain. There is a different proportion of RGCs axons that project ipsilaterally (to the same hemisphere as their side of origin) or contralaterally (to the opposite side of their side of origin) into the brain targets. This proportion varies widely between species and is directly related to the position of the eyes in the head, and consequently the degree of binocular overlap in the visual field. In primates, the number of ipsilateral RGC axons is approximately 45% while in rodents it is as low as approximately 2-3% (Jeffery et al., 2005). It has been described that there are more than 50 retinorecipient brain regions that receive direct input from RGCs (Fleming et al., 2006, Morin et al., 2014, Martersteck et al., 2017), being superior colliculus (SC) and lateral geniculate nucleus (LGN) the main RGCs recipient nuclei in the brain (Erskine et al., 2014). The SC plays an important role in visual information processing in the visual system including coordinating eye and head movements (Liang et al., 2015), suspension of locomotion (Shang et al., 2015), and escape or freezing in response to a looming object (Shang et al., 2015, Wei et al., 2015). The SC is organized into several synaptic layers, each of which has distinct sources of innervation (May 2006, Basso et al., 2017). The most superficial lamina of the SC receives direct RGC inputs from the contralateral retina while the inputs from the ipsilateral retina arrive to the lower lamina (Drager et al., 1980, Wang et al., 2013b). The SC receives projections from 85% to 90% of RGCs in mice (Ellis et al., 2016), and more than of 96% of RGC axons project to the SC in rat (Salinas-Navarro et al., 2009b). The axons of SC-projecting RGCs also pass through the LGN, being that of all RGCs projecting to the SC, ~80% also send an axon collateral to LGN in mouse brain (Ellis et al., 2016). The LGN receives input from the retina and projects to the visual cortex

(Kerschensteiner et al., 2017). Besides RGCs projection into brain target, there is also direct retino-retinal projection between the two eyes via the optic chiasm of RGCs, that constitutes 0.006% to 0.03% of the total RGC population (Nadal-Nicolas et al., 2015b).

3.2. Process of RGC neurodegeneration in glaucoma

The hypothesis that RGCs are preferentially affected in human and experimental glaucoma has received remarkable attention some time ago by Quigley and colleagues (Quigley et al., 1987, Quigley et al., 1988, Glovinsky et al., 1991). Moreover, post-mortem examination of the brains of glaucoma patients show selective neuronal loss in LGN, with greater loss in patients with more severe glaucoma (Chaturvedi et al., 1993, Gupta et al., 2006).

There is still little understanding of the pathologic events that lead to RGC loss. Since elevated IOP is a critical risk factor in glaucoma, there are some evidences that this increased IOP contributes to early stress in the retina (Nickells 2007). A theory that comprises 5 different stages was proposed, bringing together the relation of elevated IOP and the of events that culminate in cell death (Nickells 2007). The first stage is that IOP causes activation of glial cells in the ONH. The stage 2 involves the damage to the RGCs axons and degeneration, which leads to stage 3 that corresponds to the loss of neurotrophic support and apoptotic death of RGCs somas in the retina. In a stage 4, dying RGCs may adversely affect their neighbouring cells in a wave of secondary degeneration involving glutamate exposure. The last stage (stage 5), involves the function of glial cells that replace the lost of neural cells with a glial scar (Nickells 2007).

It is widely recognized that the initial site of damage in glaucoma is at the level of the lamina cribrosa in the ONH (Park et al., 2015). However, there are several "trigger events" that serve as a starting point to a number of disease mechanisms (Alqawlaq et al., 2019). These "trigger events" can be divided into three categories: mechanical, vascular, and immune factors (Alqawlaq et al., 2019). As a mechanical trigger, increased IOP is the most well-characterized contributor to glaucomatous progression (Leske et al., 2007), and a vascular deregulation has been also described in glaucoma patients (Cherecheanu et al., 2013). The immune triggers have received an increased attention as having a pivotal role in the initiation and propagation of the neurodegenerative process (Madeira et al., 2015a). Microglia activation has a preponderant role in glaucomatous damage (Rathnasamy et al., 2019), and the control of microglia-mediated neuroinflammation was demonstrated to protect RGCs from damage (Madeira et al., 2015a, Madeira et al., 2016a, Aires et al., 2019a). The concept that microglia should be considered as central players in the pathophysiology of glaucoma arises since it was observed that microglia activation occur earlier than RGC pathology, even before elevation of IOP in DBA/2J animals (Bosco et al., 2011). Moreover, even astrocytes isolated from ONH of glaucomatous patients have more than 150 upregulated genes (Hernandez et al., 2002). Besides glia activation, other mechanisms have been proposed to contribute to RGC neurodegeneration, like oxidative stress and excitotoxicity (Caprioli 2007, Munemasa et al., 2013). In fact, it seems that the relationship between IOP and glaucomatous damage is not straightforward, and whether these mechanisms are a consequence of IOP elevation still remains to be clarified.

Whatever the early events that trigger glaucoma neurodegeneration, it is certainly that this will culminate in RGC loss. As proposed by Nickells in the stage 2 of the cascade of events in glaucoma neurodegeneration, axonal damage might precede RGC death (Jakobs et al., 2005). Upon axonal damage, the neuronal degenerative response can happen by Wallerian degeneration or dying-back mechanisms (Ghaffarieh et al., 2012). In glaucoma, it is suggested that focal axon injury in the lamina cribrosa results in rapid Wallerian degeneration. In fact, a mutation in Wallerian degeneration slow allele (*Wld*^{s}) strongly protects both RGC axons and soma and substantially slow axon degeneration (Howell et al., 2007). However, others reported that axons degeneration occurs in a dying-back fashion in the DBA/2J glaucoma animal model (Schlamp et al., 2006). In fact, it was reported that both Wallerian degeneration or dying-back occurs with a nearly identical time course and to a similar magnitude in optic nerve transection animal model (Kanamori et al., 2012). As a result of axonal degeneration there is an impairment in axonal transport. Several studies have shown an impairment of axonal transport in the optic nerve in human glaucoma and in glaucoma experimental models, even before the loss of RGC soma (Mabuchi et al., 2003, Salinas-Navarro et al., 2009a, Salinas-Navarro et al., 2010, Vidal-Sanz et al., 2012, Fahy et al., 2015). Moreover, the anterograde axonal transport blockade precedes the deficits in retrograde axonal transport (Dengler-Crish et al., 2014), the blockade of both could lead to deprivation of neurotrophic signals (Quigley et al., 1979). The ultimate result of glaucomatous degeneration is the loss of RGCs by apoptotic-dependent mechanisms (Quigley et al., 1995). The death of a single RGC can lead to the spreading of the death signals, mostly by the release of intracellular glutamate from the dying cells that affects the survival of surrounding cells (Caprioli et al., 2008). Moreover, evidences show that photoreceptors are also affected both in animal models of glaucoma (Salinas-Navarro et al., 2009a, Ortin-Martinez et al., 2015) as well as in glaucoma patients (Holopigian et al., 1990, Panda et al., 1992, Nork et al., 2000).

RGCs are the main affected cells in glaucoma, which leads to an interrupting communication between the eye and brain culminating in blindness. Vision loss secondary to optic neuropathies is irreversible because RGCs do not have the capacity for self-renewal and have limited capacity for self-repair.

3.3. Obstacles to RGC survival and regeneration upon injury

The ability of RGCs to extend their axons decreases with age and the capacity to regenerate their axons is lost early in development (Goldberg et al., 2002a). In fact, cultures of RGCs (Figure 7) prepared at both embryonic day 20 (ED 20) or PND 8 extend their axons with similar calibers; however, after 3 days in culture, ED 20 RGCs extend their axons further and faster than cells isolated at PND 8. The exposure of these cells to conditioned media of SC cells further potentiates axonal growth of ED 20 RGCs without interfering with PND 8 RGCs, demonstrating that the loss of ability of RGCs axon growth is mediated by retinal maturation (Goldberg et al., 2002a). The reason behind the lost in the intrinsic ability of RGCs to regenerate upon injury has been extensively explored. Several players, including cyclic adenosine monophosphate (cAMP), phosphatase and tensin homologue (PTEN)/mammalian target of rapamycin (mTOR) and Krüppel-like family (KLF) transcript factors are implicated in the transition from the rapid axon growth of immature neurons into the poor axon growth of mature neurons in the CNS.

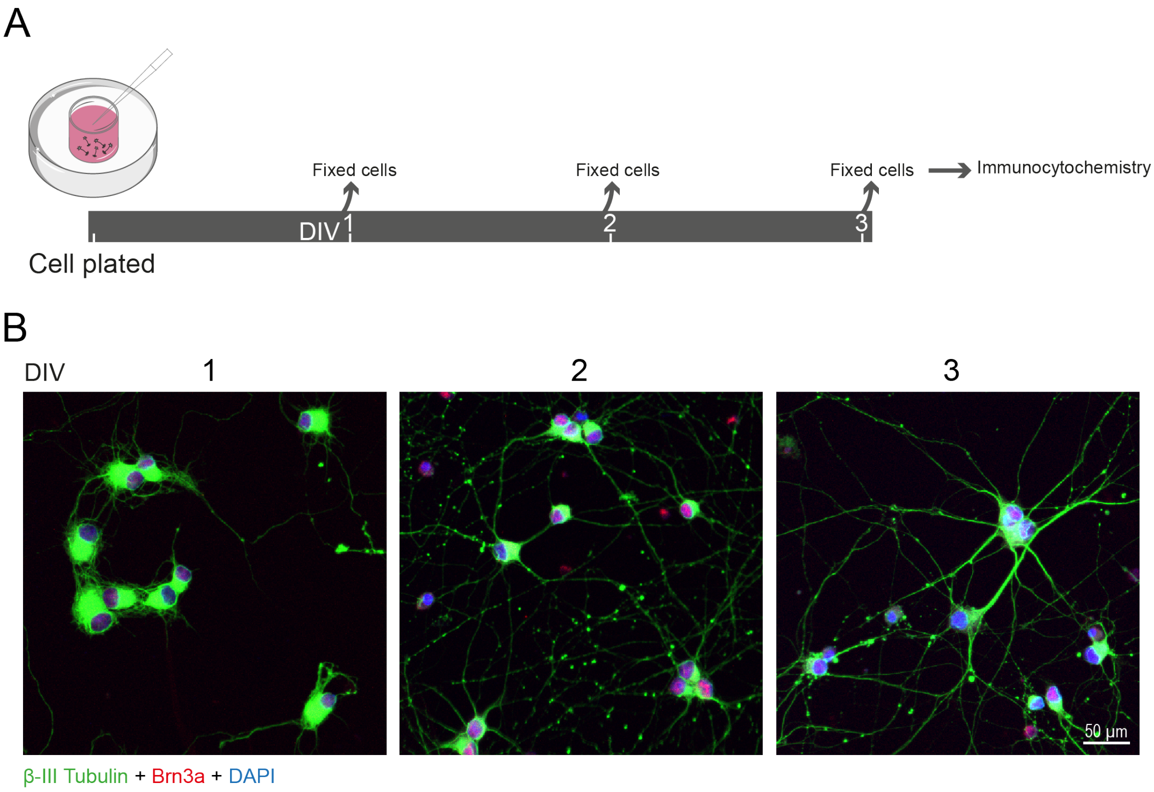

Figure 7 | Neurite growth of RGCs in culture. (**A**) Schematic representation of the experimental design. Retinas were dissected from Wistar rats at PND 5 and nearly pure RGC cultures (~93% purity assessed with anti-RBPMS antibody; Abcam, Cat. # ab194213, 1:500) were obtained by sequential immunopanning, as previously described (Barres et al., 1988, Martins et al., 2015). RGCs were cultured for DIV1, DIV2 and DIV3, followed by fixation in paraformaldehyde and processed for immunocytochemistry. (**B**) RGCs were identified by immunolabeling for Brn3a (red, Millipore, Cat. # MAB1585, 1:500), a transcription factor expressed only by these cells in the retina. The neurites, labelled with an antibody that recognizes β-tubulin III (green, BioLegend, Cat. # 802001; 1:1000), extended during the period in culture. Nuclei were stained with DAPI (blue) (Boia et al., 2020).

cAMP plays an important role in neuronal survival and axon growth and guidance (Ming et al., 1997). For example, in the goldfish, the injection of an analogue of cAMP is able to enhance axonal regeneration upon optic nerve crush (Rodger et al., 2005). Moreover, PTEN/mTOR pathway has been implicated in the failure of RGCs axons to regenerate. The deletion of PTEN in RGCs leads to the activation of phosphoinositide 3-kinases (PI3K)/mTOR pathway, increases neuronal survival and promotes robust axon regeneration after optic nerve injury (Park et al., 2008, Huang et al., 2018). Moreover, it has been reported a coordinated regulation of neurite growth by KLF transcription factors. During development, at least two growth-enhancing KLFs (KLF6 and 7) are down-regulated, and at least two growth-suppressive KLFs (KLF4 and 9) are upregulated (Moore et al., 2009). The profile of gene expression from ED 17 through PND 21 RGCs identified the zinc finger transcription factor KLF4 as the most effective suppressor of neurite outgrowth (Moore et al., 2009). Indeed, the KLF4 overexpression in ED 20 RGCs reduces their ability to extend axons and, on the other hand, KLF4 knockout enhances axon growth ability by PND 12 RGCs (Moore et al., 2009). This decline in the ability of postnatal RGCs to grow axons is associated with KLF-regulated changes in axonal growth cone morphology and protrusive dynamics (Steketee et al., 2014). The knockout of KLF4 during development increases the regenerative potential of RGCs upon optic nerve crush at adulthood (Moore et al., 2009). Amacrine cells have been implicated in the process of losing intrinsic growth capability of RGCs (Goldberg et al., 2002b). In fact, zinc (Zn^{2+}) increases in amacrine cell processes upon optic nerve injury and is transferred to RGCs via vesicular release (Li et al., 2017). The chelation of Zn^{2+} improves cell survival and axon regeneration (Li et al., 2017), raising the possibility that the dysregulation of mobile Zn^{2+} levels is responsible for the loss of axonal growth.

Other transcription factors have been studied for their role in axon growth and regeneration (reviewed in Moore et al., 2011). The tumor suppressor p53 plays a central role in the regulation of apoptosis in RGCs. The overstimulation of N-methyl-D-aspartate (NMDA) receptor activates a p53-dependent pathway of cell death (Li et al., 2002). The involvement of p53 in neurite outgrowth and axon regeneration has been explored in CNS injury (Di Giovanni et al., 2006). However, the deletion of p53 in RGCs fails to promote axonal regeneration, despite the increase in RGC survival upon optic nerve crush (Park et al., 2008), confirming the hypothesis that inducing neuronal survival is not enough to allow axonal regeneration. The activation of p53 has been implicated in the transcription of several factors responsible for apoptosis, as pro-apoptotic BAX or anti-apoptotic Bcl-2 proteins (reviewed in Maes et al., 2017). It was shown that there is an up-regulation of BAX expression after optic nerve crush injury (Isenmann et al., 1997), as well as after ischemic retinal damage (Kaneda et al., 1999). BAX deficiency completely prevents RGCs death in a glaucoma animal model (Libby et al., 2005b). However, deficient BAX expression is not sufficient to hinder axonal degeneration even without RGC death, reinforcing the idea that axon degeneration is not a consequence of RGC death (Libby et al., 2005b). A down-regulation of the anti-apoptotic protein Bcl-2 was observed in RGCs in the GCL when the onset of regenerative failure of RGCs occurs (Chen et al., 1997). Elevating the expression of Bcl-2 maintains neuronal survival even after withdrawing of all trophic factors in cultures of RGCs (Goldberg et al., 2002a). However, Bcl-2-overexpressing RGCs fail to elaborate axons or dendrites, unless axon growth-inducing signals are present, clearly demonstrating that axon growth is not a default function of a surviving neuron, but must be specifically signalled (Goldberg et al., 2002a). These evidences clearly demonstrate that manipulation of some intrinsic factors could have beneficial effects, not only in the prevention of RGC death but also in promoting axon regeneration upon injury. In the peripheral nervous system the injured neurons are able to regenerate, which does not happen in the CNS. However, the observation that CNS neurons, including RGCs, regrow into peripheral nerve grafts (Richardson et al., 1980, Vidal-Sanz et al., 1987), confirms the possibility that extrinsic factors also have a preponderant role in limiting axonal repair.

Glial scar and myelin that compose the environment of optic nerve particularly at the site of injury inhibit the axonal regeneration (reviewed in Yiu et al., 2006). Semaphorin-3 is expressed in the core of the glial scar upon CNS injury (Pasterkamp et al., 1999) and limits regenerating neurons crossing semaphorin-3A (Sema3A)-expressing regions (Pasterkamp et al., 2001). This raises the hypothesis that semaphorins may have a potential role in the glia inhibiting effect of axonal regeneration. Semaphorins have an important function in neuronal polarity and axonal guidance during RGC development or injury (van Horck et al., 2004). Sema3A is one of the extracellular factors that is involved in regulating RGC polarity (Tillo et al., 2012, Chan-Juan et al., 2019). At PND 14, when all RGCs axons reached their targets (Dallimore et al., 2002), Sema3A is elevated (de Winter et al., 2004), and increased expression of Sema3A results in strong axonal inhibition in optic nerve injury model (Zylbersztejn et al., 2012). In line with these findings and corroborating the role of semaphorin in axonal growth, the intravitreous injection of antibodies against the Sema3A-derived peptide to neutralize the function of Sema3A, caused a marked inhibition of RGC loss in an animal model of complete axotomy of the rat optic nerve (Shirvan et al., 2002). Sema5A is a semaphorin produced by oligodendrocytes that also contributes to the inhibitory environment of the injured optic nerve, heralded by the observation that RGC axonal growth increases when blocking Sema5A (Goldberg 2004). It has been demonstrated that myelin proteins inhibit axonal regeneration in adult neurons. Following an insult, nonspecific T cells accumulate at the lesion site on optic nerve (Kipnis et al., 2000, Fisher et al., 2001). Immunization with T cells specifically against myelin proteins (copolymer-1, Cop-1) reduces the post-traumatic neuronal loss after optic nerve crush (Kipnis et al., 2000, Fisher et al. 2001). Moreover, it has been shown to be an effective therapy for glutamate-induced toxicity in mice and in a rat model of chronically high IOP (Fisher et al., 2001). Although these studies were only focused on the survival of RGCs, some years after the authors demonstrated that Cop-1 treatment confer functional protection to RGCs (Bakalash et al., 2005). Other studies led to the identification of several myelin-associated inhibitors of axon growth. Nogo-A is one of the most potent oligodendrocyte-derived inhibitors for axonal regrowth in the injured adult CNS (Pernet et al., 2008, Pernet 2017) that is also expressed by RGCs (Badea et al., 2018). In cases of optic nerve injury Nogo-A is upregulated (Pernet et al., 2012), although the overexpression or down-regulation of Nogo-A does not impact the survival of injured RGCs. However, the neuronal knockout of Nogo-A diminishes the axonal growth response, demonstrating a role for Nogo-A in RGCs growth after injury (Pernet et al., 2012). On the other hand, axonal sprouting is increased in the optic nerves of oligodendrocyte-specific Nogo-A knockout mice (Vajda et al., 2015), demonstrating that the inactivation of Nogo-A in oligodendrocytes appears to be a good strategy to promote axonal regeneration. Moreover, it was reported that neutralizing Nogo-A has beneficial effects on visual recovery and plasticity after retinal injury (Mdzomba et al., 2018). Moreover, myelin-associated glycoprotein (MAG) is a component of the myelin-derived inhibition of nerve regeneration (Wong et al., 2003). It seems that a possible mechanism underlying synapse degeneration and RGCs death in glaucoma is mediated by Nogo-A (Liao et al., 2011). The antagonism of Nogo receptor (NgR) reduces RGCs loss and attenuates synaptic degeneration (Fu et al., 2011) and the knockout of NgR is effective in enhancing axonal regeneration after optic nerve crush (Su et al., 2009).

The failure to regenerate has also been attributed to an environment poor in growth-promoting trophic factors. In fact, the importance of trophic factors in promoting viability and axonal regeneration of RGCs has long been recognized (Su et al., 2009). A great variety of neurotrophins were found to induce axon growth, which include nerve growth factor (NGF), brain-derived neurotrophic factor (BDNF) and ciliary neurotrophic factor (CNTF). BDNF plays an important role in RGCs neuroprotection since the levels of BDNF are increased in response to injury (Vecino et al., 1998, Vecino et al., 1999). BDNF is also highly expressed in the superior colliculus (Hofer et al., 1990, Wetmore et al., 1990) and it is retrogradely transported to the retina. However, displaced amacrine cells in the GCL are the main source of BDNF to RGCs

(Herzog et al., 1998). The application of BDNF to the SC reduces RGC death during development (Ma et al., 1998). Moreover, several studies demonstrated that administration of BDNF into the eye increases the survival of RGCs upon injury, and ameliorate their function (Mey et al., 1993, Mansour-Robaey et al., 1994, Peinado-Ramon et al., 1996, Di Polo et al., 1998, Chen et al., 2001, Galindo-Romero et al., 2013, Domenici et al., 2014).

The survival of RGCs is increased by co-administration of BDNF and CNTF soon after optic nerve injury (Zhang et al., 2005). Moreover, RGCs extend their axons in response to BDNF and CNTF, but both together induce more axon growth than either alone (Goldberg et al., 2002a), raising the hypothesis that different factors may be responsible for different facets of axon growth. However, neurotrophins fail to induce axon growth alone. For instance, RGCs fail to survive in the presence of such trophic factors as BDNF or CNTF unless their cAMP levels are elevated (Meyer-Franke et al., 1995). CNTF overexpression promotes long-term survival and regeneration of injured adult RGCs (Leaver et al., 2006). It was described that exogenously applied CNTF stimulates RGCs partially indirectly via a mechanism that depends on astrocyte-derived CNTF (Muller et al., 2009). The NGF has also an important role in promoting RGCs survival, being the Schwann cells the main source of this factor (Maffei et al., 1990). Intraocular injection of NGF has been previously shown to promote RGC survival (Carmignoto et al., 1989).

Studying the mechanisms of glaucomatous damage has been a great opportunity to unravel the signalling pathways involved in RGC axonal degeneration and growth. Elevated IOP is the main risk factor of glaucoma and, together with other factors, it has been implicated in RGC degeneration and death (Morgan 2012). Several *in vitro* models have been developed (Aires et al., 2017) and allowed the demonstration that there are pressure-dependent changes in the length of axons and neurites of RGCs (Wu et al., 2019). When cultures of RGCs are challenged with elevated pressure there is a severe impact in axon length and in the total neurite length, with a weakened neurite extension (Figure 8), without interfering with cell body area (Wu et al., 2019). In glaucoma, the increased IOP perturbs anterograde and retrograde axonal transports that lead to deprivation of RGCs of neurotrophic factors produced by brain targets (Quigley et al. 1979). In fact, the retrograde transport of BDNF is impaired after IOP elevation, and this may contribute to RGC loss (Pease et al., 2000, Quigley et al., 2000). Recently, it was reported that intravitreal injections of BDNF leads to an increase in the levels of synaptic proteins between RGCs and bipolar cells in the IPL, meaning that this could have a beneficial effect in the function of RGCs (Park et al., 2019).

3.4. Clinical trials targeting RGCs neuroprotection

Several therapeutic strategies have been proposed in order to protect RGCs and restore visual function (Fu et al., 2019). A therapeutic strategy to optic neuropathies should protect RGCs from death but should also manipulate axonal regeneration in order to repair the visual function that was lost due to the disease. However, there is still no effective therapy for optic neuropathies. Innovative study designs and integrating therapeutic testing with biomarkers have advanced several neuroprotective and neuroenhancement compounds to clinical trials. Numerous neuroprotection strategies have been investigated for optic neuropathies, including peripheral nerve grafting, electrical stimulation, and in agreement with their well-known role in maintaining neuronal homeostasis, neurotrophic factors have been proposed as a novel therapy. However, the outcomes of the completed clinical trials were not completely satisfactory, presenting only partial or no expected effects (Greenberg et al., 2009, Allen et al., 2013, Shruthi et al., 2017, Cen et al., 2018).

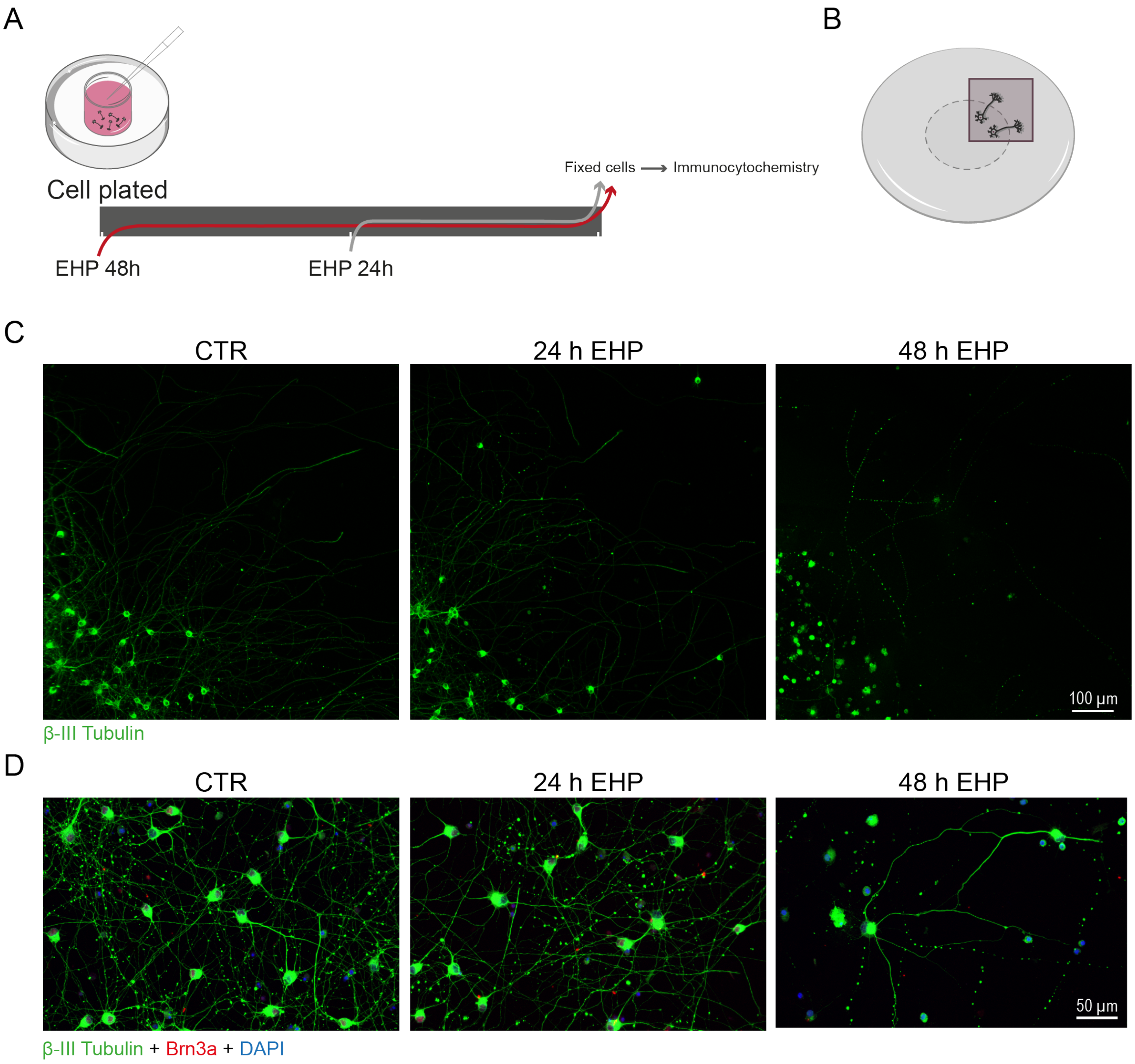

Figure 8 | Elevated hydrostatic pressure (EHP) impacts neurite growth of RGCs. (**A**) Schematic representation of the experimental design. RGCs were purified from Wistar rats at PND 5 by sequential immunopanning, as previously described (Barres et al., 1988, Martins et al., 2015) and were cultured for DIV2. RGCs were challenged with EHP (+70 mmHg above atmospheric pressure) (Madeira et al., 2015b, Aires et al., 2019a) for 24 h and 48 h and then processed for immunocytochemistry as described in the legend of Figure 7. (**C**) RGCs were plated in a coverslip with a cloning cylinder and neurite extension was observed beyond the limit established by the cylinder (**B**, grey dashed circle). Exposure to EHP decreased the length of the neurites when compared with the control (CTR) condition (normal pressure). (**D**) Higher magnification. This effect on the neurites of RGCs is dependent on the duration of the exposure to EHP (Boia et al., 2020).

There are several drugs in clinical trials that are currently being developed focused on RGC neuroprotection (Table 1). In the context of neurotrophic factors some clinical trials are available. NT-501 encapsulated cell therapy (NT-501 ECT) is a device produced by Neurotech Pharmaceuticals that consists of an intravitreal implant with a capsule filled with human cells genetically modified to secrete CNTF. NT-501 ECT is in phase 2 for glaucoma (ClinicalTrials.gov Identifier: NCT02862938) and in phase 1 for ischemic optic neuropathy (ClinicalTrials.gov Identifier: NCT01411657). For glaucoma, other therapies have been proposed such as the use of recombinant human NGF (rhNGF) (ClinicalTrials.gov Identifier: NCT02855450). In this phase 1 clinical trial the safety and tolerability of an 8-week treatment with 180 μg/mL of rhNGF eye drop solution will be determined. Additionally, the study wants to assess the changes in best corrected distance visual acuity, visual field, ERG and structural changes in GCL and NFL thickness measured by OCT at 1, 4 and 8 weeks of therapy, and at 4 and 24 weeks after therapy cessation. In another clinical trial the safety of treatment with single and multiple ascending doses of rhNGF (0.5-180 μg/mL) was tested in healthy patients (ClinicalTrials.gov Identifier: NCT01744704), and the results demonstrated that rhNGF eye drops were well tolerated by the patients (Ferrari et al., 2014).

The only modifiable risk factor for glaucoma development is elevated IOP. Brimonidine is a non-selective α2-adrenergic receptor agonist and is currently used as a treatment option in glaucoma to lower IOP (Cantor 2006). Preclinical studies demonstrated the neuroprotective properties of brimonidine (Donello et al., 2001, WoldeMussie et al., 2001), leading to the hypothesis that an implant with brimonidine can have beneficial properties for glaucoma patients. Indeed, this device is being evaluated in patients with glaucomatous optic neuropathy (ClinicalTrials.gov Identifier: NCT00693485). Moreover, cytidine-50-diphosphocholine (citicoline) is also in a phase 4 clinical trial for glaucoma (ClinicalTrials.gov Identifier: NCT00404729). Citicoline is an endogenous molecule that has a role in the biosynthesis of phospholipids of cell membranes and increases the levels of neurotransmitters, like acetylcholine, in the CNS (Grieb 2014). The neuroprotective properties of citicoline in glaucoma have been tested (Parisi et al., 1999, Parisi et al., 2018). Intramuscular treatment of citicoline improves glaucomatous visual defects (Parisi et al., 1999), RGC function (assessed by pattern ERG) and neural conduction along postretinal visual pathways (assessed by visual evoked potential) (Parisi 2005). That way, the phase 4 clinical trial aims to assess the effects of oral citicoline treatment in visual function outcomes in glaucoma patients. Memantine, a NMDA subtype of glutamate receptor antagonist, is already being used for Alzheimer's disease, and has undergone phase 3 clinical trials for glaucoma (ClinicalTrials.gov Identifier: NCT00141882 and NCT00168350). However, the drug did not show significant efficacy in preserving visual function in glaucoma patients (Weinreb et al., 2018).

Moreover, prostaglandin E1 (alprostadil) administered by intravenous infusion, is very recently in phase 2 clinical trial (ClinicalTrials.gov Identifier: NCT03851562). Prostaglandin E1 is a potent vasodilator of the microcirculation (Steigerwalt et al., 2011), and may correct the deficits in the perfusion pressure of the microcirculation that supplies the optic nerve in patients with ischemic optic neuropathy, improving visual function. In fact, intravenous prostaglandin E1 is an effective treatment for ocular and optic nerve ischemia leading to immediate visual improvement (Steigerwalt et al., 2011). On the other hand, due to the role of endothelin in glaucoma as a potent vasoconstrictor (Rosenthal et al., 2011), the antagonism of its signalling seems to be a

Table 1 | Drug-based therapies in clincial trials for optic neuropathies (Boia et al., 2020)

Condition or Disease	Intervention	ClinicalTrials.gov Identifier	Phase	Starting Date
Glaucoma	NT-501 ECT implant	NCT02862938	2	2016
Glaucoma	rhNGF	NCT02855450	1	2016
Glaucoma, Primary Open Angle	NT-501 CNTF Implant	NCT01408472	1	2011
Glaucoma, Open-Angle	Brimonidine Implant	NCT00693485	2	2008
Glaucoma and Ischemic optic neuropathy	Citicoline	NCT00404729	4	2006
Open-Angle Glaucoma	Memantine	NCT00141882	3	2005
Open-Angle Glaucoma	Memantine	NCT00168350	3	2005
Ischemic Optic Neuropathy	Alprostadil (prostaglandin E1)	NCT03851562	2	2019
Ischemic Optic Neuropathy	Bosentan	NCT02377271	3	2015
Ischemic Optic Neuropathy	Triamcinolone Acetonide	NCT02329288	3	2014
Ischemic Optic Neuropathy	NT-501 CNTF Implant	NCT01411657	1	2011
Non-arteritic Anterior Ischemic Optic Neuropathy	Prednisolone and Erythropoietin	NCT03715881	2	2018
Non-arteritic Ischemic Optic Neuropathy	RPh201	NCT03547206	3	2018
Non-arteritic Anterior Ischemic Optic Neuropathy	Citicoline	NCT03046693	4	2017
Non-arteritic Anterior Ischemic Optic Neuropathy	Methylprednisolone	NCT02439866	3	2015
Non-arteritic Ischemic Optic Neuropathy	RPh201	NCT02045212	2	2014
Non-arteritic Ischemic Optic Neuropathy	Dalfampridine	NCT01975324	4	2013
Non-arteritic Anterior Ischemic Optic Neuropathy	Avastin and Triamcinolone	NCT01330524	1 and 2	2011
Non-arteritic Anterior Ischemic Optic Neuropathy	Bevacizumab	NCT00813059	2	2008
Non-arteritic Anterior Ischemic Optic Neuropathy	Ranibizumab	NCT00561834	1	2007
Non-arteritic Anterior Ischemic Optic Neuropathy	Levodopa-carbidopa	NCT00432393	4	2007
Traumatic Optic Neuropathy	Recombinant human erythropoietin	NCT03308448	3	2017
Traumatic Optic Neuropathy	Recombinant human erythropoietin	NCT01783847	1 and 2	2013
Optic Nerve Diseases (methanol associated optic neuropathy)	Erythropoietin	NCT02376881	3	2015
Leber's Hereditary Optic Neuropathy	Idebenone	NCT02774005	4	2016
Leber's Hereditary Optic Neuropathy	Cyclosporine	NCT02176733	2	2014
Leber's Hereditary Optic Neuropathy	Idebenone	NCT00747487	2	2008

good therapeutic strategy for optic neuropathies. Bosentan, an endothelin receptor antagonist, is in phase 3 clinical trial for ischemic optic neuropathy in order to assess if the treatment could recover anatomical (NFL in OCT, optic atrophy) and functional (visual acuity, visual field) criteria (ClinicalTrials.gov Identifier: NCT02377271). The last drug-based therapy for ischemic optic neuropathy, the retrobulbar injection of triamcinolone acetonide to halt the progression of the visual acuity and visual field loss in patients improving their chances of avoiding blindness, is in phase 3 clinical trial (ClinicalTrials.gov Identifier: NCT02329288). In preclinical studies, besides the neuroprotective effects to RGCs conferred by triamcinolone acetonide, it was demonstrated that this drug also decreases the activation of retinal microglia (Wang et al., 2016a). For non-arteritic ischemic optic neuropathy there are several clinical trials targeting neuroprotection. Erythropoietin (EPO) administered by intravenous injection started recently in phase 2 clinical trial, in order to assess visual field and thickness of the retinal NFL by OCT in glaucoma patients (ClinicalTrials.gov Identifier: NCT03715881). In the same clinical trial, another aim is to assess the potential retinal neuroprotective effect of prednisolone. Moreover, methylprednisolone is also in phase 3 clinical trial (ClinicalTrials.gov Identifier: NCT02439866). Preclinical studies demonstrated that methylprednisolone inhibits the apoptosis of RGCs after optic nerve crush, probably through an up-regulation of Bcl-2 expression and a down-regulation of BAX expression (Sheng et al., 2004), two of the intrinsic factors that limit the axon regeneration described previously. Moreover, citicoline is in clinical trials for non-arteritic ischemic optic neuropathy (ClinicalTrials.gov Identifier: NCT03046693) in order to assess the function of RGCs by pattern ERG, thickness of GCL and visual field test.

RPh201 is a drug extracted from a botanical source and it has been produced by Regenera Pharma. RPh201 started recently the phase 3 clinical trial for non-arteritic ischemic optic neuropathy (ClinicalTrials.gov Identifier: NCT03547206). The results of the phase 2 clinical trial (ClinicalTrials.gov Identifier: NCT02045212) are already available. Patients showed an improvement in visual function after the treatment (Rath et al., 2019). Dalfampridine is used to improve the walking ability in multiple sclerosis patients and is in a phase 4 clinical trial for non-arteritic ischemic optic neuropathy (ClinicalTrials.gov Identifier: NCT01975324).

Anti-vascular endothelial growth factor (VEGF) antibodies (bevacizumab, avastin or ranibizumab) are used for the treatment of macular edema and neovascular AMD. However, they have also been tested for neuroprotection in optic neuropathies, and they are in three different clinical trials for non-arteritic anterior ischemic optic neuropathy (ClinicalTrials.gov Identifier: NCT01330524, NCT00813059 and NCT00561834) in order to halt the progression of visual acuity and visual field loss due to the disease. The thickness of GCL increased after the treatment with bevacizumab in diabetic macular edema (Shaheer et al., 2019). Moreover, levodopa-carbidopa is used to treat the symptoms of Parkinson's disease and it is in a phase 4 clinical trial for non-arteritic anterior ischemic optic neuropathy (ClinicalTrials.gov Identifier: NCT00432393).

A phase 1 and 2 clinical trial (ClinicalTrials.gov Identifier: NCT01783847) assessing the effect of EPO demonstrated an improvement in visual function (Kashkouli et al., 2011, Entezari et al., 2014). These beneficial effects can be due to the protection conferred to RGCs by EPO previously demonstrated in animal models of retinal degeneration (Kilic et al., 2005). Moreover, it has been tested whether EPO could improve optic nerve function and help patients to recover visual function after methanol associated optic neuropathy (ClinicalTrials.gov Identifier: NCT02376881). EPO is currently in phase 3 clinical trial for traumatic optic neuropathy (ClinicalTrials.gov Identifier: NCT03308448).

Leber's hereditary optic neuropathy is an inherited optic neuropathy characterized by mitochondrial dysfunction that leads to vision loss due to RGCs loss (Meyerson et al., 2015). Idebenone was in clinical trials for the treatment of vision loss due to Leber's hereditary optic neuropathy (ClinicalTrials.gov Identifier: NCT02774005 and NCT00747487). The beneficial effects of idebenone are due to its antioxidant properties and its ability to act as an electron carrier in the mitochondrial respiratory chain, thus resulting in the restoration of cellular energy (adenosine 5'-triphosphate, ATP) generation and contributing to the recovery of visual function in patients (reviewed in Lyseng-Williamson 2016). That way, idebenone (Raxonefi) is the first, and currently the only disease-specific treatment for Leber's hereditary optic neuropathy and the only approved for optic neuropathies aiming RGCs neuroprotection. Moreover, cyclosporine is also in a phase 2 clinical trial for Leber's hereditary optic neuropathy (ClinicalTrials.gov Identifier: NCT02176733), due to protective properties against ischemic injury-mediated mitochondrial dysfunction in RGCs (Kim et al., 2014a).

Currently, there are two clinical trials involving stem-cell based therapies targeting RGCs (Table 2). One trial aims to assess the safety and efficacy of the transplantation of autologous purified stem cells (ClinicalTrials.gov Identifier: NCT02638714) on restoring function in damaged optic nerves using autologous purified populations of bone-marrow derived stem cells in optic neuropathy. The intravitreal injection of mesenchymal stem cells (ClinicalTrials.gov Identifier: NCT03173638) aims to evaluate if the treatment may reduce the progression of axonal degeneration caused by non-arteritic ischemic optic neuropathy, but this clinical trial is focused in the evaluation of the safety of cell therapy as a new treatment for these patients.

Despite all of these clinical trials are focused on RGCs neuroprotection, until now none of them have been successfully translated to clinical practice. Nevertheless, RGC neuroprotection remains an exciting field of research with enormous potential for achieving patient visual restoration, and new targets for new therapeutic strategies should be explored.

Table 2 | Stem cell-based therapies in clinical trials for optic neuropathies (Boia et al., 2020)

Condition or Disease	Intervention	ClinicalTrials.gov Identifier	Phase	Starting Date
Optic Neuropathy	Transplantation of autologous purified stem cells	NCT02638714	1 and 2	2015
Non-arteritic Ischemic Optic Neuropathy	Intravitreal injection of mesenchymal stem cells	NCT03173638	2	2017

4. Adenosine

Adenosine is a purine nucleoside that is widely distributed throughout the body, especially in the CNS, and acts as a neuromodulator and homeostatic regulator of several physiological processes (Liu et al., 2019). In the retina, purinergic signalling regulates several events during its development as well as in the adult damaged tissue (Ventura et al., 2019). The presence of adenosine in the human, monkey, guinea pig and rat retinas was first characterized with a specific sensitive antiserum (Braas et al., 1987). Adenosine staining was detected mainly in the RGCs and their processes in the NFL, but also in the IPL and some cells in the INL (Braas et al., 1987). Despite the important function of adenosine in physiology (Xiao et al., 2019), adenosine is likely more important as a key signal of stress, damage, and/or danger (Fredholm et al., 2019).

4.1. Adenosine production and metabolism

Adenosine can be considered as a central excitatory and inhibitory neurotransmitter. Under physiological conditions the levels of adenosine are low (around 30-300 nM) in both intra- and extracellular compartment of the cells (Fredholm et al., 2001). The adenosine levels increase to low micromolar levels under extreme physiological situations, like intensive exercise or low atmospheric oxygen levels (e.g., at high altitude), and dramatically increase to high micromolar levels (30 μM) in pathological conditions (Borea et al., 2018). Even, in the retina, adenosine concentration increases after 5 min of ischemia and even during the reperfusion period (Roth et al., 1997).

The extracellular levels of adenosine are highly regulated and are mainly generated by dephosphorylation of its precursors, adenosine triphosphate (ATP), adenosine diphosphate (ADP) and adenosine monophosphate (AMP), by the ectoenzymes apyrase (CD39) and ecto-5'-nucleotidase (CD73), whilst the intracellular adenosine depend on hydrolysis of AMP and S-adenosylhomocysteine (SAH) through the endo-5'-nucleotidase and SAH hydrolase, respectively (Zimmermann 2000, Eltzschig 2009). The levels of adenosine are maintained in equilibrium by reuptake mechanisms through the action of nucleoside transporters (NTs) that are present in the cell membrane. Moreover, adenosine can be phosphorylated to AMP by adenosine kinase (ADK) or it can be degraded to inosine by adenosine deaminase (ADA) (Borea et al., 2017) (Figure 9).

The formation of adenosine is strictly dependent on the metabolic state of a cell, and in conditions with increased metabolic demand and/or lack of oxygen the adenosine levels dramatically increased. Under stress conditions or damage the main source of extracellular adenosine is from released ATP (Jacobson et al., 2019). In fact, EHP (that mimics OHT *in vitro*) increases the levels of extracellular ATP and adenosine (Madeira et al., 2015b, Rodrigues-Neves et al., 2018). Increased adenosine levels have a significant role in protecting against cell damage (Borea et al., 2016), even though there are instances in which overproduction of adenosine is pathological (Borea et al., 2017).

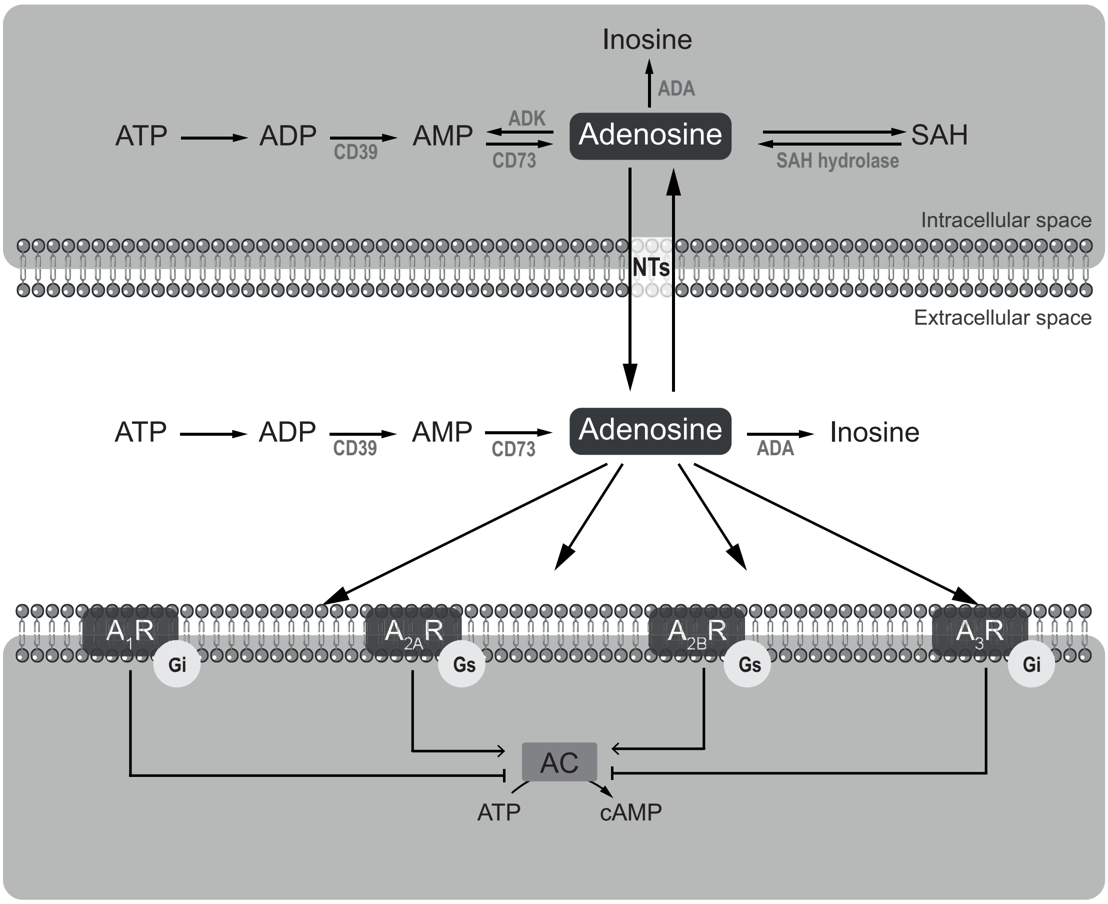

Figure 9 | Schematic representation of adenosine metabolism and intracellular response of its binding to the receptors.

4.2. Adenosine receptors

The physiological functions of adenosine are achieved through receptor mediation, acting as a transmitter stimulating each of four receptors subtypes: adenosine A_1 receptor (A_1R), adenosine A_{2A} receptor ($A_{2A}R$), adenosine A_{2B} receptor ($A_{2B}R$) and adenosine A_3 receptor (A_3R). Adenosine receptors are metabotropic receptors coupled to G proteins, being A_1R and A_3R coupled to inhibitory G_i and $A_{2A}R$ and A_{2B} to stimulatory G_s proteins that will both affect cAMP levels (Borea et al., 2018) (Figure 9). Moreover, adenosine binding to the receptors causes the dissociation of G-proteins subunits Gα, Gβ, and Gγ that will regulate the activities of secondary messengers and play an important role in transferring extracellular signals to the cytosol (Schulte et al., 2003, Borea et al., 2018). Although these receptors differ from each other in terms of the type of G protein they recruit and, thus, the downstream signalling pathways that are activated, these receptors also differ in their affinity to adenosine. The low physiological levels (nM) of adenosine lead to a basal level of adenosine receptors stimulation, especially A_1R, $A_{2A}R$ and A_3R, while $A_{2B}R$ activation mainly occurs at higher levels of adenosine (mM) (Fredholm et al., 2001).

Since adenosine receptors are widely distributed throughout the body and they have been implicated in numerous pathological conditions prompted researchers to search for novel potential drugs focused on adenosine receptors (Fredholm et al., 2011). In fact, adenosine receptors seem interesting targets for new pharmacological interventions mainly for pathophysiologic conditions

(Borea et al., 2018). Although a limited number, there are some adenosinergic drugs (agonist and antagonist of A_1R and $A_{2A}R$) now approved for clinical used (Borea et al., 2018). A_3R has been recognized as a new potential therapeutic target and great efforts are being concentrated on the development of A_3R agonists (Borea et al., 2015). In the last years, it has been proposed a broad spectrum of ligands that present an ability to interact with A_3R, including agonists, antagonists, partial agonists and inverse agonists (Muller et al., 2011). 2-Cl-IB-MECA has proved to be a very potent and a selective agonist for A_3R (inhibitory constant, Ki: 1.4 nM (human), 0.33 (rat) and 0.18 (mouse)) (Muller et al., 2020).

4.3. A_3R activation: a new therapeutic strategy

A_3R has been described to be present in several tissues which raises the possibility that this receptor might be involved in numerous physiological effects (Zhou et al., 1992, Salvatore et al., 1993). In addition, the A_3R has emerged as a potential drug target for new and effective therapeutic strategies to treatment of various pathological disorders, like cardiovascular, respiratory, immune, CNS and ocular disorders (Mailavaram et al., 2019).

The deletion of A_3R in mice enhances brain neurodegeneration in response to repeated episodes of hypoxia (Fedorova et al., 2003), and A_3R activation in ischemic brain injury is neuroprotective (Chen et al., 2006). Interestingly, in cerebral ischemia, a dual effect for A_3R activation was described: if the agonist is administered acutely, it promotes extensive neuronal loss, but if the agonist is given chronically and during post-ischemia, it improves neuronal survival (Von Lubitz et al., 1994). Besides the reported dual function of A_3R activation associated to the time of drug administration (Von Lubitz et al., 1994, Von Lubitz et al., 2001), the impact of A_3R activation on glial cells may help explain this dual effect. In fact, A_3R is expressed in astrocytes (Wittendorp et al., 2004) and microglia (Hammarberg et al., 2003). The degree of astroglial and microglial activation depends on the timing of treatment with respect to the insult itself (Von Lubitz et al., 2001). Noteworthy, the post-ischemia treatment with an A_3R agonist decreases astrogliosis and reduces microglial cell infiltration of the penumbral cortex (Von Lubitz et al., 2001). Moreover, the expression of nitric oxide synthase (NOS) is reduced with the A_3R agonist treatment during the postischemic period (Von Lubitz et al., 1999). The neuroprotective effects of A_3R agonist in brain damage after subarachnoid haemorrhage is also associated with the inhibition of microglia activation and the decrease of proinflammatory cytokine release (Luo et al., 2010). In microglial cells, A_3R activation suppresses tumor necrosis factor (TNF) in response to lipopolysaccharide exposure (Lee et al., 2006), and promotes chemotactic process extension and migration of these cells (Ohsawa et al., 2012). The activation of A_3R in astrocytes releases CCL2 (also known as MCP-1), a neuroprotective chemokine (Wittendorp et al., 2004), but high concentrations of the A_3R agonist (>10 μM) mediate apoptosis of astrocytes via Bcl-2 and caspase-3 pathways (Appel et al., 2001, Di Iorio et al., 2002). More recently, it was demonstrated that A_3R activation following traumatic brain injury protects against tissue damage, brain infarct, neural inflammation and cognitive dysfunction (Farr et al., 2020). Since the A_3R agonist has the ability of controlling inflammation mediated by glial cells in brain, it is tempting to speculate that A_3R activation may also control inflammation in the retina, prompting the hypothesis of targeting A_3R activation in glial cells as a new approach for the treatment of retinal degenerative diseases. Indeed, the activation of A_3R hinders microglia reactivity elicited by EHP, suggesting that A_3R agonists could afford protection against glaucomatous degeneration through the control of neuroinflammation (Ferreira-Silva et al., 2020).

The impact of A_3R activation on retinal degenerative diseases, such as glaucoma and ischemic diseases, has been explored (as reviewed in Santiago et al., 2020). The activation of A_3R protects the retina from excitotoxic-induced cell death, retinal I-R injury and from damage induced by partial optic nerve transection (Galvao et al., 2015). In the I-R injury model, the A_3R agonist reduces cell death in the INL, which can be an effect mediated by other cells (Galvao et al., 2015). Despite others demonstrated that A_3R may be located in neurons of the inner retina that contribute to the generation of the ERG a- and b-waves (Jonsson et al., 2017), it is possible, to some extent, that the protective effects of A_3R activation in the INL might be mediated through the control of the reactivity of glial cells. Nevertheless, the activation of A_3R with high doses of the agonist 2-Cl-IB-MECA may contribute to optic nerve and white matter damage since it induces apoptosis of oligodendrocytes and myelin loss in ischemic conditions (Gonzalez-Fernandez et al., 2014).

The activation of A_3R protects RGCs from cell death induced by a P2X7 receptor agonist (Zhang et al., 2006, Hu et al., 2010), and limits the rise in Ca^{2+} that accompanies the stimulation of NMDA receptors (Zhang et al., 2010). The protective effects may result from the direct action in RGCs, since these cells are endowed with A_3R (Zhang et al., 2006). Moreover, it was demonstrated that A_3R agonists promote neurite outgrowth of RGCs (Nakashima et al., 2018), encouraging that A_3R activation could be a good therapeutic strategy. Moreover, besides the neuroprotective potential of activation A_3R, it was demonstrated that an A_3R selective agonist has efficacy as IOP-lowering agent (Avni et al., 2010). Several clinical trials with A_3R agonists arose with the aim of controlling inflammation or IOP depending on the pathology (Table 3). The most promising A_3R full agonists, CF101 (generically known as IB-MECA) and CF102 (generically known as 2-Cl-IB-MECA), are in clinical trials, and it has been demonstrated that both present good safety profile in patients (Jacobson et al., 2019).

Table 3 | Ongoing clinical trials of adenosine A_3R agonist

Condition or Disease	Compound	ClinicalTrials.gov Identifier	Phase	Starting Date
Anti-inflammatory effect				
Dry Eye Disease	CF101	NCT00349466	2	2006
Dry Eye Disease	CF101	NCT01235234	3	2010
Rheumatoid Arthritis	CF101	NCT00556894	2	2007
Rheumatoid Arthritis	CF101	NCT01034306	2	2009
Rheumatoid Arthritis	CF101	NCT02647762	3	2016
Plaque Psoriasis	CF101	NCT01265667	2 and 3	2010
Plaque Psoriasis	CF101	NCT03168256	3	2017
Hepatocellular Carcinoma	CF102	NCT00790218	1 and 2	2008
Hepatocellular Carcinoma	CF102	NCT02128958	2	2014
Chronic Hepatitis C	CF102	NCT00790673	1 and 2	2008
Non-alcoholic Steatohepatitis	CF102	NCT02927314	2	2016
IOP lowering effect				
Glaucoma (OHT)	CF101	NCT01033422	2	2009

5. Drug administration into the eye

Aiming the administration of neuroprotective agents that can reduce the loss of RGCs and degeneration of optic nerve fibers, the drug administration must be directed towards the posterior segment of the eye. Ocular administration to the posterior segment of the eye can be performed by periocular (that includes subconjunctival, sub-Tenon's, peribulbar, retro bulbar, and posterior juxtascleral injection), suprachoroidal, subretinal and intravitreal injection (Figure 10) (Varela-Fernandez et al., 2020). In the clinical practice, the standard procedure for posterior segment drug administration is the intravitreal injection (Kim et al., 2014b). However, the need to maintain therapeutic drug levels require frequent injections that may cause several side effects such as inflammation, endophthalmitis, retinal detachment and cataracts (Sampat et al., 2010). Therefore, an increasing attention has been paid to intraocular drug delivery systems that allow the maintenance of therapeutic drug concentrations near the target site with minimal surgical invasion and reduced frequency of administration (Gote et al., 2019).

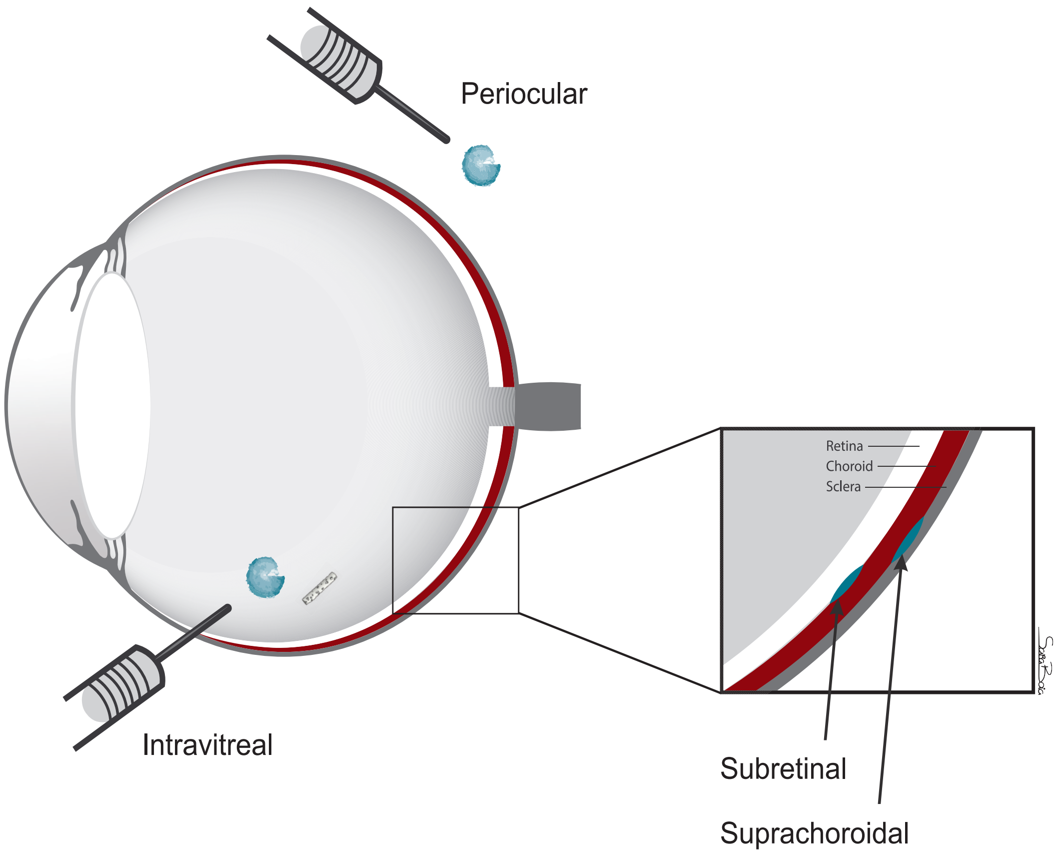

Figure 10 | Drug delivery routes to the posterior segment of the eye.

5.1. Drug delivery systems for posterior segment of the eye in clinical use

There are several intraocular delivery systems for posterior segment of the eye that had successful clinical translation and are now available for clinical use (Figure 11). Vitrasert and Retisert are maintained attached to the sclera, while Ozurdex and Iluvien are both injected into the vitreous (Yasin et al., 2014). Implantable drug delivery systems can be nonbiodegradable or biodegradable devices. One major difference is that removal and re-implantation of a new device following depletion of the drug is usually required in the case of nonbiodegradable devices (Wang et al., 2013a), while in the case of biodegradable implants the drug is either inside a reservoir or dispersed through a biodegradable matrix, conditioning its release to the degradation of the device (Kaji et al., 2018).

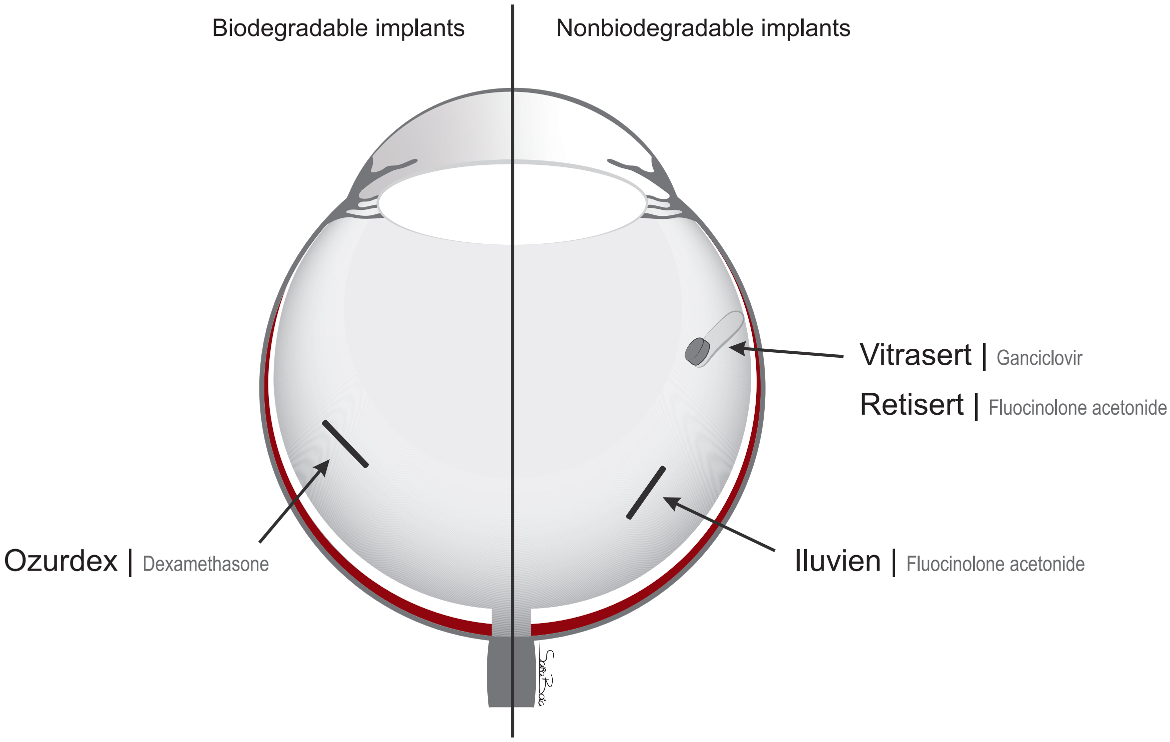

Figure 11 | Biodegradable and nonbiodegradable intraocular implants are in clinical use, and their locations in the eye upon implantation.

The first intraocular device developed for clinical use, which was released into the market in 1996 for the treatment of cytomegalovirus retinitis in acquired immunodeficiency syndrome, was the Vitrasert, a polymeric nonbiodegradable device containing ganciclovir coated with polyvinyl alcohol (PVA) and ethylene vinyl acetate (EVA) (Haghjou et al., 2011). The infection by human cytomegalovirus, which belongs to β subgroup of herpes viruses, often leads to retinitis and progressive loss of vision culminating in blindness (Egbert et al., 1980). The ganciclovir intraocular implant releases drug for up to eight months (Yasin et al., 2014) and increased the median time of disease progression when comparing with intravenous administration (Dhillon et al., 1998). Taking into consideration that Vitrasert is already in the clinical practice, it is worth more research in this field. Indeed, there are three more sustained-release corticosteroid implants that was then approved for clinical use. Retisert and Iluvien, two nonbiodegradable implants that release fluocinolone acetonide, and was approved for clinical use in 2005 and 2014, respectively. Ozurdex, that is the first biodegradable polymer implant that releases dexamethasone and was approved for clinical use in 2009 (Yasin et al., 2014).

Retisert that releases fluocinolone for up to 2.5 years, is composed by a silicone cup and a PVA membrane (Haghjou et al., 2011), and is indicated for the treatment of chronic non-infectious uveitis that affect the posterior segment of the eye (Callanan et al., 2008). Iluvien that releases drug for up to three years, consists of a cylindrical polyimide tube (Haghjou et al., 2011) and is indicated for the treatment of chronic diabetic macular edema (Soubrane et al., 2015). Ozurdex that releases drug for up to six months, is a biodegradable poly(D,L-lactic-co-glycolic)acid (PLGA) implant (Haghjou et al., 2011) for macular edema following retinal vein occlusion, diabetic macular edema, and noninfectious posterior uveitis (Haller et al., 2010, Wang et al., 2013a).

There are other intraocular devices aiming drug release to the posterior part of the eye in clinical trials (Yasin et al., 2014). The intravitreal route for intraocular drug delivery is the most suitable for the purpose of RGCs neuroprotection, indeed, the development of new intravitreal implants for drug release appears to be an effective approach for glaucoma management.

5.2. Polymer-based implants for drug release ocular diseases: the potential of poly(Ɛ-caprolactone)

Despite the advances to have an efficient drug delivery to the back of the eye, there is an unmet medical need for new drug delivery systems for new as well as already existing ophthalmic drugs. New drug delivery systems should provide maximum therapeutic efficacy and a long-term therapy solution increasing patient compliance. Moreover, one of requirements for the development of new drug delivery systems should be good biocompatibility of the delivery systems and biodegradable polymer-based drug delivery systems satisfy this requirement. Implantable polymer-based drug delivery systems have become quite appealing for eye diseases since they are designed to administer drugs without the repeated injections or self-administration of medical therapy. In fact, glaucoma patients are willing to accept an ocular drug delivery implants as an alternative to daily eye drops (Foo et al., 2012, Chong et al., 2013, Chan et al., 2015), showing that ocular drug delivery implants would be an acceptable route for drug administration.

Biodegradable polymers have been explored as the base polymers to develop new drug delivery systems. The major advantage in the use of biodegradable polymers is that the implant is degraded and clearly by the body, avoiding the need of surgical removal (Kimura et al., 2001). There are several biodegradable polymers that have been used in the research for intraocular drug delivery devices.

Among synthetic biodegradable polymers, poly(Ɛ-caprolactone) (PCL) is a polymer with good biocompatibility and biodegradability. Several studies have been focused in the use of PCL polymer for eye drug release. For glaucoma patients it has been evaluated the use of an intracameral drug delivery implant (Lance et al., 2015, Kim et al., 2016, Kim et al., 2018), providing several advantages for these patients. In fact, the use of an intracameral implant ends with the need of several eye drops instillation for drug administration. The evaluation of safety and IOP-lowering effect of DE-117, a hypotensive drug, for glaucoma treatment is in phase 3 clinical trial (ClinicalTrials.

gov Identifier: NCT02981446). To circumvent the disadvantages already described for the use of eye drops, a PCL implant loaded with DE-117 for intracameral drug delivery was recently proposed (Kim et al., 2018). This PCL implant was found to be safe and tolerable (Bernards et al., 2013, Lance et al., 2015, Kim et al., 2016) and, when loaded with DE-117, presented a long-term reduction of IOP in normotensive rabbits compared to an empty device implantation or no treatment (Kim et al., 2018).

Others proposed an implantable disc for sustained release of dorzolamide, a carbonic anhydrase inhibitor used to lower IOP in glaucoma patients (Natu et al., 2011b). The cytotoxicity for corneal endothelial cells was assessed, and after the introduction of PCL disc implant in subconjunctival pocket, it was demonstrated that dorzolamide released from the implant decreases the IOP to values similar to those obtained for drug eye drop instillation (Natu et al., 2011b).

Even to overcome most of the disadvantages of repeated intravitreal injections, intravitreous devices for long-term drug release has been studied. The use of rapamycin administered by intravitreal injection is in phase 2 clinical trials for uveitis treatment (ClinicalTrials.gov Identifier: NCT01280669). However, to bypass the problems associated with repeated intravitreal injections, an implant was developed for the release of rapamycin for the treatment of chronic uveitis (Lance et al., 2015). Moreover, a PCL implant for dexamethasone release in the vitreous was proposed some years ago, that can be used in several retinal diseases (Fialho et al., 2008). It was also proposed the use of PCL implant for sustained release of ranibizumab in the vitreous cavity over the course of several months (Lance et al., 2016), showing that even for the release of proteins during prolonged time it is possible to use this type of devices.

Even though those studies have been investigating several different ways to delivery drugs into the eye, biodegradable polymer-based intraocular implants have been receiving an increased attention.

Aims

Glaucoma is a retinal degenerative disease and a leading cause of irreversible blindness. Elevated IOP is an important risk factor in glaucoma, namely for optic nerve damage and RGC death. Current treatment is directed towards IOP lowering, but many patients continue to lose vision despite successful IOP control. Therefore, new and more effective treatments are necessary, and neuroprotection of RGCs is considered to offer potential as an additional therapy. RGCs express adenosine A_3R and its activation confers protection to RGCs following excitotoxic stimulus. These findings strongly support that A_3R activation can protect RGCs from glaucomatous damage. The intravitreal route for intraocular drug delivery is the most suitable for the purpose of RGC neuroprotection, and the development of new intravitreal implants for drug release may be an effective strategy, overcoming the side effects related with multiple intravitreal injections. Therefore, we proposed the use of a biodegradable intraocular implant loaded with the selective agonist of A_3R and investigated its neuroprotective properties using *in vitro* and animal models of glaucoma.

The main aims of the present thesis were:

1) Assess the potential of A_3R activation as a new therapeutic approach for glaucoma;

2) Assess the safety and tolerability of PCL-based implants to the retina;

3) Assess the potential of 2-Cl-IB-MECA-loaded PCL implant as a new therapeutic strategy for RGC neuroprotection.

Activation of adenosine A_3 receptor protects retinal ganglion cells from degeneration induced by ocular hypertension

Boia R, Salinas-Navarro M, Gallego-Ortega A, Galindo-Romero C, Aires ID, Agudo-Barriuso M, Ambrósio AF, Vidal-Sanz M and Santiago AR

Cell Death and Disease. 2020; 11(5):401.
doi: 10.1038/s41419-020-2593-y

1. Abstract

Glaucoma is a progressive chronic retinal degenerative disease and a leading cause of global irreversible blindness. This disease is characterized by optic nerve damage and RGC death. The current treatments available target the lowering of IOP, the main risk factor for disease onset and development. However, in some patients, vision loss progresses despite successful IOP control, indicating that new and effective treatments are needed, such as those targeting the neuroprotection of RGCs. A_3R activation confers protection to RGCs following an excitotoxic stimulus. In this work, we investigated whether the activation of A_3R could also afford protection to RGCs in the laser-induced OHT model, a well-characterized animal model of glaucoma. The intravitreal injection of 2-Cl-IB-MECA, a selective A_3R agonist, abolished the alterations induced by OHT in the negative and positive components of STR without changing a- and b-wave amplitudes both in scotopic and photopic conditions. Moreover, the treatment of OHT eyes with the A_3R agonist promoted the survival of RGCs, attenuated the impairment in retrograde axonal transport, and improved the structure of the optic nerve. Taking into consideration the beneficial effects afforded by 2-Cl-IB-MECA, we can envisage that A_3R activation can be considered a good therapeutic strategy to protect RGCs from glaucomatous damage.

Graphical Abstract

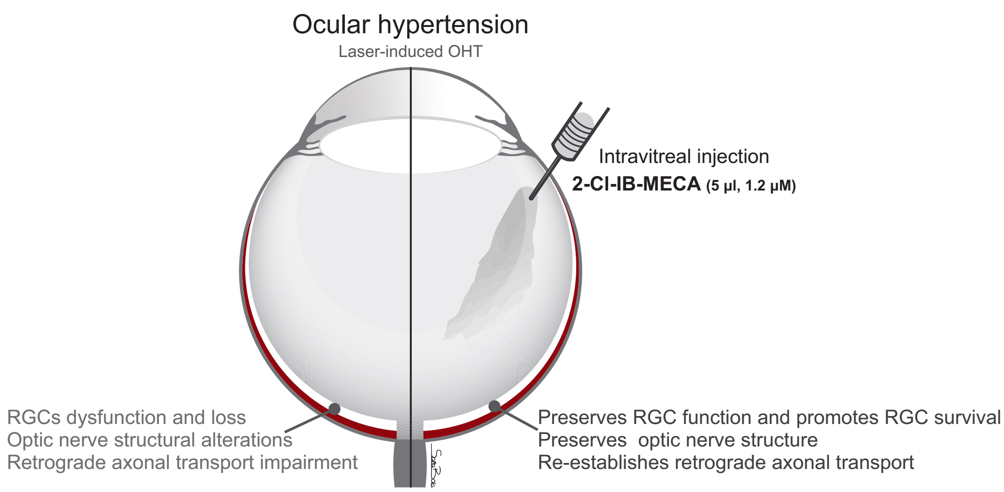

2. Introduction

Glaucoma is a leading cause of blindness worldwide. It is estimated that in 2020, the global population with moderate or severe vision impairment by glaucoma will rise to 4.5 million, and the global population that go blind because of glaucoma will rise to 3.2 million (Flaxman et al., 2017). This disease is characterized by optic nerve degeneration and loss of RGCs that contribute to the vision loss (Kuehn et al., 2005, Boia et al., 2020). The predominant and the only modifiable risk factor for the onset and progression of glaucoma is elevated IOP. Despite the growing research in the field of glaucoma, the current strategies only target lowering IOP either by topical administration of eye drops, laser, or incisional surgery. However, despite a 25% reduction in IOP in treated patients, half of them still progress in terms of visual deficits (Leske et al., 2003). Moreover, normal-tension glaucoma represents ~50% of glaucoma cases, and in the clinical practice, antihypertensive drugs remain the mainstay of treatment (Shields 2008). However, even in patients with controlled IOP the disease still progresses (Anderson et al., 2001). This demonstrates that IOP-independent mechanisms also contribute to the progression of the disease, suggesting that an effective therapeutic strategy should incorporate hypotensive drugs and neuroprotective agents, aiming at preserving RGCs (Cordeiro et al., 2011). Adenosine is a neuromodulator acting through four adenosine receptors (A_1, A_{2A}, A_{2B}, and A_3) (Borea et al., 2018). There is clinical and experimental evidence that activation of A_3R mediates protective effects in ischemic brain injury (Chen et al., 2006). Moreover, the activation of A_3R protects RGCs against P2X7 receptor agonist-induced cell death (Zhang et al., 2006, Hu et al., 2010), and it limits the rise in intracellular calcium (Ca^{2+}) concentration evoked by stimulation of the NMDA receptor (Zhang et al., 2010). The protective effects may result from the direct action on RGCs, since these cells are endowed with A_3R (Zhang et al., 2006). Moreover, we found that A_3R activation prevents retinal cell death in several *in vitro* and animal models of retinal degeneration (Galvao et al., 2015), but the beneficial properties of 2-Cl-IB-MECA were not studied in animals with OHT. In this study, we investigated the therapeutic potential of 2-Cl-IB-MECA administered by intravitreal injection immediately after inducing OHT.

3. Materials and methods

3.1. Animals

Female Sprague-Dawley rats (Charles River, Spain) 8-weeks old were housed in animal facilities of the University of Murcia, Spain, in a 12 h light/12 h dark cycle, with free access to food and water. All procedures with animals were approved by the Ethical and Animal Studies Committee of the University of Murcia, and were in accordance with the Association for Research in Vision and Ophthalmology and European Union guidelines for animal research use.

3.2. Induction of OHT and treatment with A_3R agonist

Animals were anesthetized with an intraperitoneal injection of a mixture of ketamine (60 mg/kg, Ketalar, Pfizer, USA) and xylazine (10 mg/kg, Rompun, Bayer, Germany). OHT was induced in the left eyes in a single session with a series of diode laser burns (Viridis Ophthalmic Photocoagulator-532 nm, Quantel Medical, France), as previously described (Salinas-Navarro et al., 2010, Madeira et al., 2016b). Immediately after OHT induction, both eyes (OHT and contralateral eyes) were treated with sterile saline solution (0.9% NaCl, 5 μl) or with 2-Cl-IB-MECA (1.2 μM, 5 μl) by intravitreal injection, the same dose used in our previous study (Galvao et al., 2015). Topical ointment with tobramycin (Tobrex, Alcon Cusí, S.A., Spain) was used to prevent corneal desiccation. The animals were randomly assigned into naïve, saline treated and 2-Cl-IB-MECA-treated group, and were sacrificed 7 days after OHT induction. IOP was monitored bilaterally 24 h after OHT induction. The IOP increased (35 ± 1.6 mmHg) in the left eyes, comparing with contralateral eyes (9 ± 0.2 mmHg).

3.3. Electroretinography

At 6 days after OHT induction, the animals were darkadapted overnight before the ERG recordings. To carry out the recordings, we used a dim red light (λ > 600 nm) that allowed us to handle the equipment and the animals, while the animals remained in scotopic conditions. The rats were anaesthetized with an intraperitoneal injection of a mixture of ketamine (60 mg/kg, Ketalar, Pfizer, USA) and xylazine (10 mg/kg, Rompun, Bayer, Germany), and maintained on a heating pad to keep the body temperature. Pupil mydriasis was induced by applying a topical drop of 1% tropicamide (Colircusi tropicamida 1%®, Alcon Cusí, S.A., Spain) to both eyes, 5 min before ERG testing. STR, scotopic and photopic ERG responses were recorded in response to light stimuli produced by a Ganzfeld stimulator using Burian-Allen bipolar electrodes (Hansen Labs, USA) located on the cornea. The corneal surface had been previously protected with a nonallergenic ionic conductive drop of methylcellulose (methocel 2%, OmniVision, USA). The reference electrode was placed on the mouth, and the ground electrode was a needle placed subcutaneously at the base of the tail.

The STR was recorded by stimulating both eyes with -4.7 log cd·s/m^2 of light intensity, and a series of ERG responses were averaged (~20 ERG responses) for each trace. The ERG responses were recorded by stimulating the retina with light intensities ranging between -1.69 to 2.19 log cd·s/m^2 for scotopic a-wave, -3.61 to 2.19 log cd·s/m^2 for scotopic b-wave, and 2.19 log cd·s/m^2 for photopic b-wave. For each light intensity, a series of ERG responses were averaged (~40 ERG responses for the dimmest stimulus intensities to 5 ERG responses for the brightest stimulus) with an interval between light flashes from 5 s for the dimmest stimulus intensities to 60 s for the brightest stimulus.

Electrical signals were digitized at 20 kHz using a Power Lab data acquisition board (AD Instruments, Australia) and displayed on a PC computer. The light stimuli were calibrated with a photometer (Mavo Monitor USB, Gossen, Germany). The STR was analyzed for each stimulus as follows: positive STR (pSTR) was measured from the baseline to the peak of the positive deflection, ~110-120 ms from the flash onset; negative STR (nSTR) was measured from the baseline to the peak of the negative deflection after the pSTR, ~220 ms from the onset of the flash. The investigator was blinded to the group when performing the experiment and extracting data. Standard ERG waves were analyzed according to the method recommended by the International Society for Clinical Electrophysiology of Vision (Alarcon-Martinez et al., 2009, Salinas-Navarro et al., 2009a).

3.4. Retrograde tracing of RGCs

After 24 h of laser-induced OHT procedure, animals were anesthetized using the aforementioned anesthetic protocol. Fluorogold (FG, Fluorochrome Inc., USA) was prepared at 3% concentration (w/v) in a solution of 10% dimethyl sulfoxide (DMSO)-saline, and it was applied onto the surface of both superior colliculi (SCi). The animals were sacrificed 6 days after FG application (7 days after OHT induction), and the retinas were processed for wholemount preparation.

3.5. Immunolabelling

3.5.1. In retinal wholemounts

Animals were euthanized with an intraperitoneal injection overdose of pentobarbital (Dolethal, Vetoquinol, France), and perfused with PBS followed by 4% paraformaldehyde (PFA). Then, eyecups were enucleated and fixed for an additional hour in 4% PFA. For retinal wholemounts, the eyes were maintained in PBS until dissection as flat mounts. Retinal wholemounts were permeabilized with 0.5% Triton X-100 and incubated with primary antibody (goat anti-Brn3a, catalog number sc-31984, Santa Cruz Biotechnology, USA) overnight at 4 °C. Retinas were incubated with the secondary antibody (donkey anti-goat IgG conjugated to Alexa Fluor 594, catalog number A11058, Thermo Fisher Scientific, USA), and mounted with the vitreous side up and covered with antifading mounting medium.

3.5.2. In retinal cryosections

Immunohistochemistry in retinal cryosections was performed as previously described (Boia et al., 2017). The sections were incubated overnight with the primary antibodies: rabbit anti-A_3R (catalog number sc-13938, Santa Cruz Biotechnology, USA), mouse anti-Brn3a (catalog number MAB1585, Millipore, USA), and rabbit anti-RBPMS (RNA-binding protein with multiple splicing; catalog number ab194213, Abcam, United Kingdom). The sections were rinsed with PBS followed by incubation with the corresponding secondary antibodies for 1 h at room temperature in the dark: goat anti-rabbit conjugated to Alexa Fluor 488 (catalog number A11008, Thermo Fisher Scientific, USA), goat anti-mouse conjugated to Alexa Fluor 568 (catalog number A11004, Thermo Fisher Scientific, USA), and goat anti-rabbit conjugated to Alexa Fluor 568 (catalog number A11036, Thermo Fisher Scientific, USA). For the counting of RBPMS$^+$ cells, the preparations were observed in a fluorescence microscope (Axio Observer.Z1, Zeiss, Germany), using a 20× objective (Plan Achromat 20×/0.8 M27). From each eye, four sections were analyzed and the number of RBPMS$^+$ cells was counted in the entire retinal section and normalized to the length of the respective section. The RBPMS survival rate was presented as the percentage of the ratio between the OHT-injured retina and the contralateral eye. For both RBPMS and A_3R immunohistochemistry, representative images were acquired with a 40× objective (EC Plan-Neofluar 40×/1.30 Oil DIC M27) on a confocal microscope (Zeiss LSM 710, Germany).

3.6. Acquisition of FG and Brn3a labeling in retinal wholemounts

Wholemounted retinas were acquired with a 10× objective in an epifluorescence microscope (Axioskop 2 Plus; Zeiss, Germany) equipped with a computer-driven motorized stage (ProScan H128 Series; Prior Scientific Instruments Ltd, United Kingdom), controlled by ImagePro Plus (IPP 5.1 for Windows; Media Cybernetics, USA), as previously described (Salinas-Navarro et al., 2009b). FG$^+$RGC and Brn3a$^+$RGCs were automatically quantified as reported (Salinas-Navarro et al., 2009b). Reconstructed wholemounts, made up from 185 individual frames, were further processed for representative images using Adobe Photoshop® CS 8.0.1 (Adobe Systems, Inc., USA). The Brn3a survival rate was presented as the percentage of the ratio between the OHT-injured retina and the contralateral eye.

3.7. Terminal deoxynucleotidyl transferase-mediated dUTP nick-end labeling assay

Cell death was detected in retinal cryosections with a terminal deoxynucleotidyl transferase-mediated dUTP nick-end labeling (TUNEL) assay kit, as we previously described (Boia et al., 2017). The preparations were visualized in a fluorescence microscope (Axio Observer.Z1, Zeiss, Germany) with a 20× objective (Plan Achromat 20×/0.8 M27). From each eye, four sections were analyzed and the total number of TUNEL$^+$ cells was counted in the entire retinal section and normalized to the length of the respective section.

3.8. Real-time qPCR

Total RNA was extracted from rat retinas using Trizol reagent (Invitrogen, Thermo Fisher Scientific, USA), as we previously described (Boia et al., 2017). SYBR Green-based qPCR was performed using StepOnePlus (Applied Biosystems, USA), with the following primers for Adora3 (F: GCTTGGATTACATGGTCTTC; R: TGAGTTTGTTTCGGATGATG) and Hprt1 (F: ATGGGAGGCCATCACATTGT; R: ATGTAATCCAGCAGGTCAGCAA) was the most stable gene tested, and it was used as the control gene. Ct values were converted to 'relative quantification' using the $2^{-\Delta\Delta Ct}$ method described previously (Livak et al., 2001).

3.9. Transmission electron microscopy

Following transcardial perfusion, the brain was removed, and optic nerve samples were collected close to the optic chiasm. Samples were fixed with 2.5% glutaraldehyde in 0.1 M sodium cacodylate buffer (pH 7.2) for 2 h. Following three washing steps in buffer, postfixation was performed using 1% osmium tetroxide for 90 min. Samples were then rinsed in buffer, dehydrated in a graded ethanol series (70-100%), and embedded in 2% molten agar. Sample pellets were redehydrated in ethanol (30-100%) and then, impregnated and included in Epoxy resin (Sigma-Aldrich, USA). Ultrathin sections were mounted on copper grids and observations were carried out on a FEI Tecnai G2 Spirit BioTWIN (FEI Company, USA) at 100 kV.

3.10. Statistical analysis

The results are presented as mean ± standard error of the mean (SEM). Data points were excluded if identified as outliers with the ROUT algorithm using Prism (GraphPad Software). Statistical analysis was performed with the Prism 5.03 Software for Windows (GraphPad Software, Inc, USA). The normality of the data was assessed with Shapiro-Wilk normality test, and data were analyzed with parametric or nonparametric tests, depending on data distribution.

4. Results

In order to assess the protective effects of the selective A_3R agonist, 2-Cl-IB-MECA was administered by intravitreal injection (1.2 μM, 5 μl) immediately after the induction of OHT.

4.1. Distribution of A_3R in the retina

Previous studies have identified messenger RNA (mRNA) coding for A_3R in rat RGCs (Zhang et al., 2006). In retinal vertical sections from naïve animals, the immunoreactivity of A_3R was mainly observed in the GCL in Brn3a$^+$ cells (Figure 12A), confirming that RGCs are endowed with A_3R. The effect of OHT on the levels of A_3R mRNA in the retina was determined by qPCR. OHT caused an increase of 1.7-fold in A_3R mRNA expression in the retina (Figure 12B).

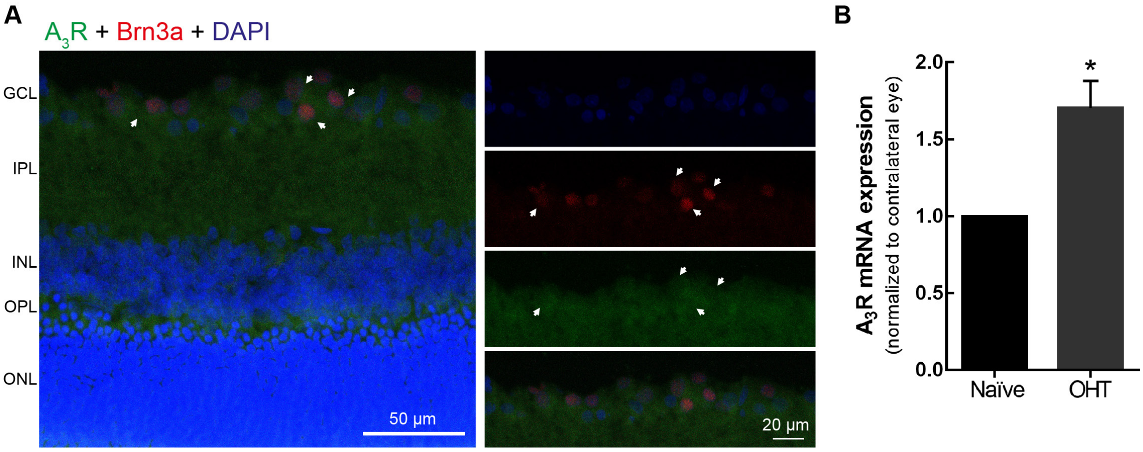

Figure 12 | A_3R is upregulated after 7 days of OHT induction. (A) Representative images of naïve retinal cryosections immunostained for A_3R (green) and Brn3a (RGCs, red) are depicted. Nuclei were stained with DAPI (blue). (**B**) A_3R mRNA expression was assessed by qPCR in naïve and OHT retinas. Results are presented as fold change of OHT eye to naïve, from seven independent experiments. *$p<0.05$, significantly different from the naïve, Wilcoxon's signed-rank test. GCL ganglion cell layer, IPL inner plexiform layer, INL inner nuclear layer, OPL outer plexiform layer, ONL outer nuclear layer.

4.2. Treatment with 2-Cl-IB-MECA attenuates the RGC dysfunction induced by OHT

Retinal function was assessed by ERG, a record of electrical responses in the eye obtained by stimulating the retina with light flashes in either dark-adapted (scotopic) or light-adapted (photopic) conditions (Figure 13A). The a-wave is the first major component of ERG that corresponds to the function of photoreceptors, being in scotopic conditions mainly due to mixed rod and cone response, and in photopic conditions mainly due to cones response (Rosolen et al., 2008). Evidence suggests that the b-wave originates in retinal cells that are postsynaptic to photoreceptors (Rosolen et al., 2008).

Generally, when retinal function deteriorates, the light-induced electrical activity in the retina reduces (Vidal-Sanz et al., 2015). As expected, the amplitude for scotopic a- and b-waves increased with the increase of light intensity in naïve animals (Figure 13B, C). In contralateral retinas, the amplitude of a-wave in scotopic conditions (Figure 13B) and of b-wave in photopic

2

conditions (Figure 13D) decreased when compared with naïve retinas, independently if treated with saline or 2-Cl-IB-MECA. In OHT retinas, the amplitudes of scotopic a- and b-waves, as well as the amplitude of photopic b-wave decreased. These effects were not modified by 2-Cl-IB-MECA, except at lower light flash stimuli in scotopic b-wave.

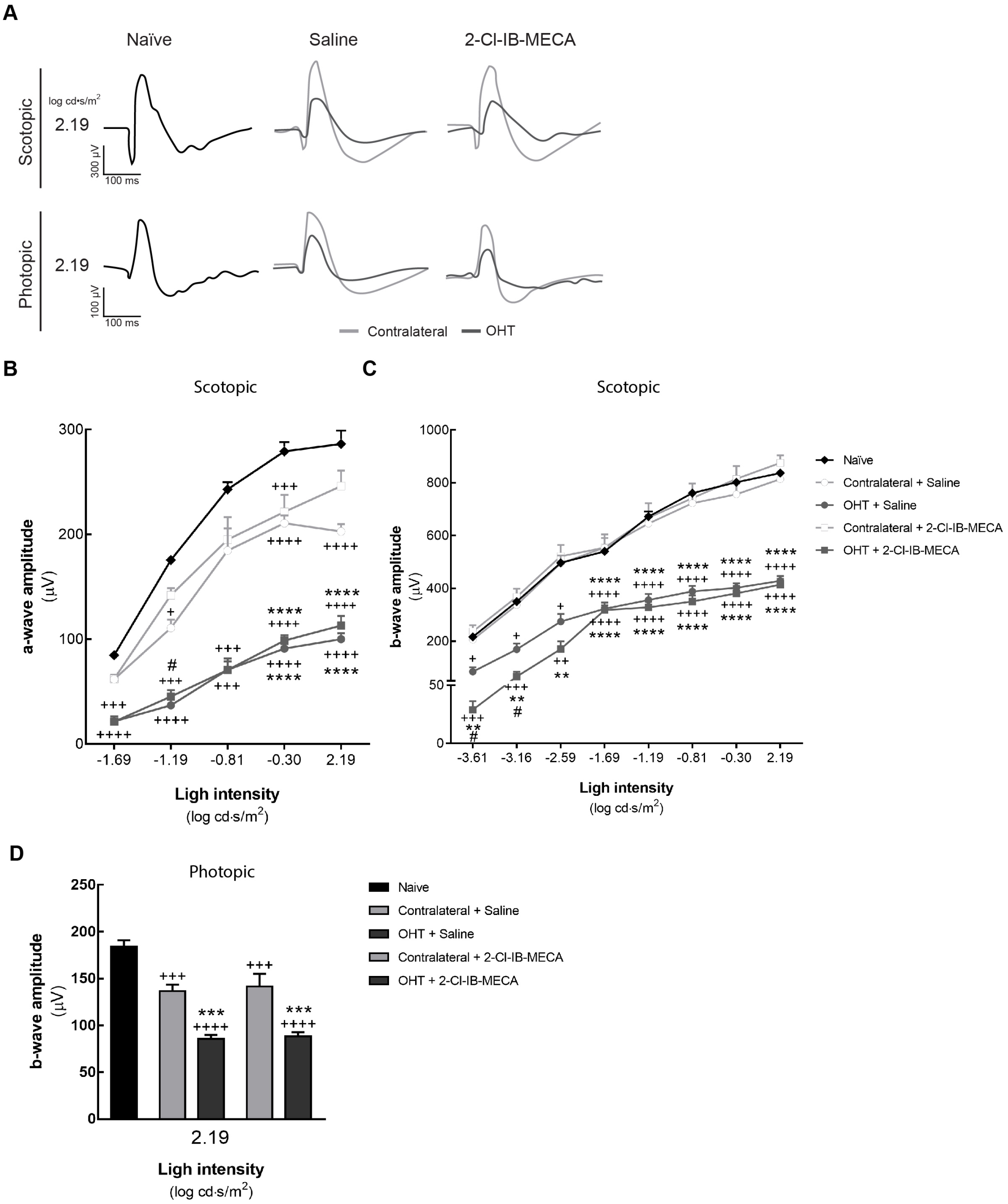

Figure 13 | Treatment with 2-Cl-IB-MECA does not change a-wave and b-wave amplitudes. Saline (5 µl) or 2-Cl-IB-MECA (5 µl, 1.2 µM) was administered by intravitreal injection immediately after laser-induced OHT, and at day 6 after OHT induction the ERG was recorded. (**A**) Representative traces of scotopic a- and b-wave amplitude and photopic b-wave at 2.19 log cd·s/m². (**B, C**) Scotopic a- and b-wave amplitudes recorded at different light intensities. (**D**) Photopic b-wave amplitudes recorded at 2.19 log cd·s/m². Results presented were obtained from 5-6 animals. +$p<0.05$, ++$p<0.01$, +++$p<0.001$, ++++$p<0.0001$, significantly different from naïve; *$p<0.05$, **$p<0.01$, ***$p<0.001$, ****$p<0.0001$, significantly different from contralateral eye; and #$p<0.05$, ##$p<0.01$, significantly different from saline-treated OHT.

The function of RGCs can be assessed by ERG using very dim light intensities after extracting the positive and negative components (Mead et al., 2016). In this work, STR was elicited with light stimuli of -4.7 log cd·s/m^2 (Figure 14A), and the amplitudes of each positive (pSTR, Figure 14B) and negative (nSTR, Figure 14C) components were extracted. OHT decreased the amplitudes of both pSTR and nSTR, and the treatment with 2-Cl-IB-MECA was able to reduce the effect of OHT in pSTR and nSTR amplitudes ($p<0.05$).

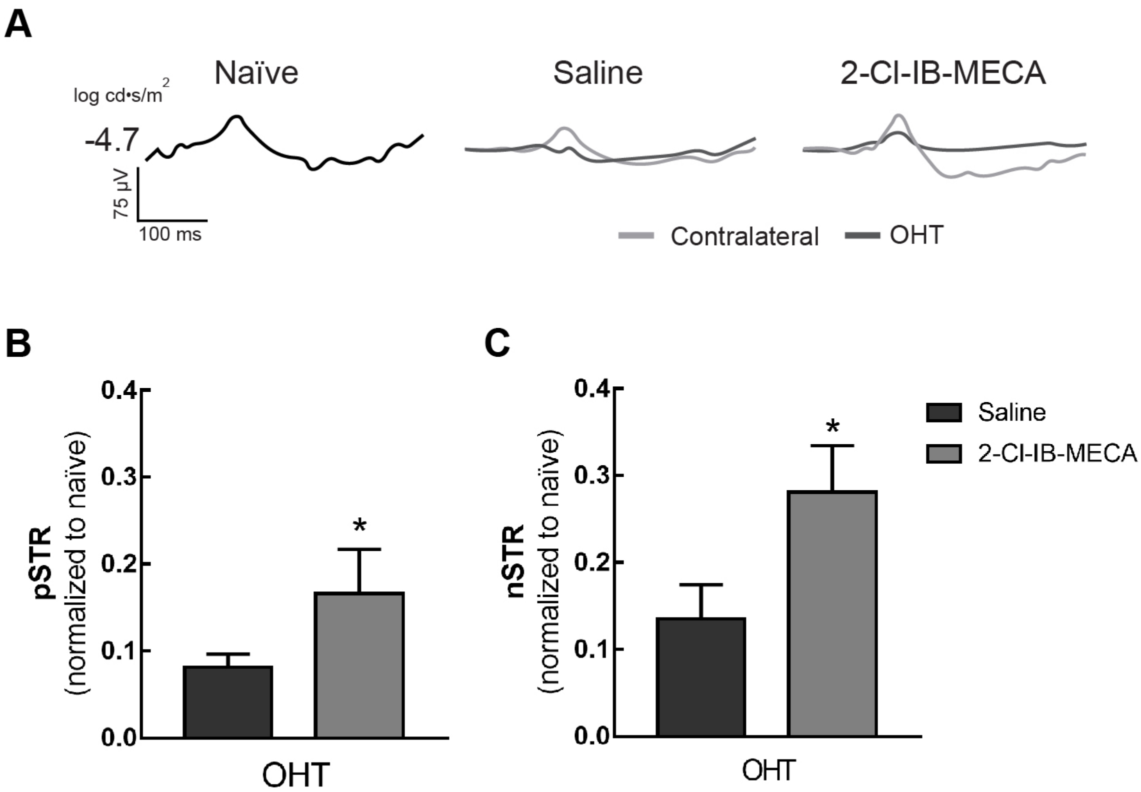

Figure 14 | Treatment with 2-Cl-IB-MECA attenuates the loss-of-function of RGCs induced by OHT. Saline (5 µl) or 2-Cl-IB-MECA (5 µl, 1.2 µM) was administered by intravitreal injection immediately after laser-induced OHT, and at day 6 after OHT induction the STR was recorded. (**A**) Representative traces of STR recordings. (**B, C**) pSTR and nSTR amplitudes recorded at -4.7 log cd·s/m^2, extracted from 5-6 animals. *$p<0.05$, significantly different from the saline-treated OHT.

4.3. A_3R agonist does not change retinal cell death induced by OHT

The TUNEL assay was performed in retinal vertical sections to quantify cell death (Figure 15). The majority of $TUNEL^+$ cells was found in the ONL and INL (Figure 15A), indicating that cells in these layers are also affected by OHT, in accordance with a previous report (Ortin-Martinez et al., 2015). No significant changes in $TUNEL^+$ cells were found in the retinas of contralateral eyes for both groups of animals (saline-treated and 2-Cl-IB-MECA-treated group), when compared with naïve animals. In the OHT-injured retinas treated with saline there were 5.8 ± 2.3 $TUNEL^+$ cells/mm ($p<0.05$, compared with naïve) and in the 2-Cl-IB-MECA-treated retinas there were 3.4 ± 1.7 $TUNEL^+$ cells/mm (Figure 15B).

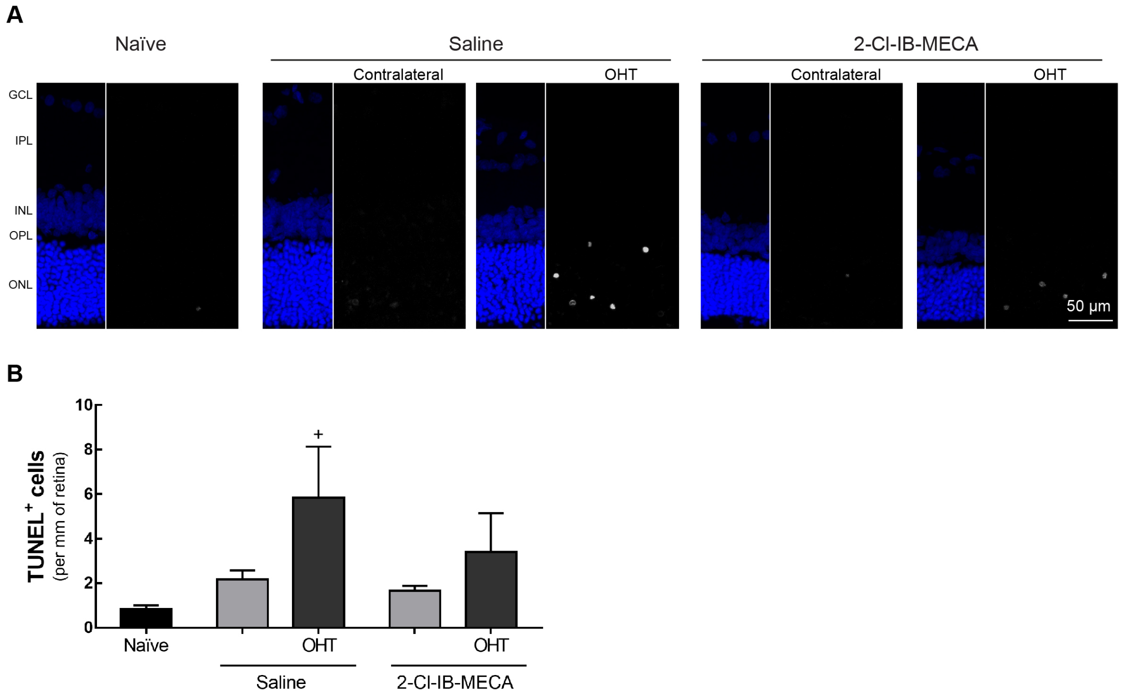

Figure 15 | Treatment with 2-Cl-IB-MECA reduces retinal cell death induced by OHT. Saline (5 µl) or 2-Cl-IB-MECA (5 µl, 1.2 µM) was administered by intravitreal injection immediately after laser-induced OHT. (**A**) Cell death was assayed in retinal cryosections by TUNEL assay (white). Nuclei were stained with DAPI (blue). Representative images are depicted. (**B**) The total number of $TUNEL^+$ cells were counted in the entire retinal section and expressed per length (mm) of the respective retinal section from 5-6 independent experiments. +$p<0.05$, significantly different from naïve. GCL, ganglion cell layer; IPL, inner plexiform layer; INL, inner nuclear layer; OPL, outer plexiform layer; ONL, outer nuclear layer.

4.4. Activation of A_3R increases the survival of RGCs in animals with OHT

Since RGCs express A_3R (Zhang et al., 2006) and 2-Cl-IB-MECA attenuated the effect of OHT in STR, we assessed whether the treatment with the A_3R agonist could protect RGCs. In retinal wholemounts, RGCs were immunolabelled for Brn3a, a specific marker of RGCs (Nadal-Nicolas et al., 2009), and the isodensity maps allowed us to visualize the distribution of RGCs (Figure 16A). The distribution of $Brn3a^+$ RGCs in both naïve and contralateral retinas is similar to a previous report (Nadal-Nicolas et al., 2009), with higher density in the superior retina and a visual-oriented horizontal strip. The total number of $Brn3a^+$ cells was automatically counted (Figure 16B). In naïve retinas, the number of $Brn3a^+$ cells was 72501 ± 1237 cells, similar to our previous work (Madeira et al., 2016b). The treatment of contralateral retinas with saline or 2-Cl-IB-MECA did not significantly affect the number of $Brn3a^+$ cells (83406 ± 5067 cells and 89689 ± 6517 cells, respectively) when compared with naïve retinas. As expected, laser-induced OHT induced a significant loss of $Brn3a^+$ cells (25328 ± 2862 cells, $p<0.01$) that was partially attenuated by the intravitreal injection of 2-Cl-IB-MECA (45299 ± 9640 cells, $p<0.05$; Figure 16B). In fact, the animals treated with 2-Cl-IB-MECA presented 48% of $Brn3a^+$ cells, which is significantly ($p<0.05$) higher when comparing with saline-treated group (survival rate of 31%; Figure 16C).

RBPMS is another RGC marker for quantitative analysis of these cells in animal models of RGC degeneration induced by IOP elevation (Kwong et al., 2010, Kwong et al., 2011). Therefore, the number of RBPMS+ cells was counted in retinal cryosections (Figure 16D). Although not so pronounced, 2-Cl-IB-MECA slightly increased the number of RBPMS+ cells present in OHT retinas (survival rate of 96%) comparing with saline-treated group (survival rate of 77%; Figure 16e).

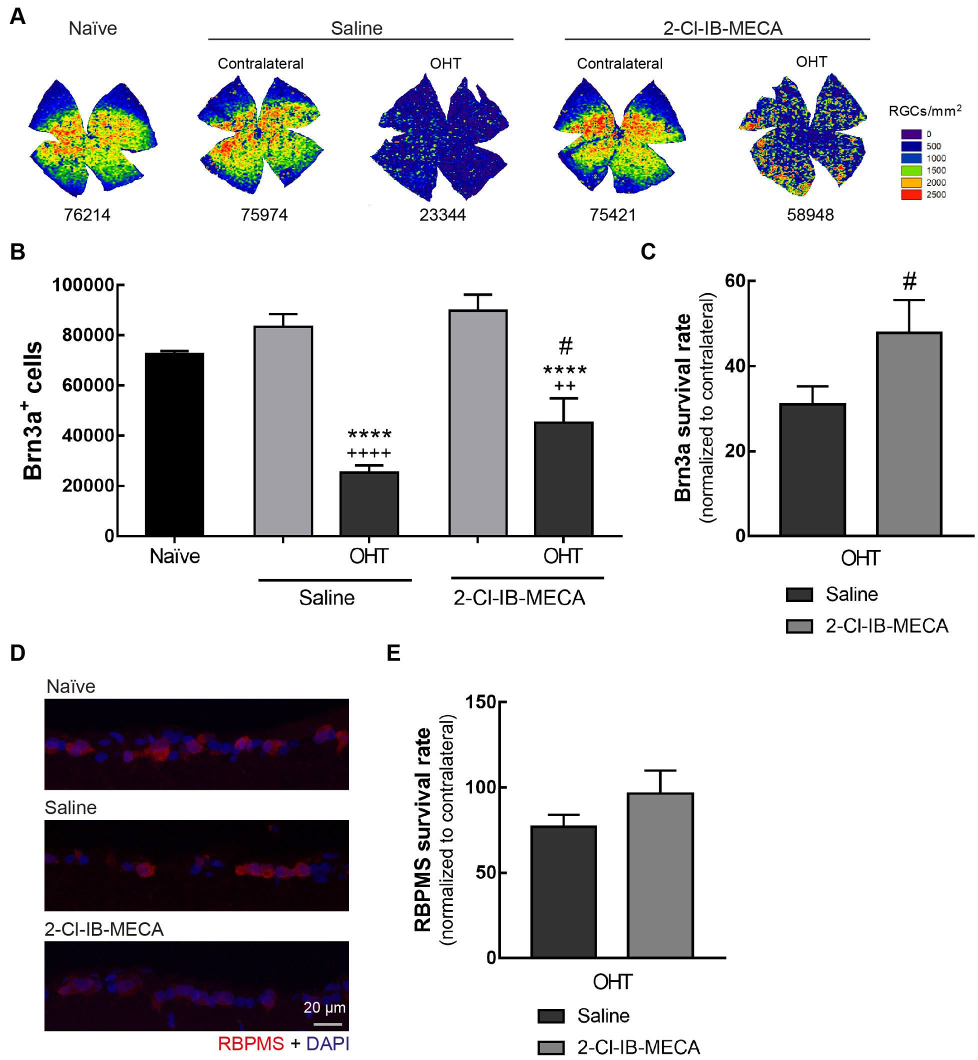

Figure 16 | A_3R agonist increases RGC survival in OHT animals. Saline (5 µl) or 2-Cl-IB-MECA (5 µl, 1.2 µM) was administered by intravitreal injection immediately after laser-induced OHT. (**A**) Representative RGC isodensity maps generated from wholemount preparations from 2-Cl-IB-MECA and saline-treated OHT, and contralateral retinas immunostained for Brn3a. (**B**) The number of total Brn3a+ cells per retina was automatically quantified from 5-6 independent retinas. (**C**) The survival rate of Brn3a+ cells was expressed as the percentage of the ratio between OHT-injured retinas and the contralateral retinas, from 5-6 independent experiments. (**D**) Representative images of retinal cryosections immunostained for RBPMS (red). Nuclei were stained with DAPI (blue). (**E**) The number of RBPMS+ cells were counted in the entire retinal section and normalized to the length of the respective section. The survival rate of RBPMS+ cells was presented as the percentage of the ratio between the OHT-injured retinas and the contralateral retinas, from 5-6 independent experiments. ++p<0.01, ++++p<0.0001, significantly different from naïve; ****p<0.0001, significantly different from the contralateral eye; and #p<0.05, significantly different from saline-treated OHT.

4.5. A_3R agonist prevents structural alterations in the optic nerve induced by OHT and ameliorates the OHT-induced impairment in the optic nerve retrograde transport

Changes in the structure of the optic nerves were assessed by transmission electron microscopy (Figure 17). The optic nerves from animals with OHT presented regions with disorganized axons, including alterations in the myelin sheath (Figure 17B, indicated by black asterisks). The treatment with 2-Cl-IB-MECA was able to partially halt the alterations caused by OHT.

One feature of laser-induced OHT is the impairment of the axonal transport through the optic nerve (Salinas-Navarro et al., 2010). Therefore, since A_3R agonist was able to protect RGCs, we assessed if the treatment with 2-Cl-IB-MECA could change the course of the disease. Optic nerve retrograde transport was assessed by counting the number of FG^+ cells in the retina after application of the dye in the SCi (Figure 18). The induction of OHT did not significantly change the number of FG^+ cells in the contralateral retinas (70067 ± 2271 cells and 63504 ± 5832 cells, for saline or 2-Cl-IB-MECA, respectively) when compared with naïve retinas (73949 ± 1653 FG^+ cells); also similar to our previous report (Madeira et al., 2016b). The number of FG^+ cells significantly decreased to 34122 ± 4090 cells in OHT retinas, but the treatment with 2-Cl-IB-MECA was able to attenuate the effect of OHT (44934 ± 9301 FG^+ cells; Figure 18B). This result suggests that A_3R agonist might improve the axonal transport through the optic nerve.

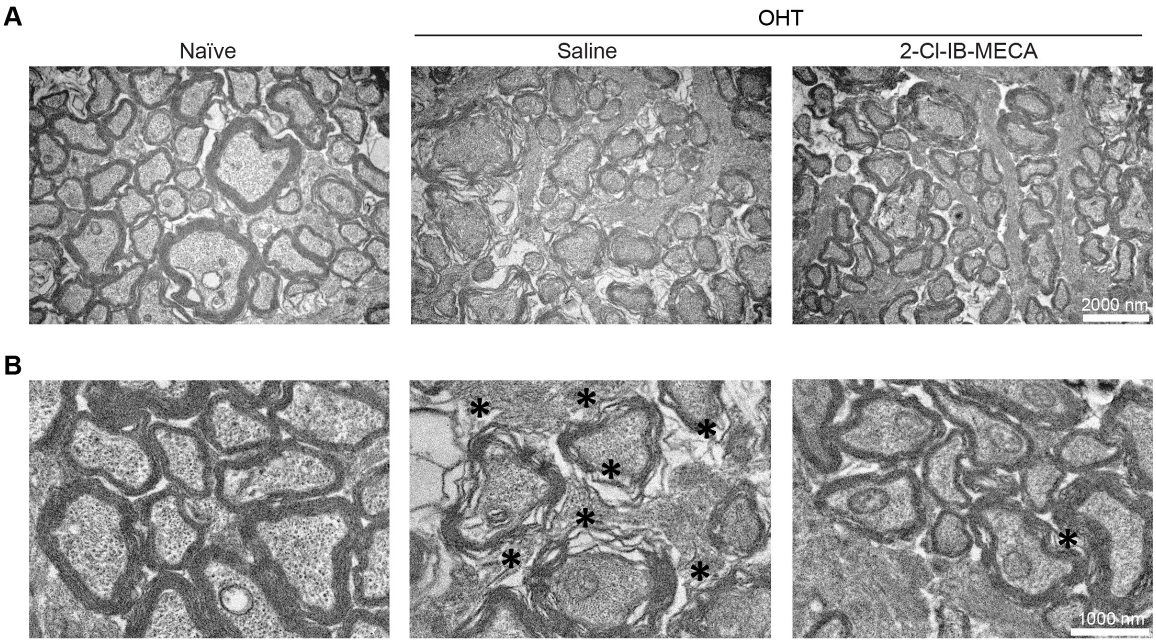

Figure 17 | Treatment with 2-Cl-IB-MECA prevents the structural alterations of optic nerve induced by OHT. Saline (5 µl) or 2-Cl-IB-MECA (5 µl,1.2 µM) was administered by intravitreal injection immediately after laser-induced OHT. Semi-thin cross sections of naïve, saline-, and 2-Cl-IB-MECAtreated OHT retinas were imaged by transmission electron microscopy. Representative images are depicted at (**A**) low magnification and (**B**) higher magnification. Structural alterations like degenerating axons and myelin disarrangement are observed in OHT animals (indicated by black asterisks).

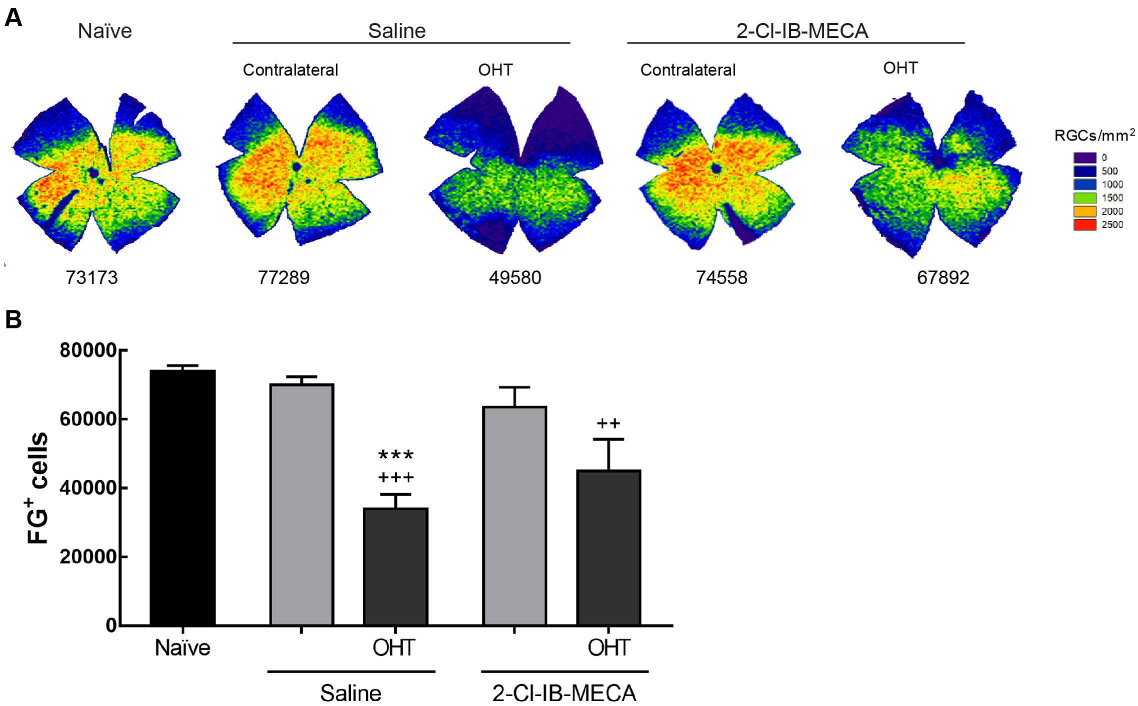

Figure 18 | Treatment with 2-Cl-IB-MECA attenuates the impairment in axonal transport induced by OHT. Saline (5 µl) or 2-Cl-IB-MECA (5 µl, 1.2 µM) was administered by intravitreal injection immediately after laser-induced OHT. (**A**) Retrograde axonal transport was assessed after FG application in the superior colliculus (SCi) at 24 h after OHT induction. Representative isodensity maps generated from wholemount preparations from 2-Cl-IB-MECA, and saline-treated OHT and contralateral retinas labeled with FG. (**B**) The total number of FG^+ cells was automatically quantified from 5-6 independent experiments. ++$p<0.01$, +++$p<0.001$ significantly different from naïve; and ***$p<0.001$ significantly different from contralateral eye.

2

5. Discussion

The results presented herein demonstrate that the treatment with an agonist of A_3R confers protection to RGCs against damage induced by OHT. In addition, we showed that the activation of A_3R attenuated the loss of function of RGCs and the alterations of their axons. Previously, we demonstrated that the activation of A_3R protects the retina, including RGCs against transient ischemic damage (Galvao et al., 2015). However, in this previous work, the A_3R agonist 2-Cl-IB-MECA was administered prior injury and the protective effects were evaluated 24 h after. In the current work, we extended the previous knowledge by evaluating the potential therapeutic properties of A_3R agonist in a model of OHT by administering the drug immediately after inducing OHT, and assessing the outcome 7 days after the treatment. Previously, we showed that the A_3R-selective antagonist (MRS 1191) abolishes the protective effects of the A_3R agonist against cell death induced by glutamatergic excitotoxicity in primary rat retinal neural cultures and in retinal organotypic cultures (Galvao et al., 2015), showing that the protective effects are mediated by A_3R activation.

Several animal models have been developed to mimic glaucoma and the laser photocauterization of the perilimbar and episcleral veins to induce OHT has been a widely used method in adult albino rats (Vidal-Sanz et al., 2015). In this animal model, IOP raises in the first 24 h post OHT induction and it is constantly maintained elevated during the first week (Ortin-Martinez et al., 2015). Our study was conducted to assess the protective properties of 2-Cl-IB-MECA against the loss of RGCs induced by OHT within the period of elevated IOP to avoid possible confounding effects of IOP normalization.

Apoptotic cell death has been described in glaucomatous patients and experimental models (Berkelaar et al., 1994, Quigley et al., 1995, Kerrigan et al., 1997). In the OHT animals, the majority of apoptotic cells ($TUNEL^+$ cells) were located at the ONL. It has been proposed that glaucoma causes not only RGC death, but also degeneration of cells in the ONL, most likely photoreceptors that are lost due to laser-induced photocoagulation (Salinas-Navarro et al., 2009a, Cuenca et al., 2010, Georgiou et al., 2014, Vidal-Sanz et al., 2015). In fact, death of photoreceptors has also been described in glaucoma patients (Holopigian et al., 1990, Panda et al., 1992, Nork et al., 2000). In the animals with OHT, the decrease in the amplitudes of a- and b-waves of the full-field ERG in scotopic and photopic conditions strongly suggests that other cells apart from RGCs are affected in glaucomatous conditions. Surprisingly, $TUNEL^+$ cells were not observed in the GCL, despite the loss of RGCs. Retinal microglia are the resident immune cells that become reactive in the retinas of laser-induced OHT eyes (de Hoz et al., 2013). One possible explanation for the lack of $TUNEL^+$ cells in GCL could be the fact that microglial cells are actively clearing the tissue from dead RGCs. In fact, we recently demonstrated that elevated pressure increases the number of engulfed $TUNEL^+$ cells by microglia (Aires et al., 2019a) and the observation of transcellularly labeled microglial cells with FG also favors this hypothesis (Nadal-Nicolas et al., 2017).

Beyond RGC dysfunction, axonal transport is also impaired in experimental glaucoma (Mabuchi et al., 2003, Salinas-Navarro et al., 2010, Calkins 2012). FG has been the tracer of choice to evaluate retrograde transport through axons of RGCs from SCi to the retina (Mead et al., 2016). The tracer can be applied in SCi and the number of FG^+ cells in the retina can be easily counted (Nadal-Nicolas et al., 2009). In the current study, FG was administered after laser photocoagulation in order to guarantee that FG^+ cells represent the RGCs with nonimpaired axonal transport. In the laser-induced OHT group, impaired retrograde axonal transport and RGC loss were found, and are in accordance with previous reports (Salinas-Navarro et al., 2010, Ortin-Martinez et al., 2015).

2

We found that OHT impacted the amplitudes of scotopic a-wave and photopic b-wave in the contralateral retinas. These alterations were never reported previously and reinforce the importance of appropriate controls (naïve and contralateral) when assessing the changes triggered by OHT. In fact, bilateral response to experimental injury in rodents has been described to cause, at least, microglial activation (Gallego et al., 2012, Choe et al., 2014) and RGC loss (Macharadze et al., 2009, Lucas-Ruiz et al., 2019).

A_3R has been implicated in many ocular diseases, like autoimmune uveitis, dry eye syndrome, and glaucoma (Fishman et al., 2013). The safety and efficacy of CF101 (IB-MECA, an agonist for A_3R) is being assessed in a randomized clinical trial in patients with elevated IOP (ClinicalTrials.gov Identifier: NCT01033422). CF101 was able to decrease IOP in a dry eye syndrome phase II clinical study (Avni et al., 2010). In fact, A_3R contributes to the regulation of IOP (Avila et al., 2002), and data from the clinical trial demonstrate that CF101 was effective as an IOP-lowering agent (Avni et al., 2010). A_3R was identified in rat RGCs (Zhang et al., 2006), and more recently also in NFL and RPE of Rhesus monkeys (Beach et al., 2018). There are no evidences of A_3R expression in the outer retina of rodents. However, it has been suggested that A_3R may be located in neurons of the inner retina that would contribute to the generation of the ERG a- and b-waves (Jonsson et al., 2017). Overall, in our experimental conditions, no changes were observed in a- and b-waves amplitudes in scotopic and photopic ERG, but different drug concentration and timepoints may help explaining these differences.

The activation of A_3R attenuated the decrease in FG^+ cells and increased the survival of $Brn3a^+$ cells induced by OHT. The degenerative process of RGCs is accompanied by structural alterations in RGC axons (Nickells 2007). The intravitreal injection of 2-Cl-IB-MECA preserved the structure of the optic nerve, consistent with the data on FG axonal transport. The A_3R agonist 2-Cl-IB-MECA promotes neurite outgrowth in cultured RGCs and axonal regeneration in the optic nerve crush model through the activation of an Akt-dependent signaling pathway (Nakashima et al., 2018). In our model, similar pathways could be activated in the RGC soma, which may contribute to the improvement in axonal transport.

It is well established that RGCs are lost in the laser-induced OHT animal model of glaucoma (Salinas-Navarro et al., 2010, Ortin-Martinez et al., 2015). Interestingly, even using different markers (Brn3a and RBPMS) and preparations for assessing RGC loss (retinal cryosections and wholemounts), the magnitude found for the protection of RGCs due to the treatment with the A_3R agonist was very similar. The A_3R agonist increases the survival of $Brn3a^+$ RGCs by 54% (survival rate: 31% in saline-treated group and 48% in 2-Cl-IB-MECA-treated group) and by 24% in the case of $RBPMS^+$RGCs (survival rate: 77% in saline-treated group and 96% in 2-Cl-IB-MECA-treated group). There is some controversy regarding the most reliable marker for RGC, especially in the case of RGC degeneration (Mead et al., 2016). Brn3a is a POU-domain transcription factor expressed in RGCs (Wegner et al., 1993) and is downregulated in injured RGCs (Nadal-Nicolas et al., 2012) in a caspase-3-dependent pathway (Sanchez-Migallon et al., 2016). However, since this downregulation occurs near the death of RGC, it does not hinder accurate counting of RGCs using Brn3a, as a cell marker (Nadal-Nicolas et al., 2009, Mead et al., 2014). Nevertheless, some authors report a downregulation of Brn3a prior RGCs loss (Mead et al., 2016), suggesting the use of other markers. RBPMS has been proposed as a marker of RGCs even in the case of neurodegeneration (Kwong et al., 2010, Kwong et al., 2011). Despite the different extension of the injury when comparing Brn3a$^+$RGCs and RBPMS$^+$RGCs, the protection conferred by 2-Cl-IB-MECA is similar comparing both markers. Therefore, regardless the most reliable marker for RGCs, there is no doubt of the protective properties of 2-Cl-IB-MECA. The STR is considered to reflect the activity of RGCs (Mead et al., 2016). Indeed, a single intravitreal injection of A_3R agonist was able to attenuate the effect of OHT on the amplitude of pSTR and nSTR elicited at -4.7 log cd·s/m^2. The mechanism by which A_3R activation mediates protection to RGCs may involve a decrease in Ca^{2+} influx (Zhang et al., 2010), although this was not addressed in this work. Indeed, it has been described that an increase in Ca^{2+} influx in RGCs mediated by transient receptor potential vanilloid 1 channel activation leads to pressure-induced RGCs death (Sappington et al., 2009).

One important consideration is that the effects mediated by A_3R agonist were only assessed 7 days after one single injection. Although repeated injections may cause several side effects, such as inflammation, endophthalmitis, retinal detachment, and cataracts (Sampat et al., 2010), one could hypothesize that the beneficial effects of A_3R activation could be potentiated if other therapeutic regimens had been adopted.

Taking together, these results demonstrate that A_3R activation may be a promising novel therapeutic strategy focusing on the protection of RGCs for the treatment of glaucoma.

6. Conclusions

Glaucoma is characterized by the loss of RGCs and degeneration of their axons, affecting cell function. The current treatments for this disease are dependent on the control of IOP, the only modifiable risk factor. However, in some patients despite having controlled IOP, the disease still progresses. Therefore, there is an emergent need for new therapeutic strategies to manage glaucoma. Drugs targeting RGCs protection may have potential to be effective for the treatment of glaucoma, additionally to IOP-lowering agents. The treatment with A_3R agonist prevented the loss of RGCs, and attenuated the loss-of-function of RGCs and the retrograde axonal transport failure induced by OHT. Concluding, our data shed light on a novel potential therapeutic strategy for glaucoma, using the A_3R activation as an IOP-independent neuroprotective therapeutic strategy for glaucoma.

Porous poly(ε-caprolactone) implants: A novel strategy for efficient intraocular drug delivery

Boia R*, Dias PAN*, Martins JM, Galindo-Romero C, Aires ID, Vidal-Sanz M, Agudo-Barriuso M, de Sousa HC, Ambrósio AF, Braga MEM, Santiago AR

* Authors contributed equally to this work

J Control Release. 2019;316:331-348.
doi:10.1016/j.jconrel.2019.09.023

1. Abstract

This work reports the development of porous PCL-based intraocular implants, prepared by green supercritical carbon dioxide ($scCO_2$)-assisted foaming/mixing method (SFM), to produce implants that degrade faster than typical slow-degrading PCL-based implants. The higher porosities and surface areas of these implants led to faster degradation rates at *in vitro* accelerated alkaline conditions than low porosity/surface area implants prepared by hot melting (HM) processing. These porous implants also presented distinct (faster) release rates of a test drug (dexamethasone). Additionally, these porous devices did not cause cell death and did not reduce the number of neurons, indicating that are not toxic to retinal cells. We further explored the impact of PCL-based implant to the retina by *in vivo* evaluation and histological analysis. Implants were surgically inserted in the vitreous of Wistar rats, and their presence did not change the function, structure and anatomy of the retina. These devices demonstrated a good intraocular tolerance, further confirming their viability for prolonged drug delivery applications. Further comprehensive studies based on this promising preliminary assessment and proof-of-concept could enable its future translation to clinical protective strategies for retinal diseases.

3

Graphical Abstract

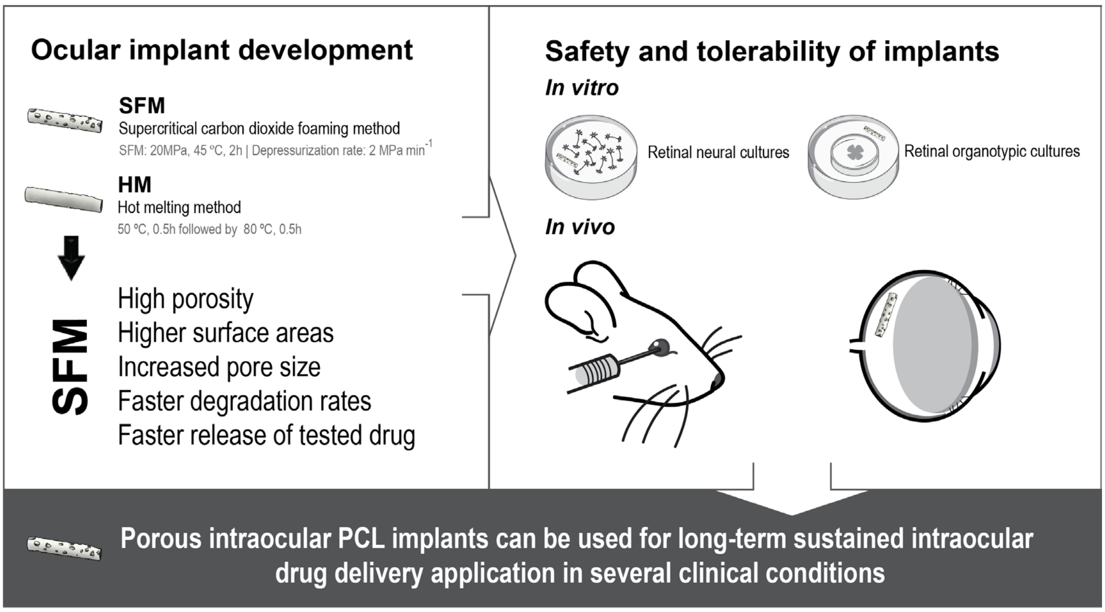

2. Introduction

Chronic retinal diseases, as AMD, glaucoma and diabetic retinopathy, represent 84% of visual impairment worldwide (Bourne et al., 2017). The therapeutic options mainly include topical drug administration using eye drops or intravitreal injections (Bourne et al., 2017). Topical drug delivery is non-invasive and easily performed by the patient (Yellepeddi et al., 2016), however the application of eye drops needs to be quite frequent and leads to poor patient compliance (Claxton et al., 2001, Nordstrom et al., 2005, Sleath et al., 2006, Reardon et al., 2011). Intravitreal injections are currently the main method to deliver drugs into the posterior segment of the eye (Kim et al., 2014b), however the need to maintain therapeutic drug levels require frequent injections that may cause several side effects such as inflammation, endophthalmitis, retinal detachment and cataracts (Sampat et al., 2010). Therefore, intraocular drug delivery systems based on biodegradable and biocompatible polymeric materials may have the potential to circumvent some of the aforementioned drawbacks (Kimura et al., 2001, Yasukawa et al., 2005, Silva-Cunha et al., 2009). These systems can be designed to maintain the therapeutic concentrations for extended periods, reducing the frequency of administration and increasing patient compliance (Kimura et al., 2001). The use of biodegradable polymeric drug delivery systems usually overcomes the need of surgical removal after the drug has been exhausted that happens in the case of non-biodegradable implants (Kimura et al., 2001, Yasukawa et al., 2011).

PCL is a biocompatible and bioresorbable synthetic polymer approved by US FDA that has been extensively studied and applied in implants for ophthalmic controlled drug delivery (Fialho et al., 2008, Silva-Cunha et al., 2009, Kim et al., 2016, Kim et al., 2018). In particular, PCL intraocular implants have been prepared for the delivery of dexamethasone (Fialho et al., 2008, Silva-Cunha et al., 2009). In addition to the controlled delivery of drugs loaded within the matrix, which is mainly controlled by water sorption and by its hydrolytic degradation, PCL presents other important advantages such as its tailorable physical and mechanical properties, and ease of shaping and processing at relatively low temperatures (Kimura et al., 2001, Woodruff et al., 2010).

Typical manufacturing techniques used to prepare these polymeric implants are HM, extrusion, 3D-printing, injection moulding or solution casting (Yasukawa et al., 2005). However, these methods may involve hazardous solvents and/or operate at processing conditions (e.g., temperature, pH) that could promote the degradation of the polymers, drugs and other additives (Yasukawa et al., 2005, de Matos et al., 2013). Alternatively, the SFM method can be used to avoid most of these problems. The temporary plasticizing effect of $scCO_2$ leads to operating temperatures considerably lower than typical polymer melting temperatures at atmospheric pressure, thus allowing sensitive drugs to be loaded at mild conditions. In addition, hazardous solvents are usually absent in this method. SFM methodologies have been successfully applied to several thermoplastic polymers, including PCL and other poly(ε-esters), to obtain materials with tuneable physical and morphological properties, such as polymer crystallinity, porosity, pore size distributions, pore interconnectivity, and surface area, just by controlling the final depressurization step rate and/or the amount of absorbed CO_2 (and varying the other operational conditions such as processing time, temperature and pressure) (Shieh et al., 2005, de Matos et al., 2013, de Matos et al., 2015, Di Maio et al., 2018, Salerno et al., 2019). The typical high porosities introduced in thermoplastic polymers by the SFM process may have the potential to increase the hydrolytic and enzymatic degradation rates of poly(Ɛ-esters), namely by increasing surface area, water sorption/swelling rates, and the available reaction sites at the surface, which are quite important advantageous features for slow degrading polymers such as PCL (Lam et al., 2008, Vidaurre et al., 2008). To the best of our knowledge, no porous implant (of the monolithic type) has yet reached the market. However, previous studies suggest that highly porous materials prepared by SFM can be designed for a better control of drug release (de Matos et al., 2013).

Therefore, the present work aimed to use the SFM method to develop and to characterize a new, biodegradable and porous intraocular implant that may present faster degradation rates and, at the same time, still control the release of drugs over time. The morphologies, thermal properties and the degradation kinetics profiles (at accelerated alkaline conditions) of prepared SFM drug-free implants were assessed and compared with non-porous implants prepared by a typical HM process. Additionally, the safety of SFM drug-free implants to the retina was assessed by extended and meticulous *in vitro* and *in vivo* studies. Finally, these new implants were tested for the incorporation yields and for the *in vitro* release kinetics of a test-drug, dexamethasone, a well-known anti-inflammatory and immuno-suppressant glucocorticoid already used for the treatment of ocular pathologies (Kaji et al., 1997, Kim et al., 1999, Chim et al., 2012, de Matos et al., 2013).

3. Materials and methods

3.1. Animals

Adult Wistar rats were housed in a standard animal room under controlled environment with free access to food and water. All procedures were approved by the Animal Welfare Committee of the Coimbra Institute for Clinical and Biomedical Research of the Faculty of Medicine of University of Coimbra (ORBEA 23/2015) and were conducted in accordance to the Portuguese law (Decreto-Lei nº113/2013) and to the Association for Research in Vision and Ophthalmology statement for animal use.

3.2. Safety for the retinal cells: *in vitro* experiments

3.2.1. Primary culture of rat retinal neural cells

Retinal neural cell cultures were obtained from 3-day-old Wistar rats, as previously described (Santiago et al., 2006). The cells were plated at a density of 2×10^6 cells cm^{-2} in 12-well plates with glass coverslips previously coated with poly-D-lysine (0.1 mg mL^{-1}; Sigma-Aldrich, Missouri, USA) and cultured in Eagle's minimum essential medium (MEM, Sigma-Aldrich, Missouri, USA), supplemented with 26 mM $NaHCO_3$, 25 mM HEPES, 10% heat-inactivated fetal bovine serum (FBS; GIBCO, Invitrogen, Life Technologies, California, USA), penicillin (100 U mL^{-1}; Sigma-Aldrich, Missouri, USA), and streptomycin (100 g mL^{-1}; Sigma-Aldrich, Missouri, USA) in a humidified atmosphere of 5% CO_2 at 37 °C for seven days. After one day in culture (one day *in vitro*, DIV1), cell cultures were incubated with PCL-based implants or with medium that was in contact with drug-free implants for 3 weeks (to check for the effects of any PCL degradation products).

3.2.2. Organotypic retinal cultures

The retinas from Wistar rats (8-10 weeks old) were dissected in Hanks' balanced salt solution (HBSS, in mM: 137 NaCl, 5.4 KCl, 0.45 KH_2PO_4, 0.34 Na_2HPO_4, 4 $NaHCO_3$, and 5 glucose; pH 7.4) and placed in tissue culture inserts with a 0.4 µm pore size (Millicell, Millipore, Massachusetts, USA), with the GCL facing up. The retinas were cultured for 4 days in Neurobasal-A medium (GIBCO, Invitrogen, Life Technologies, California, USA) supplemented with B27 (GIBCO, Invitrogen, Life Technologies, California, USA), 2 mM L-glutamine (Sigma-Aldrich, Missouri, USA) and gentamicin (50 mg mL^{-1}; GIBCO, Invitrogen, Life Technologies, California, USA), in 5% CO_2 humidified atmosphere, as previously described (Madeira et al., 2015b).

The cultures were incubated with PCL-based implant for 24 h, 48 h and 72 h or with culture medium that was previously in contact for four weeks with these implants (PCL-based metabolites) for four days.

3.3. Safety for the retina: *in vivo* experiments

3.3.1. Surgical procedure for implantation of SFM-processed drug-free PCL based implants

The animals were randomly assigned into sham-operated group or implant-inserted group. Animals were anesthetized with 2.5% isoflurane (IsoFlo; Abbott Laboratories, Illinois, USA) with 1 L min^{-1} of O_2. Oxybuprocaine (4 mg mL^{-1}, Anestocil, Edol, Portugal) and tropicamide (10 mg mL^{-1}, Tropicil Top, Edol, Portugal) were applied topically for corneal anesthesia and mydriasis, respectively. One SFM-processed drug-free PCL-based implant (92:00:08, wt.%) was introduced in the vitreous with a 24-gauge catheter after making an incision in the sclera with a 23-gauge needle. Animals were sacrificed 4 and 8 weeks after the surgery.

3.3.2. Measurement of intraocular pressure (IOP)

Animals were trained for manipulation for IOP measurement during 2 weeks before surgical procedure. After implantation, IOP was measured bilaterally with a rebound tonometer specifically designed for rodents (Tonolab®, Icare, Finland), twice a week until sacrifice, as previously described (Boia et al., 2017). An average of ten reliable measurements made in each eye was considered as one reading and reported as the IOP for that eye. The average of the IOP values obtained during the study interval was reported.

3.3.3. Optical coherence tomography (OCT)

Retinal structure was evaluated by OCT using a Micron IV (Phoenix Research Labs, California, USA) with a contact lens specifically designed for rat. The animals were anesthetized by intraperitoneal injection of ketamine (90 mg kg^{-1}; Nimatek, Dechra, UK) and xylazine (10 mg kg^{-1}; Sedaxylan, Dechra, UK). After topical anesthesia with oxybuprocaine (4 mg mL^{-1}, Anestocil, Edol, Portugal) and pupillary dilation with tropicamide (10 mg mL^{-1}, Tropicil Top, Edol, Portugal), both eyes were imaged and 13 B-scans centered in the optic nerve head were acquired. Total retinal thickness was obtained after segmentation using the semi-automatic segmentation software InSight (Phoenix Research Labs, California, USA).

3.3.4. Electroretinogram (ERG) recordings

Retinal activity was evaluated by electroretinography using corneal gold wire electrodes as previously described (Martins et al., 2011). ERGs were performed under red dim light after overnight dark adaptation of the animals. Animals were anesthetized and topical anesthetic and mydriatic were applied, as described above. Methylcellulose (Methocel 2%, OmniVision, California, USA) was applied for a good contact between cornea and gold ring electrode. A Ganzfeld stimulator (Roland Consult GmbH, Germany) with white light flashes (0.0095-9.49 cd-s m^{-2}) was used and scotopic ERG was recorded. The amplitude (μV) and latency (ms) of a-wave and b-wave in scotopic conditions (reflecting rod response) were extracted. Off-line digital filter was applied on b-wave (high frequency cut-off of 50 Hz) with the RETIport software (Roland Consult GmbH, Germany).

3.4. Immunolabelling

3.4.1. Retinal cell cultures

Cell cultures were immunostained as previously described (Madeira et al., 2016a). Cells were washed with phosphate-buffered saline (PBS, in mM: 137 NaCl, 2.7 KCl, 10 Na_2HPO_4, 1.8 KH_2PO_4; pH 7.4) and fixed with 4% PFA with 4% sucrose for 10 min. Then, cells were permeabilized with

1% Triton X-100 and blocked with 3% bovine serum albumin (BSA) and 0.2% Tween 20. The cells were incubated with the primary antibody (Table 4), followed by incubation with the secondary antibodies (Table 4). The nuclei were stained by incubation with 4',6'-diamidino-2-phenylindole (DAPI; 1:2000; Invitrogen, Life Technologies, California, USA) for 10 min. The preparations were mounted with Glycergel mounting medium (DAKO, California, USA) and were observed in a fluorescence microscope (Axio Observer.Z1, Zeiss, Germany). For each condition, 10 images per coverslip were randomly acquired with a 20× objective (Plan Achromat 20×/0.8 M27). In order to compare the different conditions, all images were acquired using identical gain and exposure settings.

3.4.2. Organotypic retinal cultures

Retinal organotypic cultures were immunostained as previously described (Madeira et al., 2015b). Briefly, retinas were washed with PBS and fixed with ice-cold 100% ethanol for 10 min at 4 °C. After washing with PBS, retinas were incubated with blocking solution (3% BSA, 10% normal goat serum and 0.1% Triton X-100) for 1 h at room temperature. Samples were then incubated with the primary antibodies (Table 4) in blocking solution for 48 h at 4 °C, followed by incubation with the secondary antibodies (Table 4) overnight at 4 °C. Nuclei were counterstained with DAPI (1:1000; Invitrogen, Life Technologies, California, USA) and the samples were then flat-mounted on glass slides with the GCL facing upwards and cover slipped with Glycergel mounting medium (DAKO, California, USA). The preparations were observed in a confocal microscope (Zeiss LSM 710, Germany) and images were randomly acquired with a 20× objective (Plan Achromat 20×/0.8 M27). From each retina, 3 images per quadrant were acquired (total of 12 images per sample). All images were acquired using identical gain and exposure settings to compare the different conditions.

3.4.3. Retinal cryosections

Retinal cryosections were prepared as previously described (Boia et al., 2017). Retinal sections were permeabilized with 0.25% Triton X-100 in PBS for 30 min and blocked in 10% normal goat serum plus 1% BSA in a humidified environment. Then, the sections were incubated with the primary antibodies (Table 4), followed by incubation with respective secondary antibodies (Table 4). Nuclei were counterstained with DAPI (1:2000; Invitrogen, Life Technologies, California, USA) and the slices were mounted with Glycergel mounting medium (DAKO, California, USA). The preparations were observed in a confocal microscope (Zeiss LSM 710, Germany) and images were acquired with a 20× objective (Plan Achromat 20×/0.8 M27).

3.4.4. Retinal wholemounts

After transcardiac perfusion of animals, eyes were enucleated and retinas were dissected as flattened wholemounts, as previously reported (Salinas-Navarro et al., 2009b). The retinas were permeabilized with 0.5% Triton X-100 and incubated with the primary antibodies (Table 4). Retinas were incubated with the secondary antibodies (Table 4) and mounted with GCL side up and covered with anti-fading mounting medium.

Wholemounted retinas were acquired with a 10× objective under an epifluorescence microscope (Axioskop 2 Plus; Zeiss Microscopy, Germany) equipped with a computer-driven motorized stage (ProScan H128 Series; Prior Scientific Instruments, UK), controlled by Image-Pro Plus (IPP 5.1 for Windows; Media Cybernetics, Maryland, USA), as previously described (Salinas-Navarro et al., 2009b). Reconstructed wholemounts, made up from 154 individual frames, were further processed when required using Adobe Photoshop® CS 8.0.1 (Adobe Systems, Inc., California, USA). The total population of Brn3a$^+$RGCs was automatically quantified by processing the individual Brn3a images taken for each retinal wholemount with a specific cell-counted routine developed for the IPP software. Isodensity maps were generated with the IPP software to evaluate the spatial distribution of Brn3a$^+$RGCs throughout the entire retinal surface (for more details, see Salinas-Navarro et al., 2009b).

Table 4 | List of primary and secondary antibodies used in this study

	Supplier	Cat. No	Host	Dilution	Sample
Primary antibodies					
anti-Arrestin	Millipore	AB15282	Rabbit	1:500	Retinal cryosections
anti-Brn3a	Millipore	MAB1585	Mouse	1:200	Organotypic retinal cultures/ Retinal cell cultures
	Santa Cruz Biotecnologies	sc-31984	Goat	1:750	Retinal wholemounts
anti-Calbindin	Swant	CB-38a	Rabbit	1:500	Retinal cryosections
Anti-Calnexin	Sicgen	AB0041-500	Goat	1:5000	Protein levels
anti-GFAP	Millipore	IF03L	Mouse	1:500	Retinal cryosections/ Protein levels
anti-Iba1	Wako	019-19741	Rabbit	1:1000	Retinal cryosections
anti-NeuN	Cell Signaling	D4G40	Rabbit	1:500	Retinal cell cultures
anti-PKCα	Santa Cruz	sc-8393	Mouse	1:500	Retinal cryosections
anti-Rhodopsin	Millipore	MABN15	Mouse	1:500	Retinal cryosections
anti-Vimentin	Abcam	AB92547	Rabbit	1:500	Retinal cryosections
Secondary antibodies					
Alexa Fluor anti-rabbit 488	Life Technologies	A11008	Goat	1:500	
Alexa Fluor anti-mouse 568	Life Technologies	A11004	Goat	1:500	
Alexa Fluor anti-goat 594	Life Technologies	A11058	Donkey	1:500	
Alexa Fluor Anti-Rabbit 568	Life Technologies	A11036	Goat	1:200	
HRP-conjugate Anti-mouse	Bio-Rad	1706516	Goat	1:10000	
AP Anti-goat	Thermo Scientific	31300	Rabbit	1:10000	

3.5. Enzyme-linked immunosorbant assay (ELISA) for quantification of TNF and IL-1β protein levels

Protein levels of interleukin-1β (IL-1β) and TNF were quantified in the culture medium supernatants and in the retinas by ELISA, according to the instructions provided by the manufacturer (PeproTech EC Ltd, UK) and as previously described (Madeira et al., 2016a).

3.6. Terminal deoxynucleotidyl transferase (TdT)-mediated dUTP nick end labeling (TUNEL) assay

Rat retinal neural cell cultures were fixed with 4% PFA with 4% sucrose for 10 min. Cell death was assessed using DeadEnd™ Fluorometric TUNEL System following the manufacturer's instructions (Promega, Wisconsin, USA). The nuclei were stained with DAPI (1:2000; Invitrogen, Life Technologies, California, USA). After washing, the preparations were mounted with Glycergel mounting medium (DAKO, California, USA). The preparations were observed in a fluorescence microscope (Axio Observer.Z1, Zeiss, Germany). For each condition, 10 images per coverslip were randomly acquired with a 20× objective (Plan Achromat 20×/0.8 M27).

3.7. Western blot

Retinas were lysed in ice-cold radioimmunoprecipitation assay (RIPA) buffer (50 mM Tris, 150 mM NaCl, 5 mM EGTA, 1% Triton X- 100, 0.5% DOC, 0.1% SDS) supplemented with 1 mM dithiothreitol (DTT, Sigma-Aldrich, Missouri, USA), complete mini protease inhibitor cocktail tablets (Roche, Sigma-Aldrich, Missouri, USA) and phosphatase inhibitors (10 mM NaF and 1 mM Na_3VO_4) and protein extracts were prepared as previously described (Baptista et al., 2014). Samples (20 μg of protein) were separated in 8% sodium dodecyl sulphate-poly(acrylamide) gel electrophoresis (SDS-PAGE) and the proteins were transferred electrophoretically to poly(vinylidene difluoride) (PVDF) membranes. The membranes were blocked in 5% skim milk in Tris-buffered saline (TBS: 137 mM NaCl, 20 mM Tris-HCl, pH 7.6) containing 0.1% Tween-20 (TBS-T) for 1 h at room temperature. The membranes were incubated with the primary antibodies (Table 4), followed by incubation with the corresponding secondary antibodies (Table 4). The membranes were processed for protein detection using enhanced chemiluminescence (ECL) (Clarity™, Bio-Rad, California, USA) or enhanced chemifluorescence (ECF™) (GE Healthcare Amersham™, UK) in accordance with the manufacturer's instructions. Digital quantification of bands intensity was performed using ImageQuant 5.0 software (Molecular Dynamics, Inc., California, USA). Membranes were reprobed for calnexin as a loading control.

3.8. Statistical analysis

The results are presented as mean ± SEM. Statistical analysis was performed with the Prism 5.03 Software for Windows (GraphPad Software, Inc, California, USA). The normality of the data was assessed with Shapiro-Wilk and Kolmogorov-Smirnov normality tests. Accordingly, data were analyzed with parametric and non-parametric tests, depending on the distribution of the data.

4. Results and discussion

4.1. *In vitro* evaluation of the effects of SFM-processed drug-free PCL-based implants

From the characterization of the implants described in the supplementary information, SFM drug-free glycofurol containing PCL-based (92:00:08, wt.%) implants were selected to proceed to biological assays. Primary retinal neural cell cultures were exposed to PCL-based implants for 6 consecutive days. The time necessary for the degradation of PCL-based materials is usually long, and the polymer degradation products can be a major factor influencing the tolerance of the developed implant (Woodruff et al., 2010). Therefore, PCL-based implants were placed in culture medium for 3 weeks, which was then used to culture the cells for 6 days. The effect of the implant or the medium containing degradation products of PCL-based implants to the death of retinal neural cells was evaluated by TUNEL assay. Furthermore, the survival of retinal neurons was determined by counting the neuronal nuclear protein (NeuN)-immunoreactive cells (neuronal marker) (Figure 19A).

The exposure of retinal cells to the implant or to the medium containing degradation products of PCL-based implants did not alter the number of TUNEL$^+$ cells (100 ± 3.3% of the control and 105 ± 4.8% of the control, respectively) when comparing with control conditions (Figure 19B). Moreover, the number of NeuN$^+$ cells in culture was not significantly different in the three conditions (Figure 19C). The degradation products of intraocular implants placed in the vitreous cavity would easily affect RGCs. Therefore, the toxicity of PCL-based implants to RGCs was also determined by exposing retinal organotypic cultures to PCL-based implants or by incubation with the medium previously in contact with the implant. The number of RGCs in cultured retinal explants was determined following immunolabeling for Brn3a (Figure 19D), a marker of RGCs (Nadal-Nicolas et al., 2009, Nadal-Nicolas et al., 2012). The presence of PCL-based implants for 24 h, 48 h or 72 h did not affect the number of RGCs in the retinal explants (115 ± 6.4% of the control; 106 ± 4.2% of the control; 103 ± 2.2% of the control, respectively), indicating that PCL implants do not elicit RGC loss in organotypic cultures. Moreover, the incubation with medium containing degradation products of PCL-based implants did not significantly change the number of RGCs (95 ± 11.6% of the control) (Figure 19E).

The use of *in vitro* models, as a simplified system, presents several advantages to study the impact of PCL-based implants to retinal neurons. In fact, these retinal cell cultures are composed by the different cell types present in the retina as neurons and glial cells (Santos-Carvalho et al., 2013). One of the limitations of retinal cell cultures is the loss of tissue architecture, which can be circumvented using retinal organotypic cultures. The vitreous body and neural retina are separated from each other by the ILM, posing a barrier for drug delivery to the retina when an implant is placed intravitreally. An additional advantage of using *in vitro* models relates to the fact that is possible to evaluate the retinal cells tolerance to the PCL-based implant without the presence of one of the barriers to drug delivery (del Amo et al., 2017). Therefore, by using these *in vitro* experimental models, we could conclude that SFM-PCL based implants could be tested in an animal model.

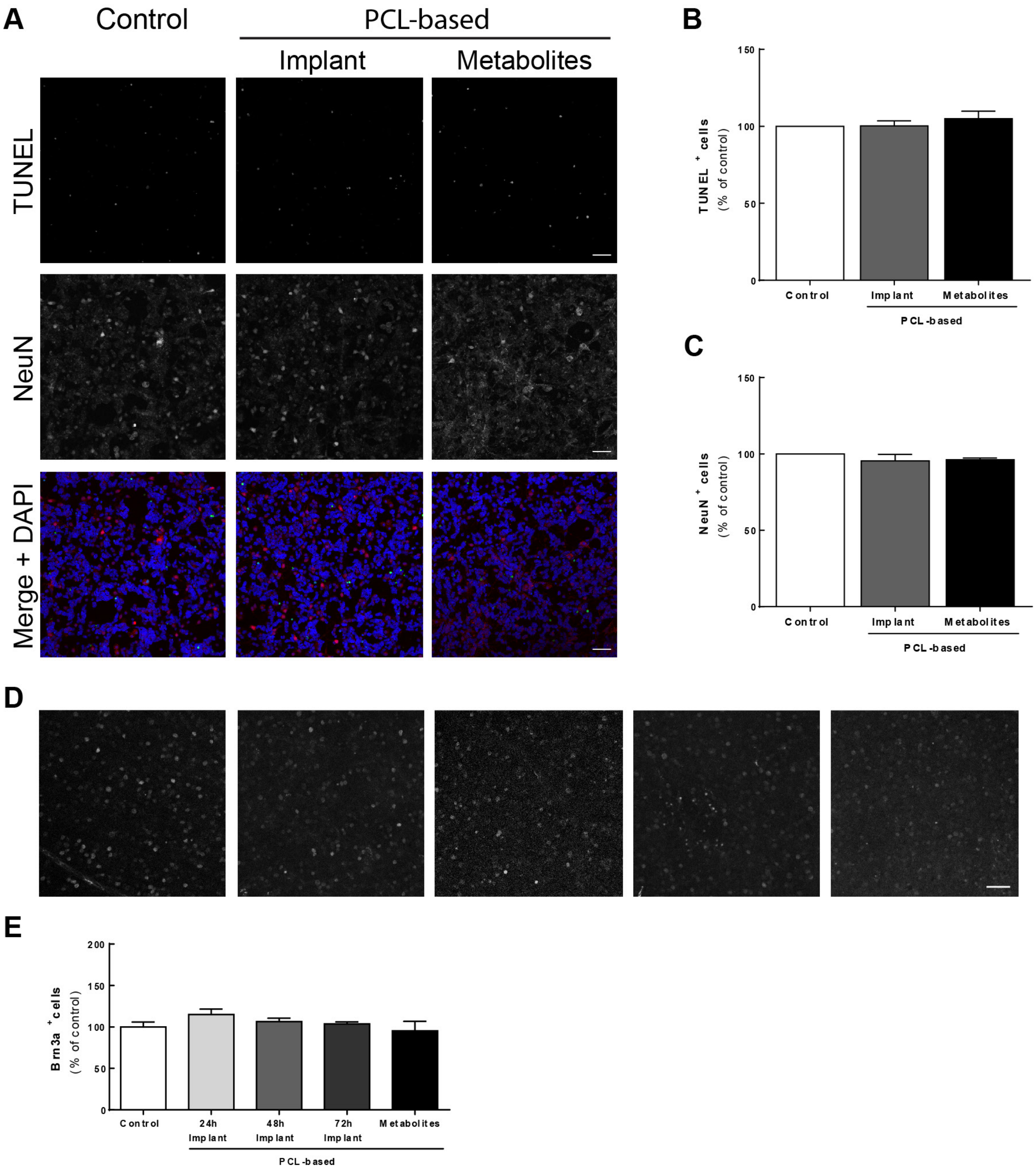

Figure 19 | The PCL-based implant (PCL:G (92:00:08, wt%)) or its degradation products did not induce cell death and neuronal loss in retinal primary neural cell cultures or RGC loss in retinal organotypic cultures. (**A**) Primary retinal neural cell cultures were incubated with PCL-based implant or with its metabolites for 6 consecutive days. Cell death was assessed by TUNEL assay and neurons were identified by immunocytochemistry with an anti-NeuN. Nuclei were counterstained with DAPI (blue) and representative images are depicted, scale bar=50 µm. (**B**) The number of TUNEL$^+$ cells per field was counted and the results are expressed as percentage of control from 3 to 6 independent experiments. (**C**) The number of NeuN-immunoreactive cells per field was counted and the results are expressed as percentage of control from 3 to 7 independent experiments. (**D**) Retinal organotypic cultures were incubated with PCL-based implants for 24 h, 48 h and 72 h or with its metabolites for 4 consecutive days. RGCs were immunostained for Brn3a and representative images are depicted, scale bar=50 µm. (**E**) The number of Brn3a$^+$ cells were counted and the results are expressed as percentage of control from 3 to 4 independent experiments.

4.2. Evaluation of the effects of SFM-processed drug-free PCL-based implants on retinal structure and function

Since there was no toxicity associated to the PCL-based implants using *in vitro* models, PCL-based implants were introduced in the vitreous of Wistar rats for 4 and 8 weeks. Sham-operated animals were also assessed to verify whether the procedure caused alterations in the retina.

Throughout the experiment the weight and the IOP of the animals were monitored. No significant differences were detected in the weight of the animals (Table 5). IOP was regularly measured and no significant changes were found as well (Table 5).

Table 5 | The PCL-based implant (PCL:G (92:00:08, wt%)) did not induce changes in animals IOP

	4 weeks				8 weeks			
	Contra	Sham	Contra	Sham	Contra	Sham	Contra	Sham
Animal weight (g)	328 ± 20		322 ± 16		332 ± 29		348 ± 23	
IOP (mmHg)	13 ± 0.4	12 ± 0.3	14 ± 0.3	11 ± 0.2	12 ± 0.4	13 ± 0.4	12 ± 0.2	12 ± 0.3

The animals weight (g) and IOP (mmHg) were determined. IOP was measured bilaterally in animals after sham-operated or implantation procedure at 4 and 8 weeks. Contra, Contralateral eye; Sham, Sham-operated eye; Implant, Implanted eye.

3

The effect of PCL-based implants for 4 or 8 weeks on retinal structure and function was evaluated by OCT (Figure 20) and ERG (Table 6 and Figure S1), respectively. These two methodologies have the advantage of being non-invasive and allow to follow the same animal throughout the course of the study.

By focusing the eye fundus image on the vitreous, it was possible to observe the PCL-based implant and confirm that the implant was not touching the retinal surface (Figure 20A). OCT is a technique frequently used in the clinics that allows a real time imaging of the retina (Fujimoto 2003). With this technique it is possible to clearly identify the different retinal layers: NFL, GCL, IPL, INL, OPL, ONL, IS/OS) and OLM (Adachi et al., 2016). There are no alterations in retinal structure in sham-operated animals, as well as, in PCL implanted animals (Figure 20C). The thickness of the total retinas was determined after image segmentation of the inner and outer limits (Figure 20D). The surgical procedure necessary for the implantation of the PCL device (sham-operated animals) did not change retinal thickness (182 ± 4.3 μm and 184 ± 4.5 μm, at 4 and 8 weeks, respectively) comparing with contralateral retinas. Also, the presence of the PCL implant did not change the thickness of the retinas (185 ± 2.9 μm; 183 ± 3.6 μm, at 4 and 8 weeks, respectively) when comparing with contralateral eye. These results suggest that both the procedure and the presence of the PCL-based implants did not elicit neither edema (that would cause an increase in retinal thickness) nor major cell loss (retinal thinning).

The retinal function was assessed by evaluating the electrical response of the retina to flash lights using ERG. The a- and b-wave amplitude and latency were extracted from scotopic ERG recordings at the maximum light intensity (9.49 cd-s m^{-2}) (Figure S1). The a-wave amplitude (181 ± 13.8 μV and 156 ± 1.0 μV) and latency (10 ± 0.2 ms and 10 ± 0.0 ms) from sham-operated animals determined after 4 and 8 weeks, respectively, were not significantly different from contralateral retinas. Moreover, the procedure did not change b-wave amplitude and latency, at 4 and 8 weeks, respectively, comparing with contralateral eye. The presence of PCL-based implants during 4 and 8 weeks did not change a- and b-wave amplitude and latency, comparing with the contralateral retina (Table 6).

These results demonstrate that PCL implants can be easily inserted into the vitreous cavity by a minimally invasive procedure, not harmful to the retina. Moreover, the polymer demonstrates a strikingly good intraocular tolerance, which is in line with others demonstrating the biocompatibility of PCL implants (Beeley et al., 2005, Fialho et al., 2008, Silva-Cunha et al., 2009, Bernards et al., 2013, Lance et al., 2015, Kim et al., 2016, Shahmoradi et al., 2017). Moreover, this study was able to go further by thoroughly characterize these PCL-based intraocular implants, using *in vivo* assessment of retinal structure and function.

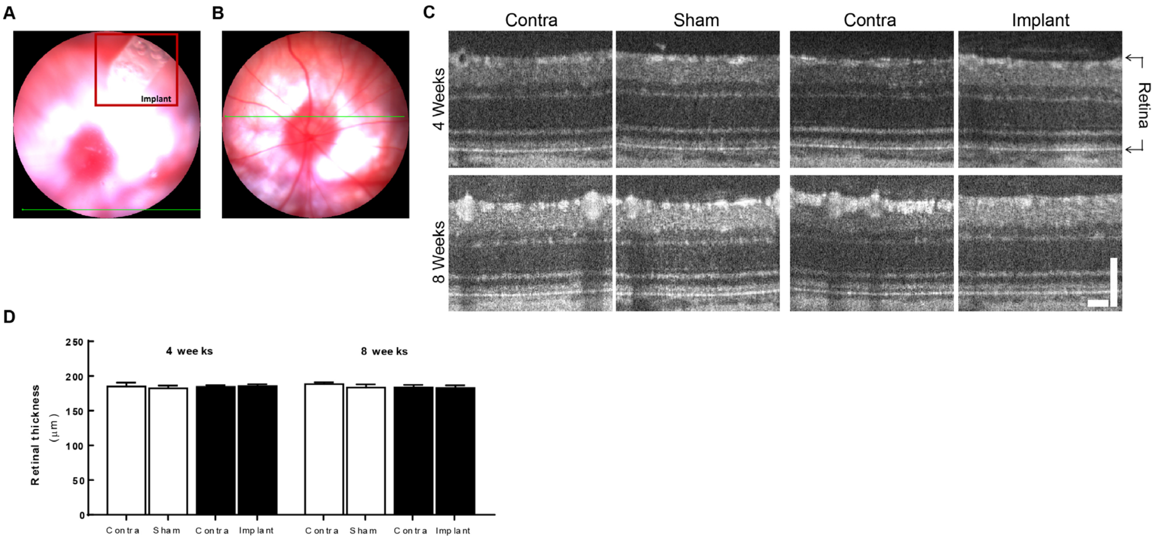

Figure 20 | The PCL-based implant (PCL:G (92:00:08, wt%)) did not change retinal structure evaluated *in vivo* by optical coherence tomography. PCL-based implant was introduced into the vitreous cavity using a 24-gauge catheter and 4 and 8 weeks after the animals were sacrificed. (**A**) Representative image of the vitreous cavity of the eye showing the presence of the implant. (**B**) Representative image of the eye fundus showing the OCT line scan (green line). (**C**) Representative images of OCT images showing the different retinal layers and the limits considered to measure total retinal thickness of the retinal layers, scale bars=50 µm. (**D**) Total retinal thickness was measured and presented from 2 to 8 animals. Contra, Contralateral eye; Sham, Sham-operated eye; Implant, Implanted eye.

Table 6 | The PCL-based implant (PCL:G (92:00:08, wt%)) did not change retinal activity evaluated by electroretinography

		4 weeks				8 weeks			
		Contra	Sham	Contra	Sham	Contra	Sham	Contra	Sham
Scotopic a-wave	amplitude (µV)	190±15	181±14	258±17	253±9	172±26	156±1	177±22	173±16
	latency (ms)	10±0.3	10±0.2	10±0.2	11±0.2	10±0.0	10±0.0	10±0.0	10±0.0
Scotopic b-wave	amplitude (µV)	266±19	259±19	365±21	360±9	265±5	251±31	260±29	265±26
	latency (ms)	42±4.8	43±4.5	50±0.4	51±0.6	48±1	48±0.0	48±0.9	49±1.1

PCL-based implant was introduced into the vitreous cavity using a 24-gauge catheter and 4 and 8 weeks after the animals were sacrificed. The intensity-response functions relatively to the scotopic a-wave amplitude and latency and scotopic b-wave amplitude and latency were presented from 2-9 animals. Contra, Contralateral eye; Sham, Sham-operated eye; Implant, Implanted eye.

4.3. Evaluation of the effects of SFM-processed drug-free PCL-based implants on retinal neurons

The effect of intraocular SFM-processed drug-free PCL-based implants on retinal neurons was assessed by immunolabelling the different cell types with specific antibodies (Figure S2): cones with anti-arrestin (Figure 21A); rods with anti-rhodopsin (Figure 21B); horizontal cells with anti-calbindin (Figure 21C); bipolar cells with anti-protein kinase C α (PKC-α) (Figure 21D); amacrine cells with anti-choline acetyltransferase (ChAT) (Figure 21E); and RGCs with anti-Brn3a (Figure 22).

Both the procedure (sham-operated animals) and the presence of the PCL-based implant did not cause alterations in the morphology and density of the different cell types in the two periods analysed (Figure 21A-E). Moreover, both the distribution (Figure 22A) and the total number (Figure 22B) of Brn3a^{+}RGCs were assessed in retinal wholemounts. Young and juvenile rats have a population of cells that project to the contralateral retina (retino-retinal projection) that constitutes 0.006% to 0.03% of the total RGC population (Nadal-Nicolas et al., 2015b). The impact of PCL-based implants on the number of RGCs in the contralateral eye would allow to determine if this population of cells is affected.

No alterations were detected in the distribution and total number of RGCs, when comparing naïve with contralateral retinas (naïve: 78411 ± 1264 RGCs mm^{-2}) (Figure S2B).

The surgical procedure did not change the number of RGCs (74173 ± 2186 RGCs mm^{-2}; 76186 ± 1983 RGCs mm^{-2}, at 4 and 8 weeks, respectively) comparing with contralateral retinas. Similarly, the presence of PCL-based implants in the vitreous for 4 and 8 weeks did not change the number of RGCs (71354 ± 5595 RGCs mm^{-2}; 77814 ± 2282 RGCs mm^{-2}, at 4 and 8 weeks, respectively) when compared with contralateral retinas (Figure 22B).

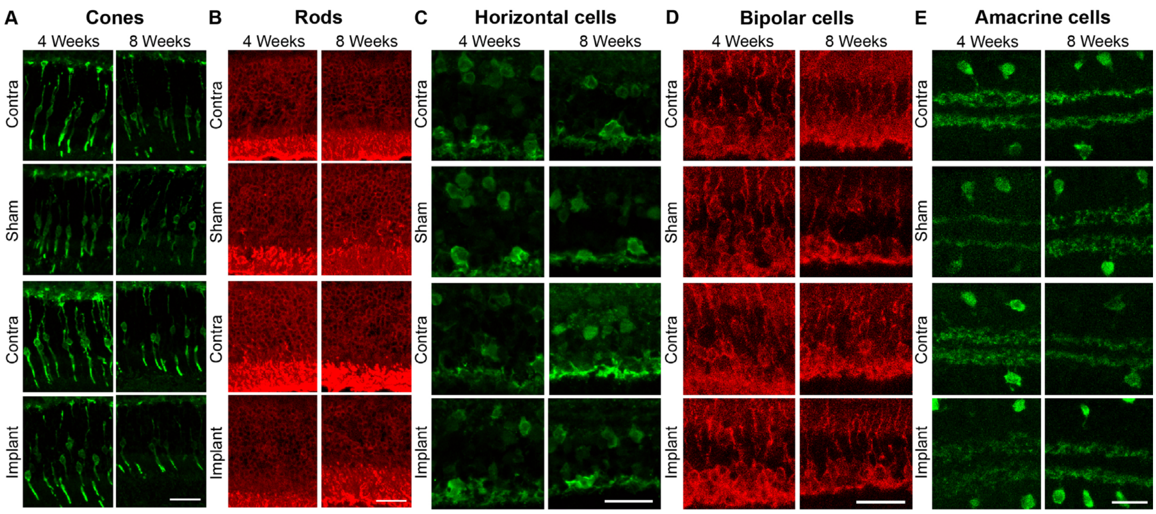

Figure 21 | The PCL-based implant (PCL:G (92:00:08, wt%)) did not induce alterations in retinal neurons. PCL-based implant was introduced into the vitreous cavity using a 24-gauge catheter and 4 and 8 weeks after the animals were sacrificed. Retinal cryosections were immunostainned for cones (arrestin) (**A**), rods (rohodopsin) (**B**), horizontal cells (calbindin) (**C**), bipolar cells (protein kinase C-α, PKC-α) (**D**) and amacrine cells (choline acetyltransferase, ChAT) (**E**). Representative images are depicted from 2 to 3 animals. Contra, Contralateral eye; Sham, Sham-operated eye; Implant, Implanted eye. Scale bar=20 µm.

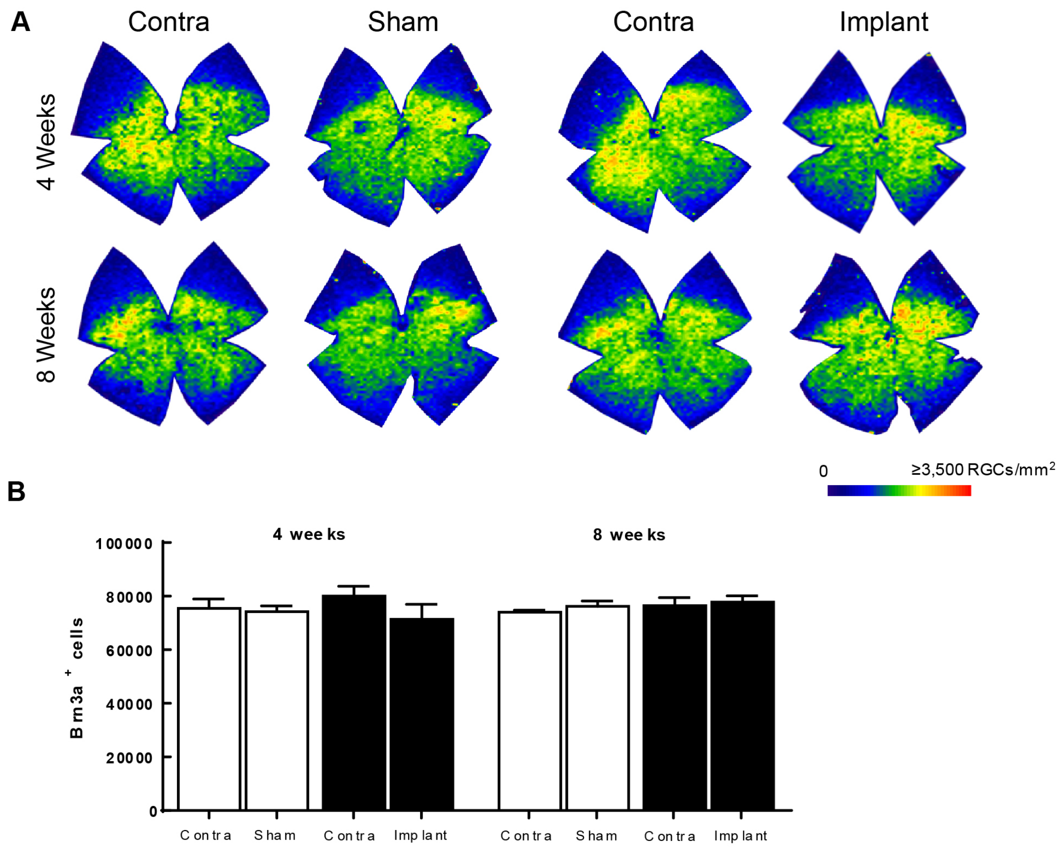

Figure 22 | The PCL-based implant (PCL:G (92:00:08, wt%)) did not change the number of RGCs. PCL-based implant was introduced into the vitreous cavity using a 24-gauge catheter and 4 and 8 weeks after the animals were sacrificed. (**A**) Retinal wholemounts were immunostained for RGCs (Brn3a). Representative isodensity maps demonstrating the topological distribution of Brn3a^{+}RGCs are depicted, within a colour code of a 28-step colour scale range from 0 (dark blue) to 3500 or higher RGCs mm^{-2} (red). (**B**) The number of Brn3a^{+}RGCs was calculated from 3 to 7 animals. Contra, Contralateral eye; Sham, Sham-operated eye; Implant, Implanted eye.

These results demonstrated that the implants are not toxic to retinal neural cells using *in vitro* and animal models. Implants prepared from PCL have been studied in the field of ophthalmology (Fialho et al., 2008, Silva-Cunha et al., 2009). The current work supports previous reports that indicate that PCL devices intravitreally implanted are well tolerated. In fact, the biocompatibility of PCL implants has been evaluated as subretinal (Beeley et al., 2005, Shahmoradi et al., 2017), intracameral (Bernards et al., 2013, Kim et al., 2016) and intravitreal (Fialho et al., 2008, Silva-Cunha et al., 2009, Lance et al., 2015) devices. Intravitreal PCL devices were shown to be well tolerated at short- and long-term, without fibrotic reaction, no sign of inflammation and minimal cell infiltration (Fialho et al., 2008, Silva-Cunha et al., 2009). However, to the best of our knowledge this is the first study that evaluated the direct impact of PCL implants to retinal neurons.

4.4. Assessment of retinal glial cells reactivity

Retinal glial cells (microglia, astrocytes and Müller cells) may become reactive as a consequence of reaction to foreign body biomaterials (Anderson et al., 2008). Chronic activation of these cells may be deleterious to the retina contributing to cell dysfunction and degeneration (Madeira et al., 2015a, Madeira et al., 2016a). The impact of the surgical procedure and the effect of the presence of SFM-processed drug-free PCL-based implants on glial cells were assessed by immunohistochemistry in retinal vertical sections. Microglial cells were labelled with an antibody that recognizes ionized calcium-binding adaptor molecule 1 (Iba1), astrocytes and Müller cell end feet were visualized by labelling GFAP, and Müller cells with vimentin (Figure 23).

Microglial cells have a key role in maintaining the homeostasis of the retinal environment and become reactive when detect alterations in the parenchyma (Wolf et al., 2017), changing their morphology, a feature that is easily observed. No major changes were observed in the number, distribution and morphology of microglia for all conditions analysed (Figure 23A).

Astrocytes have a preponderant role in the maintenance of physiological state of retina, namely neurotrophic support and the maintenance of the BRB (Vecino et al., 2016). Müller cells are the predominant glial cells in the retina, that traverse the entire retina, and modulate neuronal activity and keep homeostasis by regulating the extracellular levels of neurotransmitters (Newman et al., 1996). GFAP is expressed by astrocytes (Sofroniew et al., 2010), and it is also expressed at the end feet of retinal Müller cells in gliosis (Lupien et al., 2004), thus suggesting that increased GFAP can be used as a marker of reactive glia (Lewis et al., 2003).

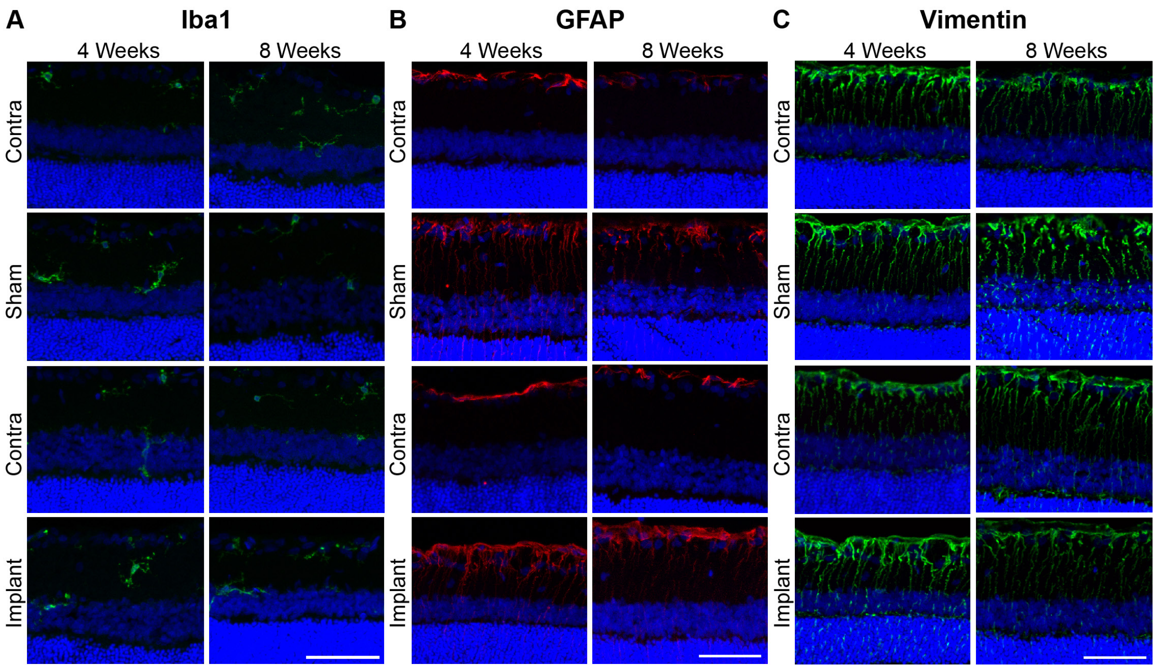

Figure 23 | The PCL-based implant (PCL:G (92:00:08, wt%)) may induce retinal stress evaluated by Müller cell gliosis. PCL-based implant was introduced into the vitreous cavity using a 24-gauge catheter and 4 and 8 weeks after the animals were sacrificed. Retinal cryosections were immunostainned for microglial cells (Iba1) (**A**), astrocytes (GFAP) (**B**) and Müller cells (vimentin) (**C**). Nuclei were stained with DAPI (blue). Representative images are depicted from 2 to 3 animals. Contra, Contralateral eye; Sham, Sham-operated eye; Implant, Implanted eye. Scale bar=50 µm.

In the contralateral retinas, the GFAP immunoreactivity was mainly observed in astrocytes, while in the retinas of the sham-operated animals or PCL implanted animals, GFAP was expressed in astrocytes but also found in the radial processes of Müller cells (Figure 23B). Nevertheless, no major changes were observed for vimentin immunoreactivity, a protein mainly expressed by Müller cells (Figure 23C). The increase in GFAP immunolabeling was further confirmed by western blot (Figure S3).

These results show that there is a foreign body reaction after PCL implantation, as well as due to surgical procedure, as assessed by the activation of Müller cells.

Müller cell reactive gliosis is a hallmark of retinal diseases (Mizutani et al., 1998, Wang et al., 2002), and this is characterized by a rapid increase in GFAP immunoreactivity that could be a sign of a disturbance in retinal homeostasis (Kimble et al., 2006). Increased GFAP in Müller cells, without alterations in microglia reactivity has been reported due to foreign body reaction (Giordano et al., 1995, Zhao et al., 2017). In fact, 2 and 4 weeks after injection of PLGA microspheres, an increase in GFAP in Müller cells was observed, returning to normal levels after 12 and 24 months after injection (Giordano et al., 1995). Similar observations were reported after injection of PLGA microspheres that may induce retinal stress as evaluated by enhanced GFAP fluorescence (Zhao et al., 2017). In the retina, there is conflicting data whether gliosis is adverse or beneficial to the tissue. Müller cell gliosis could contribute to disease development and chronic gliosis might accelerate neurodegeneration, however, Müller cells under gliosis, in such conditions, can protect neurons by releasing neurotrophic factors (Bringmann et al., 2006). The current work demonstrates that Müller cells become reactive following PCL implantation but also react to the surgical procedure, indicating that PCL implants per se do not elicit a change in these cells. This could be a response induced to protect neurons from a minimal disruption on retinal homeostasis due to surgical procedure.

4.5. Assessment of the retinal inflammatory response

Taking into consideration that an adverse inflammatory reaction could negatively impact retinal function, inflammation was assessed in the presence of SFM-processed drug-free PCL-based implants, or of their degradation products, by quantifying the protein levels and the release of IL-1β and TNF, two pro-inflammatory cytokines that are known to mediate retinal damage (Boia et al., 2017). The supernatants of primary retinal neural cell cultures (Figure 24A, B), retinal organotypic cultures (Figure 24C, D) and retinal protein extracts (Figure 24E, F) were assayed by ELISA.

Regarding primary retinal neural cell cultures, in control conditions, the extracellular levels of IL-1β and TNF were 480.6 ± 360.5 pg mL^{-1} and 1.8 ± 1.1 pg mL^{-1}, respectively.

The presence of the PCL-based implants, as well as the incubation with medium previously exposed to the implants did not change the levels of IL-1β (Figure 24A) and TNF (Figure 24B).

In organotypic cultures, the levels of IL-1β and TNF in control conditions were 427.9 ± 99.6 pg mL^{-1} and 63.2 ± 16.4 pg mL^{-1}, respectively, and the presence of PCL-based implants or of their degradation products did not change the levels of IL-1β (Figure 24C) and TNF (Figure 24D).

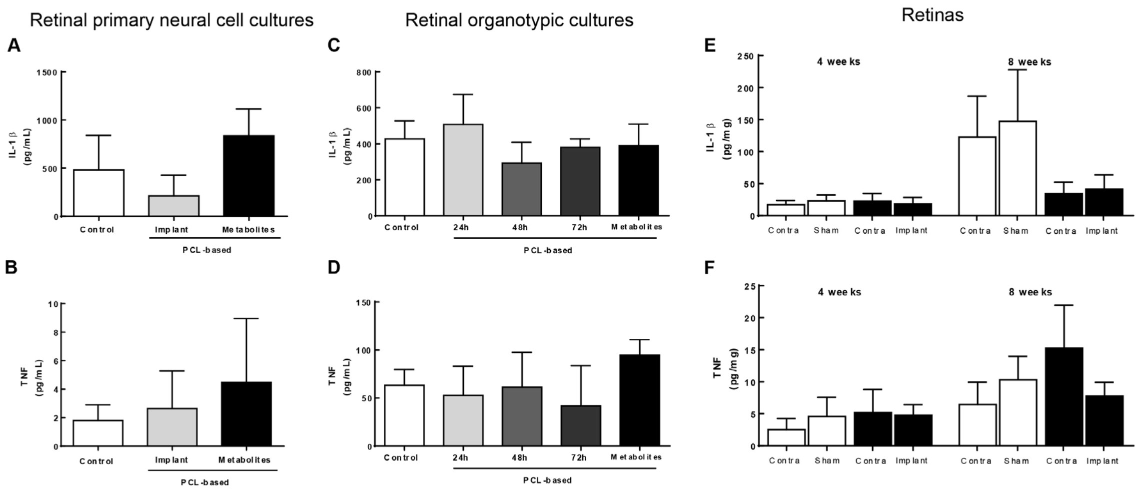

Figure 24 | The PCL-based implant (PCL:G (92:00:08, wt%)) or the degradation metabolites did not induce an inflammatory response *in vitro* or *in vivo.* Primary retinal neural cell cultures were incubated with PCL-based implants or with their metabolites for 6 consecutive days. Retinal organotypic cultures were incubated with PCLbased implants for 24 h, 48 h and 72 h or with their metabolites for 4 consecutive days. PCL-based implant was introduced into the vitreous cavity using a 24-gauge catheter and 4 and 8 weeks after the animals were sacrificed. IL-1β and TNF protein levels were assessed by ELISA in supernatant of retinal primary neural cell cultures (**A, B**) and of retinal organotypic cultures (**C, D**), and in retinal extracts (**E, F**). In culture supernatants the results are expressed in pg mL^{-1} of 2-4 independent experiments of primary cultures, and 2-12 animals independent experiments of organotypic cultures. For retinal extracts the results are expressed in pg mg^{-1} of protein of 7-11 animals. Contra, Contralateral eye; Sham, Sham-operated eye; Implant, Implanted eye.

Although there were no major effects of PCL-based implants or their degradation products when using cellular and tissue cultures, inflammation was also assessed in animals, since other signaling pathways could be involved. Retinal protein extracts from sham-operated and PCL-implanted animals (4 and 8 weeks post-surgery) were used to quantify IL-1β (Figure 24E) and TNF (Figure 24F). PCL-based implants did not significantly change the levels of IL-1β (18.4 ± 10.3 pg mL^{-1} of protein; 41.2 ± 22.4 pg mL^{-1} of protein) and TNF (4.8 ± 1.6 pg mL^{-1} of protein; 7.8 ± 2.2 pg mL^{-1} of protein) at 4 and 8 weeks, respectively, comparing with contralateral eyes. Moreover, the procedure used for the placement of the implants within the vitreous did not cause alterations in the IL-1β or TNF levels comparing with contralateral retinas.

Inflammation, secondary to implants presence, has been evaluated by the presence of cells or proteins in the vitreous or in the anterior chamber (Fialho et al., 2008, Silva-Cunha et al., 2009). In our experiments, the PCL-based implants did not promote visible retinal infiltrations assessed by OCT analysis (Figure 20). It is known that IL-1β and TNF are the main pro-inflammatory cytokines mediating retinal damage (Yoneda et al., 2001, Berger et al., 2008, Boia et al., 2017). Therefore, the evaluation of the levels of these cytokines would provide a quantitative means of evaluating *in vitro* and in the animal model whether the exposure of retinal cells to PCL metabolites or implant would cause an inflammatory response. No alterations in the levels of IL-1β and TNF were detected, suggesting that PCL-based implants do not induce an inflammatory reaction in the retina.

4.6. Long-time exposure of retinal cells to a SFM-processed PCL-based implant

Since PCL has a slow degradation rate (Woodruff et al., 2010), we assessed the effects of the presence of a SFM-processed PCL-based implant after one year of implantation. Retinal structure was assessed by OCT and Müller cell gliosis was evaluated in retinal cryosections (Figure 25).

Regarding retinal structure, even after a long period with a PCL-based device within the vitreous, no changes were found in the retinal structure (Figure 25A). Also, the total retinal thickness was determined in the OCT images, and the presence of the PCL-based implant did not cause alterations in total retinal thickness (163 ± 4.7 μm) when comparing with contralateral retinas (168 ± 3.5 μm) (Figure 25A). Taking into consideration the observations consistent with Müller cell gliosis for the earliest time points, retinal cryosections were immunolabelled for GFAP. The GFAP immunoreactivity was mostly found in the NFL, consistent with the staining of astrocytes (Figure 25B), indicating that Müller cell gliosis observed in early time points after sham-operation and PCL-implantation is transient. Most likely, the initial reaction of Müller cells was necessary to maintain retinal homeostasis after surgical procedure.

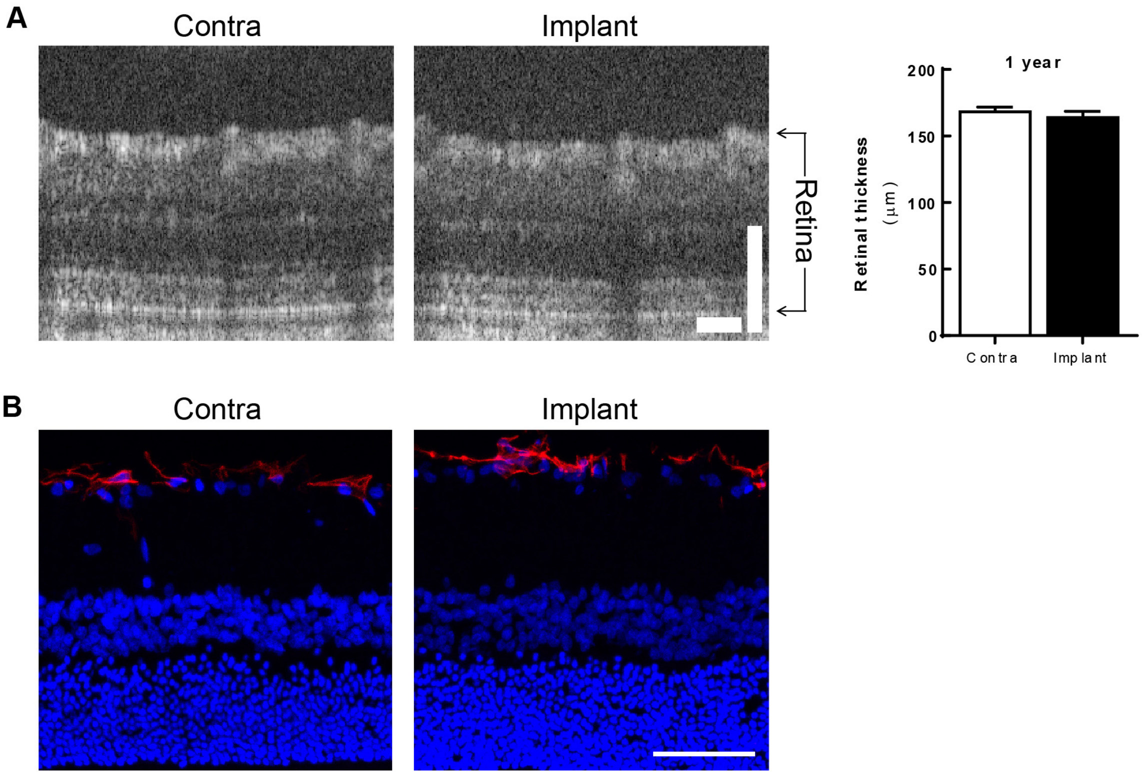

Figure 25 | Long-time exposure of retinal cells to the PCL-based implant PCL:G (92:00:08, wt%) did not change retinal structure and did not induce Müller cell activation. PCL-based implant was introduced into the vitreous cavity using a 24-gauge catheter and 4 and 8 weeks after the animals were sacrificed. (**A**) Representative images of OCT images showing the different retinal layers, scale bars=50 μm. Total retinal thickness was measured and presented from 1 animal. (**B**) Retinal cryosections were immunostainned for astrocytes (GFAP) and nuclei were stained with DAPI (blue). Representative images are depicted from 1 animal, scale bar=50 μm. Contra, Contralateral eye; Implant, Implanted eye.

5. Conclusions

In order to circumvent the adverse effects of multiple intravitreal injections for drug delivery, several types of delivery systems have been proposed. In this work, a new porous PCL-based intraocular implant was successfully developed using a SFM method (supplementary information). Glycofurol was used as a processing and compatibilizing agent between PCL and the model drug (dexamethasone, DXMT), which led to much higher incorporation yields. The higher surface areas and porosities of SFM-processed implants led to faster alkaline hydrolytic degradation rates when compared to those implants processed by the conventional HM process. Moreover, these new porous PCL-based implants also presented a faster release rate of the test-drug (DXMT), namely for the initial releasing period, while HM-processed implants present a more sustained release behaviour. These results were confirmed by two release kinetics models (diffusion-based and desorption-based models).

The *in vitro* and *in vivo* biocompatibility of these new SFM-processed PCL-based implants was assessed. By *in vitro* studies, we demonstrated that the presence of PCL implants did not increase cell death, as well as, did not decrease the number of neurons in retinal primary neural cell cultures. Moreover, PCL implants did not reduce the number of Brn3a immunoreactive RGCs in retinal organotypic cultures. By *in vivo* studies, the presence of PCL-based implants in the vitreous of Wistar rats did not change the values of IOP and did not cause changes in the retinal electrical activity nor in the structure. Moreover, PCL implants did not induce alterations to retinal neurons, in particular did not change the number of RGCs. Nevertheless, both the procedure and the presence of PCL implants may induce Müller cells reactivity, without alterations in microglial cells and astrocytes, but the impact of this to retinal physiology is not known yet. Taking into consideration the lack of retinal toxicity of the new SFM-processed PCL-based implants, we can envisage that these porous intraocular PCL implants can be used for long-term sustained intraocular drug delivery applications in several clinical conditions, thus avoiding the need of repeated intraocular injections. However, further comprehensive studies based on this promising preliminary assessment and proof-of-concept, should be performed in a near future, in order to enable the translation of these devices to the clinics.

6. Supplementary data

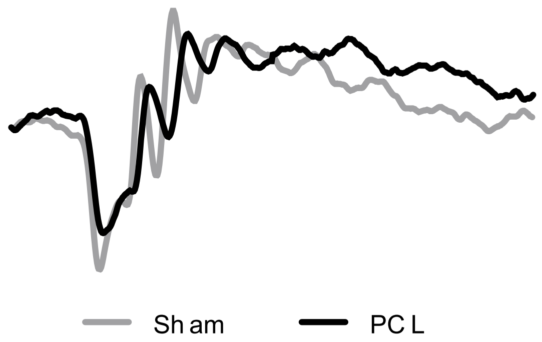

Figure S1 | The PCL-based implant (PCL:G (92:00:08, wt%)) did not change retinal activity evaluated by electroretinography. PCL-based implant was introduced into the vitreous cavity using a 24-gauge catheter and 4 and 8 weeks after the animals were sacrificed. Representative traces of individual scotopic ERGs recorded at 8 weeks after sham-operated or implant insertion procedure.

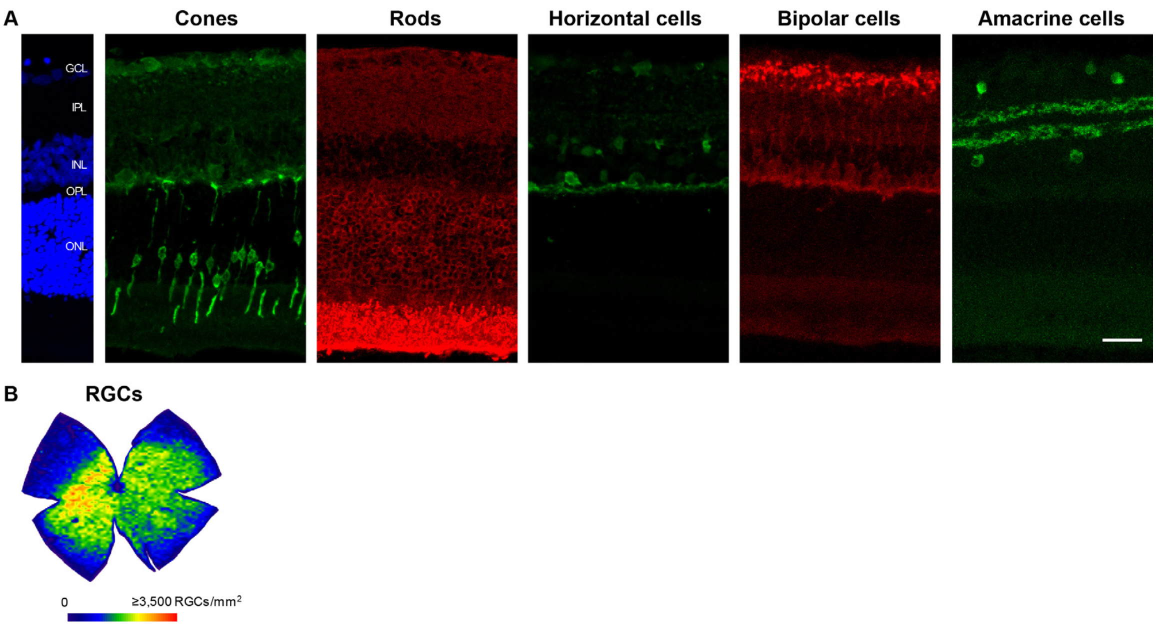

Figure S2 | (**A**) Retinal cryosections were immunostainned for cones (arrestin), rods (rohodopsin), horizontal cells (calbindin), bipolar cells (PKC-α) and amacrine cells (ChAT). Representative images of the immunostaining in retinal cryosections are depicted. Contra, Contralateral eye; Sham, Sham-operated eye; Implant, Implanted eye. Scale bar=20µm. ONL, outer nuclear layer; OPL, outer plexiform layer; INL, inner nuclear layer; IPL, inner plexiform layer; GCL, ganglion cell layer. (**B**) Retinal wholemounts were immunostained for RGCs (Brn3a). A representative isodensity map of a naïve retina demonstrating the topological distribution of Brn3a$^+$RGCs are depicted, within a color code of a 28-step color scale range from 0 (dark blue) to 3500 or higher RGCs mm^{-2} (red).

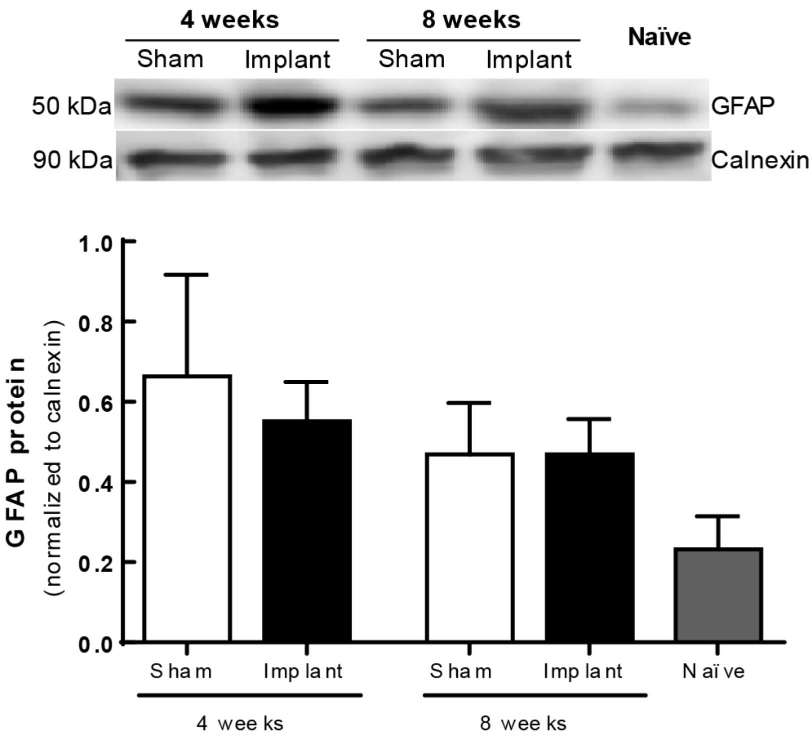

Figure S3 | The PCL-based implant (PCL:G (92:00:08, wt%)) induce a slight increase in GFAP protein levels. Drug-free PCL-based implant was introduced into the vitreous cavity using a 24-gauge catheter and 4 and 8 weeks after the animals were sacrificed. GFAP proteins levels were analyzed by Western blot in total retinal extracts. Representative images for GFAP and respective loading control (calnexin) are presented above the graph. Results are expressed as GFAP levels relative to loading control and presented as mean ± SEM of 2-3 animals.

7. Supplementary information[1]

7.1. Material and methods

7.1.1. Implants processing

PCL pellets (40 k ≤ Mn ≤ 50 kg mol^{-1}, 48 k ≤ MW ≤ 90 kg mol^{-1}; Sigma-Aldrich, Missouri, USA) were processed into powder, as described previously (de Matos et al., 2013), and mechanically sieved (sieve size 0.25 mm) to particle diameters smaller than 250 μm. PCL, dexamethasone (DXMT, ≥98%; Sigma-Aldrich) and glycofurol (G, 99%, Sigma-Aldrich), mixtures (in different compositions, Table 7), were introduced into polyurethane micro-cylinder moulds (Optiva® I.V. 24 G catheters, Smiths Medical, Minnesota, USA), and processed by a $SSCO_2$ (≥99.998%, v/v, Praxair, Portugal) SFM method, at fixed pressure (20 MPa), temperature (45 °C) and processing time (2 h) conditions. Three distinct depressurization rates (1-3 MPa min^{-1}) were employed. The employed experimental SFM set-up and the general followed procedures were previously described (de Matos et al., 2013, de Matos et al., 2015). Additionally, and for comparison purposes, two other PCL-based mixtures (Table 7) were also processed by a two-step HM method: 30 min in an oven (at 1 atm, 50 °C), followed by an additional processing period of 30 min at 80 °C. The processed materials (cylindrical implants) were removed from the micro-cylindric moulds and cut to the desired dimensions (approximately 2 × 0.46 mm, length × diameter) under a stereo microscope (Leica, Wetzlar, Germany). Three batches/replicates (using 25-30 moulds/batch) were prepared for each tested process condition. Typically, 3-4 implants were obtained from each mould.

7.1.2. Morphological characterization

Drug-free implants prepared by SFM and HM were previously sputter-coated with a gold film or with gold/palladium mixture for 15 s (around 4 nm thickness), and analysed in scanning electron microscope JSM-5310 (Jeol, Tokyo, Japan) or Vega3 (Tescan, Prague, Czech Republic), respectively, at 2 kV. Processed implants obtained from three different batches (around 25-30 moulds/batch) were analysed (5 measurements) by helium picnometry (AccuPyc® 1330, Micromeritics Instrument Corp., Georgia, USA) to obtain the real densities, by nitrogen adsorption (ASAP 2000, Micromeritics Instrument Corp., Georgia, USA) to determine surface areas (Brunauer-Emmett-Teller, BET) and average pore diameters (Barrett-Joyner-Halenda, BJH), and by mercury intrusion porosimetry (Autopore IV 9500, Micromeritics Instrument Corp., Georgia, USA) to obtain pore size distribution, porosity, bulk density, and average pore diameter. A single set of implants was measured for each process condition; and, the process variability was taken into account by measuring implants prepared from the three different processing batches for each set.

1 The conception and design of porous implants, as well as their experimental production/processing, physicochemical characterization, and degradation/*in vitro* release experiments were performed by Chemical Engineering Department of the Faculty of Sciences and Technology of the University of Coimbra.

Table 7 | Experimental design on the processing of PCL-based implants by SFM and HM: dexamethasone (DXMT) incorporation yields and correlated parameters obtained from the release kinetics diffusion and desorption models

	Experimental design		Drug incorporation		Diffusion model		Desorption model		
Method	Depressurization rate (MPa min^{-1})	PCL:DXMT:G (wt.%)	DXMT/PCL (μg mg^{-1})	DXMT loaded (%)	D (cm^2 s^{-1}) x 10^{11}	RMSE	α	τ **(days)**	RMSE
SFM 20MPa, 45°C, 2 h	1	100:00:00	-	-	-	-	-	-	-
	2	100:00:00	-	-	-	-	-	-	-
	3	100:00:00	-	-	-	-	-	-	-
	2	92:00:08	-	-	-	-	-	-	-
		74:26:00	179.5 ± 12.4	51.1 ± 3.5	-	-	-	-	-
		66:26:08	389.7 ± 2.5	98.9 ± 0.6	7.15 ± 2.18	0.0618	0.65 ± 0.01	3.79 ± 0.30	0.0337
HM 50°C, 0.5 h followed by 80°C, 0.5 h	-	92:00:08	-	-	-	-	-	-	-
		66:26:08	388.5 ± 3.1	98.6 ± 0.8	3.02 ± 0.31	0.0294	0.58 ± 0.02	7.50 ± 1.03	0.0501

7.1.3. Thermal properties

PCL powder (diameter < 250 μm) and drug-free implants prepared by SFM and HM were analysed by modulated differential scanning calorimetry (MDSC, Q100, TA Instruments, Delaware, USA). Calibration was made with Indium, and tests were performed for samples weighing ~5 mg, in aluminium pans and under a nitrogen atmosphere (50 cm^3 min^{-1}), by starting at -80 °C for 5 min, modulating at ± 0.5 °C every 40 s, and heating up to 200 °C at 2 °C min^{-1}.

Assessments were performed in duplicate to obtain the melting temperatures (T_m) and enthalpies ($\Delta H_f\,(T_m)$). The crystallinity degree ($\chi_c(\%)$) was determined by (Kong et al., 2002, Natu et al., 2008):

$$\chi_c(\%) = \frac{\Delta H_f(T_m)}{\Delta H_f^{0}(T_f^{0})} \times 100 \tag{1}$$

where ($\Delta H_f^{0}(T_f^{0})$) is the melting enthalpy of 100% crystalline PCL, which is assumed to be 139.3 J g^{-1} (Darwis et al., 1999).

7.1.4. Accelerated alkaline degradation tests

The *in vitro* hydrolysis degradation patterns of drug-free PCL-based implants formulated with glycofurol (PCL:DXMT:G, 92:00:08, wt.%) prepared by SFM and by HM were studied at accelerated alkaline conditions by adapting the method previously developed (Darwis et al., 1999). Samples of 1.3 mg (3 replicates for each tested processing method) were initially kept immersed overnight in bi-distilled water. Subsequently, samples were immersed in 3 mL of NaOH solution (5 M) (Sigma-Aldrich, Missouri, USA), in sealed glass tubes for 10 min; at room temperature, gently dried in filter paper and weighed to obtain the initial mass (m_0). The sealed tubes were kept in a thermoshaker, at 37 °C and 100 rpm, for sample degradation. Samples were removed and weighed (m_i) at several defined time intervals. The variation of mass ($\Delta m(\%)$) was determined by:

$$\Delta m(\%) = \frac{m_0 - m_i}{m_0} \times 100 \tag{2}$$

7.1.5. Drug incorporation yield and release kinetics

DXMT-loaded PCL implants prepared by SFM and HM from initial mixtures of PCL:DXMT:G (66:26:08, wt.%) were tested to determine the drug incorporation yields and the kinetics of drug release in water. Both tests were performed in triplicate and using samples of around 0.7 mg kept in sealed vials in a thermoshaker at 37 °C and 100 rpm. For the drug incorporation assessment, samples were kept in methanol (1.5 mL) and, every 2 h, aliquots (200 μL) were retrieved for analysis, and the solvent was replaced by fresh methanol. This procedure was repeated until a negligible amount of drug was detected (less than 0.5% of the accumulated drug). Kinetics of drug release experiments were performed in bi-distilled water (15 mL) under stirring (100 rpm) and aliquots (200 μL) were retrieved at defined time t intervals. The release profiles were obtained by plotting the percentage of released drug over time, which is given by:

$$\text{Released DXMT (\%)} = \frac{M_t}{M_0} \times 100 \tag{3}$$

where M_t is the amount of drug released at a given time, and M_0 is the mass of drug that was loaded into the implant. Results were correlated by applying well-known release kinetics models. The first model is based on the assumption that the drug is released from the polymer matrix simply by a diffusional process, after diffusion and absorption of water into the polymer. Assuming perfect sink conditions, the radial drug diffusion from a cylinder of radius *r* over time can be given by (Peppas et al., 1994, Siepmann et al., 1999):

$$\frac{M_t}{M_0} = 4\left(\frac{Dt}{\pi r^2}\right)^{1/2} - \frac{Dt}{r^2} \tag{4}$$

where D is the drug diffusivity within the polymer. The diffusion model presented by Eq. (4) is typically applied for less than 40% of drug released.

The release of drug from slow degrading polymeric matrices such as PCL may not be dominated only by diffusion, and the desorption of the drug from the pores surface and from the outer implant surface are probably other additional controlling steps. This can be described by the following model (Srikar et al., 2008, Natu et al., 2010):

$$\frac{M_t}{M_0} = \alpha\left[1 - \exp\left(-\frac{\pi^2}{8}\frac{t}{\tau_r}\right)\right] \tag{5}$$

where τ_r is the specific process release time, and α is the porosity factor given by:

$$\alpha = \frac{M_{s0}}{M_{s0} + M_{b0}} < 1 \tag{6}$$

M_{S0} and M_{b0} are the fractions of the mass of drug loaded at the surface and at the bulk of the matrix, respectively, with $M_0=M_{S0} + M_{b0}$.

Incorporated and released DXMT was quantified by high performance liquid chromatography (HPLC, Prominence UFLC, Shimadzu, Japan), coupled to a photo diode array detector (DAD, SPD-M20A, Shimadzu, Japan), and using a reverse phase column (Eurospher 100-5 C18 RP, Knauer, Germany, 250 × 4 mm i.d., 5 mm). The employed chromatographic conditions were described previously (Chim et al., 2012). The mobile phase, a mixture of methanol/water (9:1, v/v), was applied at the following conditions: isocratic elution (15 min), and flow rate of 1 mL min^{-1} at 35 °C. Samples (5 µL) were injected to obtain chromatograms at 239 nm, and acetonitrile runs were used to clean the column between measurements. Calibration curves (R^2=0.999) were prepared from DXMT solutions of known concentration in methanol (0-45 mg mL^{-1}, for the drug incorporation experiments), and in water (0-55 µg mL^{-1}), for the released experiments.

7.1.6. Statistical analysis

Drug release data was fitted by non-linear regression model using the JMP Pro 13 software (SAS, USA) to obtain the parameters of the diffusion and desorption models. The root-mean-square error (RMSE) was used to analyze the goodness of fit.

7.2. Results and discussion

7.2.1. Morphological and thermal characterization

Hydrophobic biodegradable polymers are used to obtain ophthalmic implants of several shapes including rods, plugs, pellets, disks and sheets (Kimura et al., 2001, Yasukawa et al., 2011). The commonly used hydrophobic polymers for these purposes are poly(lactic acid) (PLA), poly(glycolic acid) (PGA), PLGA and PCL (Kimura et al., 2001, Yasukawa et al., 2011). Cylindrical implants with dimensions of around 2 × 0.46 mm (length × diameter) were successfully obtained by SFM and HM processes. Important morphological properties of drug-free PCL-based implants were determined by helium pycnometry, nitrogen adsorption and mercury intrusion (Table 8).

Table 8 | Morphological and thermal parameters of drug-free implants prepared by the SFM and HM processes

Properties	Samples					
	PCL powder	PCL:DXMT:G (wt.%)				
		(100:00:00)			(92:00:08)	
		SFM (depressurization rate, MPa min-1)				HM
		1	2	3	2	
Nitrogen adsorption						
BET surface area (m^2 g^{-1})	-	11.15 ± 0.28	15.95 ± 0.72	15.38 ± 0.52	11.46 ± 0.42	4.18 ± 0.16
BJH Average pore diameter (Å)	-	102.26	30.35	34.07	132.77	23.12
Mercury intrusion						
Average pore diameter (μm)	-	84.86	89.19	52.37	68.66	37.99
Porosity (%)	-	41.60	56.93	62.67	62.02	12.68
Bulk density (g cm^{-3})	-	0.56	0.38	0.39	0.29	0.93
Helium pycnometry						
Real density (g cm^{-3})	-	1.04 ± 0.03	0.99 ± 0.09	1.21 ± 0.07	1.06 ± 0.12	1.22 ± 0.05
Thermal properties						
Tm (°C)	60.99 ± 0.20	61.40 ± 0.27	61.66 ± 0.27	61.23 ± 0.31	61.15 ± 0.22	60.73 ± 0.18
ΔH_f (T_m)(J g^{-1})	105.70 ± 0.60	91.71 ± 0.08	90.64 ± 2.46	95.02 ± 0.58	92.08 ± 2.38	83.12 ± 1.31
X_c (%)	75.88 ± 0.43	65.84 ± 0.06	65.07 ± 1.77	68.21 ± 0.41	66.10 ± 1.71	59.67 ± 0.94

Glycofurol (G, also known as tetraglycol, average Mn=190.24 g mol^{-1}) is a safe and FDA-approved excipient in some pharmaceutical formulations (usually used as a hydrotrope). It is relatively non-toxic and non-irritant at the concentrations normally used for pharmaceutical applications, and presents a LD_{50} of 3.5 mL kg^{-1} (mouse, intravenous) (Rowe et al., 2006). In this work, glycofurol was used as a processing agent, namely as a pre-mixing solvent for the drug (DXMT), and as a DXMT-PCL compatibilizer.

As expected and as determined by helium pycnometry, HM and SFM-prepared materials presented similar real densities of 1.0-1.2 g cm^{-3}, which are clearly within the literature values range for pure PCL (0.991.22 g cm^{-3} (Ketelaars et al., 1997, Fanovich et al., 2012)), and showing that the presence of glycofurol (similar density of 1.09 g cm^{-3}, as provided by the supplier) has a limited effect in real density.

The bulk densities of drug-free SFM-processed implants decreased with the depressurization rate from 0.56 g cm^{-3} (at 1 MPa min^{-1}) to 0.38-0.39 g cm^{-3} (at 2-3 MPa min^{-1}). Also, the addition of glycofurol led to a lower bulk density (0.29 g cm^{-3}). On the other hand, and as expected, HM-processed implants presented a bulk density of 0.93 g cm^{-3}, a value that is quite close to the real density, indicating low porosity.

Previous studies suggested that varying the final depressurization rate of the SFM-process could allow to control the porosity in PCL samples (Churro et al., 2015b, Salerno et al., 2019). In this work, the porosity of SFM-processed glycofurol-free PCL implants increased with the depressurization rate (1-3 MPa min^{-1}) from 42 to 63%, following the same trend reported elsewhere (Shieh et al., 2005, Churro 2015a).

After the polymeric matrix swelling by CO_2 saturation, a fast decrease in pressure will induce a shift in equilibrium leading to an oversaturation of gaseous CO_2 inside the polymeric matrix. Different depressurization rates, at constant temperature, will lead to dissimilar phase separation pathways, and thus to distinct nucleation rates, number of nucleation sites and cavity/bubble sizes, all of which originating final different polymer morphologies, porosities, pore sizes/diameters, and pore interconnectivities/tortuosities. For faster depressurization rates, the energy barrier for nucleation usually decreases, leading to an increase of the nucleation rate and to the formation of a large number of smaller CO_2 bubbles, which will later originate polymeric matrix presenting a large number of small size/diameter pores (mainly in the micro- and mesoporosity ranges), and high surface areas (Jacobs et al., 2008). On the contrary, for slower depressurization rates, there is more time available for the diffusion of CO_2 into the forming bubbles, as well as to bubble coalescence and size growth. As a consequence, polymeric matrices will typically present less pores however of larger pore sizes/diameters and pore interconnectivities (Fanovich et al., 2012). Therefore, as expected, average pore sizes, determined by mercury intrusion (in the 3-150 μm pore diameter measuring range), decreased from 85 to 89 to 52 μm as the depressurization rate was increased from 1 to 2 MPa min^{-1} to 3 MPa min^{-1}. For the same depressurization rate (2 MPa min^{-1}) and at the same pressure/temperature conditions, adding glycofurol slightly increased the porosity from 57 to 62%, and decreased the average pore diameter from 89 to 69 μm (Table 8). These results suggest that, at this pore diameter range, glycofurol may also be playing a porogenic role. Unsurprisingly, HM-processed implants presented a much lower porosity (~13%) and average pore diameter (~38 μm). Finally, at this pore diameter range, the average pore diameters obtained by mercury intrusion are in line with what can be observed by SEM (Figure 26). These porosity/pore diameter differences can also be observed at the cross-sections of SFM- and HM-processed implants (Figure 26). It should be noticed that SFM-processed samples are so porous that they deform during SEM sample preparation (Figure 26).

Nitrogen adsorption/desorption isotherms (in the 3-150 nm pore diameter measuring range) show that SFM-processed glycofurol-free implants presented higher BET surface areas if compared to those processed by HM (~4.2 m^2 g^{-1}). In addition, the corresponding BET surface areas increased (from 11 to 15-16 m^2 g^{-1}) as the depressurization rates were increased from 1 to 2-3 MPa min^{-1}, thus showing the typical effect of the depressurization rate on the surface areas of CO_2-saturated thermoplastic polymers (Jacobs et al., 2008). However, results also show that the addition of glycofurol decreased the BET surface area (from 16 to 11 m^2 g^{-1}) of the SFM-processed implants. Average pore sizes (BJH) obtained by this technique were within the microporous and mesoporous ranges for the SFM-processed implants, while lower values were obtained for the HM process (23 Å, in the microporous region). Again, the highest depressurization rates (2-3 MPa min-1) decreased the average pore diameters of glycofurol-free implants (from 102 to 30-34 Å), as also reported by others (Fanovich et al., 2012, Chen et al., 2019).

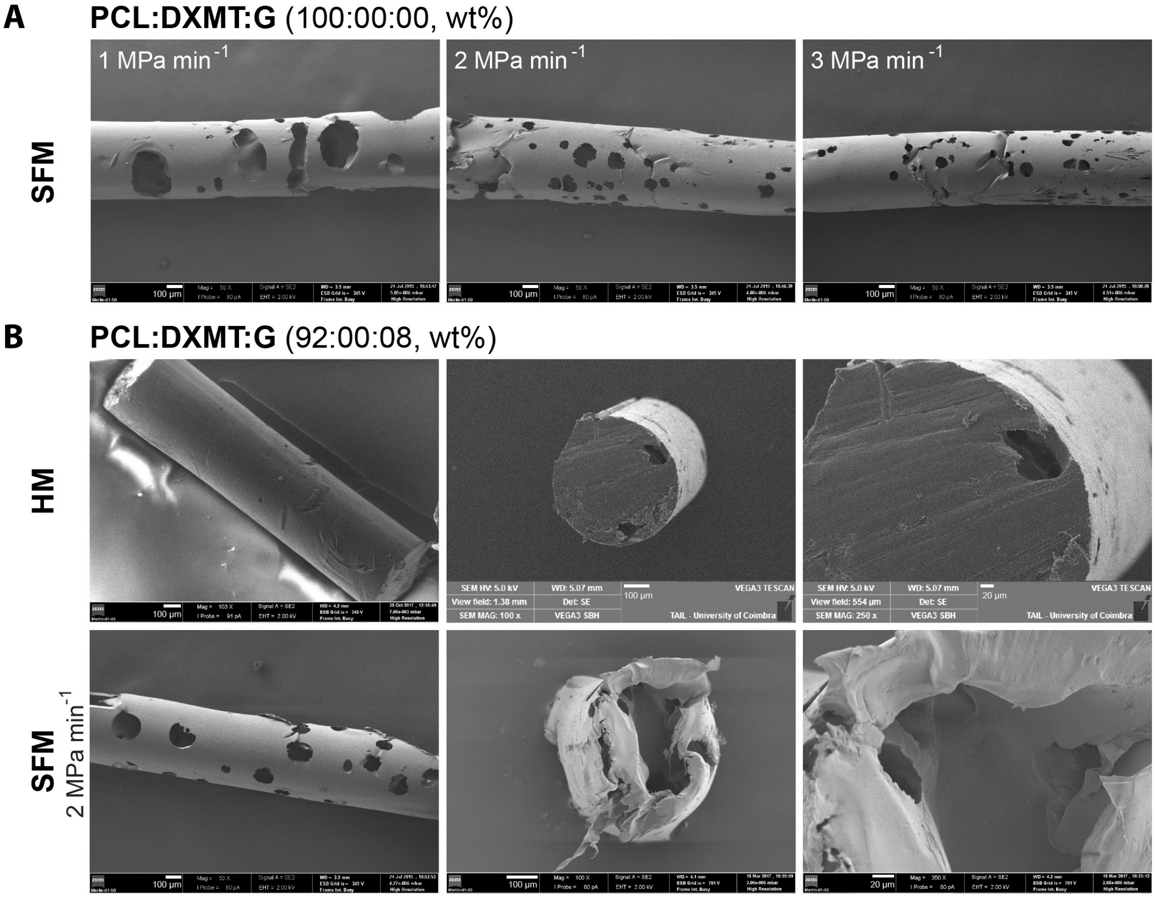

Figure 26 | SEM images of PCL (100:0:0, wt %) (**A**) or PCL:G (92:00:08, wt%) (**B**) implants processed by SFM (using different depressurization rates) and by HM. (**B**) Representative images of global views of the implants (left panel) and cross sections (middle and right panels).

Salerno et al. used ethyl lactate as an additive and as a plasticizer and a blowing agent for the PCL foaming process, and in order to promote the formation of larger pores and lower pore density of PCL than by using pure CO_2 (Salerno et al., 2013). In the current work, the addition of glycofurol seems to have a similar effect on SFM-processed implants, originating larger pore diameters (from 30 to 133 Å) and smaller surface areas (as seen, from 16 to 11 m^2 g^{-1}) in the micro- and mesoporous ranges. On the contrary, and well beyond the lower limit of the macroporous range, the addition of glycofurol decreased pore diameters and increased porosity. Therefore, and in conclusion, the pore diameter analyses of SFM-processed implants, obtained both by nitrogen adsorption and by mercury intrusion, clearly shows the SFM process "tunability" in terms of the generation of all kinds of pore diameters in these implants, *i.e.*, from quite small to quite large pores, at the micro-, meso- and macroporous ranges, and simply by manipulating the depressurization rate or by adding small amounts of glycofurol.

Micro- and mesopores (pore diameters below 50 nm), together with large surface areas (due to a large number of these small pores) are known to be important features for attaining faster degradation rates and/or for faster release of bioactive substances, while larger interconnected pores are known to be relevant for the transport of fluids and bioactive substances between implants and adjacent tissues (Shivanand et al., 1998, Srikar et al., 2008, Vidaurre et al., 2008, de Matos et al., 2015). Thus, the SFM methodology and the addition of small amounts of safe porogenic liquids clearly presents several additional advantages at the development of high porosity PCL-based implants and other materials for a wide range of pharmaceutical and biomedical applications.

Obtained MDSC thermograms presented one main melting point for all analysed samples (PCL powder and PCL-processed materials), which is typical of semi-crystalline thermoplastic polymers that went through thermal-based processing (Natu et al., 2008, de Matos et al., 2013, Salerno et al., 2019).

Typically, and during the SFM process, the sorption and the concentration of CO_2 within a semi-crystalline polymer increases as pressure increases, thus promoting a temporary plasticizing effect that enhances chain mobility and increases polymer free-volume. This process occurs firstly at the less-ordered (amorphous) regions of the polymer. As sorption continues, and as the chain mobility and free-volume keeps increasing, the ordered crystalline regions of the polymer will also be disarranged and the polymer will go easier through a phase of transition into a viscous molten state. Therefore, this transition will occur at a lower temperature than the polymer melting temperature at atmospheric pressure. The addition of a plasticizer can also help this process (Fanovich et al., 2012, Salerno et al., 2013). As explained before, after saturation and during the depressurization step, CO_2 will leave the molten polymer, forming gaseous cavities/ bubbles by nucleation and growth, ending its role as a temporary plasticizer of the polymer. This will lead to the decrease of chain mobility and free-volume, causing the polymer to freeze. During this process, the polymer chains will rearrange again into amorphous (less ordered) and crystalline (more ordered) regions, whose relative extents may not be the same before processing. This means that the post-processing crystallinity degrees and the melting temperatures of semi-crystalline polymers may change due to the SFM process. For example, some studies indicated that SFM processing can significantly change (i.e., increase or decrease) the pure PCL crystallinity degree, depending on the employed PCL properties (e.g., original crystallinity, average molecular weight and molecular weight distribution), and on the employed operational conditions (e.g., temperature, pressure, processing time) (Shieh et al., 2005, Kiran et al., 2008, Fanovich et al., 2012). In this work, the obtained melting temperature of the PCL powder (60.99 ± 0.20 °C) was within the range specified by the supplier (56-64 °C), and both processing methods (SFM and HM) did not significantly affect the typical PCL melting temperature range. However, the enthalpies of fusion and, consequently, the crystallinity degrees decreased from 76% (for PCL powder) to ~65-68% (for SFM-processed implants, with or without the addition of glycofurol), and to 60% (for HM-processed implants). The HM process led to a much more pronounced decrease in crystallinity than what was previously observed (Puga et al., 2012), however for slightly different HM operational conditions (1 h at 80 °C or at 150 °C).

7.2.2. Accelerated alkaline degradation tests

Previous studies confirmed that the *in vivo* PCL degradation follows a two-step hydrolytic-based process (Woodruff et al., 2010). First, hydrolytic cleavage of the ester linkage in the water insoluble polymer backbone occurs, producing lower molecular weight polymer segments (usually inferior to 5000). Then, these segments suffer further chain scission to produce even smaller fragments that could undergo biodegradation by phagocytosis (Kimura et al., 2001, Lam et al., 2008, Woodruff et al., 2010).

PCL is known to follow a bulk erosion mechanism that is defined by a homogeneous reduction of its molecular weight (von Burkersroda et al., 2002, Lam et al., 2008, Laycock et al., 2017). The results are coherent with typical mass loss profiles that are obtained for those polymers undergoing bulk erosion (Bat et al., 2014, Laycock et al., 2017). In general, the aqueous medium has to diffuse first into PCL to promote random hydrolytic chain scission within the polymeric structure. Then, the newly formed degradation by-products (oligomers and monomers) may diffuse out to the release medium, or remain in the polymer bulk. If the latter happens, these by-products are also reported to prompt an internal autocatalytic degradation process due to the higher concentration of carboxylic acids (at the bulk), which may lead to some potentially harmful effects, namely in terms of the degradation of incorporated bioactive substances. On the other hand, their diffusion out to the surrounding medium may cause a sudden burst in the concentration of smaller oligomers, which may lead to some adverse tissue reactions, inducing inflammation (due to the locally decreased acidic pH conditions) (Lam et al., 2008).

PCL fully degrades *in vivo* after 2-4 years (Woodruff et al., 2010), which is a time frame that is not suitable for most of the *in vitro*/*in vivo* degradation tests required to employed to check the degradation of the produced intraocular implants. However, the accelerated hydrolytic degradation of polyesters can be attained by methods such as those using high temperature or, preferably, by those using strong acidic or alkaline media (Lam et al., 2008, Laycock et al., 2017). Nevertheless, high pH alkaline solutions were found to promote faster degradation rates than those attained in acidic conditions (Jung et al., 2006, Hernández et al., 2013, Rydz et al., 2014). Thus, the degradation kinetics of drug-free 92:00:08 (wt.%) implants (processed both by SFM and by HM) were studied in a 5 M NaOH solution. These harsh and accelerated conditions allowed to determine and to compare the effects of the implant processing methodologies on their degradation rates (Figure 27).

The erosion of SFM-processed implants was significant after 4 h, then followed a quasi-linear pattern with time. In contrast, the erosion of HM-processed implants was not significant until 32 h. Then, the observed mass loss also followed a clear linear pattern. These results confirm that, in these accelerated degradation conditions, the SFM process led to implants having properties that significantly help and increase the degradation rate of PCL, by attaining 50% of mass loss within 31 h (compared to 59 h for the HM process), and 100% (full degradation) around 69 h (compared to 81 h for the HM process). It should be mentioned that the obtained results presented higher variability near the end of the degradation test. This is due to a limitation in the methodology to accurately measure lower amounts of mass.

This means that the SFM process has the ability to originate implants presenting higher porosities and surface areas, which will be the main factors responsible for the faster degradation.

These morphological properties will allow a faster water diffusion into PCL bulk, a larger number of hydrolyses sites (on surfaces), as well as a faster diffusion of the degradation products into the surrounding liquid Media. Properties such as PCL chain length, molecular weight distribution and, particularly, crystallinity, may have also an impact on the overall degradation process (Lam et al., 2008, Laycock et al., 2017). Higher values of crystallinity are known to increase the degradation time; however, slightly higher values of crystallinity were obtained for the SFM process (Table 8), which reinforces the importance of implant porosity and surface area explaining the different degradation rates obtained. Despite some expected differences, namely in terms of the periods that are indeed necessary to obtain 50% and 100% of degradation/erosion, the *in vivo* degradation of these implants are supposed to follow trends that are somehow similar to the behaviours that were observed at these accelerated conditions (Lam et al., 2008).

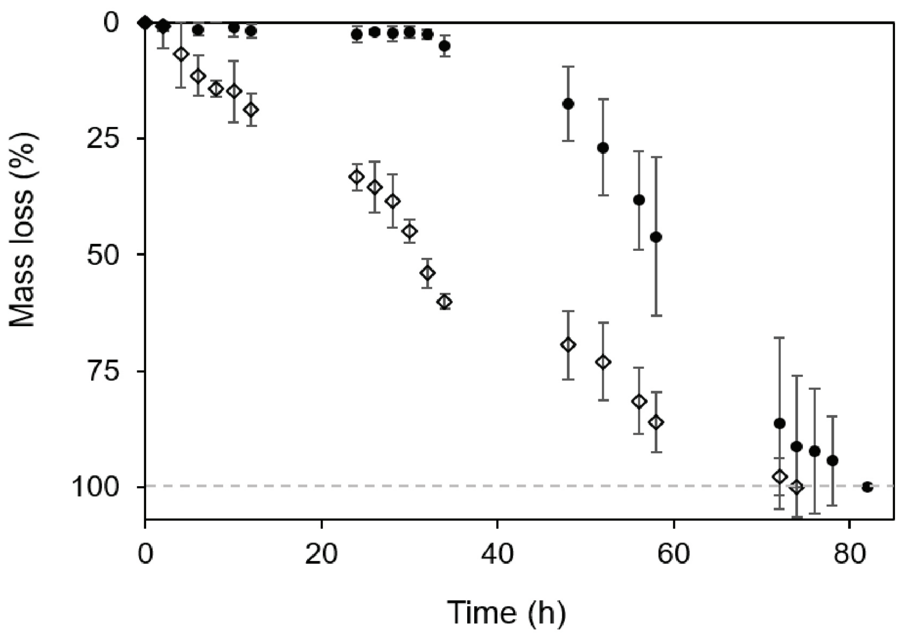

Figure 27 | Mass loss variation (%) versus time (h) for PCL:DXMT:G (92:00:08, wt%) implants prepared by: (●) HM (50 °C for 0.5 h, followed by 80 °C for 0.5 h); (◊) SFM (20 MPa, 45 °C, 2 h; depressurization rate of 2 MPa min^{-1}).

7.2.3. Drug incorporation yield and release

PCL-based implants prepared with glycofurol and loaded with DXMT (66:26:08 wt.%, PCL:DXMT:G) were prepared by both SFM and HM. DXMT is a corticosteroid used to treat eye inflammation and macular edema (Dugel et al., 2015). Its low solubility in water makes this drug a good candidate to be incorporated into the intraocular implant by the SFM process (aiming to increase its bioavailability). When using glycofurol, the drug incorporation yield achieved by the SFM process was around 99% of the initially loaded DXMT (Table 7). However, glycofurol-free implants (74:26:00 wt.%, PCL:DXMT:G) showed a considerably lower drug incorporation yield (51%). Liquid glycofurol has been used both as a co-solvent to dissolve drugs with low solubility in water (Barakat 2010) and as also proposed as a plasticizer for SFM-processed PCL-based materials (Churro et al., 2016). In this work, and based on these incorporation yields, glycofurol also seems to be acting as a compatibilizer agent between DXMT and PCL.

The *in vitro* kinetics of DXMT release from SFM- and HM-processed implants (66:26:08 wt.%, PCL:DXMT:G) was performed at near infinite sink conditions, by keeping the concentration of DXMT 10% below its saturation value in water (92-116 mg L^{-1} at 37 °C) (Yalkowsky et al., 2010, Churro et al., 2016). The kinetics of DXMT release should present two distinct phases: (i) an initial burst, due to the release of DXMT deposited at pore surfaces of the implants; and (ii) a diffusive phase (after previous water sorption by the implants), and in which the drug diffuses out the implants. Any DXMT release favoured by bulk hydrolytic degradation of PCL-based implants, or to the final and abrupt release due to the collapse of the implants, cannot be clearly observed since the degradation of PCL is a very slow process in water.

3

The kinetics of DXMT release obtained for the SFM- and HM-processed implants was assessed (Figure 28). For the initial release period, (Figure 28A), SFM-processed implants release DXMT faster than implants processed by HM. This was certainly due to a more efficient mass transfer and diffusion processes and, as discussed in section 7.2.1, mostly due to their higher porosities (~57%, in contrast with ~13% for HM-processed implants) and surface areas (~16 m^2 g^{-1}, in contrast with ~4 m^2 g^{-1} for HM-processed implants), as well as to the expected larger amounts of DXMT that were deposited on their pore surfaces (thus being more prone to be dissolved and released into the medium in a much faster way). In addition, the involved transfer and diffusion processes (of drug and/or release fluid) may also benefit from the larger pore diameters obtained for the SFM technique, both in the microporous range determined by nitrogen adsorption and well above the lower limit of the macroporous region determined by mercury intrusion. These observed distinct initial release profiles were later attenuated as the release period increased, and as the drug deposited on pore surfaces (or nearby) was released, leading to similar DXMT release profiles after 2-3 months (Figure 28B). The drug that was released, at these prolonged release periods, should essentially correspond to the DXMT impregnated (*i.e.*, molecularly dispersed) deeper into PCL struts. Moreover, and considering the initial DXMT loaded amounts (Table 7), it can be observed there was still around 35% of non-released DXMT in the implants after 80 days of release, which suggests that these porous PCL implants can even be used for longer periods of time.

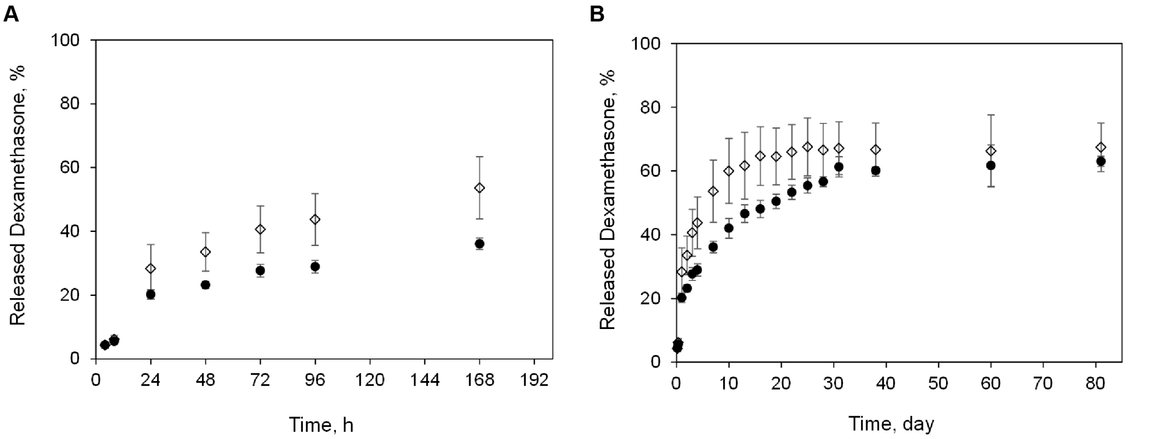

Figure 28 | Released DXMT (%) from implants (PCL:DXMT:G 66:26:08, wt.%) processed by SFM (◊) and by HM (●) considering hours (**A**) and days of drug release (**B**).

The obtained drug release data presented in Figure 28 was correlated by two non-linear regression models: a diffusion-based model (Eq. (4)) and a desorption-based model (Eqs. (5) and (6)). Correlated parameters are indicated in Table 7. The goodness of fit for both models was confirmed by the relatively small RMSE values. Despite that the diffusion-based model was fitted only to release data points below 40% of loaded drug, the correlated curves begin to deviate from the HM and SFM experimental points only after 10 and 13 days, respectively, which probably indicates an initial diffusion-controlled release process. HM-processed implants presented a smaller diffusion coefficient, thus confirming a more sustained kinetics of drug release, if compared with SFM-processed implants, and due to their lower porosities, surface areas and average pore diameters. However, this model should be applied carefully since it does not take into account any of the above referred morphological properties, all them known to strongly affect drug/fluid diffusion from/into solid polymeric matrices.

On the contrary, the desorption-based model can help us to infer about sample porosity effects on drug release kinetics. It can be observed that, and using this model, SFM-processed implants presented a higher porosity factor α (0.65) than that obtained for HM-processed implants (0.58), confirming that SFM-processed samples possess a higher fraction of DXMT deposited on pore surfaces, which is more readily available for release. On the other hand, HM-processed implants presented a higher specific process release time (7.5 days) than SFM-processed implants (3.8 days). This therefore confirms the more sustained DXMT release attained from HM-processed implants: steady state occurred after around 31 days, while it happened after 22 days for the SFM-processed implants.

The extended release periods attained for both HM and SFM-based implants were within the range reported for the commercially available Ozurdex implant (30 days) (Amsden et al., 2016). While Ozurdex releases 100% of the loaded DXMT (700 μg) over 30 days, the HM- and SFM-processed implants release in this period around 61% and 66% of the initially loaded DXMT, respectively. Therefore, and as already discussed, these implants might still release the DMXT that was deeper impregnated in PCL for an additional period of time. In particular, and due to their enhanced porosity and surface area, the potential faster degradation of the SFM-processed implants and the additional DXMT release, can also be a further advantage which could potentially increase the commercial interest of these devices.

Activation of A_3 adenosine receptor using intraocular biodegradable implants protects retinal ganglion cells from ischemic injury

Boia R, Dias PAN, Galindo-Romero C, Ferreira H, Aires ID, Vidal-Sanz M, Agudo-Barriuso M, Bernardes R, Santos PF, de Sousa HC, Ambrósio AF, Braga MEM, Santiago AR

Manuscript in preparation

4

1. Abstract

Optic neuropathies are frequent causes of visual impairment and blindness, in which RGCs are the mostly affected cells. The available therapeutic strategies for optic neuropathies have limited potential. However, the activation of A_3R emerges as a candidate strategy to protect RGCs. Drug delivery systems have potential to overcome the problems associated with repeated intravitreal injections needed in chronic diseases, such as glaucoma. Porous biodegradable intraocular implants based on PCL were loaded with the 2-Cl-IB-MECA (selective A_3R agonist) by $scCO_2$- SFM to allow the sustained activation of A_3R. This study allowed to investigate whether the PCL implants-loaded with 2-Cl-IB-MECA could afford protection to RGCs in a retinal I-R animal model. Drug-loaded SFM implants presented an extended-release of 2-Cl-IB-MECA *in vitro* (water) of around 30 days, with drug incorporation yield of around 90% at tested conditions, which corresponds to 235 ± 32 µg of 2-Cl-IB-MECA per mg of the implant.

Single-cell Ca^{2+} imaging was used as a functional measurement of 2-Cl-IB-MECA release from the implant since released 2-Cl-IB-MECA limited glutamate-evoked Ca^{2+} rise in RGCs. We then assessed the potential protective properties of 2-Cl-IB-MECA-loaded PCL implants in an animal model of I-R injury, after the implantation of 2-Cl-IB-MECA-PCL implants in the vitreous cavity of the animals. Transient retinal ischemia led to a retinal thinning, mainly a decrease in ganglion cell complex (NFL+GCL+IPL) thickness, an effect that was not prevented by the treatment with 2-Cl-IB-MECA-PCL implants. However, 2-Cl-IB-MECA-PCL implants decreased retinal cell death and promoted the survival of RGCs in the I-R injury model. Besides enhancing RGC survival, 2-Cl-IB-MECA-PCL implants also preserved optic nerve structure and re-established anterograde axonal transport. Moreover, 2-Cl-IB-MECA-loaded PCL implants were able to preserve the function of RGCs that was compromised by I-R injury.

Taking into consideration the described beneficial effects afforded by 2-Cl-IB-MECA released from the implant, we can envisage that PCL-based implants loaded with the A_3R agonist can be considered a good therapeutic strategy to protect RGCs from damage. This study provides a proof-of-concept for the use of biodegradable implants loaded with the agonist of A_3R in retinal pathologies.

Graphical Abstract

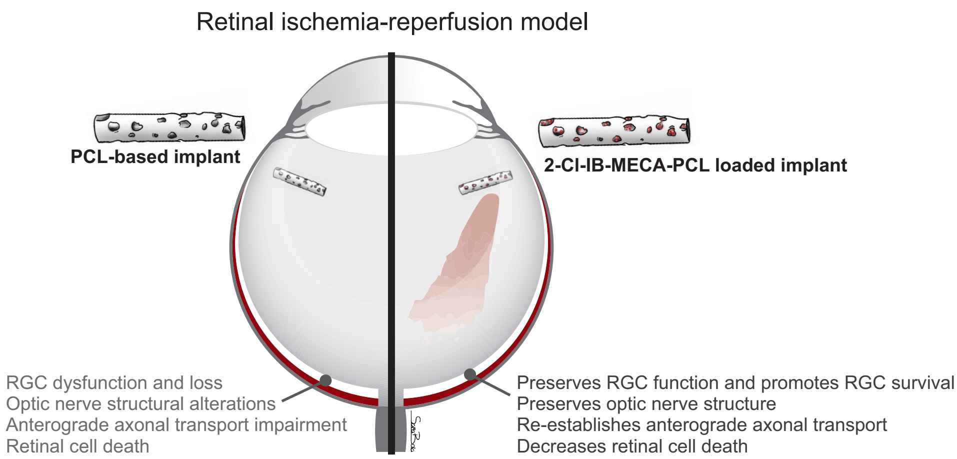

2. Introduction

RGC death and degeneration underlies several conditions which give rise to significant visual impairment and blindness. Optic neuropathies comprise a group of ocular diseases, like glaucoma (the most common), anterior ischemic optic neuropathy and retinal ischemia, in which RGCs are the main affected cells (Carelli et al., 2017). Blindness secondary to optic neuropathies is irreversible since RGCs lack the capacity for self-renewal and have a limited ability for self-repair (Goldberg et al., 2002). Currently, there are no available treatments to recover damaged RGCs, although some clinical trials focused on RGCs neuroprotection are ongoing (Boia et al., 2020). Since these chronic diseases would require multiple intravitreal injections to achieve local therapeutic drug concentrations, intraocular drug delivery systems have raised interest. Indeed, there are already clinical trials focused on the protection of RGCs using intravitreal implants. For example, a capsule filled with human cells genetically modified to secrete CNTF, a neurotrophic factor, the NT-501 encapsulated cell therapy (NT-501 ECT) is in phase 2 clinical trials for glaucoma (ClinicalTrials.gov Identifier: NCT02862938) and in phase 1 clinical trials for ischemic optic neuropathy (ClinicalTrials.gov Identifier: NCT01411657). Previously, we proposed a new biodegradable intravitreal drug delivery system using PCL as a biocompatible and bioresorbable synthetic polymer (Chapter 3). We demonstrated that the PCL implants did not cause retinal toxicity being possible to envisage their use for long-term sustained intraocular drug delivery applications in several clinical conditions (Chapter 3).

New and more effective therapeutic targets are an emergent need for RGC neuroprotection. Several therapeutic targets have been proposed, and A_3R emerged as a good candidate. RGCs are endowed with A_3R (Zhang et al., 2006), and we demonstrated that A_3R activation prevents retinal cell death in several *in vitro* and animal models of retinal degeneration (Galvao et al., 2015). Recently, we showed that the A_3R agonist 2-Cl-IB-MECA is able to confer neuroprotection to RGCs in the laser-induced OHT model (Chapter 2). We aim to extend the application of A_3R agonist for a long-term situation avoiding multiple intravitreal injections and systemic side effects. Therefore, in this work, we evaluated the potential protective effects of 2-Cl-IB-MECA-loaded PCL implants in the I-R animal model, a well characterized model (Madeira et al., 2016a, Boia et al., 2017), that has been used to identify new potential therapeutic strategies (D'Onofrio et al., 2013).

3. Materials and methods

3.1. Animals

Adult Wistar rats were housed in a standard animal room under controlled environment with free access to food and water. All procedures were approved by the Animal Welfare Committee of the Faculty of Medicine of University of Coimbra (ORBEA 23/2015) and were conducted in accordance with the European Community directive guidelines for the use of animals in laboratory (2010/63/EU), transposed into the Portuguese law in 2013 (Decreto-Lei nº113/2013) and they were also in agreement with the Association for Research in Vision and Ophthalmology statement for animal use.

3.2. Culture of retinal ganglion cells

Cultures of RGCs were obtained from the retinas of 4-5 days old Wistar rats by sequential immunopanning, as previously described (Barres et al., 1988, Winzeler et al., 2013, Martins et al., 2015), with some modifications, as follows. Rats were euthanized by direct decapitation, the eyes enucleated and the retinas dissected. Then, the retinas were digested in papain solution (16.5 U/mL; Worthington Biochemical Corporation, New Jersey, USA) containing 1.65 mM L-cysteine (Sigma-Aldrich, Missouri, USA) and 125 U/mL deoxyribonuclease I (DNase I; Sigma-Aldrich, Missouri, USA), at 37 °C for 30 min. The cell suspension was mechanically dissociated in ovomucoid (Roche, Basel, Switzerland), bovine serum albumin (BSA; Sigma-Aldrich, Missouri, USA), and DNase I (Sigma-Aldrich, Missouri, USA). RGCs were purified from the whole retina cell suspension with specific goat anti-rabbit IgG and goat anti-mouse IgM (Jackson ImmunoResearch, Cambridge, UK) and mouse anti-rat Thy1.1 (from the T11D7e hybridoma; TIB-103, ATCC, Virginia, USA).

The immunopurified cells were cultured in Neurobasal-A medium supplemented with 1x NS21 (R&D systems, Minneapolis, USA), 5 µg/mL insulin, 1 mM sodium pyruvate (Gibco, Thermo Fisher Scientific, Massachusetts, USA), 1x Sato supplement (which includes 100 µg/mL BSA, 100 µg/mL transferrin, 16 µg/mL putrescine, 60 ng/mL progesterone, 40 ng/mL sodium selenite), 40 ng/mL triiodo-L-thyronine, 2 mM L-glutamine, 5 µg/mL N-acetylcysteine, 50 µg/mL gentamicin (Gibco, Thermo Fisher Scientific, Massachusetts, USA), 50 ng/mL BDNF (Peprotech, London, UK), 10 ng/mL ciliary neurotrophic factor (Peprotech, London, UK), 10 ng/mL basic fibroblast growth factor (Gibco, Thermo Fisher Scientific, Massachusetts, USA) and 5 µM forskolin. RGCs were plated at a density of 460 cells/mm^2 using cloning cylinders on 12 mm glass coverslips coated with 10 µg/ml poly-D-lysine and 10 µg/ml laminin. The purity of cultures, determined at the first day of culture with anti-RBPMS antibody (Abcam, Cat. # ab194213, 1:500), was about 93% (Figure S4). Cell death at the first day of culture was assessed by TUNEL assay (Figure S4).

3.3. Primary culture of rat retinal neural cells

Retinal neural cell cultures were obtained from 3 to 5-day-old Wistar rats, as previously described (Aires et al., 2019a). The cells were plated at a density of 2×10^6 cells/cm^2 in 12-well plates with glass coverslips previously coated with poly-D-lysine (0.1 mg/mL; Sigma-Aldrich, Missouri, USA) and cultured in MEM (Sigma-Aldrich, Missouri, USA), supplemented with 26 mM $NaHCO_3$, 25 mM HEPES, 10% heat-inactivated FBS (GIBCO, Thermo Fisher Scientific, Massachusetts, USA), penicillin (100 U/mL; Sigma-Aldrich, Missouri, USA), and streptomycin (100 g/mL; Sigma-Aldrich, Missouri, USA) in a humidified atmosphere of 5% CO_2 at 37 °C for seven days.

3.4. Single-cell calcium imaging

RGCs were cultured for 16 h-18 h and retinal neural cell cultures were cultured for seven days at 37 °C in a humidified environment of 5% CO_2. The changes in intracellular free Ca^{2+} concentration $[Ca^{2+}]_i$ of individual cells were determined using the fluorescent probe Fluo-4. Cells were loaded with 5 μM Fluo-4-AM (Invitrogen, California, USA) for 40 min at 37 °C in HBSS (in mM: 138 NaCl, 5.3 KCl, 0.34 Na_2HPO_4, 0.44 KH_2PO_4, 5.6 D-glucose, 15 HEPES, 4.2 $NaHCO_3$, 1.8 $CaCl_2$ and 0.8 $MgCl_2$, pH 7.4). The cells were rinsed in HBSS and maintained in Mg^{2+}-free HBSS (in mM: 138 NaCl, 5.3 KCl, 0.34 Na_2HPO_4, 0.44 KH_2PO_4, 5.6 D-glucose, 15 HEPES, 4.2 $NaHCO_3$, 2.6 $CaCl_2$, pH 7.4) before data acquisition. The coverslips were mounted in a chamber-incubator for replaceable round coverslips, and cells were maintained in Mg^{2+}-free HBSS solution. Images were captured every 2 seconds in a confocal microscope (Zeiss LSM 710, Oberkochen, Germany) using a 20× objective (Plan-Apochromat 20x/0.8).

Cells were stimulated twice with 30 μM glutamate in the presence of 10 μM glycine (co-agonist of NMDA receptors) for 1 min. The cells were allowed to recover for 5 min between the first and second stimulus, and 2-Cl-IB-MECA (1 μM) was present 3 min before and 2 min after the second stimulus, a protocol that was previously described (Zhang et al., 2006). When assessing the effect of 2-Cl-IB-MECA released from the implant, cells were exposed to Mg^{2+}-free HBSS that was in contact with 2-Cl-IB-MECA-PCL implants under agitation (100 rpm) during 24 h at 37 °C.

Analysis was performed with Fiji/ImageJ software. Briefly, region of interest (ROI) were drawn around all visible cell soma that exhibited fluorescence at basal. The mean fluorescence for all ROIs defined was measured throughout the experiments. The peak of both stimuli was determined, and the maximum fluorescence of each peak was corrected for the correspondent mean baseline fluorescence determined before stimulation of the cells. The results were expressed as the ratio between the peak of the second stimulus (Delta 2, $\Delta 2$) and the peak of the first stimulus (Delta 1, $\Delta 1$). The cells that presented a $\Delta 1$ lower than 3 or that did not recover to the basal fluorescence levels after the first stimulus were excluded from the analysis.

3.5. Retinal I-R and implantation procedure

Retinal I-R injury was performed as we previously described (Boia et al., 2017). Retinal ischemia was induced for 60 min after anterior chamber cannulation with a 30-gauge needle connected to a reservoir infusing sterile saline solution. At 30 min of reperfusion, PCL implants and 2-Cl-IB-MECA-PCL implants were introduced into vitreous cavity of the animals. The animals were sacrificed 1 month after I-R induction.

3.6. Optical coherence tomography (OCT)

The animals were anaesthetized by intraperitoneal injection of ketamine (90 mg/kg; Nimatek, Dechra, UK) and xylazine (10 mg/kg; Sedaxylan, Dechra, UK) and, topical anaesthesia (oxybuprocaine hydrochloride, 4 mg/ml, Anestocil, Edol, Portugal) and pupil dilation (tropicamide, 10 mg/ml, Tropicil Top, Edol, Portugal) were applied. Corneal hydration was maintained using carmellose sodium (10 mg/ml, Celluvisc, Allergan, Ireland). B-scans were acquired using the image-guided OCT coupled to the Micron IV Retinal Imaging microscope (Phoenix Technology Group, Pleasanton, CA, USA). The volumes, composed by 512 B-scans, were acquired vertically centred and above the optic disc. The OCT data is used for the segmentation that is achieved using a fully convolutional neural network (FCNN), following a U-type architecture (Ronneberger et al., 2015), which is composed of two main parts, an encoding path and a decoding path. This architecture allows for the classification of individual pixels into one of the layers considered in this study. Furthermore, these neural networks can have short-circuit connections (Ronneberger et al., 2015). These pathways connect encoding and decoding levels providing finer grain information and more accurate pixel classification predictions. For details, see (Roy et al., 2017). While the network was designed to classify pixels into one of the six layers of the retina, the main objective is to ensure the proper discrimination at these layers' interfaces. The training set was augmented in two ways to increase the robustness of the network to distinct acquisitions: by mirroring each B-scan horizontally, and by modulating the location of the retina across the B-scan image. The segmentation provided by the neural network was then validated using manual segmentation examples provided by two graders (Hugo Ferreira and Raquel Boia).

The OCT data was segmented in order to obtain total retinal thickness, by the segmentation of inner and outer retinal limits, and to obtain the ganglion cell complex thickness (NFL+GCL+IPL), that is being used to early diagnose glaucoma (Scuderi et al., 2020).

3.7. *In vivo* detection of caspase activity

The detection of active caspases within the GCL was performed using the FAM-FLIVO® *in vivo* poly caspase assay kit (ImmunoChemistry Technologies, Minnesota, USA), similar to a previous report (Aires et al., 2019b). Animals were anesthetized with 2.5% isoflurane (IsoFlo; Abbott Laboratories, Illinois, USA) in 1 l/min O_2. Following topical anesthesia (oxybuprocaine hydrochloride, 4 mg/ml, Anestocil, Edol, Portugal) and pupil dilation (tropicamide, 10 mg/ml, Tropicil Top, Edol, Portugal), the FLIVO probe (20 ng/µL) was administered by intravitreal injection with a 36-gauge needle coupled to a Hamilton syringe. Then, 24 h later, the eyes were enucleated and fixed for 1 h in 4% (w/v) PFA. The retinas were dissected and post-fixed in 4% PFA for an additional hour. Nuclei were stained with DAPI and the retinas were mounted with fluorescent mounting media (DAKO, Agilent, California, USA). The samples were observed with a 20x objective (Plan-Apochromat 20x/0.8) on a confocal microscope (Zeiss LSM 710, Oberkochen, Germany). From each retina two images per quadrant were randomly acquired in the GCL focusing plane and the number of $FLIVO^+$ cells was counted per image.

3.8. Terminal deoxynucleotidyl transferase (TdT)-mediated dUTP nick end labelling (TUNEL) assay

Cell death was detected with a TUNEL assay kit (Promega Corporation, Wisconsin, USA) with fluorescein detection following the instructions provided by the manufacturer, and as we previously described (Boia et al., 2017). Total TUNEL$^+$ cells and TUNEL$^+$ cells in the GCL were counted directly in a fluorescence microscope (Axio Observer.Z1, Zeiss, Oberkochen, Germany) with a 20x objective (Plan Achromat 20x/0.8 M27). In each retinal section, the total number of TUNEL$^+$ cells were normalized to the respective length. Representative images were acquired in a confocal microscope (Zeiss LSM 710, Oberkochen, Germany) with a 40x objective (EC Plan-Neofluar 40x/1.30 Oil DIC M27).

3.9. Retinal wholemounts

Retinal wholemounts were prepared as we previously described (Chapters 2 and 3). The total population of Brn3a$^+$ RGCs was automatically quantified by processing the individual Brn3a images taken for each retinal wholemount with a specific cell-counted routine developed for the IPP software (IPP 5.1 for Windows; Media Cybernetics, USA). Isodensity maps were generated with the IPP software to evaluate the spatial distribution of Brn3a$^+$ RGCs throughout the entire retinal surface.

3.10. Transmission electron microscopy of optic nerves

Following transcardial perfusion with PBS (in mM: 137 NaCl, 2.7 KCl, 10 Na_2HPO_4, 1.8 KH_2PO_4; pH 7.4) followed by 4% PFA, optic nerve samples were collected close to the optic chiasm and were processed to transmission electron microscopy (TEM) as we previously described (Chapter 2). Myelin and inner tongue areas were measured using Fiji/ImageJ software, as described (Dillenburg et al., 2018). Briefly, myelin area was calculated by subtracting the area of the innermost compact myelin layer to the area of the outermost compact myelin layer. Inner tongue area was calculated by subtracting the axonal area to the area of the innermost compact myelin layer. It was analysed between 70 and 120 axons from each animal.

3.11. Anterograde tracing of RGCs

Anterograde transport assay was determined with cholera toxin B subunit (CTB). Animals were anesthetized with 2.5% isofurane (IsoFlo; Abbott Laboratories, Chicago, USA) in 1 l/min O_2, it was applied topical anesthesia (oxybuprocaine hydrochloride, 4 mg/ml, Anestocil, Edol, Portugal) and pupil dilation (tropicamide, 10 mg/ml, Tropicil Top, Edol, Portugal). CTB conjugated to Alexa Fluor™ 488 (Invitrogen, California, USA) was administered by intravitreal injection (2 μl) using a 36-gauge needle connected to an intraocular injection kit (NanoFil™ Application Kits, World Precision Instruments, Florida, USA) coupled to a 10 μl syringe and an automated pump controlled with a footswitch (Micro4; World Precision Instruments, Florida, USA). Five days after the CTB intravitreal injection, animals were transcardially perfused with PBS followed by 4% PFA, as previously described (Boia et al., 2017). The brains were dissected and kept on 4% PFA for 24 h, then transferred to a solution of 30% sucrose in PBS for 2 days and, finally, stored at -80 °C until further processing. Brain coronal cryosections (30 μm) were obtained on a cryostat (Leica CM3050 S, Leica Biosystems, Wetzlar, Germany) and nuclei were stained with the nuclear dye DAPI, diluted 1:5000. Twenty-two consecutive sections per SC, from rostral to caudal, were selected, and the SC was imaged in a fluorescence microscope (Axio Observer.Z1, Zeiss, Oberkochen, Germany) with a 5x objective (N-Achroplan 5x/0.15 M27). The area of the CTB signal in the SC of each section was outlined and the mean fluorescence was measured using Fiji/ImageJ software.

3.12. Electroretinography (ERG)

Retinal electrical activity was evaluated by ERG with corneal gold wire electrodes, as we previously described (Chapter 3). A Ganzfeld stimulator (Roland Consult GmbH, Brandenburg an der Havel, Germany) was used to deliver very dim blue light flash (0.000095 cd·s/m^2) to elicit STR and to elicit scotopic and photopic ERG responses white light flashes (0.0095-9.49 c·ds/m^2) were delivered. The amplitudes (μV) of pSTR, nSTR, and of a-wave and b-wave in scotopic conditions were extracted. Off-line digital filter was applied on STR and on b-wave (high frequency cut-off of 50 Hz) with the RETIport software (Roland Consult GmbH, Brandenburg an der Havel, Germany).

3.13. Statistical analysis

The results are presented as mean ± SEM. Statistical analysis was performed with the Prism 5.03 Software for Windows (GraphPad Software, Inc, California, USA). The normality of the data was assessed with Shapiro-Wilk normality test, and data were analysed with parametric or non-parametric tests, depending on data distribution, as indicated in the figure legends.

4. Results

4.1. 2-Cl-IB-MECA released from PCL implants prevents the glutamate-evoked increase in $[Ca^{2+}]_i$ in retinal ganglion cells

Activation of A_3R limits glutamate-evoked Ca^{2+} rise in RGCs (Zhang et al., 2010). Therefore, single-cell Ca^{2+} imaging was used as a functional readout of the release of 2-Cl-IB-MECA from the implant and the consequent activation of A_3R. RGCs were loaded with Fluo-4 Ca^{2+} probe and stimulated twice with 30 μM glutamate, in the absence (Figure 29A, Video S1) or in the presence (Figure 29B, Video S2) of 2-Cl-IB-MECA in the second stimulation. As expected, the incubation with glutamate transiently increased the $[Ca^{2+}]_i$ similarly in both stimuli (Δ2/Δ1 ratio=1.0) (Figure 29A and D). The presence of 2-Cl-IB-MECA (1 μM) decreased by 30% the $[Ca^{2+}]_i$ changes induced by glutamate (Δ2/Δ1 ratio=0.7; $p<0.05$) (Figure 29B and D). The incubation of RGCs with medium that was in contact with PCL implant did not change the response to glutamate (Δ2/Δ1 ratio=1.0) (Figure 29D). However, when the RGCs were incubated with the solution that was in contact with 2-Cl-IB-MECA-loaded PCL implant, the $[Ca^{2+}]_i$ changes were decreased by 30% (Δ2/Δ1 ratio=0.7) (Figure 29C and D, Video S3), as observed after direct incubation with 1 μM 2-Cl-IB-MECA.

The preincubation of mixed retinal neural cell cultures with 2-Cl-IB-MECA (1 μM) did not change the Ca^{2+} response to glutamate (Figure S5B and C, Video S5), as expected since these cultures have virtually no RGCs.

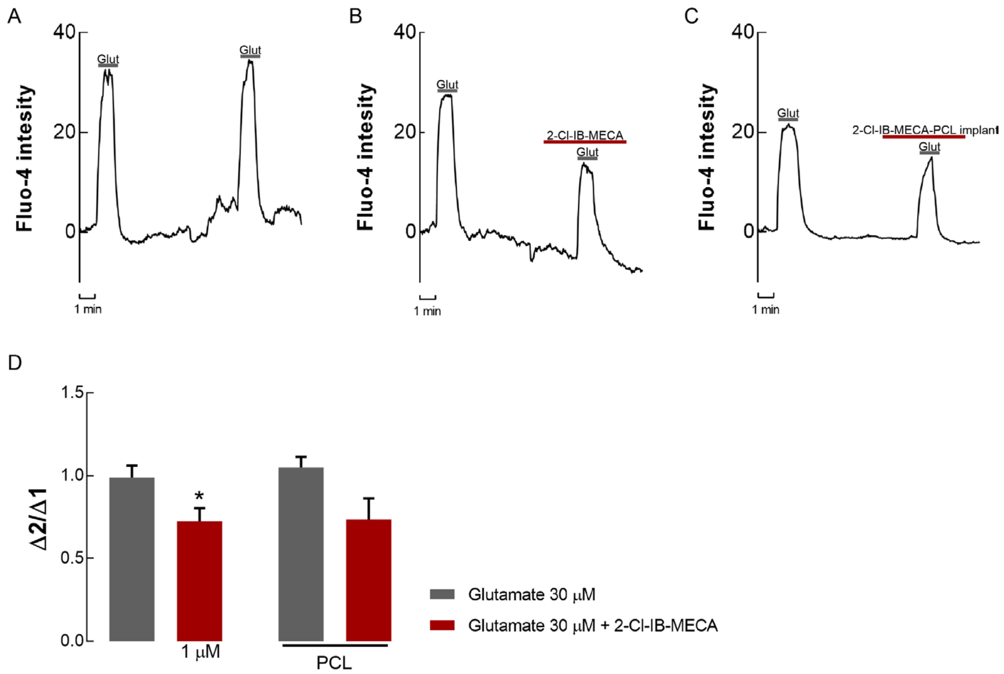

Figure 29 | 2-Cl-IB-MECA released from the implant decreased the $[Ca^{2+}]_i$ changes triggered by glutamate in RGCs. (**A**) Cells were stimulated twice with 30 μM glutamate + 10 μM glycine (referred to as Glut). (**B**) Cells were incubated with 2-Cl-IB-MECA (1 μM) 3 minutes before and 2 minutes after stimulation with Glut. (**C**) Cells were exposed to medium that was in contact with PCL implant loaded with 2-Cl-IB-MECA for 3 minutes before and 2 minutes after stimulation with glutamate. (**D**) The mean fluorescence peaks of Ca^{2+} changes were quantified, and results are presented as Δ2/Δ1 from 4 independent experiments. *$p<0.05$, significantly different from glutamate 30 μM, Unpaired t-test.

4.2. Treatment with 2-Cl-IB-MECA released from PCL implants does not prevent retinal thinning induced by retinal ischemia

Retinal thinning is a well described feature of I-R injury in which inner retinal layers are the most affected layers (Kim et al., 2013). In fact, it was described that OCT is able to detect retinal changes due to transient retinal ischemia (Sho et al., 2005). Retinal thickness was measured by OCT (Figure 30A) and, as expected, retinal I-R induced a significant decrease in total retinal thickness ($p<0.001$, 216 ± 14 μm) comparing with naïve (296 ± 4 μm), an effect that was not changed by PCL implant loaded with 2-Cl-IB-MECA (221 ± 14 μm) (Figure 30B). We observed a significant decrease in the thickness of ganglion cell complex (NFL+GCL+IPL) ($p<0.001$) that was not altered by the treatment with 2-Cl-IB-MECA-PCL implants (Figure 30B).

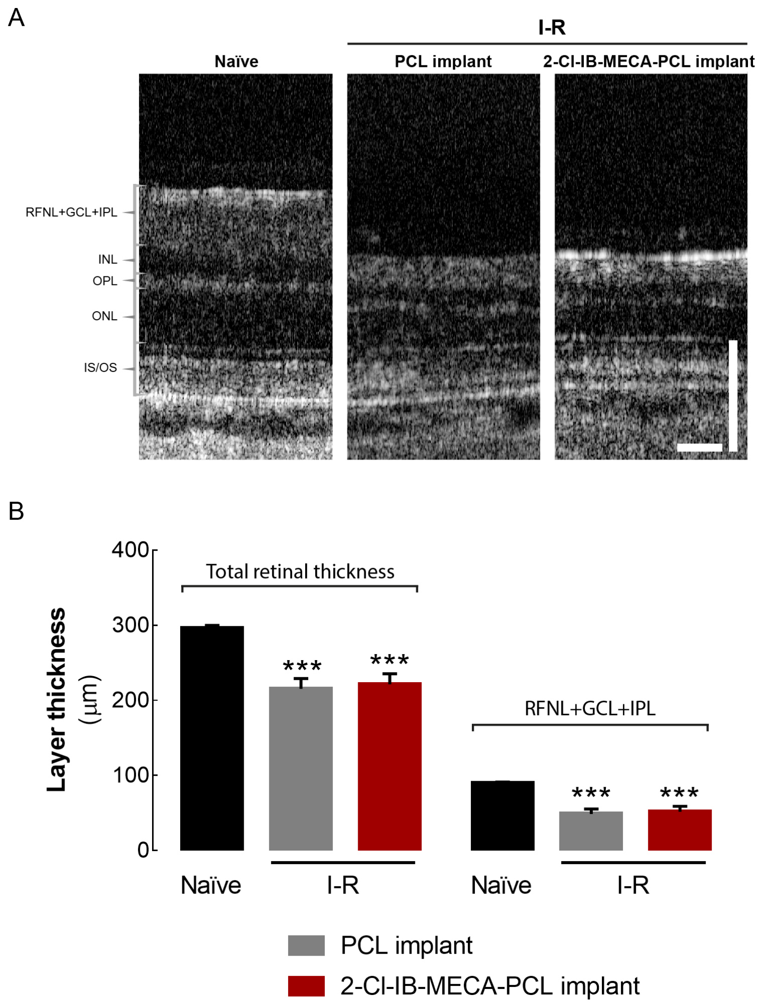

Figure 30 | Treatment with 2-Cl-IB-MECA released from PCL implants did not prevent the reduction in retinal thickness induced by retinal ischemia. (**A**) Representative images of OCT scans showing the different retinal layers and their limits, scale bars=50 μm. (**B**) Retinal volumes were acquired and total retinal thickness and ganglion cell complex (NFL+GCL+IPL) thickness were automatically calculated and presented from 5 to 8 animals. ***$p<0.001$, significantly different from naïve, One-way ANOVA, followed by Sidak's multiple comparisons test.

4.3. 2-Cl-IB-MECA released from PCL implants increases the survival of RGCs after transient retinal ischemia

Transient retinal ischemia elicits neuronal cell death (Boia et al., 2017). RGC death by caspase-dependent mechanisms has been reported in response to I-R injury (Patil et al., 2004), as well as in other retinal degenerative diseases like glaucoma (Thomas et al., 2017). Therefore, caspase$^+$ cells in the GCL were imaged following intravitreal injection of FAM-FLIVO Poly Caspase Inhibitor (FAM-VAD-FMK) (Figure 31A). I-R induced a significant increase in FLIVO$^+$ cells in the GCL ($p<0.01$), and the presence of PCL implant loaded with 2-Cl-IB-MECA attenuated the effect of I-R in the GCL (Figure 31B).

The effect of PCL implants loaded with 2-Cl-IB-MECA on retinal cell death was determined with TUNEL assay (Figure 31C). As expected, I-R significantly increased the number of retinal apoptotic cells (I-R with drug-free PCL implant) when compared with naïve retinas ($p<0.001$) (Figure 31D). The treatment of I-R undergoing retinas with PCL implants loaded with 2-Cl-IB-MECA prevented the increase in the number of TUNEL$^+$ cells triggered by I-R (Figure 31D) ($p<0.05$), suggesting that 2-Cl-IB-MECA released from the implant was able to protect retinal cells from I-R damage. Knowing that RGCs express A_3R and that I-R triggers RCG death, we specifically counted the number of TUNEL$^+$ cells in GCL. Indeed, I-R significantly increased TUNEL$^+$ cells in GCL ($p<0.05$), and the presence of 2-Cl-IB-MECA-loaded PCL implants decreased the death of cells in the GCL (Figure 31E).

RGCs were immunolabelled for Brn3a, a specific marker of RGCs (Nadal-Nicolas et al., 2009), in retinal wholemounts (Figure 32). The distribution of Brn3a$^+$ RGCs (as observed by the reconstructed isodensity maps; Figure 32A), with higher density in the superior retina and a visual-oriented horizontal strip, in naïve retinas was similar to previous reports (Nadal-Nicolas et al., 2009, Madeira et al., 2016b). The total number of Brn3a$^+$ cells was automatically counted (Figure 32B), and the number of RGCs in naïve retinas (77241 ± 8861 cells) was similar to our previous reports (Madeira et al., 2016b). I-R induced a significant loss of Brn3a$^+$ cells (39681 ± 8062 cells) that was prevented ($p<0.05$) by the treatment with PCL implants loaded with 2-Cl-IB-MECA (65093 ± 5793 cells) (Figure 32B).

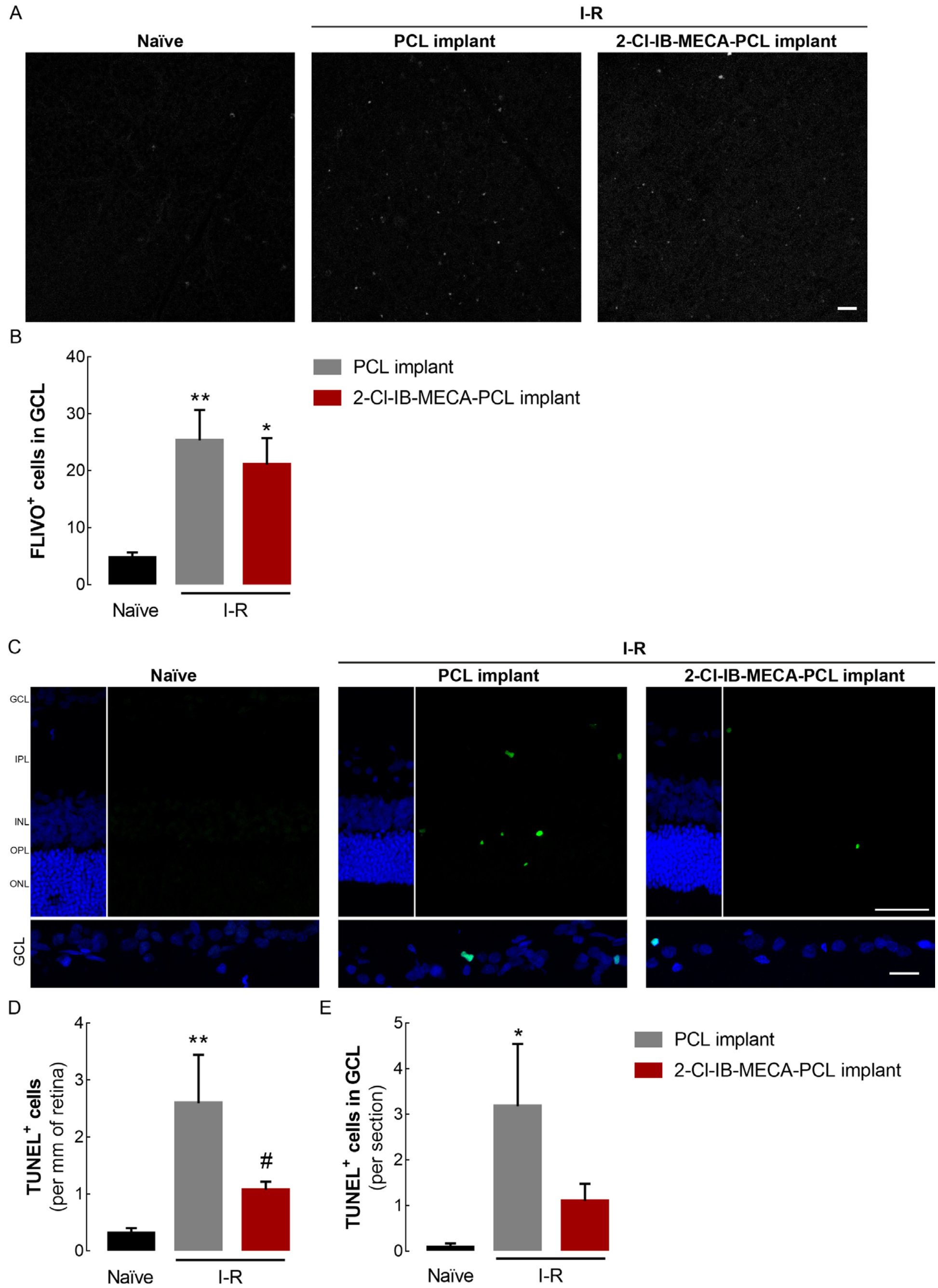

Figure 31 | 2-Cl-IB-MECA released from the implant attenuated caspase+ cells in the GCL and reduced cell death induced by I-R. (**A**) The presence of active caspases in the GCL was assessed with FAM-FLIVO (white) and representative images are depicted. Scale bar: 50 μm. (**B**) The number of FLIVO+ cells in the GCL was counted from 10-12 animals. *$p<0.05$, **$p<0.01$ significantly different from naïve, Kruskal-Wallis test, followed by Dunn's multiple comparisons test. (**C**) Cell death was detected in retinal cryosections by TUNEL assay (green). Nuclei were stained with DAPI (blue) and representative images are depicted. Scale bars: 50 μm (top image) and 20 μm (bottom image). (**D**) TUNEL+ cells in the retina were counted and expressed per mm of retina from 6-11 independent experiments. **$p<0.01$, significantly different from naïve; #$p<0.05$ significantly different from I-R + PCL implant, One-way ANOVA, followed by Sidak's multiple comparisons test. (**E**) TUNEL+ cells in the GCL were counted and expressed per section from 6-11 animals. *$p<0.05$, significantly different from naïve, Kruskal-Wallis test, followed by Dunn's multiple comparisons test.

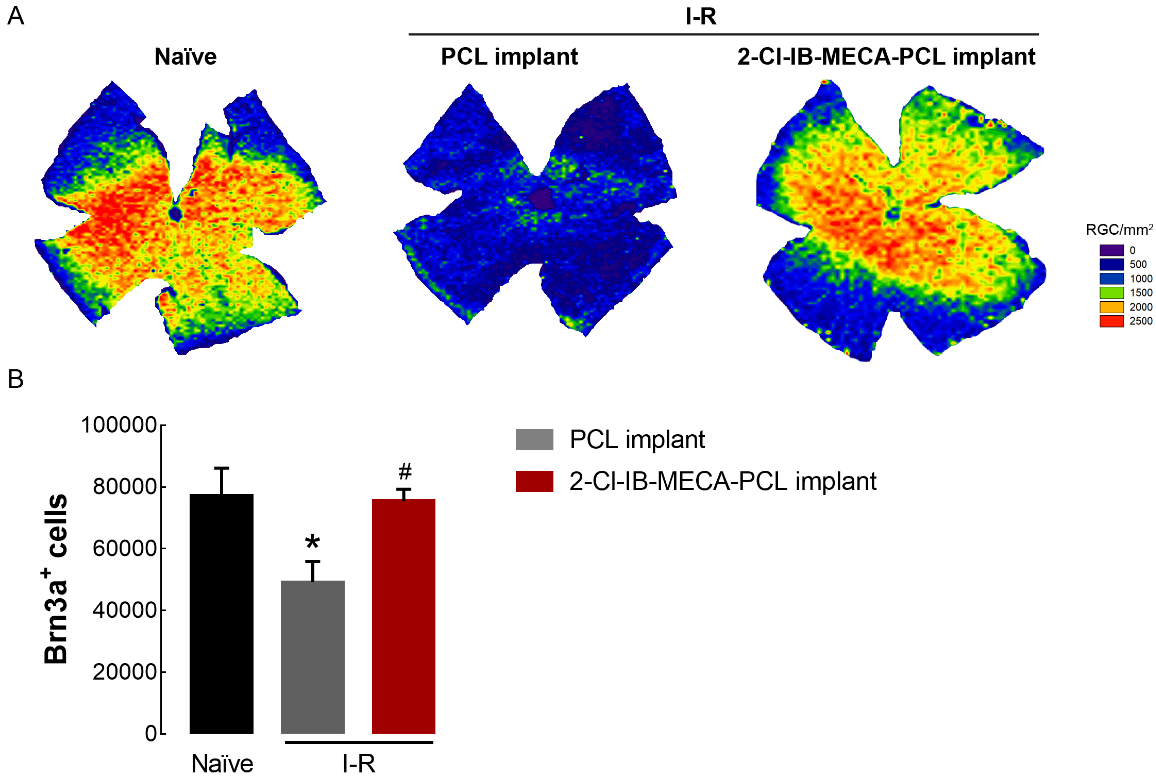

Figure 32 | 2-Cl-IB-MECA released from the implant reduced the RGC loss induced by I-R. (**A**) Representative RGC isodensity maps generated from wholemount preparations immunostained for RGCs (Brn3a), demonstrating the topological distribution of Brn3a^{+}RGCs, within a colour code of a 28-step colour scale range from 0 (purple) to 2500 or higher (red) RGCs mm^{2}. (**B**) The number of Brn3a^{+} RGCs per retina was automatically calculated from 4-6 animals. *p<0.05, significantly different from naïve; #p<0.05, significantly different from I-R + PCL implant, One-way ANOVA, followed by Sidak's multiple comparisons test.

4.4. 2-Cl-IB-MECA released from PCL implants preserve the structure of optic nerve and the anterograde axonal transport of RGCs

Some reports point the optic nerve as a structure severely affected by glaucoma (Jakobs et al., 2005, Balaratnasingam et al., 2007), and in this I-R model these alterations have been also described (Renner et al., 2017). In that way we analysed the alterations in the structure of the optic nerve by TEM (Figure 33A). In adult vertebrate CNS, axons that form optic nerve are surrounded by compact myelin (Stassart et al., 2018), as observed in optic nerves from naïve animals. Despite the observation of a disorganized axons in I-R undergoing animals, including alterations in the myelin sheath, the myelin area was not altered by I-R (Figure 33B). Moreover, the treatment with PCL implants loaded with 2-Cl-IB-MECA did not change the myelin area (Figure 33B). In contrast, inner tongue abnormalities were clearly observed in I-R animals, resulting in a significant increase in the inner tongue area ($p<0.05$, 0.13 ± 0.02 μm^{2}) due to I-R injury comparing with naïve animals (0.06 ± 0.01 μm^{2}) (Figure 33C).

The treatment with PCL implants loaded with 2-Cl-IB-MECA attenuated the abnormalities in the inner tongue caused by I-R and decreased their area (0.08 ± 0.01 μm^{2}) (Figure 33C).

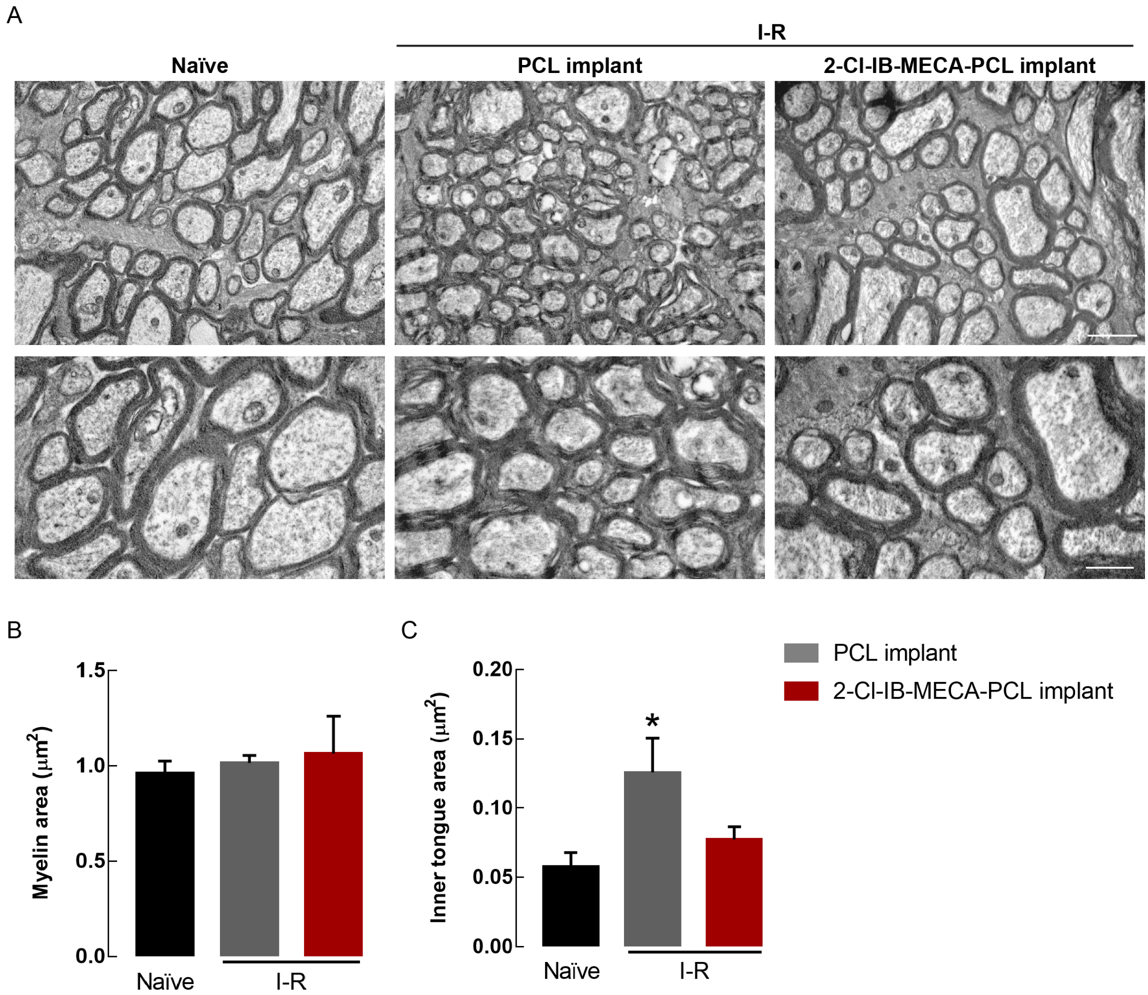

Figure 33 | 2-Cl-IB-MECA released from the implant prevented the alterations induced by I-R in the optic nerve structure. (**A**) Semi-thin cross-sections of optic nerves from naïve, PCL implant- and 2-Cl-IB-MECA-PCL implant-treated I-R retinas were imaged by transmission electron microscopy. Representative images are depicted. Scale bars: 2000 nm (top image) and 1000 nm (bottom image). (**B**) Myelin area was calculated by subtracting the area of the innermost compact myelin layer to the area of the outermost compact myelin layer. (**C**) Inner tongue thickness was calculated by subtracting the axonal area to the area of the innermost compact myelin layer. Results were obtained from 4 animals. *$p<0.05$, significantly different from naïve, One-way ANOVA, followed by Sidak's multiple comparisons test.

The optic nerve consists almost entirely of the fibers of the RGCs that mainly project in the superior colliculus in rodents (Busse 2018). Impairment of the axonal transport may precede RGC death (Munemasa et al., 2013, Le Roux et al., 2020). Therefore, we analysed anterograde transport by injecting CTB in the vitreous and measuring the mean fluorescence in the SC (arbitrary units, a.u.) (Figure 34A). I-R injury leads to a decrease in the mean fluorescence of CTB (365 ± 25 a.u.) comparing with naïve (469 ± 32 a.u.), an effect that was attenuated by the treatment with PCL implants loaded with 2-Cl-IB-MECA (500 ± 89 a.u.) (Figure 34B).

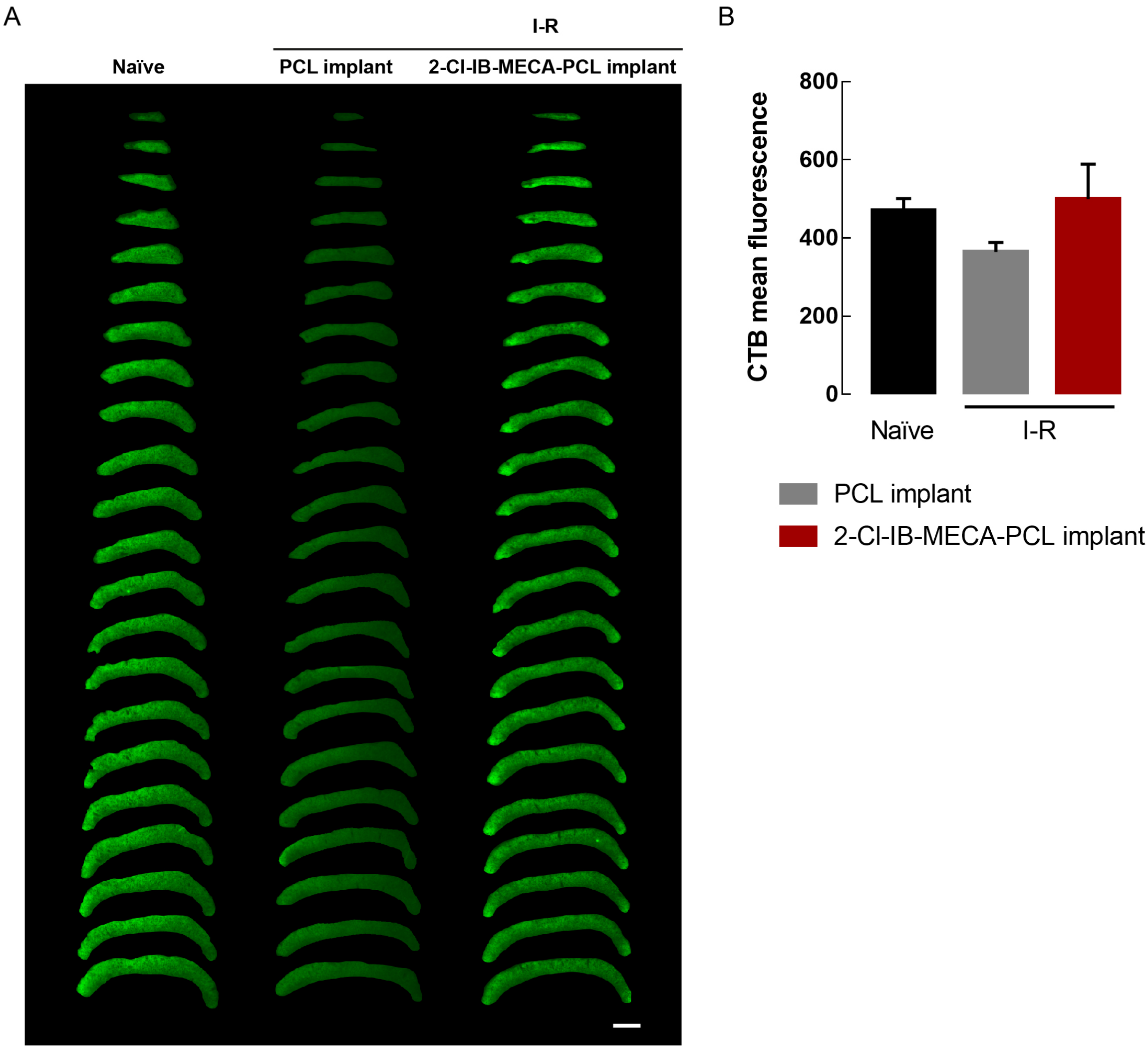

Figure 34 | 2-Cl-IB-MECA released from the implant attenuated the impairment in anterograde axonal transport induced by I-R. (**A**) Anterograde axonal transport was assessed following intravitreal injection of CTB (green). Representatives images of retinal terminal projections in the SC were depicted. Scale bar: 500 μm (**B**) CTB mean fluorescence was measured from 3-5 animals.

4.5. Treatment with 2-Cl-IB-MECA released from PCL implants attenuates RGC dysfunction induced by I-R

The function of RGCs was assessed by ERG using very dim blue light flashes (0.000095 cd·s/m^2), after extracting the amplitudes of the positive (pSTR) and negative (nSTR) components (Figure 35A). The amplitudes of both pSTR and nSTR decreased by 30% and 40%, respectively, in the retinas subjected to I-R that had PCL implants when compared with naïve animals, suggesting loss of function of RGCs induced by I-R injury. The presence of 2-Cl-IB-MECA-loaded PCL implants significantly reduced the effect of I-R in pSTR ($p<0.05$) and nSTR amplitudes (Figure 35B).

The function of other retinal cells was also assessed by ERG by exposing the animals to several light flash intensities in scotopic conditions (Figure S6A). The amplitudes of a- and b-waves that correspond to the function of retinal cells of the outer and innermost retinal layers, photoreceptors and bipolar cells, respectively, were extracted at the maximum light intensity (9.49 cd·s/m^2). I-R decreased the amplitudes of a-wave and b-wave, an effect that was not modified by the presence of PCL implants loaded with 2-Cl-IB-MECA (Figure S6B).

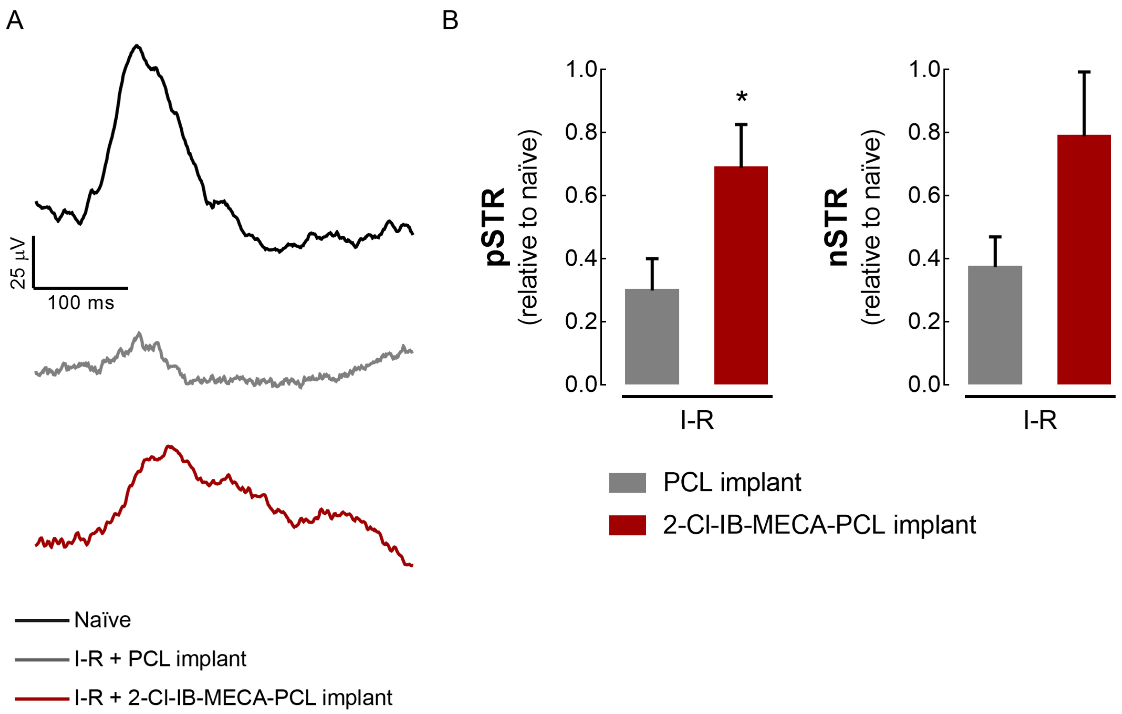

Figure 35 | 2-Cl-IB-MECA released from the implant decreased the RGC loss-of-function induced by I-R. (**A**) Representative traces of STR. (**B**) The pSTR and nSTR amplitudes from I-R eyes treated with PCL implant or 2-Cl-IB-MECA-loaded implant were normalized to the responses obtained from naïve eyes. Results were obtained from 7-8 animals. *p<0.05, significantly different from I-R + PCL implant condition, Unpaired t-test.

5. Discussion

Neuroprotection of RGCs is a valuable strategy to treat optic neuropathies that are characterized by RGC loss. We previously demonstrated that A_3R activation confers neuroprotection to RGCs in an animal model of laser-induced OHT (Chapter 2). In the present work, we proposed a new therapeutic strategy by the incorporation of 2-Cl-IB-MECA in a biodegradable intravitreal drug delivery system that we demonstrated to be safe and biocompatible upon insertion in the vitreous cavity of the animals (Chapter 3). The results presented herein demonstrate that the treatment with 2-Cl-IB-MECA-loaded PCL implants confers protection to RGCs and optic nerve against damage induced by retinal ischemia.

The use of biodegradable intraocular implants has the potential to replace the need of several intravitreal injections that are required in chronic retinal diseases (Kim et al., 2014b). The main advantage of PCL-based implants prepared by SFM is the fact that this methodology does not require harmful solvents and extreme processing temperatures that could degrade the components (polymers, drugs, and additives), resulting in solvent-free materials after processing (Chapter 3, supplementary information). The PCL-based implants loaded with 2-Cl-IB-MECA were developed in collaboration with the Chemical Engineering Department of the Faculty of Sciences and Technology of the University of Coimbra (supplementary information). 2-Cl-IB-MECA-loaded PCL implant presented an extended-release of 2-Cl-IB-MECA of around 30 days, corresponding to an average drug release of 1.6 ng/day. This value is within the same order of magnitude of the amount delivered by intravitreal injection for 2-Cl-IB-MECA (around 3.27 ng) that we reported neuroprotective to the retina (Galvao et al., 2015), and further confirming the therapeutic potential of this drug delivery system.

Prior the assessment of the neuroprotective activity of 2-Cl-IB-MECA-loaded PCL implants, we wanted to evaluate whether the released 2-Cl-IB-MECA presented functional activity. Knowing that RGCs express A_3R (Zhang et al., 2006) and that stimulation of the A_3R limits the rise in Ca^{2+} induced by glutamate (Zhang et al., 2010), single-cell Ca^{2+} imaging was performed as a functional readout of the activity of 2-Cl-IB-MECA released from the implant. In the current work, the activation of the A_3R with 1 μM of 2-Cl-IB-MECA decreased the Ca^{2+} changes induced by glutamate, which is in accordance with the literature (Zhang et al., 2010). The confirmation that 2-Cl-IB-MECA released from the PCL-implants has functional activity was achieved by the observation that the incubation of RGCs with medium that was in contact with 2-Cl-IB-MECA-loaded PCL implant also decreased the Ca^{2+} entrance induced by glutamate. This effect was specific of RGCs since in the primary cultures of retinal neural cells, with residual numbers of RGCs, 2-Cl-IB-MECA did not change the Ca^{2+} response to glutamate.

The protective activity of 2-Cl-IB-MECA-loaded PCL implants were assessed in an animal model of I-R injury. We first assessed the retinal thickness, since a thinning of the retina, mainly NFL, may reflect RGC loss (Chauhan et al., 2012, Chidlow et al., 2014). In fact, ganglion cell complex thickness (NFL+GCL+IPL) is being used to early diagnose glaucoma (Scuderi et al., 2020). We observed a decrease in total retinal thickness, in which the main affected retinal layers are NFL+GCL+IPL. Despite no beneficial effects in retinal thickness were observed with the treatment with 2-Cl-IB-MECA-PCL implants, we further explored retinal cell death, mainly RGC loss after ischemic injury.

RGC death by caspase-dependent mechanisms has been reported in response to I-R injury (Patil et al., 2004), as well as in other retinal degenerative diseases like glaucoma (Thomas et al., 2017). Caspases are a family of cysteine proteases known to be involved in the initiation and execution of apoptosis and have been implicated in the death of RGCs (Thomas et al., 2017). The death of a single RGC can lead to the spreading of death signals, mostly by the release of intracellular glutamate from the dying cells that affects the survival of surrounding cells (Caprioli et al., 2008). It has been estimated that 50% of the cellular population of GCL are RGCs, but the GCL is also composed of astrocytes and displaced amacrine cells (Schlamp et al., 2013, Nadal-Nicolas et al., 2015a). This might explain the lack of effect of 2-Cl-IB-MECA-loaded PCL implants in reducing the number FLIVO$^+$ cells, since we might be counting RGCs and the other cells in the GCL, amacrine cells for example (Schmid et al., 2014, Palmhof et al., 2019) that might be affected by I-R. Besides cell death in the GCL, the majority of TUNEL$^+$ cells were found in ONL. Previous reports describe a second wave of cell death that mainly affects outer retinal layers and occurs at later time points (21 days after ischemic injury) (Schmid et al., 2014), which may help explaining our observations since cell death was evaluated 30 days post I-R.

Caspase activation is the main driver of the apoptotic process. Caspase-mediated apoptotic death occurs by the activation of initiator caspases that trigger a cascade to amplify the response leading to the activation of the effector caspases (a "no return" point) that culminates in DNA fragmentation (Pollard et al., 2017). It means that the assessment of activated caspases by FAM-FLIVO Poly Caspase Inhibitor (FAM-VAD-FMK) and the assessment of cell death (apoptotic DNA cleavage) by TUNEL assay provide different conclusions regarding different points of the apoptotic process. In fact, it seems that 2-Cl-IB-MECA-loaded PCL implants do not decrease the number of cells with active caspases, but could prevent cells from undergoing the cell death process, since we observed that 2-Cl-IB-MECA released from the implant was able to prevent the increase in TUNEL$^+$ cells without interfering with FLIVO$^+$ cells. Another explanation could reside in the involvement of other proteases. Apart from caspases, Ca^{2+}-dependent proteases known as calpains play a role in the execution of apoptosis (Momeni 2011). Calpains are activated under conditions of elevated IOP (Huang et al., 2010), and knowing that the activation of A_3R leads to a decrease in intracellular Ca^{2+} in RGCs (Zhang et al., 2010), one possible explanation to the protection afforded by 2-Cl-IB-MECA-PCL implant could be the decrease in calpains activation, as was suggested for the neuroprotection observed in a model of cerebral ischemia (Von Lubitz et al., 1999).

Enhancing RGC survival is a critical first step for the development of new therapeutic strategies, and 2-Cl-IB-MECA released from the implant prevented the Brn3a$^+$ RGCs loss induced by I-R. However, for RGCs that already present axonal injury merely preventing apoptosis will not enhance regrowth of axons (Boia et al., 2020). Moreover, the impact of retinal I-R injury extends to the optic nerve (Renner et al., 2017). Therefore, we extended the study to the effects of 2-Cl-IB-MECA-loaded PCL implants in the structure of optic nerve and anterograde transport. Optic nerve axons are surrounded by myelin sheaths that are lost after retinal I-R injury (Renner et al., 2017). We observed disorganized myelin sheaths, but this did not interfere with the area of the myelin sheath. However, the enlargement of axonal inner tongue due to ischemic injury was attenuated by the treatment with 2-Cl-IB-MECA-PCL implant. RGCs unmyelinated axons bundle in the optic nerve head and become myelinated as it traverses the lamina cribrosa (Yanoff et al., 2015). Oligodendrocytes are responsible for myelination and metabolic support of RGC axons (Simons et al., 2015). How an oligodendrocyte "wraps" its plasma membrane around the axons is still an issue under investigation, but it was demonstrated that the inner tongue is the primary growth zone in growing myelin sheaths (Snaidero et al., 2014). Oligodendrocyte loss has been implicated in OHT injury, and it has been proposed that this is the mechanism through which the axons are damaged leading to the subsequent RGC death (Nakazawa et al., 2006, Son et al., 2010). Even in retinal ischemic injury, the function of oligodendrocytes is impaired (Renner et al., 2017). Moreover, others reported that A_3R activation leads to oligodendrocyte apoptosis but using a much higher concentration of the agonist (2-Cl-IB-MECA between 10 μM and 1 mM) (Gonzalez-Fernandez et al., 2014). Although we cannot determine the concentration that reaches the retina after being released from the implant, in a previous work we injected in the vitreous 1.2 μM of 2-Cl-IB-MECA that was sufficient to confer neuroprotection to RGCs and to preserve the structure of the optic nerve in an animal model of laser-induced OHT (Chapter 2).

RGC axonal projections form the optic nerve and conduct the visual signal from the retina to the visual centers in the brain (mainly SCi in rat brain) (Busse 2018). It was reported that anterograde axonal transport blockade precedes the deficits in retrograde axonal transport (Dengler-Crish et al., 2014). Retinal I-R leads to a depletion of CTB transport from the retina to SC that is in line with other reports in DBA/2J glaucoma animal model (Crish et al., 2010). In fact, besides axonal regeneration it is important that new therapies also rebuild connections from the eye to the brain, and the treatment with 2-Cl-IB-MECA-loaded PCL implants was able to preserve the anterograde axonal transport to the same levels of control.

ERG has been used to asses retinal function *in vivo*, and the ERG response after exposing the animals to a very dim light flashes reflects the function of RGCs (Bui et al., 2004). In that way a decrease in the amplitude of both pSTR and nSTR reflects RGC injury (Perez de Lara et al., 2014). The beneficial effects of 2-Cl-IB-MECA-loaded PCL implants reflected by a decrease of the impact of I-R on STR, reveals that 2-Cl-IB-MECA-loaded PCL implants were able to preserve the function of RGCs, but did not inhibit the loss of function of other retinal cells. In fact, we previously described that the treatment with intravitreal injection of the A_3R agonist attenuated the effect of OHT on STR while it did not affect the amplitudes of a- and b-waves under scotopic conditions (Chapter 2). These results demonstrate that the beneficial effects of the activation of A_3R can be specific and directed to RGCs.

The treatment with 2-Cl-IB-MECA-loaded PCL implants preserved the structure of the optic nerve and increase the anterograde axonal transport, which is consistent with the preservation of RGC function and indicates that RGCs are protected from I-R damage. Our results support that A_3R could be considered a novel therapeutic target and the incorporation of A_3R agonist in a biodegradable intraocular implant may be a promising therapeutic strategy for the treatment of optic neuropathies.

6. Supplementary data

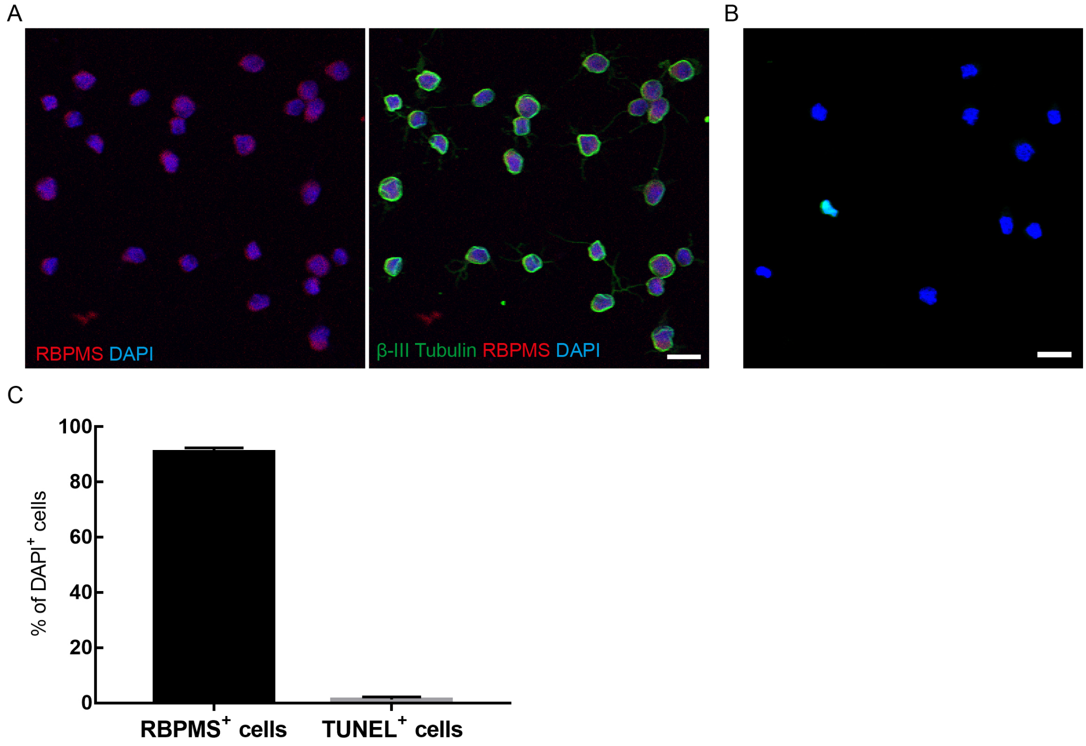

Figure S4 | Purity and viability of immunopurified RGCs at DIV1 of culture. The preparations were observed in a fluorescence microscope (Axio Observer.Z1, Zeiss, Germany), using a 20x objective (Plan Achromat 20x/0.8 M27). The number of RBPMS+ retinal ganglion cells (**A**) and TUNEL+ cells (**B**) per field were counted and normalized to the total number of cells (DAPI+ cells) (**C**).

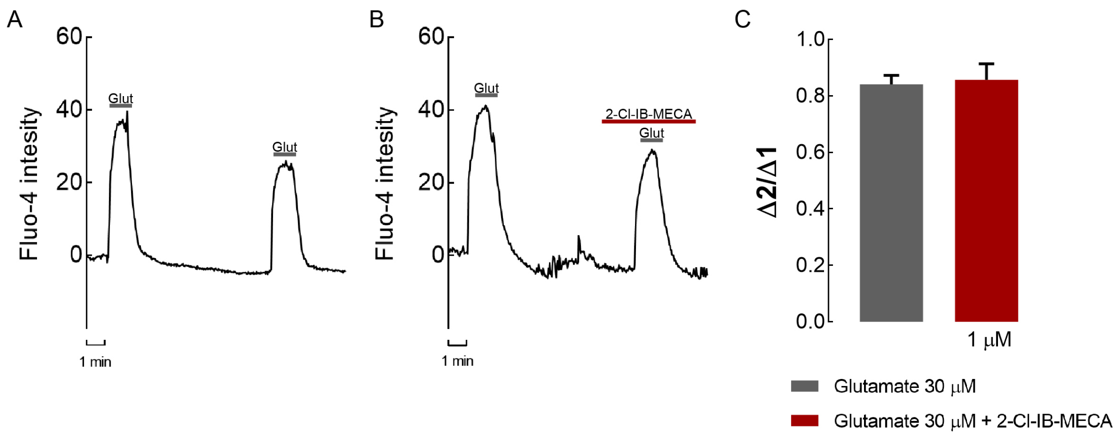

Figure S5 | A_3R agonist 2-Cl-IB-MECA did not modify the Ca^{2+} changes triggered by glutamate in primary retinal neural cell cultures. (**A**) Cells were stimulated twice with 30 μM glutamate + 10 μM glycine (referred to as Glut) with 5 min interval. (**B**) Cells were pre-incubated with 2-Cl-IB-MECA (1 μM) 3 minutes before and 2 minutes after stimulation with glutamate. (**C**) The mean fluorescence peak of Ca^{2+} changes were quantified, and results are presented as Δ2/Δ1 from 4 independent experiments.

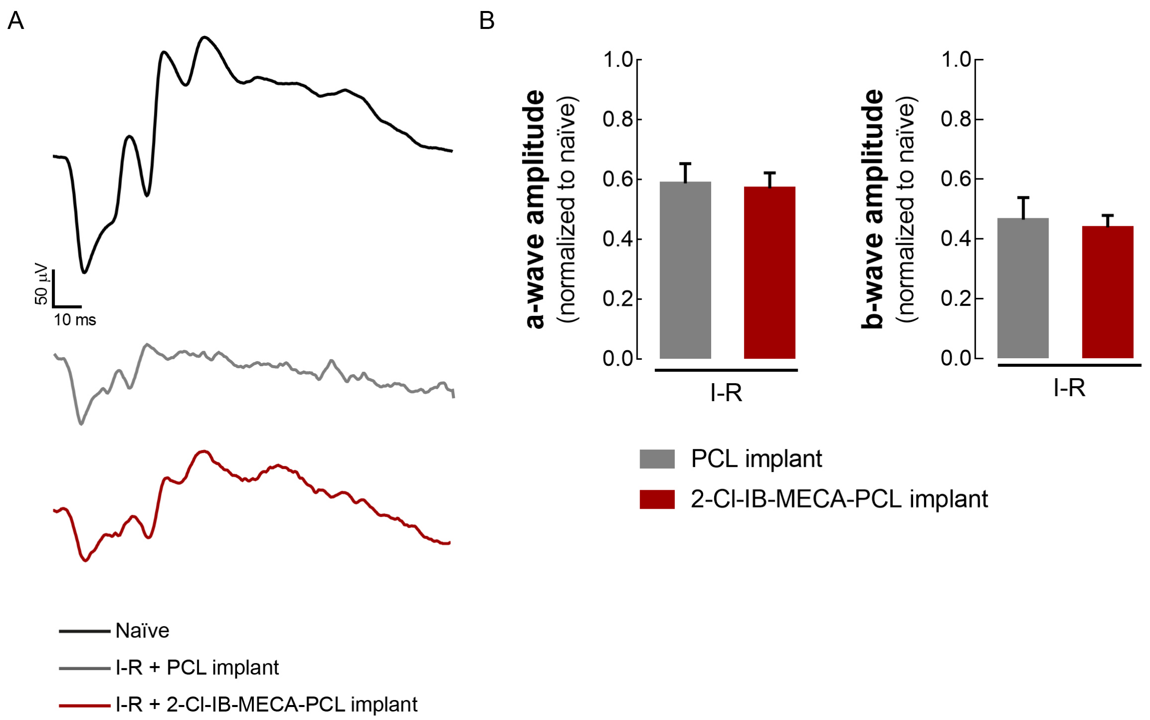

Figure S6 | 2-Cl-IB-MECA released from the implant did not change the a-wave and b-wave amplitudes following I-R injury. (**A**) Representative traces of scotopic response. (**B**) The amplitudes of scotopic a-wave and b-wave from I-R eyes treated with PCL implant or 2-Cl-IB-MECA implant were normalized to the responses from naïve eyes. Results are presented as mean ± SEM from 10-11 animals.

7. Supplementary videos

Video S1 | RGCs were stimulated twice with glutamate
http://bit.ly/Video_S1

Video S2 | RGCs stimulated twice with glutamate in the presence of 2-Cl-IB-MECA in the second stimulation.
http://bit.ly/Video_S2

Video S3 | RGCs stimulated twice with glutamate in the presence of medium that was in contact with 2-Cl-IB-MECA-PCL implant in the second stimulation.
http://bit.ly/Video_S3

Video S4 | Retinal mixed cultues were stimulated twice with glutamate.
http://bit.ly/Video_S4

Video S5 | Retinal mixed cultues were stimulated twice with glutamate in the presence of 2-Cl-IB-MECA in the second stimulus.
http://bit.ly/Video_S5

8. Supplementary information[1]

8.1. Materials and methods

8.1.1. Preparation of PCL implants loaded with 2-Cl-IB-MECA

Powder of PCL (40k ≤ Mn ≤ 50 kg/mol, Sigma-Aldrich, Missouri, USA) was obtained as previously described (de Matos et al., 2013), and mechanically sieved to particle diameters smaller than 250 µm. Glycofurol (G, 99%, Sigma-Aldrich, Missouri, USA) was used as a compatibilizer to homogenize the 2-Cl-IB-MECA (Tocris Bioscience, Bristol, UK) and PCL mixture (Chapter 3). Preliminary tests were used to define the concentration ratios of the mixture (data not shown) and the depressurization rate (2 and 3 MPa/min were tested) (Braga et al., 2017). Physically mixed combinations of PCL:2-Cl-IB-MECA:G (66:26:08, wt.%) were introduced into polyurethane micro-cylinder moulds and were processed by SFM at 20 MPa and 45 °C for 2 h. The system was then depressurized at 2 MPa/min. The employed experimental SFM set-up and the followed general procedures were described elsewhere (Chapter 3).The processed materials (cylindrical implants) were removed from the micro-cylindric moulds and cut to dimensions of approximately 2 mm × 0.46 mm (length × diameter) under a stereomicroscope (Leica, Wetzlar, Germany).

8.1.2. Release profile of 2-Cl-IB-MECA from the PCL implant

The 2-Cl-IB-MECA-loaded PCL implants prepared by SFM were tested to determine the drug incorporation yields and the drug release curves in water by a chromatographic method. A total of two and three replicates were used for the drug incorporation and for the drug release test, respectively. Samples were kept in sealed vials in a thermoshaker at 37 °C and 100 rpm while performing both tests.

For the drug incorporation assessment, samples were kept in methanol. Aliquots were retrieved for analysis every 2 h, followed by a complete replacement of the solution with fresh solvent. This procedure was repeated until a negligible amount of drug was detected (less than 0.5% of the accumulated drug). Solubility data retrieved from the literature was used to define the conditions applied for the drug release test (Braga et al., 2017, manuscript in preparation). These experiments were performed in Milli-Q water (15 mL), with aliquots (200 µL) being retrieved at defined time t intervals. The release profiles were obtained by plotting over time the percentage of the released drug, which is given by Eq. 7:

$$\text{Released 2-Cl-IB-MECA (\%)} = \frac{M_t}{M_0} \times 100 \qquad (7)$$

where Mt is the amount of drug released at a given time, and M_0 is the mass of drug that was loaded into the implant.

1 The conception and design of porous implants, as well as their experimental production/processing, physicochemical characterization, and degradation/*in vitro* release experiments were performed by Chemical Engineering Department of the Faculty of Sciences and Technology of the University of Coimbra.

Incorporated and released 2-Cl-IB-MECA was quantified by high performance liquid chromatography (HPLC, Prominence UFLC, Shimadzu, Japan), coupled to a photo diode array detector (DAD, SPD-M20A, Shimadzu, Japan) and using a reverse-phase column C18 RP (250 × 4 mm i.d., 5 mm). The mobile phase was a mixture of acetonitrile/water (8:2, v/v) in isocratic elution (12 min), and flow rate of 1 mL/min at 35 °C, with quantification at 270 nm and injection volume of 5 µL. Calibration curves were prepared from 2-Cl-IB-MECA solutions of known concentration in methanol from 0 up to 228 µg/mL (R^2=0.9995) for the drug incorporation experiments, and in water from 0 to 5 µg/mL (R^2=0.9930) for the drug release tests.

8.2. Results

8.2.1. Profile for 2-Cl-IB-MECA release from PCL implants

The porosity of PCL implants increased for higher depressurization rates (1 to 3 MPa/min) from 42% to 63%, while the addition of glycofurol, for the same depressurization rate of 2 MPa/min, leads to slightly increased porosity from 57% to 62%, as we previously described (Chapter 3). At this SFM conditions (20 MPa and 45 °C for 2 h, and depressurization rate of 2 MPa/min) implants are highly porous with a surface area of around 11-16 m^2/g (Chapter 3). Besides the porogenic effect, glycofurol was used as a pre-processing mixing solvent of the drug, and as a compatibilizer between the drug and PCL, as previously reported (Chapter 3).

The 2-Cl-IB-MECA incorporation yield in the produced implants was determined by applying a quantification method using methanol as an extraction solvent, due to the higher solubility of the drug in methanol when compared with water-based systems (manuscript in preparation). The 2-Cl-IB-MECA loaded implants presented an incorporation yield of 90.7 ± 12.4% at defined conditions (Figure 36), which corresponds to 235 ± 32 µg/mg (mass of drug per mass of implant). Since the drug is kept in the polymeric matrix, it is also usual to present drug loading in terms of the mass of 2-Cl-IB-MECA per mass of PCL, which was 357.5 ± 49.0 µg/mg. It should be noted that these results are valid only for the considered dimensions used for the implants (2 mm × 0.46 mm, length × diameter). Therefore, for different implant dimensions and drug concentrations additional studies should be developed since the solubility in the polymer-additive-solvent mixtures must be considered in the SFM processing.

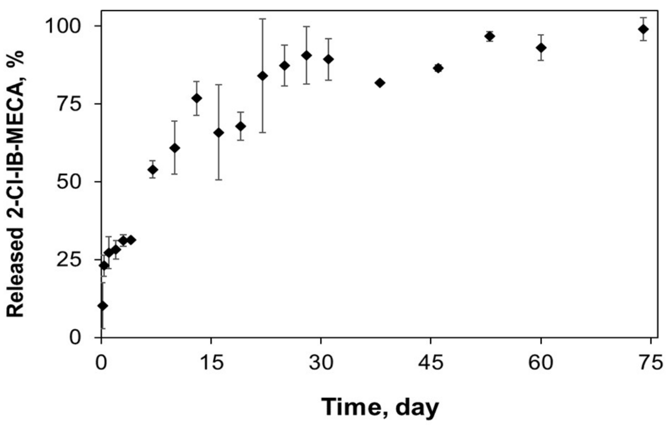

Figure 36 | Released 2-Cl-IB-MECA (%) in water from intraocular PCL-based implants (PCL:2-Cl-IB-MECA:G proportion 66:26:08, wt.%) processed by SFM.

4

General discussion

General discussion

Optic neuropathies comprise a group of ocular diseases, like glaucoma (the most common), anterior ischemic optic neuropathy and retinal ischemia. Glaucoma is a leading cause of irreversible blindness and the main risk factor for disease development is elevated IOP (Weinreb et al., 2014). RGCs are the main affected cells (Carelli et al., 2017) and blindness secondary to optic neuropathies is irreversible since RGCs lack the capacity for self-renewal and have a limited ability for self-repair (Goldberg et al., 2002). Currently, the treatments are focused on lowering the IOP, but vision loss progresses in some patients despite successful IOP control, suggesting that there are other mechanisms beside OHT that lead to the loss of RGCs. Therefore, new and more effective treatments are needed, and RGCs neuroprotection have emerged as a strategy with great potential (Boia et al., 2020).

The A_3R is an adenosine receptor that preferentially couples to G_i proteins (Borea et al., 2015). In the past years, great attention has been given to the potential of the modulation of A_3R activity since it has been demonstrated that the activation of A_3R confers neuroprotection in several animal models of CNS pathological conditions, like cerebral ischemic conditions (Chen et al., 2006, Pugliese et al., 2007, Choi et al., 2011) or traumatic brain injury (Farr et al., 2020). Moreover, the genetic knockout of A_3R in animals leads to an increase in neurodegeneration in response to repeated episodes of hypoxia (Fedorova et al., 2003). Regarding the retina, the activation of A_3R using selective agonists was shown to confer neuroprotection (Galvao et al., 2015), and particularly neuroprotection to RGCs (Zhang et al., 2006, Hu et al., 2010). The effects of 2-Cl-IB-MECA are abolished in the presence of A_3R antagonist (MRS 1191), confirming the selectivity of 2-Cl-IB-MECA in mediating the activation of A_3R (Galvao et al., 2015). In a phase 2 clinical trial for the treatment of dry eye syndrome, an A_3R selective agonist demonstrated to have efficacy as an IOP-lowering agent (Avni et al., 2010, Fishman et al., 2013). Nevertheless, others have previously reported A_3R antagonists as hypotensive drugs for the treatment of glaucoma (Avila et al., 2001, Avila et al., 2002, Yang et al., 2005, Wang et al., 2010), but this discrepancy can be due in differences in the treatment protocol and the time-point at which the IOP was measured (Avni et al., 2010). Indeed, CF101 (IB-MECA, A_3R agonist) entered a phase 2 clinical trial (ClinicalTrials.gov identifier: NCT01033422) to assess the safety and efficacy of daily oral administration in subjects with elevated IOP.

In addition to neuroprotection and the IOP lowering effect, A_3R activation also improves the outcome of several pathological conditions by reducing the inflammatory milieu (Choi et al., 2011, Ohsawa et al., 2012). Indeed, A_3R agonists have been in several clinical trials aiming the control of inflammation in several pathologies (Table 3, Chapter 1). Knowing that microglia-mediated neuroinflammation contributes to neurodegeneration in glaucoma (Madeira et al., 2015a), A_3R activation was studied to evaluate whether it could control microglia reactivity triggered by EHP. In fact, the incubation of microglia exposed to EHP with 2-Cl-IB-MECA was able to hinder retinal microglia reactivity induced by EHP, suggesting that A_3R agonists could afford protection against glaucomatous degeneration through the control of retinal neuroinflammation (Ferreira-Silva et al., 2020). All of these evidences reinforce the hypothesis that the A_3R agonist might be a suitable treatment for glaucoma.

The fact that 2-Cl-IB-MECA is a selective ligand for both human and rodent A_3Rs allows the use of rodents as a model for the evaluation of protective effects of A_3R activation. In this work, two different animal models were used to mimic several features occurring in glaucoma: the laser-induced OHT (Chapter 2) and retinal I-R injury (Chapter 4). The laser-induced OHT leads to a chronic increase of IOP that persists for consecutive days to weeks, depending on the number of laser burns (Biermann et al., 2012), and the retinal I-R encompasses the induction of retinal ischemia by acute IOP increase followed by reperfusion (Johnson et al., 2010). Despite these differences the outcome of both animal models is the dysfunction and ultimately death of RGCs, two characteristics of glaucoma (Johnson et al., 2010).

Knowing from literature that RGCs express A_3R (Zhang et al., 2006) and that the activation of A_3R confers protection to RGCs following excitotoxic stimulus (Zhang et al., 2006, Hu et al., 2010, Galvao et al., 2015), in Chapter 2, it was investigated the potential of 2-Cl-IB-MECA to protect the retina from glaucomatous damage.

In a previous work, the A_3R agonist (2-Cl-IB-MECA, 1.2 μM) was administered by intravitreal injection 2 h prior the ischemic insult (Galvao et al., 2015). One of the reasons for the failure of several neuroprotective agents identified in preclinical studies in clinical trials has been argued to be the timing of drug administration (Danesh-Meyer et al., 2009). In most preclinical studies, the drug is given before inducing injury, different from the clinical trials in which the patient is enrolled after acute injury or disease establishment, when the neurons are already committed to death (Danesh-Meyer et al., 2009). Knowing from the previous study that A_3R activation has the potential to protect RGCs from glaucomatous damage (Galvao et al., 2015), the A_3R agonist was delivered by intravitreal injection to the eyes of OHT animals, immediately after inducing injury, aiming a more relevant and translational study. The treatment with A_3R agonist increased the RGC survival and attenuated the impairment in the retrograde axonal transport induced by OHT, which is consistent with the preservation of the optic nerve structure. These beneficial effects of A_3R activation may be contributing to the maintenance of the RGC function in the OHT animals, as determined by the STR components. In order to perform a preclinical study that can be extrapolated into a clinical study an accurate and reliable assessment of RGC numbers along with appropriate testing of RGC function is required. Several preclinical studies in animal models of disease rely on the assessment of RGC number. The quantification of RGC loss in experimental glaucoma include counting RGCs using specific markers, as Brn3a or RBPMS (Nadal-Nicolas et al., 2009, Kwong et al., 2010) that can be done in histological retinal cryosections or wholemounts (Mead et al., 2016). The most reliable preparation is wholemount, but retinal sections also provide a qualitative result with equal fidelity (Mead et al., 2014). In Chapter 2, the survival of RGCs was assessed by immunolabeling for Brn3a or RBPMS in retinal wholemounts and cryosections, respectively. The magnitude of the determined protection was similar in the two approaches, further confirming that both are reliable to assess RGC neuroprotection. Despite being a gold standard method in preclinical research, this is an endpoint experiment that can not be assessed in humans. However, the assessment of individual RGC apoptosis in humans is being validated using DARC technology (Cordeiro et al., 2017). It is therefore essential to have a standard procedure for preclinical assessment when evaluating RGC loss and survival, combining both histological and structural/functional analysis.

The study was completed by the assessment of RGC function, and the treatment with 2-Cl-IB-MECA attenuated the effect of OHT. Since the degenerative process of RGCs is accompanied by structural alterations in RGC axons, the evaluation of optic nerve structure revealed that 2-Cl-IB-MECA preserved the structure of the optic nerve, which is consistent with the data on FG retrograde axonal transport. The results demonstrating the beneficial effects of the treatment with 2-Cl-IB-MECA in OHT animals are supported by others that show the role of A_3R activation in RGC axonal regeneration, using cultured RGCs and the optic nerve crush animal model (Nakashima et al., 2018). In this study, the authors revealed that the activation of an Akt-dependent signalling pathway promotes neurite outgrowth (Nakashima et al., 2018). In the OHT animal model, similar pathways could be activated in the RGC soma and may contribute to the improvement in the axonal transport and optic nerve structure. Moreover, other mechanisms by which A_3R activation mediates protection to RGCs may be involved, like a decrease in Ca^{2+} influx (Zhang et al., 2010).

Currently, the most common method of pharmacological intervention in glaucoma therapy is the topical instillation of eye drops, indeed it was reported that 90% of ophthalmic drug formulations are for topical use (Edelhauser et al., 2010). However, when aiming drug administration to the posterior segment of the eye, the eye drops face several barriers to achieve the target site with an effective and therapeutic drug concentration (Agrahari et al., 2016, Varela-Fernandez et al., 2020). Moreover, topical eye drops are associated with poor patient compliance which is the most important reason for treatment dropout in glaucoma patients (Claxton et al., 2001, Sleath et al., 2006, Harasymowycz et al., 2016). Therefore, intravitreal injections are widely used to deliver drugs near the retina, bypassing the ocular barriers and decreasing the need of higher drug concentrations to attain a therapeutic effect (Meyer et al., 2016). The need of repetitive injections presents several side-effects that might include raised IOP, retinal detachment, cataract, and endophthalmitis (Jager et al., 2004, Sampat et al., 2010). Intraocular drug delivery systems are receiving a lot of attention in the last years, once they allow to overcome the various ocular barriers (Gote et al., 2019). Although the implantation of intravitreal devices also requires a surgical intervention that is not free of injection-related complications, they provide the maintenance of therapeutic drug concentrations at the target site along time with only one injection avoiding the cumulative side effects of repeated intravitreal injections. In fact, it was found that 62.8% of glaucoma patients were willing to accept a subconjunctival implant instead of eye drops, even though the implantation procedure is more invasive (Foo et al., 2012). Indeed, sustained drug release systems are now routinely used in patients (Wang et al., 2013)a.

With the aim to overcome the need of multiple intravitreal injections, a new biodegradable intraocular implant for controlled drug release was developed in collaboration with the Chemical Engineering Department of the Faculty of Sciences and Technology of the University of Coimbra (Chapter 3, supplementary information). The PCL-based implant was successfully developed using a SFM method and was physicochemical characterized. The application of PCL as a biomaterial return into the spotlight with a particular focus on medical devices, drug delivery and tissue engineering (Woodruff et al., 2010). Regarding intraocular drug delivery devices, the potential of PCL-based devices has been explored as subretinal (Beeley et al., 2005, Shahmoradi et al., 2017), intracameral (Bernards et al., 2013, Kim et al., 2016) and intravitreal (Fialho et al., 2008, Silva-Cunha et al., 2009, Lance et al., 2015) devices. Moreover, PCL-based devices have been designed for glaucoma treatment by the incorporation of a IOP-lowering drug and by subconjunctival placement (Natu et al., 2011a, Natu et al., 2011b). All of these proposed PCL-based devices presented good ocular compatibility, however, they were prepared using methods that may involve hazardous solvents and/or operate at processing conditions (e.g., temperature, pH) that could promote the degradation of the polymers, drugs and other additives. In order to circumvent the above-mentioned problems alternative methods based on supercritical fluids, and namely on $scCO_2$, have been proposed (de Matos et al., 2013). The SFM method allows to produce a porous implant in which the higher surface area contributes to a faster degradation when compared to implants processed by the conventional HM processes. Moreover, SFM-processed implants also presented a faster release rate of the test-drug. Thus, the potential of PCL-based implants prepared by SFM to be used as intraocular drug delivery devices was assessed (Chapter 3). Since nonclinical studies should be conducted using *in vitro* approaches before using *in vivo* animal models (Andrade et al., 2016), the safety of PCL-based implants was determined using retinal primary neural cell cultures and retinal organotypic cultures. Two approaches were defined to test the safety of the implants to retinal cells: exposing the cells directly to the implant and exposing the cells to the degradation products of the PCL-based implants, since the polymer degradation products can be a major factor influencing the tolerance of the developed implant (Woodruff et al., 2010). PCL degradation can occur via surface erosion that involves the hydrolytic cleavage of the polymer backbone only at the surface, or via bulk degradation that occurs when water penetrates the entire polymer bulk, causing hydrolysis throughout the entire polymer matrix (Woodruff et al., 2010). In our experimental conditions, whether PCL-based implants are being degraded by surface erosion or by bulk degradation is not known. However, in both preparations, the presence of the PCL implant or the degradation products did not cause neuronal cell death, particularly did not affect the number of RGCs, reinforcing the possibility to test the safety of PCL-based implant in animal models. Taking into account that PCL-based implants were not toxic to retinal cells, the devices were introduced in the vitreous of Wistar rats. PCL implants can be easily inserted into the vitreous cavity by a minimally invasive procedure that is not harmful to the retina, as observed in sham-operated experimental group. The implantation was performed in order to avoid the obstruction of the visual axis, and throughout the course to the study no change in the location of the device was observed. The presence of PCL-based implants in vitreous cavity did not elicit neither edema (that would cause an increase in retinal thickness) nor major cell loss (retinal thinning) as assessed by analysis of the B-scans acquired by OCT, and the retinal electrical function was also not affected. Moreover, histological data showed that intraocular PCL implants did not cause changes to retinal neurons, specifically loss of RGCs, further confirming that the implants are not toxic to retinal neural cells. Additionally, despite no major signs of inflammation, like microglia activation or increased levels of cytokines, both the surgical procedure and the presence of the implants induced Müller cell activation. The expression of GFAP in Müller cells is a feature of gliosis and could be a sign of a disturbance in retinal homeostasis (Mizutani et al., 1998, Wang et al., 2002, Kimble et al., 2006). Enhanced GFAP immunostaining in Müller cells, without alterations in microglia reactivity has been reported due to foreign body reaction (Giordano et al., 1995, Zhao et al., 2017), which may explain the results obtained. Since the Müller cell gliosis observed in early time points is a transient effect, not being observed 1 year after the procedure, one could suggest that the initial reaction of Müller cells is necessary to maintain retinal homeostasis after the surgical intervention to place the PCL implant in the vitreous. In fact, this transient expression of GFAP in Müller cells has been reported previously by others (Giordano et al., 1995, Zhao et al., 2017). Since, Müller cells become reactive following PCL implantation but also react to the surgical procedure, allowed us to conclude that this is a typical retinal response after surgical procedure. The injection of PLGA microspheres in the retina of rabbits triggered GFAP increase in Müller cells that was normalized after 12 and 24 months (Giordano et al., 1995). Similarly, the intravitreal injection of PLGA microspheres in the eyes of Wistar rats caused an increase in GFAP fluorescence in activated Müller cells (Zhao et al., 2017). The fact that Müller cell gliosis was also observed in rabbits, apart from rats, and with other type of drug delivery system (PLGA microspheres) reinforces that this reaction is due to the surgical procedure. Given that PCL presents a slow degradation rate (Woodruff et al., 2010) arises the need to evaluate the impact of the implants in the eye during a longer period of time (1 year). However, the exposure to the PCL for 1 year did not cause Müller cells gliosis, or alterations in retinal structure and thickness.

Taking into consideration the lack of retinal toxicity, the new SFM-processed PCL-based implants can be envisaged for long-term intraocular drug delivery in several ophthalmological conditions, avoiding the need of repeated intraocular injections. Since the activation of A_3R confers protection to the retina, in particular to RGCs, these implants loaded with A_3R agonist could be a new strategy to protect the retina from degeneration. Therefore, a biodegradable PCL intraocular implant loaded with A_3R agonist (2-Cl-IB-MECA) was developed and its neuroprotective potential was addressed (Chapter 4).

2-Cl-IB-MECA-loaded PCL implants were developed in collaboration with the Chemical Engineering Department of the Faculty of Sciences and Technology of the University of Coimbra (Chapter 4, supplementary information). The release profile of 2-Cl-IB-MECA from the PCL implant revealed an extended-release of 2-Cl-IB-MECA of around 30 days, corresponding to an average drug release of 1.6 ng/day, which is within the same order of magnitude of the amount delivered by an intravitreal injection for 2-Cl-IB-MECA (5 μl, 1.2 μM) that we reported to be neuroprotective to the retina (Galvao et al., 2015). Besides confirming that 2-Cl-IB-MECA is being released from the implant, it is also important to study whether the drug released from the implant maintains functional activity to the receptor. Knowing that A_3R activation blocks the Ca^{2+} rise in RGC cultures induced by the P2X7 agonist (Zhang et al., 2006) or by the stimulation of NMDA receptors (Zhang et al., 2010), single-cell Ca^{2+} imaging was used as a functional readout of the release of 2-Cl-IB-MECA from the implant. Purified RGC cultures were prepared and Ca^{2+} imaging was performed. In order to ensure that the amount of drug release from the implant is compatible with the time-frame of Ca^{2+} experiments, 2-Cl-IB-MECA-loaded PCL-based implants were immersed in a saline solution for 24 h that was used to stimulate the cells. This period of time was sufficient to have around 30% of drug released from the implant (Chapter 4, supplementary information). 2-Cl-IB-MECA released from the implant was able to reduce the Ca^{2+} response of RGCs to glutamate, showing that more important than being released from the implant is the fact that the methodology used to produce the device does not interfere with the ability of the drug to activate the A_3R. Indeed, this result clearly indicate that 2-Cl-IB-MECA released from the implant activates A_3R.

The neuroprotective properties of 2-Cl-IB-MECA-loaded PCL-based implants were further evaluated in the retinal I-R animal model. Although this is considered an animal model of global retinal degeneration (Johnson et al., 2010), it triggers apoptosis in RGCs (Palmhof et al., 2019) which are the main affected cells in glaucoma and the goal read out of our study. Furthermore, this is an animal model is well-established and it has been widely used by our group to asses new neuroprotective strategies namely to RGCs (Madeira et al., 2016a, Boia et al., 2017).

The PCL implants loaded with 2-Cl-IB-MECA preserved the structure of the optic nerve and increased the anterograde axonal transport, which is consistent with the preservation of RGC function and indicates that RGCs are protected from I-R damage. The use of PCL-based devices for intravitreal drug released has been explored (Fialho et al., 2008, Silva-Cunha et al., 2009, Lance et al., 2015). Generally, these studies show that PCL-based devices can be used for long-term drug release, since PCL has a slow degradation rate.

Intravitreal devices offer a therapeutic advantage and have been considered to replace the clinical practice of monthly injections. For example in the case of AMD, the anti-VEGF therapies present a significant burden for the patients (Edelhauser et al., 2010). The Port Delivery System with ranibizumab developed by Genentech is a novel, innovative, long-acting drug delivery system that enables the continuous delivery of a customized formulation of ranibizumab in the vitreous (Campochiaro et al., 2019). The implant is in phase 3 of the randomized Archway trial (ClinicalTrials.gov Identifier: NCT03677934) and could ease treatment burden by reducing the number of injections needed (Regillo 2020). Moreover, aiming RGCs neuroprotection there is one intravitreal implant for sustained release of soluble CNTF that is in phase 2 clinical trial for glaucoma (ClinicalTrials.gov Identifier: NCT02862938). Although there is still a long way to go, pertinent future challenges and opportunities in the development of intraocular implants are arising.

The activation of A_3R could be considered a novel therapeutic target and the incorporation of A_3R agonist in a biodegradable intraocular implant may be a promising therapeutic strategy for the treatment of optic neuropathies. There is a major unmet need in the treatment of optic neuropathies, specifically for glaucoma. Although the adequate control of IOP obtained with topical drugs decreases the progression of disease, an effective treatment to protect RGCs from damage is far from available. An effective therapeutic strategy should be able to control elevated IOP, but also should induce a protective effect on RGCs. That way the most successful therapeutic strategy could rely on combining IOP lowering agents that are being used in clinical practice with neuroprotective strategies to protect RGCs. Despite some clinical trials focused on RGCs neuroprotection are ongoing (Boia et al., 2020), a treatment for optic nerve or RGC neurodegeneration is still largely unavailable. This work constitutes a step forwardin the search for new and improved treatments for patients with compromised visual function due to optic neuropathies.

6

Main conclusions

Conclusions

This work demonstrated that A_3R represents a potential drug target for the development of an additional therapeutic strategy for glaucoma. Moreover, the incorporation of 2-Cl-IB-MECA in a biodegradable intraocular implant may be a promising therapeutic approach conferring long time protection to RGCs.

This thesis is composed by three complementary chapters, which allowed to obtain a range of different conclusions:

- Chapter 2: The intravitreal injection of A_3R agonist (2-Cl-IB-MECA, 5 μl, 1.2 μM) increased the RGC survival and attenuated the impairment in the retrograde axonal transport induced by OHT, which is consistent with the preservation of the optic nerve structure. These beneficial effects of A_3R activation may be contributing to the maintenance of the RGC function in the OHT animals. Indeed, we proposed that A_3R could be considered a good therapeutic target to protect RGCs from glaucomatous damage.

- Chapter 3: A biodegradable intraocular implant for controlled drug release was developed in collaboration with the Chemical Engineering Department of the Faculty of Sciences and Technology of the University of Coimbra (supplementary information). Both *in vitro* and *in vivo* studies demonstrated that PCL implant is not toxic to retinal cells. However, the presence of PCL implant in the vitreous may induce transient reactivity of Müller cells. However, after one year with the PCL-based implant within the vitreous, no changes were found in the retinal structure nor in total retinal thickness. We concluded that PCL-based implants can be used for long-term sustained intraocular drug delivery applications.

- Chapter 4: 2-Cl-IB-MECA-loaded PCL implants were developed in collaboration with the Chemical Engineering Department of the Faculty of Sciences and Technology of the University of Coimbra (supplementary information). The release profile of 2-Cl-IB-MECA from the PCL implant revealed an extended-release of 2-Cl-IB-MECA of around 30 days, and 2-Cl-IB-MECA released from the implant maintains its ability to activate de A_3R, despite the methodology used to produce the device. The implantation of 2-Cl-IB-MECA-loaded PCL implants in the vitreous after inducing retinal ischemia, revealed that 2-Cl-IB-MECA preserved the structure of the optic nerve and attenuated the impairment in anterograde axonal transport induced by I-R, which is consistent with the preservation of RGC function, indicating that RGCs are protected from I-R damage.

This work meets one of the major needs in glaucoma management that is finding new strategies to protect the retina from glaucomatous neurodegeneration, minimizing the number of intravitreal injections. In order to progress in the preclinical study, the experiments should be performed under Good Laboratory Practices (GLP), as described in International Organization for Standardization (ISO) standard ISO-10993, that regulates the biological evaluation of medical devices. Moreover, the assessment of the rodent visual function with behavioural vision tests, as visual water tank and optomotor response, should be considered in the future work.

Although much work lies ahead, this work sheds light on a new therapeutic strategy to RGC neuroprotection using the A_3R agonist (2-Cl-IB-MECA), already in several clinical trials, incorporated in a new biodegradable implant for sustained drug release.

7

References

References

Abbott, C. J., T. E. Choe, C. F. Burgoyne, G. Cull, L. Wang and B. Fortune (2014). "Comparison of retinal nerve fiber layer thickness in vivo and axonal transport after chronic intraocular pressure elevation in young versus older rats." PLoS One 9(12): e114546. DOI: 10.1371/journal.pone.0114546.

Adachi, K., S. Takahashi, K. Yamauchi, N. Mounai, R. Tanabu and M. Nakazawa (2016). "Optical coherence tomography of retinal degeneration in royal college of surgeons rats and its correlation with morphology and electroretinography." PLoS One 11(9): e0162835. DOI: 10.1371/journal.pone.0162835.

AGIS (2000). "The advanced glaucoma intervention study (agis): 7. The relationship between control of intraocular pressure and visual field deterioration.The agis investigators." Am J Ophthalmol 130(4): 429-440. DOI: 10.1016/s0002-9394(00)00538-9.

Agrahari, V., A. Mandal, V. Agrahari, H. M. Trinh, M. Joseph, A. Ray, H. Hadji, R. Mitra, D. Pal and A. K. Mitra (2016). "A comprehensive insight on ocular pharmacokinetics." Drug Deliv Transl Res 6(6): 735-754. DOI: 10.1007/s13346-016-0339-2.

Aires, I. D., A. F. Ambrosio and A. R. Santiago (2017). "Modeling human glaucoma: Lessons from the in vitro models." Ophthalmic Res 57(2): 77-86. DOI: 10.1159/000448480.

Aires, I. D., R. Boia, A. C. Rodrigues-Neves, M. H. Madeira, C. Marques, A. F. Ambrosio and A. R. Santiago (2019a). "Blockade of microglial adenosine A2A receptor suppresses elevated pressure-induced inflammation, oxidative stress, and cell death in retinal cells." Glia 67(5): 896-914. DOI: 10.1002/glia.23579.

Aires, I. D., M. H. Madeira, R. Boia, A. C. Rodrigues-Neves, J. M. Martins, A. F. Ambrosio and A. R. Santiago (2019b). "Intravitreal injection of adenosine A2A receptor antagonist reduces neuroinflammation, vascular leakage and cell death in the retina of diabetic mice." Sci Rep 9(1): 17207. DOI: 10.1038/s41598-019-53627-y.

Alarcon-Martinez, L., P. de la Villa, M. Aviles-Trigueros, R. Blanco, M. P. Villegas-Perez and M. Vidal-Sanz (2009). "Short and long term axotomy-induced erg changes in albino and pigmented rats." Mol Vis 15: 2373-2383.

Allen, S. J., J. J. Watson, D. K. Shoemark, N. U. Barua and N. K. Patel (2013). "Gdnf, ngf and bdnf as therapeutic options for neurodegeneration." Pharmacol Ther 138(2): 155-175. DOI: 10.1016/j.pharmthera.2013.01.004.

Almasieh, M. and L. A. Levin (2017). "Neuroprotection in glaucoma: Animal models and clinical trials." Annual Review of Vision Science 3(1): 91-120. DOI: 10.1146/annurev-vision-102016-061422.

Almasieh, M., A. M. Wilson, B. Morquette, J. L. Cueva Vargas and A. Di Polo (2012). "The molecular basis of retinal ganglion cell death in glaucoma." Progress in Retinal and Eye Research 31(2): 152-181. DOI: 10.1016/j.preteyeres.2011.11.002.

Alqawlaq, S., J. G. Flanagan and J. M. Sivak (2019). "All roads lead to glaucoma: Induced retinal injury cascades contribute to a common neurodegenerative outcome." Exp Eye Res 183: 88-97. DOI: 10.1016/j.exer.2018.11.005.

Amsden, B. G. and D. Marecak (2016). "Long-term sustained release from a biodegradable photo-cross-linked network for intraocular corticosteroid delivery." Mol Pharm 13(9): 3004-3012. DOI: 10.1021/acs.molpharmaceut.6b00358.

Anderson, D. R., S. M. Drance, M. Schulzer and G. Collaborative Normal-Tension Glaucoma Study (2001). "Natural history of normal-tension glaucoma." Ophthalmology 108(2): 247-253. DOI: 10.1016/s0161-6420(00)00518-2.

Anderson, J. M., A. Rodriguez and D. T. Chang (2008). "Foreign body reaction to biomaterials." Semin Immunol 20(2): 86-100. DOI: 10.1016/j.smim.2007.11.004.

Anderson, M. G., R. S. Smith, N. L. Hawes, A. Zabaleta, B. Chang, J. L. Wiggs and S. W. John (2002). "Mutations in genes encoding melanosomal proteins cause pigmentary glaucoma in DBA/2J mice." Nat Genet 30(1): 81-85. DOI: 10.1038/ng794.

Andrade, E. L., A. F. Bento, J. Cavalli, S. K. Oliveira, C. S. Freitas, R. Marcon, R. C. Schwanke, J. M. Siqueira and J. B. Calixto (2016). "Non-clinical studies required for new drug development - part i: Early in silico and *in vitro* studies, new target discovery and validation, proof of principles and robustness of animal studies." Braz J Med Biol Res 49(11): e5644. DOI: 10.1590/1414-431X20165644.

Appel, E., G. Kazimirsky, E. Ashkenazi, S. G. Kim, K. A. Jacobson and C. Brodie (2001). "Roles of BCL-2 and caspase 3 in the adenosine A3 receptor-induced apoptosis." J Mol Neurosci 17(3): 285-292. DOI: 10.1385/JMN:17:3:285.

Avila, M. Y., R. A. Stone and M. M. Civan (2001). "A(1)-, A(2A)- and A(3)-subtype adenosine receptors modulate intraocular pressure in the mouse." Br J Pharmacol 134(2): 241-245. DOI: 10.1038/sj.bjp.0704267.

Avila, M. Y., R. A. Stone and M. M. Civan (2002). "Knockout of A3 adenosine receptors reduces mouse intraocular pressure." Invest Ophthalmol Vis Sci 43(9): 3021-3026.

Avni, I., H. J. Garzozi, I. S. Barequet, F. Segev, D. Varssano, G. Sartani, N. Chetrit, E. Bakshi, D. Zadok, O. Tomkins, G. Litvin, K. A. Jacobson, S. Fishman, Z. Harpaz, M. Farbstein, S. B. Yehuda, M. H. Silverman, W. D. Kerns, D. R. Bristol, I. Cohn and P. Fishman (2010). "Treatment of dry eye syndrome with orally administered CF101: Data from a phase 2 clinical trial." Ophthalmology 117(7): 1287-1293. DOI: 10.1016/j.ophtha.2009.11.029.

Badea, T. C., A. M. Solomon, T. Westbrook, G. D. Field and A. W. McGee (2018). "Nogo receptor 1 is expressed by nearly all retinal ganglion cells." Plos One 13(5): e0196565. DOI: 10.1371/journal.pone.0196565.

Baden, T., P. Berens, K. Franke, M. Roman Roson, M. Bethge and T. Euler (2016). "The functional diversity of retinal ganglion cells in the mouse." Nature 529(7586): 345-350. DOI: 10.1038/nature16468.

Bakalash, S., G. Ben-Shlomo, E. Aloni, I. Shaked, L. Wheeler, R. Ofri and M. Schwartz (2005). "T-cell-based vaccination for morphological and functional neuroprotection in a rat model of chronically elevated intraocular pressure." J Mol Med (Berl) 83(11): 904-916. DOI: 10.1007/s00109-005-0689-6.

Balaratnasingam, C., W. H. Morgan, L. Bass, G. Matich, S. J. Cringle and D.-Y. Yu (2007). "Axonal transport and cytoskeletal changes in the laminar regions after elevated intraocular pressure." Investigative Opthalmology & Visual Science 48(8): 3632. DOI: 10.1167/iovs.06-1002.

Ban, N., C. J. Siegfried and R. S. Apte (2018). "Monitoring neurodegeneration in glaucoma: Therapeutic implications." Trends Mol Med 24(1): 7-17. DOI: 10.1016/j.molmed.2017.11.004.

Baptista, F. I., M. J. Pinto, F. Elvas, T. Martins, R. D. Almeida and A. F. Ambrosio (2014). "Diabetes induces changes in kif1a, kif5b and dynein distribution in the rat retina: Implications for axonal transport." Exp Eye Res 127: 91-103. DOI: 10.1016/j.exer.2014.07.011.

Barakat, N. S. (2010). "Evaluation of glycofurol-based gel as a new vehicle for topical application of naproxen." AAPS PharmSciTech 11(3): 1138-1146. DOI: 10.1208/s12249-010-9485-x.

Barres, B. A., B. E. Silverstein, D. P. Corey and L. L. Chun (1988). "Immunological, morphological, and electrophysiological variation among retinal ganglion cells purified by panning." Neuron 1(9): 791-803. DOI: 10.1016/0896-6273(88)90127-4.

Basso, M. A. and P. J. May (2017). "Circuits for action and cognition: A view from the superior colliculus." Annu Rev Vis Sci 3: 197-226. DOI: 10.1146/annurev-vision-102016-061234.

Bat, E., Z. Zhang, J. Feijen, D. W. Grijpma and A. A. Poot (2014). "Biodegradable elastomers for biomedical applications and regenerative medicine." Regenerative Medicine 9(3): 385-398. DOI: 10.2217/rme.14.4.

Beach, K. M., L. F. Hung, B. Arumugam, E. L. Smith, 3rd and L. A. Ostrin (2018). "Adenosine receptor distribution in rhesus monkey ocular tissue." Exp Eye Res 174: 40-50. DOI: 10.1016/j.exer.2018.05.020.

Beeley, N. R., J. V. Rossi, P. A. Mello-Filho, M. I. Mahmoud, G. Y. Fujii, E. de Juan, Jr. and S. E. Varner (2005). "Fabrication, implantation, elution, and retrieval of a steroid-loaded polycaprolactone subretinal implant." J Biomed Mater Res A 73(4): 437-444. DOI: 10.1002/jbm.a.30294.

Berger, S., S. I. Savitz, S. Nijhawan, M. Singh, J. David, P. S. Rosenbaum and D. M. Rosenbaum (2008). "Deleterious role of tnf-alpha in retinal ischemia-reperfusion injury." Invest Ophthalmol Vis Sci 49(8): 3605-3610. DOI: 10.1167/iovs.07-0817.

Berkelaar, M., D. B. Clarke, Y. C. Wang, G. M. Bray and A. J. Aguayo (1994). "Axotomy results in delayed death and apoptosis of retinal ganglion cells in adult rats." J Neurosci 14(7): 4368-4374.

Bernards, D. A., R. B. Bhisitkul, P. Wynn, M. R. Steedman, O. T. Lee, F. Wong, S. Thoongsuwan and T. A. Desai (2013). "Ocular biocompatibility and structural integrity of micro- and nanostructured poly(caprolactone) films." J Ocul Pharmacol Ther 29(2): 249-257. DOI: 10.1089/jop.2012.0152.

Beykin, G., A. M. Norcia, V. J. Srinivasan, A. Dubra and J. L. Goldberg (2020). "Discovery and clinical translation of novel glaucoma biomarkers." Prog Retin Eye Res: 100875. DOI: 10.1016/j.preteyeres.2020.100875.

Biermann, J., C. van Oterendorp, C. Stoykow, C. Volz, T. Jehle, D. Boehringer and W. A. Lagreze (2012). "Evaluation of intraocular pressure elevation in a modified laser-induced glaucoma rat model." Exp Eye Res 104: 7-14. DOI: 10.1016/j.exer.2012.08.011.

Boia, R., F. Elvas, M. H. Madeira, I. D. Aires, A. C. Rodrigues-Neves, P. Tralhao, E. C. Szabo, Y. Baqi, C. E. Muller, A. R. Tome, R. A. Cunha, A. F. Ambrosio and A. R. Santiago (2017). "Treatment with A2A receptor antagonist kw6002 and caffeine intake regulate microglia reactivity and protect retina against transient ischemic damage." Cell Death Dis 8(10): e3065. DOI: 10.1038/cddis.2017.451.

Boia, R., N. Ruzafa, I. D. Aires, X. Pereiro, A. F. Ambrosio, E. Vecino and A. R. Santiago (2020). "Neuroprotective strategies for retinal ganglion cell degeneration: Current status and challenges ahead." Int J Mol Sci 21(7). DOI: 10.3390/ijms21072262.

Boland, M. V., L. Zhang, A. T. Broman, H. D. Jampel and H. A. Quigley (2008). "Comparison of optic nerve head topography and visual field in eyes with open-angle and angle-closure glaucoma." Ophthalmology 115(2): 239-245 e232. DOI: 10.1016/j.ophtha.2007.03.086.

Borea, P. A., S. Gessi, S. Merighi and K. Varani (2016). "Adenosine as a multi-signalling guardian angel in human diseases: When, where and how does it exert its protective effects?" Trends Pharmacol Sci 37(6): 419-434. DOI: 10.1016/j.tips.2016.02.006.

Borea, P. A., S. Gessi, S. Merighi, F. Vincenzi and K. Varani (2017). "Pathological overproduction: The bad side of adenosine." Br J Pharmacol 174(13): 1945-1960. DOI: 10.1111/bph.13763.

Borea, P. A., S. Gessi, S. Merighi, F. Vincenzi and K. Varani (2018). "Pharmacology of adenosine receptors: The state of the art." Physiol Rev 98(3): 1591-1625. DOI: 10.1152/physrev.00049.2017.

Borea, P. A., K. Varani, F. Vincenzi, P. G. Baraldi, M. A. Tabrizi, S. Merighi and S. Gessi (2015). "The A3 adenosine receptor: History and perspectives." Pharmacol Rev 67(1): 74-102. DOI: 10.1124/pr.113.008540.

Bosco, A., C. O. Romero, K. T. Breen, A. A. Chagovetz, M. R. Steele, B. K. Ambati and M. L. Vetter (2015). "Neurodegeneration severity can be predicted from early microglia alterations monitored in vivo in a mouse model of chronic glaucoma." Dis Model Mech 8(5): 443-455. DOI: 10.1242/dmm.018788.

Bosco, A., M. R. Steele and M. L. Vetter (2011). "Early microglia activation in a mouse model of chronic glaucoma." J Comp Neurol 519(4): 599-620. DOI: 10.1002/cne.22516.

Boulton, M. and P. Dayhaw-Barker (2001). "The role of the retinal pigment epithelium: Topographical variation and ageing changes." Eye (Lond) 15(Pt 3): 384-389. DOI: 10.1038/eye.2001.141.

Bourne, R. R. A., S. R. Flaxman, T. Braithwaite, M. V. Cicinelli, A. Das, J. B. Jonas, J. Keeffe, J. H. Kempen, J. Leasher, H. Limburg, K. Naidoo, K. Pesudovs, S. Resnikoff, A. Silvester, G. A. Stevens, N. Tahhan, T. Y. Wong, H. R. Taylor and G. Vision Loss Expert (2017). "Magnitude, temporal trends, and projections of the global prevalence of blindness and distance and near vision impairment: A systematic review and meta-analysis." Lancet Glob Health 5(9): e888-e897. DOI: 10.1016/S2214-109X(17)30293-0.

Braas, K. M., M. A. Zarbin and S. H. Snyder (1987). "Endogenous adenosine and adenosine receptors localized to ganglion cells of the retina." Proc Natl Acad Sci U S A 84(11): 3906-3910. DOI: 10.1073/pnas.84.11.3906.

Braga, M. E. M., S. Bizarro, P. A. N. Dias and H. C. de Sousa (2017). New porous ocular implants prepared by a green supercritical foaming/mixing technology for sustained release of 2-Cl-IB-MECA. 46th World Chemistry Congress IUPAC (46th WCC IUPAC 2017), São Paulo , Brazil.

Bringmann, A., T. Pannicke, J. Grosche, M. Francke, P. Wiedemann, S. N. Skatchkov, N. N. Osborne and A. Reichenbach (2006). "Müller cells in the healthy and diseased retina." Prog Retin Eye Res 25(4): 397-424. DOI: 10.1016/j.preteyeres.2006.05.003.

Bui, B. V. and B. Fortune (2004). "Ganglion cell contributions to the rat full-field electroretinogram." J Physiol 555(Pt 1): 153-173. DOI: 10.1113/jphysiol.2003.052738.

Busse, L. (2018). "The mouse visual system and visual perception." 27: 53-68. DOI: 10.1016/b978-0-12-812012-5.00004-5.

Calkins, D. J. (2012). "Critical pathogenic events underlying progression of neurodegeneration in glaucoma." Prog Retin Eye Res 31(6): 702-719. DOI: 10.1016/j.preteyeres.2012.07.001.

Callanan, D. G., G. J. Jaffe, D. F. Martin, P. A. Pearson and T. L. Comstock (2008). "Treatment of posterior uveitis with a fluocinolone acetonide implant: Three-year clinical trial results." Arch Ophthalmol 126(9): 1191-1201. DOI: 10.1001/archopht.126.9.1191.

Campochiaro, P. A., D. M. Marcus, C. C. Awh, C. Regillo, A. P. Adamis, V. Bantseev, Y. Chiang, J. S. Ehrlich, S. Erickson, W. D. Hanley, J. Horvath, K. F. Maass, N. Singh, F. Tang and G. Barteselli (2019). "The port delivery system with ranibizumab for neovascular age-related macular degeneration." Ophthalmology 126(8): 1141-1154. DOI: 10.1016/j.ophtha.2019.03.036.

Cantor, L. B. (2006). "Brimonidine in the treatment of glaucoma and ocular hypertension." Ther Clin Risk Manag 2(4): 337-346. DOI: 10.2147/tcrm.2006.2.4.337.

Caprioli, J. (2007). "Glaucoma is a neuronal disease." Eye 21(S1): S6-S10. DOI: 10.1038/sj.eye.6702879.

Caprioli, J. and N. Piri (2008). "Neuroprotection in glaucoma." 423-442. DOI: 10.1016/b978-012370585-3.50021-2.

Carelli, V., C. La Morgia, F. N. Ross-Cisneros and A. A. Sadun (2017). "Optic neuropathies: The tip of the neurodegeneration iceberg." Hum Mol Genet 26(R2): R139-R150. DOI: 10.1093/hmg/ddx273.

Carmignoto, G., L. Maffei, P. Candeo, R. Canella and C. Comelli (1989). "Effect of ngf on the survival of rat retinal ganglion cells following optic nerve section." J Neurosci 9(4): 1263-1272.

Cen, L. P. and T. K. Ng (2018). "Stem cell therapy for retinal ganglion cell degeneration." Neural Regen Res 13(8): 1352-1353. DOI: 10.4103/1673-5374.235237.

Chan-Juan, H., L. Sen, A. Li-Qianyu, Y. Jian and Y. Rong-Di (2019). "MicroRNA-30b regulates the polarity of retinal ganglion cells by inhibiting semaphorin-3A." Mol Vis 25: 722-730.

Chan, H. H., T. T. Wong, E. Lamoureux and S. Perera (2015). "A survey on the preference of sustained glaucoma drug delivery systems by singaporean chinese patients: A comparison between subconjunctival, intracameral, and punctal plug routes." J Glaucoma 24(7): 485-492. DOI: 10.1097/IJG.0000000000000197.

Chaturvedi, N., E. T. Hedley-Whyte and E. B. Dreyer (1993). "Lateral geniculate nucleus in glaucoma." Am J Ophthalmol 116(2): 182-188. DOI: 10.1016/s0002-9394(14)71283-8.

Chauhan, B. C., K. T. Stevens, J. M. Levesque, A. C. Nuschke, G. P. Sharpe, N. O'Leary, M. L. Archibald and X. Wang (2012). "Longitudinal in vivo imaging of retinal ganglion cells and retinal thickness changes following optic nerve injury in mice." PLoS One 7(6): e40352. DOI: 10.1371/journal.pone.0040352.

Chen, C.-X., H.-H. Peng, Y.-X. Guan and S.-J. Yao (2019). "Morphological study on the pore growth profile of poly(Ɛ-caprolactone) bi-modal porous foams using a modified supercritical CO2 foaming process." The Journal of Supercritical Fluids 143: 72-81. DOI: 10.1016/j.supflu.2018.07.029.

Chen, D. F., G. E. Schneider, J. C. Martinou and S. Tonegawa (1997). "Bcl-2 promotes regeneration of severed axons in mammalian cns." Nature 385(6615): 434-439. DOI: 10.1038/385434a0.

Chen, G. J., B. K. Harvey, H. Shen, J. Chou, A. Victor and Y. Wang (2006). "Activation of adenosine A3 receptors reduces ischemic brain injury in rodents." J Neurosci Res 84(8): 1848-1855. DOI: 10.1002/jnr.21071.

Chen, H. and A. J. Weber (2001). "BDNF enhances retinal ganglion cell survival in cats with optic nerve damage." Invest Ophthalmol Vis Sci 42(5): 966-974.

Cherecheanu, A. P., G. Garhofer, D. Schmidl, R. Werkmeister and L. Schmetterer (2013). "Ocular perfusion pressure and ocular blood flow in glaucoma." Curr Opin Pharmacol 13(1): 36-42. DOI: 10.1016/j.coph.2012.09.003.

Chidlow, G., T. E. Choe, C. J. Abbott, C. Piper, L. Wang and B. Fortune (2014). "Comparison of longitudinal in vivo measurements of retinal nerve fiber layer thickness and retinal ganglion cell density after optic nerve transection in rat." PLoS ONE 9(11): e113011. DOI: 10.1371/journal.pone.0113011.

Chim, R. B., M. B. C. de Matos, M. E. M. Braga, A. M. A. Dias and H. C. de Sousa (2012). "Solubility of dexamethasone in supercritical carbon dioxide." Journal of Chemical & Engineering Data 57(12): 3756-3760. DOI: 10.1021/je301065f.

Choe, T. E., C. J. Abbott, C. Piper, L. Wang and B. Fortune (2014). "Comparison of longitudinal in vivo measurements of retinal nerve fiber layer thickness and retinal ganglion cell density after optic nerve transection in rat." PLoS One 9(11): e113011. DOI: 10.1371/journal.pone.0113011.

Choi, I. Y., J. C. Lee, C. Ju, S. Hwang, G. S. Cho, H. W. Lee, W. J. Choi, L. S. Jeong and W. K. Kim (2011). "A3 adenosine receptor agonist reduces brain ischemic injury and inhibits inflammatory cell migration in rats." Am J Pathol 179(4): 2042-2052. DOI: 10.1016/j.ajpath.2011.07.006.

Chong, R. S., D. H. Su, A. Tsai, Y. Jiang, H. M. Htoon, E. L. Lamoureux, T. Aung and T. T. Wong (2013). "Patient acceptance and attitude toward an alternative method of subconjunctival injection for the medical treatment of glaucoma." J Glaucoma 22(3): 190-194. DOI: 10.1097/IJG.0b013e318237c6c4.

Churro, R. M. M. (2015a). Supercritical foaming/mixing on the preparation of pcl/mesoporous silica based composites for hard tissue engineering applications. Master's Thesis, Faculty of Sciences and Technology of University of Coimbra

Churro, R. M. M., A. B. S. Rosa, M. E. Braga and H. C. Sousa (2016). Supercritical CO2 foaming/mixing for the preparation of plasticized porous pcl/sba-15 composite biomaterials. Prosciba 2016 - IV Iberoamerican Conference on Supercritical Fluids, Chile.

Churro, R. M. M., A. B. S. Rosa, M. B. de Matos, C. Alvarez-Lorenzo, A. Concheiro, M. E. Braga and H. C. de Sousa (2015b). Safer and greener plasticizers, compatibilizers and foaming agents for the preparation of PCL/silica nanoparticles composite biomaterials. 2nd EuGSC – 2nd EuCheMS Congress on Green and Sustainable Chemistry, Lisbon, Portugal.

Claxton, A. J., J. Cramer and C. Pierce (2001). "A systematic review of the associations between dose regimens and medication compliance." Clin Ther 23(8): 1296-1310.

Cordeiro, M. F. and L. A. Levin (2011). "Clinical evidence for neuroprotection in glaucoma." Am J Ophthalmol 152(5): 715-716. DOI: 10.1016/j.ajo.2011.06.015.

Cordeiro, M. F., E. M. Normando, M. J. Cardoso, S. Miodragovic, S. Jeylani, B. M. Davis, L. Guo, S. Ourselin, R. A'Hern and P. A. Bloom (2017). "Real-time imaging of single neuronal cell apoptosis in patients with glaucoma." Brain 140(6): 1757-1767. DOI: 10.1093/brain/awx088.

Crish, S. D., R. M. Sappington, D. M. Inman, P. J. Horner and D. J. Calkins (2010). "Distal axonopathy with structural persistence in glaucomatous neurodegeneration." Proc Natl Acad Sci U S A 107(11): 5196-5201. DOI: 10.1073/pnas.0913141107.

Cuenca, N., I. Pinilla, L. Fernandez-Sanchez, M. Salinas-Navarro, L. Alarcon-Martinez, M. Aviles-Trigueros, P. de la Villa, J. Miralles de Imperial, M. P. Villegas-Perez and M. Vidal-Sanz (2010). "Changes in the inner and outer retinal layers after acute increase of the intraocular pressure in adult albino swiss mice." Exp Eye Res 91(2): 273-285. DOI: 10.1016/j.exer.2010.05.020.

Cunha-Vaz, J. G. (2004). "The blood-retinal barriers system. Basic concepts and clinical evaluation." Exp Eye Res 78(3): 715-721. DOI: 10.1016/s0014-4835(03)00213-6.

Curcio, C. A. and K. A. Allen (1990). "Topography of ganglion cells in human retina." J Comp Neurol 300(1): 5-25. DOI: 10.1002/cne.903000103.

Cvenkel, B. and M. Kolko (2020). "Current medical therapy and future trends in the management of glaucoma treatment." J Ophthalmol 2020: 6138132. DOI: 10.1155/2020/6138132.

D'Onofrio, P. M. and P. D. Koeberle (2013). "What can we learn about stroke from retinal ischemia models?" Acta Pharmacol Sin 34(1): 91-103. DOI: 10.1038/aps.2012.165.

Dallimore, E. J., Q. Cui, L. D. Beazley and A. R. Harvey (2002). "Postnatal innervation of the rat superior colliculus by axons of late-born retinal ganglion cells." European Journal of Neuroscience 16(7): 1295-1304. DOI: 10.1046/j.1460-9568.2002.02178.x.

Danesh-Meyer, H. V. and L. A. Levin (2009). "Neuroprotection: Extrapolating from neurologic diseases to the eye." American Journal of Ophthalmology 148(2): 186-191.e182. DOI: 10.1016/j.ajo.2009.03.029.

Darwis, D., H. Mitomo and F. Yoshii (1999). "Degradability of radiation crosslinked pcl in the supercooled state under various environments." Polymer Degradation and Stability 65(2): 279-285. DOI: 10.1016/s0141-3910(99)00017-8.

Das, A. and J. Byrd (2014). "Retinal vasculature: Structure and pathologies." 2137-2161. DOI: 10.1016/b978-0-12-386456-7.04709-2.

de Hoz, R., B. I. Gallego, A. I. Ramirez, B. Rojas, J. J. Salazar, F. J. Valiente-Soriano, M. Aviles-Trigueros, M. P. Villegas-Perez, M. Vidal-Sanz, A. Trivino and J. M. Ramirez (2013). "Rod-like microglia are restricted to eyes with laser-induced ocular hypertension but absent from the microglial changes in the contralateral untreated eye." PLoS One 8(12): e83733. DOI: 10.1371/journal.pone.0083733.

de Hoz, R., B. Rojas, A. I. Ramírez, J. J. Salazar, B. I. Gallego, A. Triviño and J. M. Ramírez (2016). "Retinal macroglial responses in health and disease." BioMed Research International 2016: 1-13. DOI: 10.1155/2016/2954721.

de Matos, M. B., A. P. Piedade, C. Alvarez-Lorenzo, A. Concheiro, M. E. Braga and H. C. de Sousa (2013). "Dexamethasone-loaded poly(epsilon-caprolactone)/silica nanoparticles composites prepared by supercritical co2 foaming/mixing and deposition." Int J Pharm 456(2): 269-281. DOI: 10.1016/j.ijpharm.2013.08.042.

de Matos, M. B., A. M. Puga, C. Alvarez-Lorenzo, A. Concheiro, M. E. Braga and H. C. de Sousa (2015). "Osteogenic poly(epsilon-caprolactone)/poloxamine homogeneous blends prepared by supercritical foaming." Int J Pharm 479(1): 11-22. DOI: 10.1016/j.ijpharm.2014.12.041.

De Moraes, C. G., S. Demirel, S. K. Gardiner, J. M. Liebmann, G. A. Cioffi, R. Ritch, M. O. Gordon, M. A. Kass and G. Ocular Hypertension Treatment Study (2012). "Effect of treatment on the rate of visual field change in the ocular hypertension treatment study observation group." Invest Ophthalmol Vis Sci 53(4): 1704-1709. DOI: 10.1167/iovs.11-8186.

de Winter, F., Q. Cui, N. Symons, J. Verhaagen and A. R. Harvey (2004). "Expression of class-3 semaphorins and their receptors in the neonatal and adult rat retina." Investigative Opthalmology & Visual Science 45(12): 4554. DOI: 10.1167/iovs.04-0173.

del Amo, E. M., A.-K. Rimpelä, E. Heikkinen, O. K. Kari, E. Ramsay, T. Lajunen, M. Schmitt, L. Pelkonen, M. Bhattacharya, D. Richardson, A. Subrizi, T. Turunen, M. Reinisalo, J. Itkonen, E. Toropainen, M. Casteleijn, H. Kidron, M. Antopolsky, K.-S. Vellonen, M. Ruponen and A. Urtti (2017). "Pharmacokinetic aspects of retinal drug delivery." Progress in Retinal and Eye Research 57: 134-185. DOI: 10.1016/j.preteyeres.2016.12.001.

Dengler-Crish, C. M., M. A. Smith, D. M. Inman, G. N. Wilson, J. W. Young and S. D. Crish (2014). "Anterograde transport blockade precedes deficits in retrograde transport in the visual projection of the DBA/2J mouse model of glaucoma." Frontiers in Neuroscience 8. DOI: 10.3389/fnins.2014.00290.

Dhillon, B., A. Kamal and C. Leen (1998). "Intravitreal sustained-release ganciclovir implantation to control cytomegalovirus retinitis in aids." Int J STD AIDS 9(4): 227-230. DOI: 10.1258/0956462981922098.

Di Giovanni, S., C. D. Knights, M. Rao, A. Yakovlev, J. Beers, J. Catania, M. L. Avantaggiati and A. I. Faden (2006). "The tumor suppressor protein p53 is required for neurite outgrowth and axon regeneration." EMBO J 25(17): 4084-4096. DOI: 10.1038/sj.emboj.7601292.

Di Iorio, P., S. Kleywegt, R. Ciccarelli, U. Traversa, C. M. Andrew, C. E. Crocker, E. S. Werstiuk and M. P.

Rathbone (2002). "Mechanisms of apoptosis induced by purine nucleosides in astrocytes." Glia 38(3): 179-190. DOI: 10.1002/glia.10055.

Di Maio, E. and E. Kiran (2018). "Foaming of polymers with supercritical fluids and perspectives on the current knowledge gaps and challenges." The Journal of Supercritical Fluids 134: 157-166. DOI: 10.1016/j.supflu.2017.11.013.

Di Polo, A., L. J. Aigner, R. J. Dunn, G. M. Bray and A. J. Aguayo (1998). "Prolonged delivery of brain-derived neurotrophic factor by adenovirus-infected muller cells temporarily rescues injured retinal ganglion cells." Proc Natl Acad Sci U S A 95(7): 3978-3983. DOI: 10.1073/pnas.95.7.3978.

Diao, L., W. Sun, Q. Deng and S. He (2004). "Development of the mouse retina: Emerging morphological diversity of the ganglion cells." J Neurobiol 61(2): 236-249. DOI: 10.1002/neu.20041.

Dillenburg, A., G. Ireland, R. K. Holloway, C. L. Davies, F. L. Evans, M. Swire, M. E. Bechler, D. Soong, T. J. Yuen, G. H. Su, J. C. Becher, C. Smith, A. Williams and V. E. Miron (2018). "Activin receptors regulate the oligodendrocyte lineage in health and disease." Acta Neuropathol 135(6): 887-906. DOI: 10.1007/s00401-018-1813-3.

Domenici, L., N. Origlia, B. Falsini, E. Cerri, D. Barloscio, C. Fabiani, M. Sanso and L. Giovannini (2014). "Rescue of retinal function by bdnf in a mouse model of glaucoma." PLoS One 9(12): e115579. DOI: 10.1371/journal.pone.0115579.

Donello, J. E., E. U. Padillo, M. L. Webster, L. A. Wheeler and D. W. Gil (2001). "Alpha(2)-adrenoceptor agonists inhibit vitreal glutamate and aspartate accumulation and preserve retinal function after transient ischemia." J Pharmacol Exp Ther 296(1): 216-223.

Drager, U. C. and J. F. Olsen (1980). "Origins of crossed and uncrossed retinal projections in pigmented and albino mice." J Comp Neurol 191(3): 383-412. DOI: 10.1002/cne.901910306.

Dratviman-Storobinsky, O., M. Hasanreisoglu, D. Offen, Y. Barhum, D. Weinberger and N. Goldenberg-Cohen (2008). "Progressive damage along the optic nerve following induction of crush injury or rodent anterior ischemic optic neuropathy in transgenic mice." Mol Vis 14: 2171-2179.

Dugel, P. U., F. Bandello and A. Loewenstein (2015). "Dexamethasone intravitreal implant in the treatment of diabetic macular edema." Clin Ophthalmol 9: 1321-1335. DOI: 10.2147/OPTH.S79948.

Edelhauser, H. F., C. L. Rowe-Rendleman, M. R. Robinson, D. G. Dawson, G. J. Chader, H. E. Grossniklaus, K. D. Rittenhouse, C. G. Wilson, D. A. Weber, B. D. Kuppermann, K. G. Csaky, T. W. Olsen, U. B. Kompella, V. M. Holers, G. S. Hageman, B. C. Gilger, P. A. Campochiaro, S. M. Whitcup and W. T. Wong (2010). "Ophthalmic drug delivery systems for the treatment of retinal diseases: Basic research to clinical applications." Invest Ophthalmol Vis Sci 51(11): 5403-5420. DOI: 10.1167/iovs.10-5392.

Egbert, P. R., R. B. Pollard, J. G. Gallagher and T. C. Merigan (1980). "Cytomegalovirus retinitis in immunosuppressed hosts. Ii. Ocular manifestations." Ann Intern Med 93(5): 664-670. DOI: 10.7326/0003-4819-93-5-664.

EGS (2017). "European glaucoma society terminology and guidelines for glaucoma, 4th edition - chapter 3: Treatment principles and optionssupported by the egs foundation." British Journal of Ophthalmology 101(6): 130-195. DOI: 10.1136/bjophthalmol-2016-EGSguideline.003.

Ellis, E. M., G. Gauvain, B. Sivyer and G. J. Murphy (2016). "Shared and distinct retinal input to the mouse superior colliculus and dorsal lateral geniculate nucleus." J Neurophysiol 116(2): 602-610. DOI: 10.1152/jn.00227.2016.

Eltzschig, H. K. (2009). "Adenosine: An old drug newly discovered." Anesthesiology 111(4): 904-915. DOI: 10.1097/ALN.0b013e3181b060f2.

Entezari, M., M. Esmaeili and M. Yaseri (2014). "A pilot study of the effect of intravenous erythropoetin on improvement of visual function in patients with recent indirect traumatic optic neuropathy." Graefes Arch Clin Exp Ophthalmol 252(8): 1309-1313. DOI: 10.1007/s00417-014-2691-6.

Erskine, L. and E. Herrera (2014). "Connecting the retina to the brain." ASN Neuro 6(6). DOI: 10.1177/1759091414562107.

Euler, T., S. Haverkamp, T. Schubert and T. Baden (2014). "Retinal bipolar cells: Elementary building blocks of vision." Nat Rev Neurosci 15(8): 507-519. DOI: 10.1038/nrn3783.

Fahy, E. T., V. Chrysostomou and J. G. Crowston (2015). "Impaired axonal transport and glaucoma." Current Eye Research: 1-11. DOI: 10.3109/02713683.2015.1037924.

Fanovich, M. A. and P. Jaeger (2012). "Sorption and diffusion of compressed carbon dioxide in polycaprolactone for the development of porous scaffolds." Materials Science and Engineering: C 32(4): 961-968. DOI: 10.1016/j.msec.2012.02.021.

Farr, S. A., S. Cuzzocrea, E. Esposito, M. Campolo, M. L. Niehoff, T. M. Doyle and D. Salvemini (2020). "Adenosine a3 receptor as a novel therapeutic target to reduce secondary events and improve neurocognitive functions following traumatic brain injury." Journal of Neuroinflammation 17(1). DOI: 10.1186/s12974-020-02009-7.

Farris, W. and J. R. Waymack (2020). Central retinal artery occlusion. Statpearls. Treasure Island (FL).

Fedorova, I. M., M. A. Jacobson, A. Basile and K. A. Jacobson (2003). "Behavioral characterization of mice lacking the a3 adenosine receptor: Sensitivity to hypoxic neurodegeneration." Cell Mol Neurobiol 23(3): 431-447. DOI: 10.1023/a:1023601007518.

Ferrari, M. P., F. Mantelli, M. Sacchetti, M. I. Antonangeli, F. Cattani, G. D'Anniballe, F. Sinigaglia, P. A. Ruffini and A. Lambiase (2014). "Safety and pharmacokinetics of escalating doses of human recombinant nerve growth factor eye drops in a double-masked, randomized clinical trial." BioDrugs 28(3): 275-283. DOI: 10.1007/s40259-013-0079-5.

Ferreira-Silva, J., I. D. Aires, R. Boia, A. F. Ambrósio and A. R. Santiago (2020). "Activation of adenosine A3 receptor inhibits microglia reactivity elicited by elevated pressure." International Journal of Molecular Sciences 21(19): 7218. DOI: 10.3390/ijms21197218.

Fialho, S. L., F. Behar-Cohen and A. Silva-Cunha (2008). "Dexamethasone-loaded poly(epsilon-caprolactone) intravitreal implants: A pilot study." Eur J Pharm Biopharm 68(3): 637-646. DOI: 10.1016/j.ejpb.2007.08.004.

Fisher, J., H. Levkovitch-Verbin, H. Schori, E. Yoles, O. Butovsky, J. F. Kaye, A. Ben-Nun and M. Schwartz (2001). "Vaccination for neuroprotection in the mouse optic nerve: Implications for optic neuropathies." J Neurosci 21(1): 136-142.

Fishman, P., S. Cohen and S. Bar-Yehuda (2013). "Targeting the A3 adenosine receptor for glaucoma treatment (review)." Mol Med Rep 7(6): 1723-1725. DOI: 10.3892/mmr.2013.1413.

Flaxman, S. R., R. R. A. Bourne, S. Resnikoff, P. Ackland, T. Braithwaite, M. V. Cicinelli, A. Das, J. B. Jonas, J. Keeffe, J. H. Kempen, J. Leasher, H. Limburg, K. Naidoo, K. Pesudovs, A. Silvester, G. A. Stevens, N. Tahhan, T. Y. Wong, H. R. Taylor, R. Bourne, P. Ackland, A. Arditi, Y. Barkana, B. Bozkurt, T. Braithwaite, A. Bron, D. Budenz, F. Cai, R. Casson, U. Chakravarthy, J. Choi, M. V. Cicinelli, N. Congdon, R. Dana, R. Dandona, L. Dandona, A. Das, I. Dekaris, M. Del Monte, J. deva, L. Dreer, L. Ellwein, M. Frazier, K. Frick, D. Friedman, J. Furtado, H. Gao, G. Gazzard, R. George, S. Gichuhi, V. Gonzalez, B. Hammond, M. E. Hartnett, M. He, J. Hejtmancik, F. Hirai, J. Huang, A. Ingram, J. Javitt, J. Jonas, C. Joslin, J. Keeffe, J. Kempen, M. Khairallah, R. Khanna, J. Kim, G. Lambrou, V. C. Lansingh, P. Lanzetta, J. Leasher, J. Lim, H. Limburg, K. Mansouri, A. Mathew, A. Morse, B. Munoz, D. Musch, K. Naidoo, V. Nangia, M. Palaiou, M. B. Parodi, F. Y. Pena, K. Pesudovs, T. Peto, H. Quigley, M. Raju, P. Ramulu, Z. Rankin, S. Resnikoff, D. Reza, A. Robin, L. Rossetti, J. Saaddine, M. Sandar, J. Serle, T. Shen, R. Shetty, P. Sieving, J. C. Silva, A. Silvester, R. S. Sitorus, D. Stambolian, G. Stevens, H. Taylor, J. Tejedor, J. Tielsch, M. Tsilimbaris, J. van Meurs, R. Varma, G. Virgili, Y. X. Wang, N.-L. Wang, S. West, P. Wiedemann, T. Wong, R. Wormald and Y. Zheng (2017). "Global causes of blindness and distance vision impairment 1990–2020: A systematic review and meta-analysis." The Lancet Global Health 5(12): e1221-e1234. DOI: 10.1016/s2214-109x(17)30393-5.

Fleming, M. D., R. M. Benca and M. Behan (2006). "Retinal projections to the subcortical visual system in congenic albino and pigmented rats." Neuroscience 143(3): 895-904. DOI: 10.1016/j.neuroscience.2006.08.016.

Foo, R. C., E. L. Lamoureux, R. C. Wong, S. W. Ho, P. P. Chiang, G. Rees, T. Aung and T. T. Wong (2012). "Acceptance, attitudes, and beliefs of singaporean chinese toward an ocular implant for glaucoma drug delivery." Invest Ophthalmol Vis Sci 53(13): 8240-8245. DOI: 10.1167/iovs.12-10393.

Fredholm, B. B. (2014). "Adenosine-a physiological or pathophysiological agent?" J Mol Med (Berl) 92(3): 201-206. DOI: 10.1007/s00109-013-1101-6.

Fredholm, B. B., I. J. AP, K. A. Jacobson, K. N. Klotz and J. Linden (2001). "International union of pharmacology. Xxv. Nomenclature and classification of adenosine receptors." Pharmacol Rev 53(4): 527-552.

Fredholm, B. B., I. J. AP, K. A. Jacobson, J. Linden and C. E. Muller (2011). "International union of basic and clinical pharmacology. Lxxxi. Nomenclature and classification of adenosine receptors--an update." Pharmacol Rev 63(1): 1-34. DOI: 10.1124/pr.110.003285.

Fu, L., S. S. Kwok, Y. K. Chan, J. S. Ming Lai, W. Pan, L. Nie and K. C. Shih (2019). "Therapeutic strategies for attenuation of retinal ganglion cell injury in optic neuropathies: Concepts in translational research and therapeutic implications." BioMed Research International 2019: 1-10. DOI: 10.1155/2019/8397521.

Fu, Q.-L., X.-X. Liao, X. Li, D. Chen, J. Shi, W. Wen, D. H. S. Lee and K.-F. So (2011). "Soluble Nogo-66 receptor prevents synaptic dysfunction and rescues retinal ganglion cell loss in chronic glaucoma." Investigative Opthalmology & Visual Science 52(11): 8374. DOI: 10.1167/iovs.11-7667.

Fujimoto, J. G. (2003). "Optical coherence tomography for ultrahigh resolution in vivo imaging." Nat Biotechnol 21(11): 1361-1367. DOI: 10.1038/nbt892.

Galindo-Romero, C., F. J. Valiente-Soriano, M. Jiménez-López, D. García-Ayuso, M. P. Villegas-Pérez, M. Vidal-Sanz and M. Agudo-Barriuso (2013). "Effect of brain-derived neurotrophic factor on mouse axotomized retinal ganglion cells and phagocytic microglia." Investigative Opthalmology & Visual Science 54(2): 974. DOI: 10.1167/iovs.12-11207.

Gallego, B. I., J. J. Salazar, R. de Hoz, B. Rojas, A. I. Ramirez, M. Salinas-Navarro, A. Ortin-Martinez, F. J. Valiente-Soriano, M. Aviles-Trigueros, M. P. Villegas-Perez, M. Vidal-Sanz, A. Trivino and J. M. Ramirez (2012). "IOP induces upregulation of GFAP and MHC-II and microglia reactivity in mice retina contralateral to experimental glaucoma." J Neuroinflammation 9: 92. DOI: 10.1186/1742-2094-9-92.

Galloway, N. R., W. M. K. Amoaku, P. H. Galloway and A. C. Browning (2006). Common eye diseases and their management.

Galvao, J., F. Elvas, T. Martins, M. F. Cordeiro, A. F. Ambrosio and A. R. Santiago (2015). "Adenosine A3 receptor activation is neuroprotective against retinal neurodegeneration." Exp Eye Res 140: 65-74. DOI: 10.1016/j.exer.2015.08.009.

Garcia-Valenzuela, E., S. Shareef, J. Walsh and S. C. Sharma (1995). "Programmed cell death of retinal ganglion cells during experimental glaucoma." Experimental Eye Research 61(1): 33-44. DOI: 10.1016/s0014-4835(95)80056-5.

Gazzard, G., E. Konstantakopoulou, D. Garway-Heath, A. Garg, V. Vickerstaff, R. Hunter, G. Ambler, C. Bunce, R. Wormald, N. Nathwani, K. Barton, G. Rubin, M. Buszewicz, G. Ambler, K. Barton, R. Bourne, D. Broadway, C. Bunce, M. Buszewicz, A. Davis, A. Garg, D. Garway-Heath, G. Gazzard, R. Hunter, H. Jayaram, Y. Jiang, E. Konstantakopoulou, S. Lim, J. Liput, T. Manners, S. Morris, N. Nathwani, G. Rubin, N. Strouthidis, V. Vickerstaff, S. Wilson, R. Wormald and H. Zhu (2019). "Selective laser trabeculoplasty versus eye drops for first-line treatment of ocular hypertension and glaucoma (light): A multicentre randomised controlled trial." The Lancet 393(10180): 1505-1516. DOI: 10.1016/s0140-6736(18)32213-x.

Georgiou, A. L., L. Guo, M. Francesca Cordeiro and T. E. Salt (2014). "Electroretinogram and visual-evoked potential assessment of retinal and central visual function in a rat ocular hypertension model of glaucoma." Curr Eye Res 39(5): 472-486. DOI: 10.3109/02713683.2013.848902.

Ghaffarieh, A. and L. A. Levin (2012). "Optic nerve disease and axon pathophysiology." 105: 1-17. DOI: 10.1016/b978-0-12-398309-1.00002-0.

Giordano, G. G., P. Chevez-Barrios, M. F. Refojo and C. A. Garcia (1995). "Biodegradation and tissue reaction to intravitreous biodegradable poly(d,l-lactic-co-glycolic)acid microspheres." Curr Eye Res 14(9): 761-768. DOI: 10.3109/02713689508995797.

Glovinsky, Y., H. A. Quigley and G. R. Dunkelberger (1991). "Retinal ganglion cell loss is size dependent in experimental glaucoma." Invest Ophthalmol Vis Sci 32(3): 484-491.

Goel, M., R. G. Picciani, R. K. Lee and S. K. Bhattacharya (2010). "Aqueous humor dynamics: A review." Open Ophthalmol J 4: 52-59. DOI: 10.2174/1874364101004010052.

Goldberg, J. L. (2004). "An oligodendrocyte lineage-specific semaphorin, sema5a, inhibits axon growth by retinal ganglion cells." Journal of Neuroscience 24(21): 4989-4999. DOI: 10.1523/jneurosci.4390-03.2004.

Goldberg, J. L., J. S. Espinosa, Y. Xu, N. Davidson, G. T. Kovacs and B. A. Barres (2002a). "Retinal ganglion cells do not extend axons by default: Promotion by neurotrophic signaling and electrical activity." Neuron 33(5): 689-702. DOI: 10.1016/s0896-6273(02)00602-5.

Goldberg, J. L., M. P. Klassen, Y. Hua and B. A. Barres (2002b). "Amacrine-signaled loss of intrinsic axon growth ability by retinal ganglion cells." Science 296(5574): 1860-1864. DOI: 10.1126/science.1068428.

Gonzalez-Fernandez, E., M. V. Sanchez-Gomez, A. Perez-Samartin, R. O. Arellano and C. Matute (2014). "A3 adenosine receptors mediate oligodendrocyte death and ischemic damage to optic nerve." Glia 62(2): 199-216. DOI: 10.1002/glia.22599.

Gote, V., S. Sikder, J. Sicotte and D. Pal (2019). "Ocular drug delivery: Present innovations and future challenges." Journal of Pharmacology and Experimental Therapeutics 370(3): 602-624. DOI: 10.1124/jpet.119.256933.

Greenberg, M. E., B. Xu, B. Lu and B. L. Hempstead (2009). "New insights in the biology of bdnf synthesis and release: Implications in cns function." J Neurosci 29(41): 12764-12767. DOI: 10.1523/JNEUROSCI.3566-09.2009.

Grieb, P. (2014). "Neuroprotective properties of citicoline: Facts, doubts and unresolved issues." CNS Drugs 28(3): 185-193. DOI: 10.1007/s40263-014-0144-8.

Guerin, M. B., D. P. McKernan, C. J. O'Brien and T. G. Cotter (2006). "Retinal ganglion cells: Dying to survive." Int J Dev Biol 50(8): 665-674. DOI: 10.1387/ijdb.062159mg.

Gupta, N., L. C. Ang, L. Noel de Tilly, L. Bidaisee and Y. H. Yucel (2006). "Human glaucoma and neural degeneration in intracranial optic nerve, lateral geniculate nucleus, and visual cortex." Br J Ophthalmol 90(6): 674-678. DOI: 10.1136/bjo.2005.086769.

Gupta, N. and Y. H. Yucel (2007a). "Glaucoma as a neurodegenerative disease." Curr Opin Ophthalmol 18(2): 110-114. DOI: 10.1097/ICU.0b013e3280895aea.

Gupta, R. B. and J.-J. Shim (2007b). Solubility in supercritical carbon dioxide. Boca Raton, CRC Press.

Haghjou, N., M. Soheilian and M. J. Abdekhodaie (2011). "Sustained release intraocular drug delivery devices for treatment of uveitis." J Ophthalmic Vis Res 6(4): 317-329.

Halfter, W., S. Dong, A. Dong, A. W. Eller and R. Nischt (2008). "Origin and turnover of ecm proteins from the inner limiting membrane and vitreous body." Eye (Lond) 22(10): 1207-1213. DOI: 10.1038/eye.2008.19.

Haller, J. A., F. Bandello, R. Belfort, Jr., M. S. Blumenkranz, M. Gillies, J. Heier, A. Loewenstein, Y. H. Yoon, M. L. Jacques, J. Jiao, X. Y. Li, S. M. Whitcup and O. G. S. Group (2010). "Randomized, sham-controlled trial of dexamethasone intravitreal implant in patients with macular edema due to retinal vein occlusion." Ophthalmology 117(6): 1134-1146 e1133. DOI: 10.1016/j.ophtha.2010.03.032.

Hammarberg, C., G. Schulte and B. B. Fredholm (2003). "Evidence for functional adenosine A3 receptors in microglia cells." J Neurochem 86(4): 1051-1054. DOI: 10.1046/j.1471-4159.2003.01919.x.

Harasymowycz, P., C. Birt, P. Gooi, L. Heckler, C. Hutnik, D. Jinapriya, L. Shuba, D. Yan and R. Day (2016). "Medical management of glaucoma in the 21st century from a canadian perspective." J Ophthalmol 2016: 6509809. DOI: 10.1155/2016/6509809.

Harwerth, R. S., A. S. Vilupuru, N. V. Rangaswamy and E. L. Smith, 3rd (2007). "The relationship between nerve fiber layer and perimetry measurements." Invest Ophthalmol Vis Sci 48(2): 763-773. DOI: 10.1167/iovs.06-0688.

Heijl, A., B. Bengtsson and S. E. Oskarsdottir (2013). "Prevalence and severity of undetected manifest glaucoma: Results from the early manifest glaucoma trial screening." Ophthalmology 120(8): 1541-1545. DOI: 10.1016/j.ophtha.2013.01.043.

Heijl, A., M. C. Leske, B. Bengtsson, L. Hyman, B. Bengtsson, M. Hussein and G. Early Manifest Glaucoma Trial (2002). "Reduction of intraocular pressure and glaucoma progression: Results from the early manifest glaucoma trial." Arch Ophthalmol 120(10): 1268-1279. DOI: 10.1001/archopht.120.10.1268.

Hernández, A. R., O. C. Contreras, J. C. Acevedo and L. G. N. Moreno (2013). "Poly(Ɛ-caprolactone) degradation under acidic and alkaline conditions." American Journal of Polymer Science 3(4): 70-75. DOI: 10.5923/j.ajps.20130304.02.

Hernandez, M. R., O. A. Agapova, P. Yang, M. Salvador-Silva, C. S. Ricard and S. Aoi (2002). "Differential gene expression in astrocytes from human normal and glaucomatous optic nerve head analyzed by cdna microarray." Glia 38(1): 45-64. DOI: 10.1002/glia.10051.

Herrmann, R., S. J. Heflin, T. Hammond, B. Lee, J. Wang, R. R. Gainetdinov, M. G. Caron, E. D. Eggers, L. J. Frishman, M. A. McCall and V. Y. Arshavsky (2011). "Rod vision is controlled by dopamine-dependent sensitization of rod bipolar cells by gaba." Neuron 72(1): 101-110. DOI: 10.1016/j.neuron.2011.07.030.

Herzog, K. H. and C. S. von Bartheld (1998). "Contributions of the optic tectum and the retina as sources of brain-derived neurotrophic factor for retinal ganglion cells in the chick embryo." J Neurosci 18(8): 2891-2906.

Hofer, M., S. R. Pagliusi, A. Hohn, J. Leibrock and Y. A. Barde (1990). "Regional distribution of brain-derived neurotrophic factor mrna in the adult mouse brain." EMBO J 9(8): 2459-2464.

Holopigian, K., W. Seiple, C. Mayron, R. Koty and M. Lorenzo (1990). "Electrophysiological and psychophysical flicker sensitivity in patients with primary open-angle glaucoma and ocular hypertension." Invest Ophthalmol Vis Sci 31(9): 1863-1868.

Hood, D. C. (2019). "Does retinal ganglion cell loss precede visual field loss in glaucoma?" J Glaucoma 28(11): 945-951. DOI: 10.1097/IJG.0000000000001380.

Howell, G. R., R. T. Libby, T. C. Jakobs, R. S. Smith, F. C. Phalan, J. W. Barter, J. M. Barbay, J. K. Marchant, N. Mahesh, V. Porciatti, A. V. Whitmore, R. H. Masland and S. W. John (2007). "Axons of retinal ganglion cells are insulted in the optic nerve early in DBA/2J glaucoma." J Cell Biol 179(7): 1523-1537. DOI: 10.1083/jcb.200706181.

Hu, H., W. Lu, M. Zhang, X. Zhang, A. J. Argall, S. Patel, G. E. Lee, Y. C. Kim, K. A. Jacobson, A. M. Laties and C. H. Mitchell (2010). "Stimulation of the P2X7 receptor kills rat retinal ganglion cells in vivo." Exp Eye Res 91(3): 425-432. DOI: 10.1016/j.exer.2010.06.017.

Hu, Y. and J. Danias (2018). "Noninvasive intraocular pressure measurement in animals models of glaucoma." Methods Mol Biol 1695: 49-61. DOI: 10.1007/978-1-4939-7407-8_5.

Huang, T., J. Cui, L. Li, P. F. Hitchcock and Y. Li (2012). "The role of microglia in the neurogenesis of zebrafish retina." Biochem Biophys Res Commun 421(2): 214-220. DOI: 10.1016/j.bbrc.2012.03.139.

Huang, W., J. Fileta, I. Rawe, J. Qu and C. L. Grosskreutz (2010). "Calpain activation in experimental glaucoma." Invest Ophthalmol Vis Sci 51(6): 3049-3054. DOI: 10.1167/iovs.09-4364.

Huang, Z. R., H. Y. Chen, Z. Z. Hu, P. Xie and Q. H. Liu (2018). "PTEN knockdown with the Y444F mutant AAV2 vector promotes axonal regeneration in the adult optic nerve." Neural Regen Res 13(1): 135-144. DOI: 10.4103/1673-5374.224381.

Hurley, J. B. (2009). "Phototransduction." 687-692. DOI: 10.1016/b978-008045046-9.00914-1.

Isenmann, S., C. Wahl, S. Krajewski, J. C. Reed and M. Bahr (1997). "Up-regulation of bax protein in degenerating retinal ganglion cells precedes apoptotic cell death after optic nerve lesion in the rat." Eur J Neurosci 9(8): 1763-1772. DOI: 10.1111/j.1460-9568.1997.tb01534.x.

Jacobs, L. J. M., M. F. Kemmere and J. T. F. Keurentjes (2008). "Sustainable polymer foaming using high pressure carbon dioxide: A review on fundamentals, processes and applications." Green Chemistry 10(7): 731. DOI: 10.1039/b801895b.

Jacobson, K. A., D. K. Tosh, S. Jain and Z. G. Gao (2019). "Historical and current adenosine receptor agonists in preclinical and clinical development." Front Cell Neurosci 13: 124. DOI: 10.3389/fncel.2019.00124.

Jager, R. D., L. P. Aiello, S. C. Patel and E. T. Cunningham, Jr. (2004). "Risks of intravitreous injection: A comprehensive review." Retina 24(5): 676-698. DOI: 10.1097/00006982-200410000-00002.

Jakobs, T. C., R. T. Libby, Y. Ben, S. W. John and R. H. Masland (2005). "Retinal ganglion cell degeneration is topological but not cell type specific in DBA/2J mice." J Cell Biol 171(2): 313-325. DOI: 10.1083/jcb.200506099.

Jammal, A. A., A. C. Thompson, E. B. Mariottoni, T. Estrela, L. S. Shigueoka, S. I. Berchuck and F. A. Medeiros (2020). "Real-world impact of intraocular pressure control on rates of retinal nerve fiber layer loss in a large clinical population." Ophthalmology. DOI: 10.1016/j.ophtha.2020.06.027.

Jeffery, G. and L. Erskine (2005). "Variations in the architecture and development of the vertebrate optic chiasm." Prog Retin Eye Res 24(6): 721-753. DOI: 10.1016/j.preteyeres.2005.04.005.

Jeoung, J. W., Y. J. Choi, K. H. Park and D. M. Kim (2013). "Macular ganglion cell imaging study: Glaucoma diagnostic accuracy of spectral-domain optical coherence tomography." Invest Ophthalmol Vis Sci 54(7): 4422-4429. DOI: 10.1167/iovs.12-11273.

Johnson, T. V. and S. I. Tomarev (2010). "Rodent models of glaucoma." Brain Res Bull 81(2-3): 349-358. DOI: 10.1016/j.brainresbull.2009.04.004.

Jonsson, G. and T. Eysteinsson (2017). "Retinal A2A and A3 adenosine receptors modulate the components of the rat electroretinogram." Vis Neurosci 34: E001. DOI: 10.1017/S0952523816000171.

Jung, J. H., M. Ree and H. Kim (2006). "Acid- and base-catalyzed hydrolyses of aliphatic polycarbonates and polyesters." Catalysis Today 115(1-4): 283-287. DOI: 10.1016/j.cattod.2006.02.060.

Jutley, G., S. M. H. Luk, M. H. Dehabadi and M. F. Cordeiro (2017). "Management of glaucoma as a neurodegenerative disease." Neurodegenerative Disease Management 7(2): 157-172. DOI: 10.2217/nmt-2017-0004.

Kaji, H., N. Nagai, M. Nishizawa and T. Abe (2018). "Drug delivery devices for retinal diseases." Adv Drug Deliv Rev 128: 148-157. DOI: 10.1016/j.addr.2017.07.002.

Kaji, H., T. Sugimoto, M. Kanatani, K. Nishiyama and K. Chihara (1997). "Dexamethasone stimulates osteoclast-like cell formation by directly acting on hemopoietic blast cells and enhances osteoclast-like cell formation stimulated by parathyroid hormone and prostaglandin e2." Journal of Bone and Mineral Research 12(5): 734-741. DOI: 10.1359/jbmr.1997.12.5.734.

Kanamori, A., M.-M. Catrinescu, J. M. Belisle, S. Costantino and L. A. Levin (2012). "Retrograde and wallerian axonal degeneration occur synchronously after retinal ganglion cell axotomy." The American Journal of Pathology 181(1): 62-73. DOI: 10.1016/j.ajpath.2012.03.030.

Kaneda, K., S. Kashii, T. Kurosawa, S. Kaneko, A. Akaike, Y. Honda, M. Minami and M. Satoh (1999). "Apoptotic DNA fragmentation and upregulation of bax induced by transient ischemia of the rat retina." Brain Res 815(1): 11-20. DOI: 10.1016/s0006-8993(98)01074-9.

Kaplan, H. J. (2007). "Anatomy and function of the eye." Chem Immunol Allergy 92: 4-10. DOI: 10.1159/000099236.

Kashkouli, M. B., F. Pakdel, M. S. Sanjari, A. Haghighi, M. Nojomi, M. H. Homaee and A. Heirati (2011). "Erythropoietin: A novel treatment for traumatic optic neuropathy-a pilot study." Graefes Arch Clin Exp Ophthalmol 249(5): 731-736. DOI: 10.1007/s00417-010-1534-3.

Kass, M. A., D. K. Heuer, E. J. Higginbotham, C. A. Johnson, J. L. Keltner, J. P. Miller, R. K. Parrish, 2nd, M. R. Wilson and M. O. Gordon (2002). "The ocular hypertension treatment study: A randomized trial determines that topical ocular hypotensive medication delays or prevents the onset of primary open-angle glaucoma." Arch Ophthalmol 120(6): 701-713; discussion 829-730. DOI: 10.1001/archopht.120.6.701.

Kawaguchi, I., T. Higashide, S. Ohkubo, H. Takeda and K. Sugiyama (2006). "In vivo imaging and quantitative evaluation of the rat retinal nerve fiber layer using scanning laser ophthalmoscopy." Invest Ophthalmol Vis Sci 47(7): 2911-2916. DOI: 10.1167/iovs.05-1169.

Kerrigan, L. A., D. J. Zack, H. A. Quigley, S. D. Smith and M. E. Pease (1997). "Tunel-positive ganglion cells in human primary open-angle glaucoma." Arch Ophthalmol 115(8): 1031-1035. DOI: 10.1001/archopht.1997.01100160201010.

Kerschensteiner, D. and W. Guido (2017). "Organization of the dorsal lateral geniculate nucleus in the mouse." Vis Neurosci 34: E008. DOI: 10.1017/S0952523817000062.

Ketelaars, A. A. J., Y. Papantoniou and K. Nakayama (1997). "Analysis of the density and the enthalpy of poly(ε-caprolactone)-polycarbonate blends: Amorphous phase compatibility and the effect of secondary crystallization." Journal of Applied Polymer Science 66(5): 921-927. DOI: 10.1002/(sici)1097-4628(19971031)66:5<921::aid-app12>3.0.co;2-q.

Kilic, U., E. Kilic, J. Soliz, C. I. Bassetti, M. Gassmann and D. M. Hermann (2005). "Erythropoietin protects from axotomy-induced degeneration of retinal ganglion cells by activating ERK-1/-2." FASEB J 19(2): 249-251. DOI: 10.1096/fj.04-2493fje.

Killer, H. E. and A. Pircher (2018). "Normal tension glaucoma: Review of current understanding and mechanisms of the pathogenesis." Eye (Lond) 32(5): 924-930. DOI: 10.1038/s41433-018-0042-2.

Kim, B. J., T. A. Braun, R. J. Wordinger and A. F. Clark (2013). "Progressive morphological changes and impaired retinal function associated with temporal regulation of gene expression after retinal ischemia/reperfusion injury in mice." Mol Neurodegener 8: 21. DOI: 10.1186/1750-1326-8-21.

Kim, C. H., S. L. Cheng and G. S. Kim (1999). "Effects of dexamethasone on proliferation, activity, and cytokine secretion of normal human bone marrow stromal cells: Possible mechanisms of glucocorticoid-induced bone loss." J Endocrinol 162(3): 371-379.

Kim, J., M. Kudisch, N. R. K. da Silva, H. Asada, E. Aya-Shibuya, M. M. Bloomer, S. Mudumba, R. B. Bhisitkul and T. A. Desai (2018). "Long-term intraocular pressure reduction with intracameral polycaprolactone glaucoma devices that deliver a novel anti-glaucoma agent." J Control Release 269: 45-51. DOI: 10.1016/j.jconrel.2017.11.008.

Kim, J., M. Kudisch, S. Mudumba, H. Asada, E. Aya-Shibuya, R. B. Bhisitkul and T. A. Desai (2016). "Biocompatibility and pharmacokinetic analysis of an intracameral polycaprolactone drug delivery implant for glaucoma." Invest Ophthalmol Vis Sci 57(10): 4341-4346. DOI: 10.1167/iovs.16-19585.

Kim, S. Y., M. S. Shim, K. Y. Kim, R. N. Weinreb, L. A. Wheeler and W. K. Ju (2014a). "Inhibition of cyclophilin d by cyclosporin a promotes retinal ganglion cell survival by preventing mitochondrial alteration in ischemic injury." Cell Death & Disease 5(3): e1105-e1105. DOI: 10.1038/cddis.2014.80.

Kim, Y. C., B. Chiang, X. Wu and M. R. Prausnitz (2014b). "Ocular delivery of macromolecules." J Control Release 190: 172-181. DOI: 10.1016/j.jconrel.2014.06.043.

Kimble, T. D., M. E. Fitzgerald and A. Reiner (2006). "Sustained upregulation of glial fibrillary acidic protein in muller cells in pigeon retina following disruption of the parasympathetic control of choroidal blood flow." Exp Eye Res 83(5): 1017-1030. DOI: 10.1016/j.exer.2006.05.006.

Kimura, H. and Y. Ogura (2001). "Biodegradable polymers for ocular drug delivery." Ophthalmologica 215(3): 143-155. DOI: 10.1159/000050849.

Kipnis, J., E. Yoles, Z. Porat, A. Cohen, F. Mor, M. Sela, I. R. Cohen and M. Schwartz (2000). "T cell immunity to copolymer 1 confers neuroprotection on the damaged optic nerve: Possible therapy for optic neuropathies." Proceedings of the National Academy of Sciences 97(13): 7446-7451. DOI: 10.1073/pnas.97.13.7446.

Kiran, E., K. Liu and K. Ramsdell (2008). "Morphological changes in poly(Ɛ-caprolactone) in dense carbon dioxide." Polymer 49(7): 1853-1859. DOI: 10.1016/j.polymer.2008.02.017.

Kolb, H., E. Fernandez and R. Nelson (1995). Webvision: The organization of the retina and visual system. Salt Lake City (UT): University of Utah Health Sciences Center.

Kong, Y. and J. N. Hay (2002). "The measurement of the crystallinity of polymers by dsc." Polymer 43(14): 3873-3878. DOI: 10.1016/s0032-3861(02)00235-5.

Kuehn, M. H., J. H. Fingert and Y. H. Kwon (2005). "Retinal ganglion cell death in glaucoma: Mechanisms and neuroprotective strategies." Ophthalmol Clin North Am 18(3): 383-395, vi. DOI: 10.1016/j.ohc.2005.04.002.

Kutsarova, E., M. Munz and E. S. Ruthazer (2016). "Rules for shaping neural connections in the developing brain." Front Neural Circuits 10: 111. DOI: 10.3389/fncir.2016.00111.

Kwong, J. M., J. Caprioli and N. Piri (2010). "Rna binding protein with multiple splicing: A new marker for retinal ganglion cells." Invest Ophthalmol Vis Sci 51(2): 1052-1058. DOI: 10.1167/iovs.09-4098.

Kwong, J. M., A. Quan, H. Kyung, N. Piri and J. Caprioli (2011). "Quantitative analysis of retinal ganglion cell survival with rbpms immunolabeling in animal models of optic neuropathies." Invest Ophthalmol Vis Sci 52(13): 9694-9702. DOI: 10.1167/iovs.11-7869.

Lam, C. X., M. M. Savalani, S. H. Teoh and D. W. Hutmacher (2008). "Dynamics of in vitro polymer degradation of polycaprolactone-based scaffolds: Accelerated versus simulated physiological conditions." Biomed Mater 3(3): 034108. DOI: 10.1088/1748-6041/3/3/034108.

Lance, K. D., D. A. Bernards, N. A. Ciaccio, S. D. Good, T. S. Mendes, M. Kudisch, E. Chan, M. Ishikiriyama, R. B. Bhisitkul and T. A. Desai (2016). "In vivo and in vitro sustained release of ranibizumab from a nanoporous thin-film device." Drug Deliv Transl Res 6(6): 771-780. DOI: 10.1007/s13346-016-0298-7.

Lance, K. D., S. D. Good, T. S. Mendes, M. Ishikiriyama, P. Chew, L. S. Estes, K. Yamada, S. Mudumba, R. B. Bhisitkul and T. A. Desai (2015). "In vitro and in vivo sustained zero-order delivery of rapamycin (sirolimus) from a biodegradable intraocular device." Invest Ophthalmol Vis Sci 56(12): 7331-7337. DOI: 10.1167/iovs.15-17757.

Larrea, B. A., M. G. Iztueta, L. M. Indart and N. M. Alday (2014). "Early axonal damage detection by ganglion cell complex analysis with optical coherence tomography in nonarteritic anterior ischaemic optic neuropathy." Graefes Arch Clin Exp Ophthalmol 252(11): 1839-1846. DOI: 10.1007/s00417-014-2697-0.

Laycock, B., M. Nikolić, J. M. Colwell, E. Gauthier, P. Halley, S. Bottle and G. George (2017). "Lifetime prediction of biodegradable polymers." Progress in Polymer Science 71: 144-189. DOI: 10.1016/j.progpolymsci.2017.02.004.

Le Roux, L. G., X. Qiu, M. C. Jacobsen, M. D. Pagel, S. T. Gammon, D. R. Piwnica-Worms and D. Schellingerhout (2020). "Axonal transport as an in vivo biomarker for retinal neuropathy." Cells 9(5). DOI: 10.3390/cells9051298.

Leaver, S. G., Q. Cui, G. W. Plant, A. Arulpragasam, S. Hisheh, J. Verhaagen and A. R. Harvey (2006). "Aav-mediated expression of cntf promotes long-term survival and regeneration of adult rat retinal ganglion cells." Gene Ther 13(18): 1328-1341. DOI: 10.1038/sj.gt.3302791.

Lee, J. E., K. J. Liang, R. N. Fariss and W. T. Wong (2008). "Ex vivo dynamic imaging of retinal microglia using time-lapse confocal microscopy." Invest Ophthalmol Vis Sci 49(9): 4169-4176. DOI: 10.1167/iovs.08-2076.

Lee, J. Y., B. S. Jhun, Y. T. Oh, J. H. Lee, W. Choe, H. H. Baik, J. Ha, K. S. Yoon, S. S. Kim and I. Kang (2006). "Activation of adenosine a3 receptor suppresses lipopolysaccharide-induced tnf-alpha production through inhibition of pi 3-kinase/akt and nf-kappab activation in murine bv2 microglial cells." Neurosci Lett 396(1): 1-6. DOI: 10.1016/j.neulet.2005.11.004.

Leske, M. C., A. Heijl, M. Hussein, B. Bengtsson, L. Hyman, E. Komaroff and G. Early Manifest Glaucoma Trial (2003). "Factors for glaucoma progression and the effect of treatment: The early manifest glaucoma trial." Arch Ophthalmol 121(1): 48-56. DOI: 10.1001/archopht.121.1.48.

Leske, M. C., A. Heijl, L. Hyman, B. Bengtsson, L. Dong, Z. Yang and E. Group (2007). "Predictors of long-term progression in the early manifest glaucoma trial." Ophthalmology 114(11): 1965-1972. DOI: 10.1016/j.ophtha.2007.03.016.

Leung, C. K., W. M. Chan, W. H. Yung, A. C. Ng, J. Woo, M. K. Tsang and R. K. Tse (2005). "Comparison of macular and peripapillary measurements for the detection of glaucoma: An optical coherence tomography study." Ophthalmology 112(3): 391-400. DOI: 10.1016/j.ophtha.2004.10.020.

Levkovitch-Verbin, H., H. A. Quigley, K. R. Martin, D. Valenta, L. A. Baumrind and M. E. Pease (2002). "Translimbal laser photocoagulation to the trabecular meshwork as a model of glaucoma in rats." Invest Ophthalmol Vis Sci 43(2): 402-410.

Lewis, G. P. and S. K. Fisher (2003). "Up-regulation of glial fibrillary acidic protein in response to retinal injury: Its potential role in glial remodeling and a comparison to vimentin expression." 230: 263-290. DOI: 10.1016/s0074-7696(03)30005-1.

Li, Y., L. Andereggen, K. Yuki, K. Omura, Y. Yin, H. Y. Gilbert, B. Erdogan, M. S. Asdourian, C. Shrock, S. de Lima, U. P. Apfel, Y. Zhuo, M. Hershfinkel, S. J. Lippard, P. A. Rosenberg and L. Benowitz (2017). "Mobile zinc increases rapidly in the retina after optic nerve injury and regulates ganglion cell survival and optic nerve regeneration." Proc Natl Acad Sci U S A 114(2): E209-E218. DOI: 10.1073/pnas.1616811114.

Li, Y., C. L. Schlamp, G. L. Poulsen, M. W. Jackson, A. E. Griep and R. W. Nickells (2002). "P53 regulates apoptotic retinal ganglion cell death induced by n-methyl-d-aspartate." Mol Vis 8: 341-350.

Liang, F., X. R. Xiong, B. Zingg, X. Y. Ji, L. I. Zhang and H. W. Tao (2015). "Sensory cortical control of a visually induced arrest behavior via corticotectal projections." Neuron 86(3): 755-767. DOI: 10.1016/j.neuron.2015.03.048.

Liao, X. X., D. Chen, J. Shi, Y. Q. Sun, S. J. Sun, K. F. So and Q. L. Fu (2011). "The expression patterns of nogo-a, myelin associated glycoprotein and oligodendrocyte myelin glycoprotein in the retina after ocular hypertension: The expression of myelin proteins in the retina in glaucoma." Neurochem Res 36(11): 1955-1961. DOI: 10.1007/s11064-011-0518-y.

Libby, R. T., M. G. Anderson, I. H. Pang, Z. H. Robinson, O. V. Savinova, I. M. Cosma, A. Snow, L. A. Wilson, R. S. Smith, A. F. Clark and S. W. John (2005a). "Inherited glaucoma in DBA/2J mice: Pertinent disease features for studying the neurodegeneration." Vis Neurosci 22(5): 637-648. DOI: 10.1017/S0952523805225130.

Libby, R. T., Y. Li, O. V. Savinova, J. Barter, R. S. Smith, R. W. Nickells and S. W. John (2005b). "Susceptibility to neurodegeneration in a glaucoma is modified by bax gene dosage." PLoS Genet 1(1): 17-26. DOI: 10.1371/journal.pgen.0010004.

Lisboa, R., M. T. Leite, L. M. Zangwill, A. Tafreshi, R. N. Weinreb and F. A. Medeiros (2012). "Diagnosing preperimetric glaucoma with spectral domain optical coherence tomography." Ophthalmology 119(11): 2261-2269. DOI: 10.1016/j.ophtha.2012.06.009.

Liu, Y. J., J. Chen, X. Li, X. Zhou, Y. M. Hu, S. F. Chu, Y. Peng and N. H. Chen (2019). "Research progress on adenosine in central nervous system diseases." CNS Neurosci Ther 25(9): 899-910. DOI: 10.1111/cns.13190.

Livak, K. J. and T. D. Schmittgen (2001). "Analysis of relative gene expression data using real-time quantitative pcr and the 2(-delta delta c(t)) method." Methods 25(4): 402-408. DOI: 10.1006/meth.2001.1262.

Lucas-Ruiz, F., C. Galindo-Romero, K. T. Rodriguez-Ramirez, M. Vidal-Sanz and M. Agudo-Barriuso (2019). "Neuronal death in the contralateral un-injured retina after unilateral axotomy: Role of microglial cells." Int J Mol Sci 20(22). DOI: 10.3390/ijms20225733.

Luo, C., B. Yi, G. Tao, M. Li, Z. Chen, W. Tang, J. H. Zhang and H. Feng (2010). "Adenosine A3 receptor agonist reduces early brain injury in subarachnoid haemorrhage." Neuroreport 21(13): 892-896. DOI: 10.1097/WNR.0b013e32833dbd13.

Lupien, C., M. Brenner, S. L. Guerin and C. Salesse (2004). "Expression of glial fibrillary acidic protein in primary cultures of human muller cells." Exp Eye Res 79(3): 423-429. DOI: 10.1016/j.exer.2004.05.008.

Lyseng-Williamson, K. A. (2016). "Idebenone: A review in leber's hereditary optic neuropathy." Drugs 76(7): 805-813. DOI: 10.1007/s40265-016-0574-3.

Ma, Y. T., T. Hsieh, M. E. Forbes, J. E. Johnson and D. O. Frost (1998). "BDNF injected into the superior colliculus reduces developmental retinal ganglion cell death." J Neurosci 18(6): 2097-2107.

Mabuchi, F., M. Aihara, M. R. Mackey, J. D. Lindsey and R. N. Weinreb (2003). "Optic nerve damage in experimental mouse ocular hypertension." Invest Ophthalmol Vis Sci 44(10): 4321-4330. DOI: 10.1167/iovs.03-0138.

Macharadze, T., J. Goldschmidt, M. Marunde, T. Wanger, H. Scheich, W. Zuschratter, E. D. Gundelfinger and M. R. Kreutz (2009). "Interretinal transduction of injury signals after unilateral optic nerve crush." Neuroreport 20(3): 301-305. DOI: 10.1097/WNR.0b013e32832027e6.

Madeira, M. H., R. Boia, F. Elvas, T. Martins, R. A. Cunha, A. F. Ambrosio and A. R. Santiago (2016a). "Selective a2a receptor antagonist prevents microglia-mediated neuroinflammation and protects retinal ganglion cells from high intraocular pressure-induced transient ischemic injury." Transl Res 169: 112-128. DOI: 10.1016/j.trsl.2015.11.005.

Madeira, M. H., R. Boia, P. F. Santos, A. F. Ambrosio and A. R. Santiago (2015a). "Contribution of microglia-mediated neuroinflammation to retinal degenerative diseases." Mediators Inflamm 2015: 673090. DOI: 10.1155/2015/673090.

Madeira, M. H., F. Elvas, R. Boia, F. Q. Goncalves, R. A. Cunha, A. F. Ambrosio and A. R. Santiago (2015b). "Adenosine a2ar blockade prevents neuroinflammation-induced death of retinal ganglion cells caused by elevated pressure." J Neuroinflammation 12: 115. DOI: 10.1186/s12974-015-0333-5.

Madeira, M. H., A. Ortin-Martinez, F. Nadal-Nicolas, A. F. Ambrosio, M. Vidal-Sanz, M. Agudo-Barriuso and A. R. Santiago (2016b). "Caffeine administration prevents retinal neuroinflammation and loss of retinal ganglion cells in an animal model of glaucoma." Sci Rep 6: 27532. DOI: 10.1038/srep27532.

Maes, M. E., C. L. Schlamp and R. W. Nickells (2017). "Bax to basics: How the BCL2 gene family controls the death of retinal ganglion cells." Prog Retin Eye Res 57: 1-25. DOI: 10.1016/j.preteyeres.2017.01.002.

Maffei, L., G. Carmignoto, V. H. Perry, P. Candeo and G. Ferrari (1990). "Schwann cells promote the survival of rat retinal ganglion cells after optic nerve section." Proc Natl Acad Sci U S A 87(5): 1855-1859. DOI: 10.1073/pnas.87.5.1855.

Mailavaram, R. P., O. H. A. Al-Attraqchi, S. Kar and S. Ghosh (2019). "Current status in the design and development of agonists and antagonists of adenosine A3 receptor as potential therapeutic agents." Curr Pharm Des 25(25): 2772-2787. DOI: 10.2174/1381612825666190716114056.

Malhotra, A., F. J. Minja, A. Crum and D. Burrowes (2011). "Ocular anatomy and cross-sectional imaging of the eye." Semin Ultrasound CT MR 32(1): 2-13. DOI: 10.1053/j.sult.2010.10.009.

Mansour-Robaey, S., D. B. Clarke, Y. C. Wang, G. M. Bray and A. J. Aguayo (1994). "Effects of ocular injury and administration of brain-derived neurotrophic factor on survival and regrowth of axotomized retinal ganglion cells." Proc Natl Acad Sci U S A 91(5): 1632-1636. DOI: 10.1073/pnas.91.5.1632.

Martersteck, E. M., K. E. Hirokawa, M. Evarts, A. Bernard, X. Duan, Y. Li, L. Ng, S. W. Oh, B. Ouellette, J. J. Royall, M. Stoecklin, Q. Wang, H. Zeng, J. R. Sanes and J. A. Harris (2017). "Diverse central projection patterns of retinal ganglion cells." Cell Rep 18(8): 2058-2072. DOI: 10.1016/j.celrep.2017.01.075.

Martins, J., M. Castelo-Branco, A. Batista, B. Oliveiros, A. R. Santiago, J. Galvao, E. Fernandes, F. Carvalho, C. Cavadas and A. F. Ambrosio (2011). "Effects of 3,4-methylenedioxymethamphetamine administration on retinal physiology in the rat." PLoS One 6(12): e29583. DOI: 10.1371/journal.pone.0029583.

Martins, J., F. Elvas, D. Brudzewsky, T. Martins, B. Kolomiets, P. Tralhao, C. R. Gotzsche, C. Cavadas, M. Castelo-Branco, D. P. Woldbye, S. Picaud, A. R. Santiago and A. F. Ambrosio (2015). "Activation of neuropeptide Y receptors modulates retinal ganglion cell physiology and exerts neuroprotective actions in vitro." ASN Neuro 7(4). DOI: 10.1177/1759091415598292.

May, P. J. (2006). "The mammalian superior colliculus: Laminar structure and connections." Prog Brain Res 151: 321-378. DOI: 10.1016/S0079-6123(05)51011-2.

Mdzomba, J. B., N. Jordi, L. Rodriguez, S. Joly, F. Bretzner and V. Pernet (2018). "Nogo-a inactivation improves visual plasticity and recovery after retinal injury." Cell Death & Disease 9(7). DOI: 10.1038/s41419-018-0780-x.

Mead, B., A. Thompson, B. A. Scheven, A. Logan, M. Berry and W. Leadbeater (2014). "Comparative evaluation of methods for estimating retinal ganglion cell loss in retinal sections and wholemounts." PLoS One 9(10): e110612. DOI: 10.1371/journal.pone.0110612.

Mead, B. and S. Tomarev (2016). "Evaluating retinal ganglion cell loss and dysfunction." Exp Eye Res 151: 96-106. DOI: 10.1016/j.exer.2016.08.006.

Medeiros, F. A., R. Lisboa, R. N. Weinreb, J. M. Liebmann, C. Girkin and L. M. Zangwill (2013). "Retinal ganglion cell count estimates associated with early development of visual field defects in glaucoma." Ophthalmology 120(4): 736-744. DOI: 10.1016/j.ophtha.2012.09.039.

Mey, J. and S. Thanos (1993). "Intravitreal injections of neurotrophic factors support the survival of axotomized retinal ganglion cells in adult rats in vivo." Brain Res 602(2): 304-317. DOI: 10.1016/0006-8993(93)90695-j.

Meyer-Franke, A., M. R. Kaplan, F. W. Pfrieger and B. A. Barres (1995). "Characterization of the signaling interactions that promote the survival and growth of developing retinal ganglion cells in culture." Neuron 15(4): 805-819. DOI: 10.1016/0896-6273(95)90172-8.

Meyer, C. H., T. U. Krohne, P. Charbel Issa, Z. Liu and F. G. Holz (2016). "Routes for drug delivery to the eye and retina: Intravitreal injections." Dev Ophthalmol 55: 63-70. DOI: 10.1159/000431143.

Meyerson, C., G. Van Stavern and C. McClelland (2015). "Leber hereditary optic neuropathy: Current perspectives." Clin Ophthalmol 9: 1165-1176. DOI: 10.2147/OPTH.S62021.

Miki, A., F. A. Medeiros, R. N. Weinreb, S. Jain, F. He, L. Sharpsten, N. Khachatryan, N. Hammel, J. M. Liebmann, C. A. Girkin, P. A. Sample and L. M. Zangwill (2014). "Rates of retinal nerve fiber layer thinning in glaucoma suspect eyes." Ophthalmology 121(7): 1350-1358. DOI: 10.1016/j.ophtha.2014.01.017.

Ming, G. L., H. J. Song, B. Berninger, C. E. Holt, M. Tessier-Lavigne and M. M. Poo (1997). "cAMP-dependent growth cone guidance by netrin-1." Neuron 19(6): 1225-1235. DOI: 10.1016/s0896-6273(00)80414-6.

Mizutani, M., C. Gerhardinger and M. Lorenzi (1998). "Müller cell changes in human diabetic retinopathy." Diabetes 47(3): 445-449. DOI: 10.2337/diabetes.47.3.445.

Momeni, H. R. (2011). "Role of calpain in apoptosis." Cell J 13(2): 65-72.

Moore, D. L., M. G. Blackmore, Y. Hu, K. H. Kaestner, J. L. Bixby, V. P. Lemmon and J. L. Goldberg (2009). "KLF family members regulate intrinsic axon regeneration ability." Science 326(5950): 298-301. DOI: 10.1126/science.1175737.

Moore, D. L. and J. L. Goldberg (2011). "Multiple transcription factor families regulate axon growth and regeneration." Dev Neurobiol 71(12): 1186-1211. DOI: 10.1002/dneu.20934.

Morgan, J. E. (2012). "Retina ganglion cell degeneration in glaucoma: An opportunity missed? A review." Clinical & Experimental Ophthalmology 40(4): 364-368. DOI: 10.1111/j.1442-9071.2012.02789.x.

Morgan, J. E. and J. R. Tribble (2015). "Microbead models in glaucoma." Exp Eye Res 141: 9-14. DOI: 10.1016/j.exer.2015.06.020.

Morin, L. P. and K. M. Studholme (2014). "Retinofugal projections in the mouse." J Comp Neurol 522(16): 3733-3753. DOI: 10.1002/cne.23635.

Morrison, J. C., W. O. Cepurna and E. C. Johnson (2015). "Modeling glaucoma in rats by sclerosing aqueous outflow pathways to elevate intraocular pressure." Exp Eye Res 141: 23-32. DOI: 10.1016/j.exer.2015.05.012.

Morrison, J. C., C. G. Moore, L. M. Deppmeier, B. G. Gold, C. K. Meshul and E. C. Johnson (1997). "A rat model of chronic pressure-induced optic nerve damage." Exp Eye Res 64(1): 85-96. DOI: 10.1006/exer.1996.0184.

Muller, A., T. G. Hauk, M. Leibinger, R. Marienfeld and D. Fischer (2009). "Exogenous cntf stimulates axon regeneration of retinal ganglion cells partially via endogenous cntf." Mol Cell Neurosci 41(2): 233-246. DOI: 10.1016/j.mcn.2009.03.002.

Muller, C. E., Y. Baqi and V. Namasivayam (2020). "Agonists and antagonists for purinergic receptors." Methods Mol Biol 2041: 45-64. DOI: 10.1007/978-1-4939-9717-6_3.

Muller, C. E. and K. A. Jacobson (2011). "Recent developments in adenosine receptor ligands and their potential as novel drugs." Biochim Biophys Acta 1808(5): 1290-1308. DOI: 10.1016/j.bbamem.2010.12.017.

Munemasa, Y. and Y. Kitaoka (2013). "Molecular mechanisms of retinal ganglion cell degeneration in glaucoma and future prospects for cell body and axonal protection." Frontiers in Cellular Neuroscience 6. DOI: 10.3389/fncel.2012.00060.

Murcia-Belmonte, V. and L. Erskine (2019). "Wiring the binocular visual pathways." Int J Mol Sci 20(13). DOI: 10.3390/ijms20133282.

Mwanza, J. C., M. K. Durbin, D. L. Budenz, F. E. Sayyad, R. T. Chang, A. Neelakantan, D. G. Godfrey, R. Carter and A. S. Crandall (2012). "Glaucoma diagnostic accuracy of ganglion cell-inner plexiform layer thickness: Comparison with nerve fiber layer and optic nerve head." Ophthalmology 119(6): 1151-1158. DOI: 10.1016/j.ophtha.2011.12.014.

Na, J. H., K. Lee, J. R. Lee, S. Baek, S. J. Yoo and M. S. Kook (2013). "Detection of macular ganglion cell loss in preperimetric glaucoma patients with localized retinal nerve fibre defects by spectral-domain optical coherence tomography." Clin Exp Ophthalmol 41(9): 870-880. DOI: 10.1111/ceo.12142.

Nadal-Nicolas, F. M., M. Jimenez-Lopez, M. Salinas-Navarro, P. Sobrado-Calvo, J. J. Alburquerque-Bejar, M.

Vidal-Sanz and M. Agudo-Barriuso (2012). "Whole number, distribution and co-expression of Brn3 transcription factors in retinal ganglion cells of adult albino and pigmented rats." PLoS One 7(11): e49830. DOI: 10.1371/journal.pone.0049830.

Nadal-Nicolas, F. M., M. Jimenez-Lopez, M. Salinas-Navarro, P. Sobrado-Calvo, M. Vidal-Sanz and M. Agudo-Barriuso (2017). "Microglial dynamics after axotomy-induced retinal ganglion cell death." J Neuroinflammation 14(1): 218. DOI: 10.1186/s12974-017-0982-7.

Nadal-Nicolas, F. M., M. Jimenez-Lopez, P. Sobrado-Calvo, L. Nieto-Lopez, I. Canovas-Martinez, M. Salinas-Navarro, M. Vidal-Sanz and M. Agudo (2009). "Brn3a as a marker of retinal ganglion cells: Qualitative and quantitative time course studies in naive and optic nerve-injured retinas." Invest Ophthalmol Vis Sci 50(8): 3860-3868. DOI: 10.1167/iovs.08-3267.

Nadal-Nicolas, F. M., P. Sobrado-Calvo, M. Jimenez-Lopez, M. Vidal-Sanz and M. Agudo-Barriuso (2015). "Long-term effect of optic nerve axotomy on the retinal ganglion cell layer." Invest Ophthalmol Vis Sci 56(10): 6095-6112. DOI: 10.1167/iovs.15-17195.

Nadal-Nicolas, F. M., F. J. Valiente-Soriano, M. Salinas-Navarro, M. Jimenez-Lopez, M. Vidal-Sanz and M. Agudo-Barriuso (2015). "Retino-retinal projection in juvenile and young adult rats and mice." Exp Eye Res 134: 47-52. DOI: 10.1016/j.exer.2015.03.015.

Nagata, A., T. Higashide, S. Ohkubo, H. Takeda and K. Sugiyama (2009). "In vivo quantitative evaluation of the rat retinal nerve fiber layer with optical coherence tomography." Investigative Opthalmology & Visual Science 50(6): 2809. DOI: 10.1167/iovs.08-2764.

Nakashima, K. I., K. Iwao, T. Inoue, A. Haga, T. Tsutsumi, M. I. Mochita, T. Fujimoto and H. Tanihara (2018). "Stimulation of the adenosine A3 receptor, not the A1 or A2 receptors, promote neurite outgrowth of retinal ganglion cells." Exp Eye Res 170: 160-168. DOI: 10.1016/j.exer.2018.02.019.

Nakazawa, T., C. Nakazawa, A. Matsubara, K. Noda, T. Hisatomi, H. She, N. Michaud, A. Hafezi-Moghadam, J. W. Miller and L. I. Benowitz (2006). "Tumor necrosis factor-alpha mediates oligodendrocyte death and delayed retinal ganglion cell loss in a mouse model of glaucoma." J Neurosci 26(49): 12633-12641. DOI: 10.1523/JNEUROSCI.2801-06.2006.

Nathans, J. (1999). "The evolution and physiology of human color vision: Insights from molecular genetic studies of visual pigments." Neuron 24(2): 299-312. DOI: 10.1016/s0896-6273(00)80845-4.

Natu, M. V., H. C. de Sousa and M. H. Gil (2010). "Effects of drug solubility, state and loading on controlled release in bicomponent electrospun fibers." International Journal of Pharmaceutics 397(1-2): 50-58. DOI: 10.1016/j.ijpharm.2010.06.045.

Natu, M. V., M. N. Gaspar, C. A. Fontes Ribeiro, A. M. Cabrita, H. C. de Sousa and M. H. Gil (2011a). "In vitro and in vivo evaluation of an intraocular implant for glaucoma treatment." Int J Pharm 415(1-2): 73-82. DOI: 10.1016/j.ijpharm.2011.05.047.

Natu, M. V., M. N. Gaspar, C. A. Ribeiro, I. J. Correia, D. Silva, H. C. de Sousa and M. H. Gil (2011b). "A poly(epsilon-caprolactone) device for sustained release of an anti-glaucoma drug." Biomed Mater 6(2): 025003. DOI: 10.1088/1748-6041/6/2/025003.

Natu, M. V., M. H. Gil and H. C. de Sousa (2008). "Supercritical solvent impregnation of poly(Ɛ-caprolactone)/poly(oxyethylene-b-oxypropylene-b-oxyethylene) and poly(Ɛ-caprolactone)/poly(ethylene-vinyl acetate) blends for controlled release applications." The Journal of Supercritical Fluids 47(1): 93-102. DOI: 10.1016/j.supflu.2008.05.006.

Newman, E. and A. Reichenbach (1996). "The muller cell: A functional element of the retina." Trends Neurosci 19(8): 307-312. DOI: 10.1016/0166-2236(96)10040-0.

Nickells, R. W. (2007). "From ocular hypertension to ganglion cell death: A theoretical sequence of events leading to glaucoma." Can J Ophthalmol 42(2): 278-287. DOI: 10.3129/can j ophthalmol.i07-036.

Nordstrom, B. L., D. S. Friedman, E. Mozaffari, H. A. Quigley and A. M. Walker (2005). "Persistence and adherence with topical glaucoma therapy." Am J Ophthalmol 140(4): 598-606. DOI: 10.1016/j.ajo.2005.04.051.

Nork, T. M., J. N. Ver Hoeve, G. L. Poulsen, R. W. Nickells, M. D. Davis, A. J. Weber, Vaegan, S. H. Sarks, H. L. Lemley and L. L. Millecchia (2000). "Swelling and loss of photoreceptors in chronic human and experimental glaucomas." Arch Ophthalmol 118(2): 235-245. DOI: 10.1001/archopht.118.2.235.

Nouri-Mahdavi, K., S. Nowroozizadeh, N. Nassiri, N. Cirineo, S. Knipping, J. Giaconi and J. Caprioli (2013). "Macular ganglion cell/inner plexiform layer measurements by spectral domain optical coherence tomography for detection of early glaucoma and comparison to retinal nerve fiber layer measurements." Am J Ophthalmol 156(6): 1297-1307 e1292. DOI: 10.1016/j.ajo.2013.08.001.

Ohsawa, K., T. Sanagi, Y. Nakamura, E. Suzuki, K. Inoue and S. Kohsaka (2012). "Adenosine A3 receptor is involved in adp-induced microglial process extension and migration." J Neurochem 121(2): 217-227. DOI: 10.1111/j.1471-4159.2012.07693.x.

Ortin-Martinez, A., M. Salinas-Navarro, F. M. Nadal-Nicolas, M. Jimenez-Lopez, F. J. Valiente-Soriano, D. Garcia-Ayuso, J. M. Bernal-Garro, M. Aviles-Trigueros, M. Agudo-Barriuso, M. P. Villegas-Perez and M. Vidal-Sanz (2015). "Laser-induced ocular hypertension in adult rats does not affect non-RGC neurons in the ganglion cell layer but results in protracted severe loss of cone-photoreceptors." Exp Eye Res 132: 17-33. DOI: 10.1016/j.exer.2015.01.006.

Osborne, N. N., R. J. Casson, J. P. Wood, G. Chidlow, M. Graham and J. Melena (2004). "Retinal ischemia: Mechanisms of damage and potential therapeutic strategies." Prog Retin Eye Res 23(1): 91-147. DOI: 10.1016/j.preteyeres.2003.12.001.

Palmhof, M., V. Frank, P. Rappard, E. Kortenhorn, J. Demuth, N. Biert, G. Stute, H. B. Dick and S. C. Joachim (2019). "From ganglion cell to photoreceptor layer: Timeline of deterioration in a rat ischemia/reperfusion model." Front Cell Neurosci 13: 174. DOI: 10.3389/fncel.2019.00174.

Panda, S. and J. B. Jonas (1992). "Decreased photoreceptor count in human eyes with secondary angle-closure glaucoma." Invest Ophthalmol Vis Sci 33(8): 2532-2536.

Parisi, V. (2005). "Electrophysiological assessment of glaucomatous visual dysfunction during treatment with cytidine-5'-diphosphocholine (citicoline): A study of 8 years of follow-up." Doc Ophthalmol 110(1): 91-102. DOI: 10.1007/s10633-005-7348-7.

Parisi, V., G. Manni, G. Colacino and M. G. Bucci (1999). "Cytidine-5'-diphosphocholine (citicoline) improves retinal and cortical responses in patients with glaucoma." Ophthalmology 106(6): 1126-1134. DOI: 10.1016/S0161-6420(99)90269-5.

Parisi, V., F. Oddone, L. Ziccardi, G. Roberti, G. Coppola and G. Manni (2018). "Citicoline and retinal ganglion cells: Effects on morphology and function." Curr Neuropharmacol 16(7): 919-932. DOI: 10.2174/1570159X15666170703111729.

Park, H. L., S. W. Kim, J. H. Kim and C. K. Park (2019). "Increased levels of synaptic proteins involved in synaptic plasticity after chronic intraocular pressure elevation and modulation by brain-derived neurotrophic factor in a glaucoma animal model." Dis Model Mech 12(6). DOI: 10.1242/dmm.037184.

Park, K. K., K. Liu, Y. Hu, P. D. Smith, C. Wang, B. Cai, B. Xu, L. Connolly, I. Kramvis, M. Sahin and Z. He (2008). "Promoting axon regeneration in the adult cns by modulation of the pten/mtor pathway." Science 322(5903): 963-966. DOI: 10.1126/science.1161566.

Park, S. C., J. Brumm, R. L. Furlanetto, C. Netto, Y. Liu, C. Tello, J. M. Liebmann and R. Ritch (2015). "Lamina cribrosa depth in different stages of glaucoma." Investigative Opthalmology & Visual Science 56(3): 2059. DOI: 10.1167/iovs.14-15540.

Pasterkamp, R. J., P. N. Anderson and J. Verhaagen (2001). "Peripheral nerve injury fails to induce growth of lesioned ascending dorsal column axons into spinal cord scar tissue expressing the axon repellent semaphorin3a." Eur J Neurosci 13(3): 457-471. DOI: 10.1046/j.0953-816x.2000.01398.x.

Pasterkamp, R. J., R. J. Giger, M. J. Ruitenberg, A. J. G. D. Holtmaat, J. De Wit, F. De Winter and J. Verhaagen (1999). "Expression of the gene encoding the chemorepellent semaphorin iii is induced in the fibroblast component of neural scar tissue formed following injuries of adult but not neonatal cns." Molecular and Cellular Neuroscience 13(2): 143-166. DOI: 10.1006/mcne.1999.0738.

Patil, K. and S. C. Sharma (2004). "Broad spectrum caspase inhibitor rescues retinal ganglion cells after ischemia." Neuroreport 15(6): 981-984. DOI: 10.1097/00001756-200404290-00010.

Pattamatta, U., Z. McPherson and A. White (2016). "A mouse retinal explant model for use in studying neuroprotection in glaucoma." Exp Eye Res 151: 38-44. DOI: 10.1016/j.exer.2016.07.010.

Pease, M. E., S. J. McKinnon, H. A. Quigley, L. A. Kerrigan-Baumrind and D. J. Zack (2000). "Obstructed axonal transport of bdnf and its receptor trkb in experimental glaucoma." Invest Ophthalmol Vis Sci 41(3): 764-774.

Peinado-Ramon, P., M. Salvador, M. P. Villegas-Perez and M. Vidal-Sanz (1996). "Effects of axotomy and intraocular administration of NT-4, NT-3, and brain-derived neurotrophic factor on the survival of adult rat retinal ganglion cells. A quantitative in vivo study." Invest Ophthalmol Vis Sci 37(4): 489-500.

Peppas, N. A. and L. Brannon-Peppas (1994). "Water diffusion and sorption in amorphous macromolecular systems and foods." Journal of Food Engineering 22(1-4): 189-210. DOI: 10.1016/0260-8774(94)90030-2.

Perez de Lara, M. J., C. Santano, A. Guzman-Aranguez, F. J. Valiente-Soriano, M. Aviles-Trigueros, M. Vidal-Sanz, P. de la Villa and J. Pintor (2014). "Assessment of inner retina dysfunction and progressive ganglion cell loss in a mouse model of glaucoma." Exp Eye Res 122: 40-49. DOI: 10.1016/j.exer.2014.02.022.

Pernet, V. (2017). "Nogo-a in the visual system development and in ocular diseases." Biochimica et Biophysica Acta (BBA) - Molecular Basis of Disease 1863(6): 1300-1311. DOI: 10.1016/j.bbadis.2017.04.008.

Pernet, V., S. Joly, F. Christ, L. Dimou and M. E. Schwab (2008). "Nogo-a and myelin-associated glycoprotein differently regulate oligodendrocyte maturation and myelin formation." Journal of Neuroscience 28(29): 7435-7444. DOI: 10.1523/jneurosci.0727-08.2008.

Pernet, V., S. Joly, D. Dalkara, O. Schwarz, F. Christ, D. Schaffer, J. G. Flannery and M. E. Schwab (2012). "Neuronal nogo-a upregulation does not contribute to er stress-associated apoptosis but participates in the regenerative response in the axotomized adult retina." Cell Death Differ 19(7): 1096-1108. DOI: 10.1038/cdd.2011.191.

Pollard, T. D., W. C. Earnshaw, J. Lippincott-Schwartz and G. T. Johnson (2017). Programmed cell death. Cell biology: 797-815.

Puga, A. M., A. Rey-Rico, B. Magarinos, C. Alvarez-Lorenzo and A. Concheiro (2012). "Hot melt poly-epsilon-caprolactone/poloxamine implantable matrices for sustained delivery of ciprofloxacin." Acta Biomater 8(4): 1507-1518. DOI: 10.1016/j.actbio.2011.12.020.

Pugliese, A. M., E. Coppi, R. Volpini, G. Cristalli, R. Corradetti, L. S. Jeong, K. A. Jacobson and F. Pedata (2007). "Role of adenosine A3 receptors on ca1 hippocampal neurotransmission during oxygen-glucose deprivation episodes of different duration." Biochem Pharmacol 74(5): 768-779. DOI: 10.1016/j.bcp.2007.06.003.

Quigley, H. A. (2018a). "21st century glaucoma care." Eye 33(2): 254-260. DOI: 10.1038/s41433-018-0227-8.

Quigley, H. A. (2018b). "Use of animal models and techniques in glaucoma research: Introduction." Methods Mol Biol 1695: 1-10. DOI: 10.1007/978-1-4939-7407-8_1.

Quigley, H. A., G. R. Dunkelberger and W. R. Green (1988). "Chronic human glaucoma causing selectively greater loss of large optic nerve fibers." Ophthalmology 95(3): 357-363. DOI: 10.1016/s0161-6420(88)33176-3.

Quigley, H. A., J. Guy and D. R. Anderson (1979). "Blockade of rapid axonal transport. Effect of intraocular pressure elevation in primate optic nerve." Arch Ophthalmol 97(3): 525-531. DOI: 10.1001/archopht.1979.01020010269018.

Quigley, H. A., S. J. McKinnon, D. J. Zack, M. E. Pease, L. A. Kerrigan-Baumrind, D. F. Kerrigan and R. S. Mitchell (2000). "Retrograde axonal transport of bdnf in retinal ganglion cells is blocked by acute iop elevation in rats." Invest Ophthalmol Vis Sci 41(11): 3460-3466.

Quigley, H. A., R. W. Nickells, L. A. Kerrigan, M. E. Pease, D. J. Thibault and D. J. Zack (1995). "Retinal ganglion cell death in experimental glaucoma and after axotomy occurs by apoptosis." Invest Ophthalmol Vis Sci 36(5): 774-786.

Quigley, H. A., R. M. Sanchez, G. R. Dunkelberger, N. L. L'Hernault and T. A. Baginski (1987). "Chronic glaucoma selectively damages large optic nerve fibers." Invest Ophthalmol Vis Sci 28(6): 913-920.

Rath, E. Z., Z. Hazan, K. Adamsky, A. Solomon, Z. I. Segal and L. A. Levin (2019). "Randomized controlled phase 2a study of rph201 in previous nonarteritic anterior ischemic optic neuropathy." J Neuroophthalmol 39(3): 291-298. DOI: 10.1097/WNO.0000000000000786.

Rathnasamy, G., W. S. Foulds, E. A. Ling and C. Kaur (2019). "Retinal microglia - a key player in healthy and diseased retina." Prog Neurobiol 173: 18-40. DOI: 10.1016/j.pneurobio.2018.05.006.

Reardon, G., S. Kotak and G. F. Schwartz (2011). "Objective assessment of compliance and persistence among patients treated for glaucoma and ocular hypertension: A systematic review." Patient Prefer Adherence 5: 441-463. DOI: 10.2147/PPA.S23780.

Regillo, C. (2020). Long-acting drug delivery in namd: Archway phase 3 results. EURETINA 2020 virtual.

Reichenbach, A. and A. Bringmann (2013). "New functions of muller cells." Glia 61(5): 651-678. DOI: 10.1002/glia.22477.

Remington, L. A. (2012). "Retina." 61-92. DOI: 10.1016/b978-1-4377-1926-0.10004-9.

Renner, M., G. Stute, M. Alzureiqi, J. Reinhard, S. Wiemann, H. Schmid, A. Faissner, H. B. Dick and S. C. Joachim (2017). "Optic nerve degeneration after retinal ischemia/reperfusion in a rodent model." Front Cell Neurosci 11: 254. DOI: 10.3389/fncel.2017.00254.

Rheaume, B. A., A. Jereen, M. Bolisetty, M. S. Sajid, Y. Yang, K. Renna, L. Sun, P. Robson and E. F. Trakhtenberg (2018). "Single cell transcriptome profiling of retinal ganglion cells identifies cellular subtypes." Nat Commun 9(1): 2759. DOI: 10.1038/s41467-018-05134-3.

Richardson, P. M., U. M. McGuinness and A. J. Aguayo (1980). "Axons from cns neurones regenerate into pns grafts." Nature 284(5753): 264-265. DOI: 10.1038/284264a0.

Riva, I., E. Micheletti, F. Oddone, C. Bruttini, S. Montescani, G. De Angelis, L. Rovati, R. N. Weinreb and L. Quaranta (2020). "Anterior chamber angle assessment techniques: A review." J Clin Med 9(12). DOI: 10.3390/jcm9123814.

Rodger, J., H. Goto, Q. Cui, P. B. Chen and A. R. Harvey (2005). "cAMP regulates axon outgrowth and guidance during optic nerve regeneration in goldfish." Molecular and Cellular Neuroscience 30(3): 452-464. DOI: 10.1016/j.mcn.2005.08.009.

Rodrigues-Neves, A. C., I. D. Aires, J. Vindeirinho, R. Boia, M. H. Madeira, F. Q. Gonçalves, R. A. Cunha, P. F. Santos, A. F. Ambrósio and A. R. Santiago (2018). "Elevated pressure changes the purinergic system of microglial cells." Frontiers in Pharmacology 9. DOI: 10.3389/fphar.2018.00016.

Ronneberger, O., P. Fischer and T. Brox (2015). "U-net: Convolutional networks for biomedical image segmentation. In: Lecture notes in computer science (including subseries lecture notes in artificial intelligence and lecture notes in bioinformatics)." 9351: 234-241. DOI: 10.1007/978-3-319-24574-4_28.

Rosenthal, R. and M. Fromm (2011). "Endothelin antagonism as an active principle for glaucoma therapy." Br J Pharmacol 162(4): 806-816. DOI: 10.1111/j.1476-5381.2010.01103.x.

Rosolen, S. G., B. Kolomiets, O. Varela and S. Picaud (2008). "Retinal electrophysiology for toxicology studies: Applications and limits of erg in animals and ex vivo recordings." Exp Toxicol Pathol 60(1): 17-32. DOI: 10.1016/j.etp.2007.11.012.

Roth, S., P. S. Rosenbaum, J. Osinski, S. S. Park, A. Y. Toledano, B. Li and A. A. Moshfeghi (1997). "Ischemia induces significant changes in purine nucleoside concentration in the retina-choroid in rats." Experimental Eye Research 65(6): 771-779. DOI: 10.1006/exer.1997.0391.

Rowe, R. C., P. J. Sheskey, S. n. C. Owen and American Pharmacists Association. (2006). Handbook of pharmaceutical excipients / edited by raymond c. Rowe, paul j. Sheskey, siân c. Owen. London ; Greyslake, IL Washington, DC, Pharmaceutical Press ; American Pharmacists Association.

Roy, A. G., S. Conjeti, S. P. K. Karri, D. Sheet, A. Katouzian, C. Wachinger and N. Navab (2017). "Relaynet: Retinal layer and fluid segmentation of macular optical coherence tomography using fully convolutional networks." Biomedical Optics Express 8(8): 3627. DOI: 10.1364/boe.8.003627.

Rydz, J., W. Sikorska, M. Kyulavska and D. Christova (2014). "Polyester-based (bio)degradable polymers as environmentally friendly materials for sustainable development." Int J Mol Sci 16(1): 564-596. DOI: 10.3390/ijms16010564.

Salerno, A. and C. Domingo (2019). "Polycaprolactone foams prepared by supercritical CO2 batch foaming of polymer/organic solvent solutions." The Journal of Supercritical Fluids 143: 146-156. DOI: 10.1016/j.supflu.2018.08.006.

Salerno, A. and C. D. Pascual (2013). "A clean and sustainable route towards the design and fabrication of biodegradable foams by means of supercritical CO2/ethyl lactate solid-state foaming." RSC Advances 3(38): 17355. DOI: 10.1039/c3ra42345j.

Salinas-Navarro, M., L. Alarcon-Martinez, F. J. Valiente-Soriano, M. Jimenez-Lopez, S. Mayor-Torroglosa, M. Aviles-Trigueros, M. P. Villegas-Perez and M. Vidal-Sanz (2010). "Ocular hypertension impairs optic nerve axonal transport leading to progressive retinal ganglion cell degeneration." Exp Eye Res 90(1): 168-183. DOI: 10.1016/j.exer.2009.10.003.

Salinas-Navarro, M., L. Alarcon-Martinez, F. J. Valiente-Soriano, A. Ortin-Martinez, M. Jimenez-Lopez, M. Aviles-Trigueros, M. P. Villegas-Perez, P. de la Villa and M. Vidal-Sanz (2009a). "Functional and morphological effects of laser-induced ocular hypertension in retinas of adult albino swiss mice." Mol Vis 15: 2578-2598.

Salinas-Navarro, M., S. Mayor-Torroglosa, M. Jimenez-Lopez, M. Aviles-Trigueros, T. M. Holmes, R. D. Lund, M. P. Villegas-Perez and M. Vidal-Sanz (2009b). "A computerized analysis of the entire retinal ganglion cell population and its spatial distribution in adult rats." Vision Res 49(1): 115-126. DOI: 10.1016/j.visres.2008.09.029.

Salvatore, C. A., M. A. Jacobson, H. E. Taylor, J. Linden and R. G. Johnson (1993). "Molecular cloning and characterization of the human a3 adenosine receptor." Proc Natl Acad Sci U S A 90(21): 10365-10369. DOI: 10.1073/pnas.90.21.10365.

Sampat, K. M. and S. J. Garg (2010). "Complications of intravitreal injections." Curr Opin Ophthalmol 21(3): 178-183. DOI: 10.1097/ICU.0b013e328338679a.

Samsel, P. A., L. Kisiswa, J. T. Erichsen, S. D. Cross and J. E. Morgan (2011). "A novel method for the induction of experimental glaucoma using magnetic microspheres." Invest Ophthalmol Vis Sci 52(3): 1671-1675. DOI: 10.1167/iovs.09-3921.

Sanchez-Migallon, M. C., F. J. Valiente-Soriano, F. M. Nadal-Nicolas, M. Vidal-Sanz and M. Agudo-Barriuso (2016). "Apoptotic retinal ganglion cell death after optic nerve transection or crush in mice: Delayed rgc loss with bdnf or a caspase 3 inhibitor." Invest Ophthalmol Vis Sci 57(1): 81-93. DOI: 10.1167/iovs.15-17841.

Sánchez-Migallón, M. C., F. J. Valiente-Soriano, M. Salinas-Navarro, F. M. Nadal-Nicolás, M. Jiménez-López, M. Vidal-Sanz and M. Agudo-Barriuso (2018). "Nerve fibre layer degeneration and retinal ganglion cell loss long term after optic nerve crush or transection in adult mice." Experimental Eye Research 170: 40-50. DOI: 10.1016/j.exer.2018.02.010.

Sanes, J. R. and R. H. Masland (2015). "The types of retinal ganglion cells: Current status and implications for neuronal classification." Annu Rev Neurosci 38: 221-246. DOI: 10.1146/annurev-neuro-071714-034120.

Santiago, A. R., R. Boia, I. D. Aires, A. F. Ambrosio and R. Fernandes (2018). "Sweet stress: Coping with vascular dysfunction in diabetic retinopathy." Front Physiol 9: 820. DOI: 10.3389/fphys.2018.00820.

Santiago, A. R., M. H. Madeira, R. Boia, I. D. Aires, A. C. Rodrigues-Neves, P. F. Santos and A. F. Ambrósio (2020). "Keep an eye on adenosine: Its role in retinal inflammation." Pharmacology & Therapeutics 210: 107513. DOI: 10.1016/j.pharmthera.2020.107513.

Santiago, A. R., T. S. Pereira, M. J. Garrido, A. J. Cristovao, P. F. Santos and A. F. Ambrosio (2006). "High glucose and diabetes increase the release of [3H]-d-aspartate in retinal cell cultures and in rat retinas." Neurochem Int 48(6-7): 453-458. DOI: 10.1016/j.neuint.2005.10.013.

Santos-Carvalho, A., C. A. Aveleira, F. Elvas, A. F. Ambrosio and C. Cavadas (2013). "Neuropeptide Y receptors Y1 and Y2 are present in neurons and glial cells in rat retinal cells in culture." Invest Ophthalmol Vis Sci 54(1): 429-443. DOI: 10.1167/iovs.12-10776.

Sappington, R. M., B. J. Carlson, S. D. Crish and D. J. Calkins (2010). "The microbead occlusion model: A paradigm for induced ocular hypertension in rats and mice." Invest Ophthalmol Vis Sci 51(1): 207-216. DOI: 10.1167/iovs.09-3947.

Sappington, R. M., T. Sidorova, D. J. Long and D. J. Calkins (2009). "Trpv1: Contribution to retinal ganglion cell apoptosis and increased intracellular Ca2+ with exposure to hydrostatic pressure." Invest Ophthalmol Vis Sci 50(2): 717-728. DOI: 10.1167/iovs.08-2321.

Schafer, D. P., E. K. Lehrman, A. G. Kautzman, R. Koyama, A. R. Mardinly, R. Yamasaki, R. M. Ransohoff, M. E. Greenberg, B. A. Barres and B. Stevens (2012). "Microglia sculpt postnatal neural circuits in an activity and complement-dependent manner." Neuron 74(4): 691-705. DOI: 10.1016/j.neuron.2012.03.026.

Schlamp, C. L., Y. Li, J. A. Dietz, K. T. Janssen and R. W. Nickells (2006). "Progressive ganglion cell loss and optic nerve degeneration in dba/2j mice is variable and asymmetric." BMC Neurosci 7: 66. DOI: 10.1186/1471-2202-7-66.

Schlamp, C. L., A. D. Montgomery, C. E. Mac Nair, C. Schuart, D. J. Willmer and R. W. Nickells (2013). "Evaluation of the percentage of ganglion cells in the ganglion cell layer of the rodent retina." Mol Vis 19: 1387-1396.

Schmid, H., M. Renner, H. B. Dick and S. C. Joachim (2014). "Loss of inner retinal neurons after retinal ischemia in rats." Investigative Opthalmology & Visual Science 55(4): 2777. DOI: 10.1167/iovs.13-13372.

Schulte, G. and B. B. Fredholm (2003). "Signalling from adenosine receptors to mitogen-activated protein kinases." Cell Signal 15(9): 813-827. DOI: 10.1016/s0898-6568(03)00058-5.

Schuman, J. S., M. R. Hee, C. A. Puliafito, C. Wong, T. Pedut-Kloizman, C. P. Lin, E. Hertzmark, J. A. Izatt, E. A. Swanson and J. G. Fujimoto (1995). "Quantification of nerve fiber layer thickness in normal and glaucomatous eyes using optical coherence tomography." Arch Ophthalmol 113(5): 586-596. DOI: 10.1001/archopht.1995.01100050054031.

Schuster, A. K., C. Erb, E. M. Hoffmann, T. Dietlein and N. Pfeiffer (2020). "The diagnosis and treatment of glaucoma." Dtsch Arztebl Int 117(13): 225-234. DOI: 10.3238/arztebl.2020.0225.

Scuderi, G., S. Fragiotta, L. Scuderi, C. M. Iodice and A. Perdicchi (2020). "Ganglion cell complex analysis in glaucoma patients: What can it tell us?" Eye Brain 12: 33-44. DOI: 10.2147/EB.S226319.

Shaheer, M., A. Amjad and Z. Saleem (2019). "Retinal ganglion cell complex changes after intravitreal bevacizumab for diabetic macular edema." J Coll Physicians Surg Pak 29(5): 426-429. DOI: 10.29271/jcpsp.2019.05.426.

Shahmoradi, S., F. Yazdian, F. Tabandeh, Z. S. Soheili, A. S. Hatamian Zarami and M. Navaei-Nigjeh (2017). "Controlled surface morphology and hydrophilicity of polycaprolactone toward human retinal pigment epithelium cells." Mater Sci Eng C Mater Biol Appl 73: 300-309. DOI: 10.1016/j.msec.2016.11.076.

Shahsuvaryan, M. L. (2013). "Glaucomatous optic neuropathy management: The role of neuroprotective agents." Med Hypothesis Discov Innov Ophthalmol 2(2): 41-46.

Shang, C., Z. Liu, Z. Chen, Y. Shi, Q. Wang, S. Liu, D. Li and P. Cao (2015). "Brain circuits. A parvalbumin-positive excitatory visual pathway to trigger fear responses in mice." Science 348(6242): 1472-1477. DOI: 10.1126/science.aaa8694.

Sheng, Y., Y. Zhu and L. Wu (2004). "Effect of high dosage of methylprednisolone on rat retinal ganglion cell apoptosis after optic nerve crush." Yan Ke Xue Bao 20(3): 181-186.

Shieh, Y.-T. and H.-S. Yang (2005). "Morphological changes of polycaprolactone with high-pressure CO2 treatment." The Journal of Supercritical Fluids 33(2): 183-192. DOI: 10.1016/j.supflu.2004.06.002.

Shields, M. B. (2008). "Normal-tension glaucoma: Is it different from primary open-angle glaucoma?" Curr Opin Ophthalmol 19(2): 85-88. DOI: 10.1097/ICU.0b013e3282f3919b.

Shirvan, A., M. Kimron, V. Holdengreber, I. Ziv, Y. Ben-Shaul, S. Melamed, E. Melamed, A. Barzilai and A. S. Solomon (2002). "Anti-semaphorin 3a antibodies rescue retinal ganglion cells from cell death following optic nerve axotomy." J Biol Chem 277(51): 49799-49807. DOI: 10.1074/jbc.M204793200.

Shivanand, P. and O. L. Sprockel (1998). "A controlled porosity drug delivery system." International Journal of Pharmaceutics 167(1-2): 83-96. DOI: 10.1016/s0378-5173(98)00047-7.

Sho, K., K. Takahashi, T. Fukuchi and M. Matsumura (2005). "Quantitative evaluation of ischemia-reperfusion injury by optical coherence tomography in the rat retina." Jpn J Ophthalmol 49(2): 109-113. DOI: 10.1007/s10384-004-0150-3.

Shruthi, S., R. Sumitha, A. M. Varghese, S. Ashok, B. K. Chandrasekhar Sagar, T. N. Sathyaprabha, A. Nalini, B. W. Kramer, T. R. Raju, K. Vijayalakshmi and P. A. Alladi (2017). "Brain-derived neurotrophic factor facilitates functional recovery from als-cerebral spinal fluid-induced neurodegenerative changes in the nsc-34 motor neuron cell line." Neurodegener Dis 17(1): 44-58. DOI: 10.1159/000447559.

Siepmann, J., F. Lecomte and R. Bodmeier (1999). "Diffusion-controlled drug delivery systems: Calculation of the required composition to achieve desired release profiles." Journal of Controlled Release 60(2-3): 379-389. DOI: 10.1016/s0168-3659(99)00093-0.

Silva-Cunha, A., S. L. Fialho, M. C. Naud and F. Behar-Cohen (2009). "Poly-epsilon-caprolactone intravitreous devices: An in vivo study." Invest Ophthalmol Vis Sci 50(5): 2312-2318. DOI: 10.1167/iovs.08-2969.

Silverman, S. M. and W. T. Wong (2018). "Microglia in the retina: Roles in development, maturity, and disease." Annual Review of Vision Science 4(1): 45-77. DOI: 10.1146/annurev-vision-091517-034425.

Simons, M. and K. A. Nave (2015). "Oligodendrocytes: Myelination and axonal support." Cold Spring Harb Perspect Biol 8(1): a020479. DOI: 10.1101/cshperspect.a020479.

Sleath, B., A. L. Robin, D. Covert, J. E. Byrd, G. Tudor and B. Svarstad (2006). "Patient-reported behavior and problems in using glaucoma medications." Ophthalmology 113(3): 431-436. DOI: 10.1016/j.ophtha.2005.10.034.

Smith, R. S., A. Zabaleta, O. V. Savinova and S. W. John (2001). "The mouse anterior chamber angle and trabecular meshwork develop without cell death." BMC Dev Biol 1: 3. DOI: 10.1186/1471-213x-1-3.

Snaidero, N., W. Mobius, T. Czopka, L. H. Hekking, C. Mathisen, D. Verkleij, S. Goebbels, J. Edgar, D. Merkler, D. A. Lyons, K. A. Nave and M. Simons (2014). "Myelin membrane wrapping of cns axons by pi(3,4,5)p3-dependent polarized growth at the inner tongue." Cell 156(1-2): 277-290. DOI: 10.1016/j.cell.2013.11.044.

Sofroniew, M. V. and H. V. Vinters (2010). "Astrocytes: Biology and pathology." Acta Neuropathol 119(1): 7-35. DOI: 10.1007/s00401-009-0619-8.

Son, J. L., I. Soto, E. Oglesby, T. Lopez-Roca, M. E. Pease, H. A. Quigley and N. Marsh-Armstrong (2010). "Glaucomatous optic nerve injury involves early astrocyte reactivity and late oligodendrocyte loss." Glia: NA-NA. DOI: 10.1002/glia.20962.

Soubrane, G. and F. Behar-Cohen (2015). "Fluocinolone acetonide (iluvien(r)) micro-implant for chronic diabetic macular edema." J Fr Ophtalmol 38(2): 159-167. DOI: 10.1016/j.jfo.2014.09.007.

Srikar, R., A. L. Yarin, C. M. Megaridis, A. V. Bazilevsky and E. Kelley (2008). "Desorption-limited mechanism of release from polymer nanofibers." Langmuir 24(3): 965-974. DOI: 10.1021/la702449k.

Stassart, R. M., W. Mobius, K. A. Nave and J. M. Edgar (2018). "The axon-myelin unit in development and degenerative disease." Front Neurosci 12: 467. DOI: 10.3389/fnins.2018.00467.

Steigerwalt, R. D., Jr., M. R. Cesarone, A. Pascarella, M. De Angelis, M. Nebbioso, G. Belcaro and B. Feragalli (2011). "Ocular and optic nerve ischemia: Recognition and treatment with intravenous prostaglandin e1." Panminerva Med 53(3 Suppl 1): 119-124.

Steketee, M. B., C. Oboudiyat, R. Daneman, E. Trakhtenberg, P. Lamoureux, J. E. Weinstein, S. Heidemann, B. A. Barres and J. L. Goldberg (2014). "Regulation of intrinsic axon growth ability at retinal ganglion cell growth cones." Invest Ophthalmol Vis Sci 55(7): 4369-4377. DOI: 10.1167/iovs.14-13882.

Su, Y., F. Wang, Y. Teng, S. G. Zhao, H. Cui and S. H. Pan (2009). "Axonal regeneration of optic nerve after crush in nogo66 receptor knockout mice." Neurosci Lett 460(3): 223-226. DOI: 10.1016/j.neulet.2009.05.072.

Susanna, R., C. G. De Moraes, G. A. Cioffi and R. Ritch (2015). "Why do people (still) go blind from glaucoma?" Translational Vision Science & Technology 4(2): 1. DOI: 10.1167/tvst.4.2.1.

Tham, Y.-C., X. Li, T. Y. Wong, H. A. Quigley, T. Aung and C.-Y. Cheng (2014). "Global prevalence of glaucoma and projections of glaucoma burden through 2040." Ophthalmology 121(11): 2081-2090. DOI: 10.1016/j.ophtha.2014.05.013.

Thomas, C. N., M. Berry, A. Logan, R. J. Blanch and Z. Ahmed (2017). "Caspases in retinal ganglion cell death and axon regeneration." Cell Death Discov 3: 17032. DOI: 10.1038/cddiscovery.2017.32.

Tillo, M., C. Ruhrberg and F. Mackenzie (2012). "Emerging roles for semaphorins and vegfs in synaptogenesis and synaptic plasticity." Cell Adh Migr 6(6): 541-546. DOI: 10.4161/cam.22408.

Vajda, F., N. Jordi, D. Dalkara, S. Joly, F. Christ, B. Tews, M. E. Schwab and V. Pernet (2015). "Cell type-specific nogo-a gene ablation promotes axonal regeneration in the injured adult optic nerve." Cell Death Differ 22(2): 323-335. DOI: 10.1038/cdd.2014.147.

van Horck, F. P., C. Weinl and C. E. Holt (2004). "Retinal axon guidance: Novel mechanisms for steering." Curr Opin Neurobiol 14(1): 61-66. DOI: 10.1016/j.conb.2004.01.002.

Varela-Fernandez, R., V. Diaz-Tome, A. Luaces-Rodriguez, A. Conde-Penedo, X. Garcia-Otero, A. Luzardo-Alvarez, A. Fernandez-Ferreiro and F. J. Otero-Espinar (2020). "Drug delivery to the posterior segment of the eye: Biopharmaceutic and pharmacokinetic considerations." Pharmaceutics 12(3). DOI: 10.3390/pharmaceutics12030269.

Vecino, E., E. Caminos, M. Ugarte, D. Martín-Zanca and N. N. Osborne (1998). "Immunohistochemical distribution of neurotrophins and their receptors in the rat retina and the effects of ischemia and reperfusion." General Pharmacology: The Vascular System 30(3): 305-314. DOI: 10.1016/s0306-3623(97)00361-3.

Vecino, E., F. D. Rodriguez, N. Ruzafa, X. Pereiro and S. C. Sharma (2016). "Glia-neuron interactions in the mammalian retina." Prog Retin Eye Res 51: 1-40. DOI: 10.1016/j.preteyeres.2015.06.003.

Vecino, E., M. Ugarte, M. S. Nash and N. N. Osborne (1999). "NMDA induces bdnf expression in the albino rat retina in vivo." Neuroreport 10(5): 1103-1106. DOI: 10.1097/00001756-199904060-00036.

Ventura, A. L. M., A. Dos Santos-Rodrigues, C. H. Mitchell and M. P. Faillace (2019). "Purinergic signaling in the retina: From development to disease." Brain Res Bull 151: 92-108. DOI: 10.1016/j.brainresbull.2018.10.016.

Vidal-Sanz, M., G. M. Bray, M. P. Villegas-Perez, S. Thanos and A. J. Aguayo (1987). "Axonal regeneration and synapse formation in the superior colliculus by retinal ganglion cells in the adult rat." J Neurosci 7(9): 2894-2909.

Vidal-Sanz, M., M. Salinas-Navarro, F. M. Nadal-Nicolas, L. Alarcon-Martinez, F. J. Valiente-Soriano, J. M. de Imperial, M. Aviles-Trigueros, M. Agudo-Barriuso and M. P. Villegas-Perez (2012). "Understanding glaucomatous damage: Anatomical and functional data from ocular hypertensive rodent retinas." Prog Retin Eye Res 31(1): 1-27. DOI: 10.1016/j.preteyeres.2011.08.001.

Vidal-Sanz, M., F. J. Valiente-Soriano, A. Ortin-Martinez, F. M. Nadal-Nicolas, M. Jimenez-Lopez, M. Salinas-Navarro, L. Alarcon-Martinez, D. Garcia-Ayuso, M. Aviles-Trigueros, M. Agudo-Barriuso and M. P. Villegas-Perez (2015). "Retinal neurodegeneration in experimental glaucoma." Prog Brain Res 220: 1-35. DOI: 10.1016/bs.pbr.2015.04.008.

Vidaurre, A., J. M. M. Dueñas, J. M. Estellés and I. C. Cortázar (2008). "Influence of enzymatic degradation on physical properties of poly(Ɛ-caprolactone) films and sponges." Macromolecular Symposia 269(1): 38-46. DOI: 10.1002/masy.200850907.

von Burkersroda, F., L. Schedl and A. Gopferich (2002). "Why degradable polymers undergo surface erosion or bulk erosion." Biomaterials 23(21): 4221-4231. DOI: 10.1016/S0142-9612(02)00170-9.

Von Lubitz, D. K., R. C. Lin, M. Boyd, N. Bischofberger and K. A. Jacobson (1999). "Chronic administration of adenosine a3 receptor agonist and cerebral ischemia: Neuronal and glial effects." Eur J Pharmacol 367(2-3): 157-163. DOI: 10.1016/s0014-2999(98)00977-7.

Von Lubitz, D. K., R. C. Lin, P. Popik, M. F. Carter and K. A. Jacobson (1994). "Adenosine A3 receptor stimulation and cerebral ischemia." Eur J Pharmacol 263(1-2): 59-67. DOI: 10.1016/0014-2999(94)90523-1.

Von Lubitz, D. K., K. L. Simpson and R. C. Lin (2001). "Right thing at a wrong time? Adenosine A3 receptors and cerebroprotection in stroke." Ann N Y Acad Sci 939: 85-96. DOI: 10.1111/j.1749-6632.2001.tb03615.x.

Wang, J., S. Chen, X. Zhang, W. Huang and J. B. Jonas (2016a). "Intravitreal triamcinolone acetonide, retinal microglia and retinal ganglion cell apoptosis in the optic nerve crush model." Acta Ophthalmologica 94(5): e305-e311. DOI: 10.1111/aos.12698.

Wang, J., A. Jiang, M. Joshi and J. Christoforidis (2013a). "Drug delivery implants in the treatment of vitreous inflammation." Mediators Inflamm 2013: 780634. DOI: 10.1155/2013/780634.

Wang, L., G. A. Cioffi, G. Cull, J. Dong and B. Fortune (2002). "Immunohistologic evidence for retinal glial cell changes in human glaucoma." Invest Ophthalmol Vis Sci 43(4): 1088-1094.

Wang, M., W. Ma, L. Zhao, R. N. Fariss and W. T. Wong (2011). "Adaptive Müller cell responses to microglial activation mediate neuroprotection and coordinate inflammation in the retina." J Neuroinflammation 8: 173. DOI: 10.1186/1742-2094-8-173.

Wang, M., X. Wang, L. Zhao, W. Ma, I. R. Rodriguez, R. N. Fariss and W. T. Wong (2014). "Macroglia-microglia interactions via tspo signaling regulates microglial activation in the mouse retina." J Neurosci 34(10): 3793-3806. DOI: 10.1523/JNEUROSCI.3153-13.2014.

Wang, Q. and A. Burkhalter (2013b). "Stream-related preferences of inputs to the superior colliculus from areas of dorsal and ventral streams of mouse visual cortex." J Neurosci 33(4): 1696-1705. DOI: 10.1523/JNEUROSCI.3067-12.2013.

Wang, X., L. Zhao, J. Zhang, R. N. Fariss, W. Ma, F. Kretschmer, M. Wang, H. H. Qian, T. C. Badea, J. S. Diamond, W. B. Gan, J. E. Roger and W. T. Wong (2016b). "Requirement for microglia for the maintenance of synaptic function and integrity in the mature retina." J Neurosci 36(9): 2827-2842. DOI: 10.1523/JNEUROSCI.3575-15.2016.

Wang, Z., C. W. Do, M. Y. Avila, K. Peterson-Yantorno, R. A. Stone, Z. G. Gao, B. Joshi, P. Besada, L. S. Jeong, K. A. Jacobson and M. M. Civan (2010). "Nucleoside-derived antagonists to A3 adenosine receptors lower mouse intraocular pressure and act across species." Exp Eye Res 90(1): 146-154. DOI: 10.1016/j.exer.2009.10.001.

Wassle, H. (2004). "Parallel processing in the mammalian retina." Nat Rev Neurosci 5(10): 747-757. DOI: 10.1038/nrn1497.

Wassle, H., C. Puller, F. Muller and S. Haverkamp (2009). "Cone contacts, mosaics, and territories of bipolar cells in the mouse retina." J Neurosci 29(1): 106-117. DOI: 10.1523/JNEUROSCI.4442-08.2009.

Wax, M. B., G. Tezel, S. Kobayashi and M. R. Hernandez (2000). "Responses of different cell lines from ocular tissues to elevated hydrostatic pressure." Br J Ophthalmol 84(4): 423-428. DOI: 10.1136/bjo.84.4.423.

Wegner, M., D. W. Drolet and M. G. Rosenfeld (1993). "Pou-domain proteins: Structure and function of developmental regulators." Curr Opin Cell Biol 5(3): 488-498. DOI: 10.1016/0955-0674(93)90015-i.

Wei, P., N. Liu, Z. Zhang, X. Liu, Y. Tang, X. He, B. Wu, Z. Zhou, Y. Liu, J. Li, Y. Zhang, X. Zhou, L. Xu, L. Chen, G. Bi, X. Hu, F. Xu and L. Wang (2015). "Corrigendum: Processing of visually evoked innate fear by a non-canonical thalamic pathway." Nat Commun 6: 8228. DOI: 10.1038/ncomms9228.

Weinreb, R. N., T. Aung and F. A. Medeiros (2014). "The pathophysiology and treatment of glaucoma: A review." JAMA 311(18): 1901-1911. DOI: 10.1001/jama.2014.3192.

Weinreb, R. N., J. M. Liebmann, G. A. Cioffi, I. Goldberg, J. D. Brandt, C. A. Johnson, L. M. Zangwill, S. Schneider, H. Badger and M. Bejanian (2018). "Oral memantine for the treatment of glaucoma: Design and results of 2 randomized, placebo-controlled, phase 3 studies." Ophthalmology 125(12): 1874-1885. DOI: 10.1016/j.ophtha.2018.06.017.

Weinreb, R. N. and J. D. Lindsey (2005). "The importance of models in glaucoma research." J Glaucoma 14(4): 302-304. DOI: 10.1097/01.ijg.0000169395.47921.02.

Wetmore, C., P. Ernfors, H. Persson and L. Olson (1990). "Localization of brain-derived neurotrophic factor mrna to neurons in the brain by in situ hybridization." Exp Neurol 109(2): 141-152. DOI: 10.1016/0014-4886(90)90068-4.

Wiggs, J. L. (2013). "Glaucoma." 1-15. DOI: 10.1016/b978-0-12-383834-6.00144-0.

Wilsey, L. J. and B. Fortune (2016). "Electroretinography in glaucoma diagnosis." Curr Opin Ophthalmol 27(2): 118-124. DOI: 10.1097/ICU.0000000000000241.

Winzeler, A. and J. T. Wang (2013). "Purification and culture of retinal ganglion cells from rodents." Cold Spring Harb Protoc 2013(7): 643-652. DOI: 10.1101/pdb.prot074906.

Wittendorp, M. C., H. W. Boddeke and K. Biber (2004). "Adenosine A3 receptor-induced CCL2 synthesis in cultured mouse astrocytes." Glia 46(4): 410-418. DOI: 10.1002/glia.20016.

WoldeMussie, E., G. Ruiz, M. Wijono and L. A. Wheeler (2001). "Neuroprotection of retinal ganglion cells by brimonidine in rats with laser-induced chronic ocular hypertension." Invest Ophthalmol Vis Sci 42(12): 2849-2855.

Wolf, S. A., H. W. Boddeke and H. Kettenmann (2017). "Microglia in physiology and disease." Annu Rev Physiol 79: 619-643. DOI: 10.1146/annurev-physiol-022516-034406.

Wong, E. V., S. David, M. H. Jacob and D. G. Jay (2003). "Inactivation of myelin-associated glycoprotein enhances optic nerve regeneration." J Neurosci 23(8): 3112-3117.

Wong, R. C., S. L. Cloherty, M. R. Ibbotson and B. J. O'Brien (2012). "Intrinsic physiological properties of rat retinal ganglion cells with a comparative analysis." J Neurophysiol 108(7): 2008-2023. DOI: 10.1152/jn.01091.2011.

Woodruff, M. A. and D. W. Hutmacher (2010). "The return of a forgotten polymer-polycaprolactone in the 21st century." Progress in Polymer Science 35(10): 1217-1256. DOI: 10.1016/j.progpolymsci.2010.04.002.

Wu, J., H. K. Mak, Y. K. Chan, C. Lin, C. Kong, C. K. S. Leung and H. C. Shum (2019). "An in vitro pressure model towards studying the response of primary retinal ganglion cells to elevated hydrostatic pressures." Scientific Reports 9(1). DOI: 10.1038/s41598-019-45510-7.

Wu, Z. and F. A. Medeiros (2018). "Recent developments in visual field testing for glaucoma." Current Opinion in Ophthalmology 29(2): 141-146. DOI: 10.1097/icu.0000000000000461.

Xiao, C., N. Liu, K. A. Jacobson, O. Gavrilova and M. L. Reitman (2019). "Physiology and effects of nucleosides in mice lacking all four adenosine receptors." PLOS Biology 17(3): e3000161. DOI: 10.1371/journal.pbio.3000161.

Xiao, H., X. Liu, P. Lian, L. L. Liao and Y. M. Zhong (2020). "Different damage patterns of retinal nerve fiber layer and ganglion cell-inner plexiform layer between early glaucoma and non-glaucomatous optic neuropathy." Int J Ophthalmol 13(6): 893-901. DOI: 10.18240/ijo.2020.06.06.

Yalkowsky, S., Y. He and P. Jain (2010). Handbook of aqueous solubility data, CRC Press.

Yang, H., M. Y. Avila, K. Peterson-Yantorno, M. Coca-Prados, R. A. Stone, K. A. Jacobson and M. M. Civan (2005). "The cross-species A3 adenosine-receptor antagonist MRS 1292 inhibits adenosine-triggered human nonpigmented ciliary epithelial cell fluid release and reduces mouse intraocular pressure." Curr Eye Res 30(9): 747-754. DOI: 10.1080/02713680590953147.

Yang, X. L. (2004). "Characterization of receptors for glutamate and GABA in retinal neurons." Prog Neurobiol 73(2): 127-150. DOI: 10.1016/j.pneurobio.2004.04.002.

Yanoff, M. and J. W. Sassani (2015). "Optic nerve." 441-465.e444. DOI: 10.1016/b978-1-4557-2874-9.00013-2.

Yasin, M. N., D. Svirskis, A. Seyfoddin and I. D. Rupenthal (2014). "Implants for drug delivery to the posterior segment of the eye: A focus on stimuli-responsive and tunable release systems." Journal of Controlled Release 196: 208-221. DOI: 10.1016/j.jconrel.2014.09.030.

Yasukawa, T., Y. Ogura, E. Sakurai, Y. Tabata and H. Kimura (2005). "Intraocular sustained drug delivery using implantable polymeric devices." Adv Drug Deliv Rev 57(14): 2033-2046. DOI: 10.1016/j.addr.2005.09.005.

Yasukawa, T., Y. Tabata, H. Kimura and Y. Ogura (2011). "Recent advances in intraocular drug delivery systems." Recent Pat Drug Deliv Formul 5(1): 1-10.

Yellepeddi, V. K. and S. Palakurthi (2016). "Recent advances in topical ocular drug delivery." J Ocul Pharmacol Ther 32(2): 67-82. DOI: 10.1089/jop.2015.0047.

Yiu, G. and Z. He (2006). "Glial inhibition of cns axon regeneration." Nature Reviews Neuroscience 7(8): 617-627. DOI: 10.1038/nrn1956.

Yoneda, S., H. Tanihara, N. Kido, Y. Honda, W. Goto, H. Hara and N. Miyawaki (2001). "Interleukin-1beta mediates ischemic injury in the rat retina." Exp Eye Res 73(5): 661-667. DOI: 10.1006/exer.2001.1072.

Yu, C., C. Roubeix, F. Sennlaub and D. R. Saban (2020). "Microglia versus monocytes: Distinct roles in degenerative diseases of the retina." Trends in Neurosciences 43(6): 433-449. DOI: 10.1016/j.tins.2020.03.012.

Zhang, C.-W., Q. Lu, S.-W. You, Y. Zhi, H. K. Yip, W. Wu, K.-F. So and Q. Cui (2005). "CNTF and BDNF have similar effects on retinal ganglion cell survival but differential effects on nitric oxide synthase expression soon after optic nerve injury." Investigative Opthalmology & Visual Science 46(4): 1497. DOI: 10.1167/iovs.04-0664.

Zhang, M., M. T. Budak, W. Lu, T. S. Khurana, X. Zhang, A. M. Laties and C. H. Mitchell (2006). "Identification of the a3 adenosine receptor in rat retinal ganglion cells." Mol Vis 12: 937-948.

Zhang, M., H. Hu, X. Zhang, W. Lu, J. Lim, T. Eysteinsson, K. A. Jacobson, A. M. Laties and C. H. Mitchell (2010). "The A3 adenosine receptor attenuates the calcium rise triggered by nmda receptors in retinal ganglion cells." Neurochem Int 56(1): 35-41. DOI: 10.1016/j.neuint.2009.08.011.

Zhang, X., M. Zhang, A. M. Laties and C. H. Mitchell (2006). "Balance of purines may determine life or death of retinal ganglion cells as A3 adenosine receptors prevent loss following P2X7 receptor stimulation." J Neurochem 98(2): 566-575. DOI: 10.1111/j.1471-4159.2006.03900.x.

Zhao, M., E. Rodriguez-Villagra, L. Kowalczuk, M. Le Normand, M. Berdugo, R. Levy-Boukris, I. El Zaoui, B. Kaufmann, R. Gurny, I. Bravo-Osuna, I. T. Molina-Martinez, R. Herrero-Vanrell and F. Behar-Cohen (2017). "Tolerance of high and low amounts of PLGA microspheres loaded with mineralocorticoid receptor antagonist in retinal target site." J Control Release 266: 187-197. DOI: 10.1016/j.jconrel.2017.09.029.

Zhou, Q. Y., C. Li, M. E. Olah, R. A. Johnson, G. L. Stiles and O. Civelli (1992). "Molecular cloning and characterization of an adenosine receptor: The A3 adenosine receptor." Proc Natl Acad Sci U S A 89(16): 7432-7436. DOI: 10.1073/pnas.89.16.7432.

Zimmermann, H. (2000). "Extracellular metabolism of atp and other nucleotides." Naunyn Schmiedebergs Arch Pharmacol 362(4-5): 299-309. DOI: 10.1007/s002100000309.

Zylbersztejn, K., M. Petkovic, A. Burgo, M. Deck, S. Garel, S. Marcos, E. Bloch-Gallego, F. Nothias, G. Serini, D. Bagnard, T. Binz and T. Galli (2012). "The vesicular snare synaptobrevin is required for semaphorin 3a axonal repulsion." J Cell Biol 196(1): 37-46. DOI: 10.1083/jcb.201106113.